

A Detailed Kinetic and Mechanistic Investigation into the Rate of Chloride Substitution from Chloro Terpyridine Platinum(II) and Analogous Complexes by a Series of Azole Nucleophiles

By

Kate J. Gillham

BSc (Honours) (University of KwaZulu Natal)

Master of Science

Jaanaary 2010



**UNIVERSITY OF
KWAZULU-NATAL**

School of Chemistry
Pietermaritzburg

A Detailed Kinetic and Mechanistic Investigation into the Rate of Chloride Substitution from Chloro Terpyridine Platinum(II) and Analogous Complexes by a Series of Azole Nucleophiles

Submitted in the fulfillment of the requirements for the degree of

Master of Science

By

Kate J. Gillham

BSc (Honours) (University of KwaZulu Natal)

February 2010

School of Chemistry

University of KwaZulu-Natal

Pietermaritzburg

The financial assistance of the National Research Foundation (NRF) towards this research is hereby acknowledged. Opinions expressed and conclusions arrived at, are those of the author and are not necessarily to be attributed to the NRF.

FACULTY OF SCIENCE AND AGRICULTURE

DECLARATION - PLAGIARISM

I, Kate J. Gillham, declare that

1. The research reported in this thesis, except where otherwise indicated, is my original research.
2. This thesis has not been submitted for any degree or examination at any other university.
3. This thesis does not contain other persons' data, pictures, graphs or other information, unless specifically acknowledged as being sourced from other persons.
4. This thesis does not contain other persons' writing, unless specifically acknowledged as being sourced from other researchers. Where other written sources have been quoted, then:
 - a. Their words have been re-written but the general information attributed to them has been referenced
 - b. Where their exact words have been used, then their writing has been placed in italics and inside quotation marks, and referenced.
5. This thesis does not contain text, graphics or tables copied and pasted from the Internet, unless specifically acknowledged, and the source being detailed in the thesis and in the References sections.

Signed.....

Kate J. Gillham

I hereby certify that this is correct.

Signed.....

..

Dr. D. Reddy

Supervisor

Signed.....

..

Prof. D. Jaganyi

Co-supervisor

Abstract

The substitution kinetics of the complexes: [Pt(terpy)Cl]Cl·2H₂O (**PtL1**), [Pt(^tBu₃terpy)Cl]ClO₄ (**PtL2**), [Pt{4'-(2'''-CH₃-Ph)terpy}Cl]BF₄ (**PtL3**), [Pt{4'-(2'''-CF₃-Ph)terpy}Cl]CF₃SO₄ (**PtL4**), [Pt{4'-(2'''-CF₃-Ph)-6-Ph-bipy}Cl] (**PtL5**) and [Pt{4'-(2'''-CH₃-Ph)-6-2''-pyrazinyl-2,2'-bipy}Cl]CF₃SO₃ (**PtL6**) with the nucleophiles: imidazole (**Im**), 1-methylimidazole (**MIm**), 1,2-dimethylimidazole (**DIm**), pyrazole (**pyz**) and 1,2,4-triazole (**Trz**) were investigated in a methanolic solution of constant ionic strength. Substitution of the chloride ligand from the metal complexes by the nucleophiles was investigated as a function of nucleophile concentration and temperature under *pseudo* first-order condition using UV/Visible and stopped-flow spectrophotometric techniques.

The results obtained indicate that by either changing the substituents on the terpy backbone or by slight modification of the chelate itself leads to changes in the π -acceptor ability of the chelate. This in turn controls the electrophilicity of the metal centre and hence its reactivity. In the case of **PtL3** and **PtL4**, the *ortho* substituent on the phenyl ring at the 4'-position on the terpy backbone is either electron-donating or electron-withdrawing respectively. For an electron-donating group (CH₃, **PtL3**) the reactivity of the metal centre is decreased whilst an electron-withdrawing group (CF₃, **PtL4**) lead to a moderate increase in reactivity. Electron-donating groups attached directly to the terpy moiety (^tBu₃, **PtL2**) also leads to a decrease in the rate of chloride substitution. Placing a strong σ -donor *cis* to the leaving group (**PtL5**) greatly decreases the reactivity of a complex while the addition of a good π -acceptor group (**PtL6**) significantly enhances the reactivity. The results obtained for **PtL5** and **PtL6** indicate that the group present in the *cis* position activates the metal centre in a different manner than when in the *trans* position.

The experimental results obtained were supported by DFT calculations at the B3LYP/LACVP+** level of theory, with the NBO charges showing a less electrophilic Pt(II) centre when a strong σ -donor *cis* to the leaving group was present such as in **PtL5** and a more electrophilic centre for complexes with good π -acceptor groups such as with **PtL6**. Surprisingly, the results indicate that in the case of **PtL5**, when the metal centre was less electrophilic it also appears to be less selective.

The nucleophiles followed a general trend dependent on the basicity of the azole with the exception of **DIm**. Although **DIm** is the most basic of the nucleophiles, it has reduced reactivity due to added steric bulk. **MIm** is basic and hence the most reactive of the nucleophiles with **Trz** being the least basic with the slowest reactivity. The temperature dependence studies support an associative mode of activation. X-ray crystal structures of **Pyz** bound to **PtL1** and **PtL3** as well as structures of **MIm** and **DIm** bound to **PtL1** were obtained in order to determine the manner in which these nucleophiles bind to the metal centre.

Contents

Acknowledgements	I
Previous Publications	II
List of Abbreviations	III
List of Figures	V
List of Tables	XI
Chapter 1: Introduction	1
1.1 <i>Platinum(II) Chemistry</i>	1
1.1.1 Chemical Properties of Platinum	1
1.1.2 Applications of Platinum	3
1.2 <i>Cancer Chemotherapy Involving Platinum Complexes</i>	5
1.2.1 Introduction to Cancer	5
1.2.2 The Anti-Tumour Activity of Platinum Complexes	6
1.2.3 Structure-Activity Relationships of Platinum Complexes	7
1.2.4 Mechanisms of Action of Platinum Anti-Cancer Agents	9
1.2.5 Development of New Platinum Anti-Cancer Complexes	13
1.3 <i>Pt(II) Terpyridine Complexes</i>	16
1.3.1 The Role of Platinum(II) Terpyridine Complexes in Modern Chemistry	16
1.3.2 Previous Platinum(II) Terpyridine Investigations	18
1.4 <i>Azoles</i>	23
1.4.1 Azoles in Biological Systems	23
1.4.2 Previous Azole Studies	26
1.5 <i>Aims of Current Study</i>	28
1.6 <i>References</i>	30
Chapter 2: Substitution Reactions	34
2.1 <i>Stoichiometric and Intimate Mechanisms</i>	36
2.2 <i>Coordination Number and Substitution Mechanism</i>	38
2.3 <i>Substitution in Square-Planar Complexes</i>	38
2.3.1 The Kinetics and Mechanisms of Substitution	40

2.3.2	Geometries of the Transition States and Intermediates	43
2.3.3	Factors Controlling the Reactivity of Square-Planar Complexes	44
2.3.4	The Dissociative Mechanism in Square-Planar Complexes	53
2. 4	<i>References</i>	55
Chapter 3: Reaction Kinetics		57
3.1	<i>Introduction</i>	57
3.2	<i>The Rate Law</i>	59
3.3	<i>Integrated Rate Laws</i>	59
3.3.1	First Order Reactions	59
3.3.2	Reversible First Order Reactions	61
3.3.3	Second Order Reactions	63
3.3.4	Reversible Second Order Reactions	65
3.4	<i>Temperature Dependence and Activation Parameters</i>	67
3.4.1	Arrhenius Equation	68
3.4.2	Transition State Theory	68
3.4.3	Pressure Dependence and Volumes of Activation	70
3.5	<i>Experimental Kinetic Techniques</i>	71
3.5.1	UV/Visible Spectrophotometry	72
3.5.2	Stopped-flow Techniques	74
3.6	<i>References</i>	77
Chapter 4: Experimental		79
4.1	<i>General Methods</i>	79
4.2	<i>Synthesis of Complexes</i>	80
4.2.1	Synthesis of Dichloro(1,5-cyclooctadiene)platinum(II)	80
4.2.2	Synthesis of [Pt(terpy)Cl]Cl·2H ₂ O (PtL1)	81
4.2.3	Synthesis of [Pt(tBu ₃ terpy)Cl]ClO ₄ (PtL2)	82
4.2.4	Synthesis of [Pt{4'-(2'''-CH ₃ -Ph)terpy}Cl]BF ₄ (PtL3)	83
4.2.5	Synthesis of [Pt{4'-(2'''-CF ₃ -Ph)terpy}Cl]CF ₃ SO ₄ (PtL4)	84
4.2.6	Synthesis of [Pt{4'-(2'''-CF ₃ -Ph)-6-Ph-bipy}Cl] (PtL5)	86
4.2.7	Synthesis of [Pt{4'-(2''-CH ₃ -Ph)-6-2''pyraz-2,2' bipy}Cl] CF ₃ SO ₃ (PtL6)	87

4.3	<i>X-ray Crystal Structures</i>	89
4.4	<i>Preparation of Complex and Nucleophile Solutions for Kinetic Analysis</i>	90
4.5	<i>Instrumentation and Measurements</i>	90
4.5.1	Microanalysis	90
4.5.2	NMR Spectroscopy	91
4.5.3	Infrared Spectroscopy	91
4.5.4	Mass Spectrometry	91
4.5.5	Computational modelling	91
4.5.6	X-ray Structure Determination	92
4.5.7	Kinetic Measurements	94
4.6	<i>References</i>	95
Chapter 5:	X-ray Crystallography	98
5.1	<i>X-ray structure of PtL1-MIm</i>	98
5.2	<i>X-ray structures of PtL1-DIm, PtL1-Pyz and PtL3-Pyz</i>	103
5.3	<i>References</i>	111
Chapter 6:	Results and Discussion	112
6.1	<i>Results</i>	112
6.1.1	Ligand Synthesis	112
6.1.2	Complex Synthesis	114
6.1.3	Kinetic Measurements	119
6.2	<i>Discussion</i>	128
6.2.1	Reactivity of Metal Complexes	128
6.2.2	Reactivity of Nucleophiles	137
6.2.3	Activation Parameters	145
6.2.4	Conclusion	146
6.3	<i>References</i>	148
Chapter 7:	Conclusions and Future Work	151
7.1	<i>Conclusions</i>	151
7.2	<i>Current Work</i>	154
7.2.1	Other Reactions Attempted During this Study	154

7.2.2 Experiments Conducted	158
7.3 <i>Future Work</i>	162
7.3.1 Extension of Nucleophile Study	162
7.4 <i>References</i>	165
Appendix A	167
Appendix B	178
Appendix C	186
Appendix D	210
Appendix E	212
Appendix F	216

Acknowledgements

I would like to acknowledge both my supervisors, Dr. Reddy and Prof. Jaganyi, for their support over the last year. I am very grateful to Dr. Reddy for having an open-door policy (most of the time) and for his endless advice and explanations. I thank him for his constant guidance and tireless patience as he not only taught me how to use all the necessary instruments but also shared general skills and knowledge. I appreciate the Friday morning meetings with Prof. Jaganyi as he could always put me back on track when I had gone off course. I thank him for always trying to extend me and for the constant words of encouragement, without which I may not have moved so quickly.

I am very grateful to Craig Grimmer for all his time and help. His assistance with NMR spectroscopy as well as his general support has been much appreciated.

I feel privileged to have been able to study at the Chemistry Department on the Pietermaritzburg campus of the University of KwaZulu-Natal, the environment and the people make the work interesting and enjoyable. I would also like to thank the NRF for the funding that has allowed me to study this degree.

I appreciate all the support that my family has given me. Their understanding and financial support has been invaluable. I would also like to thank my future family for their interest especially Mary-Ann for proof-reading my work.

I don't know if I can thank my fiancé enough for everything he has done for me – not only this year but over the past three years. Thank you Matt for taking me to University at all strange hours of the night and over weekends – your understanding and patience has meant a lot. Thank you for running all my X-ray structures, teaching me how to use instruments and programmes, reading through and correcting my work and just for your continual support and words of encouragement.

Previous Publications

1. O. Q. Munro, K. Gillham and M. P. Akerman, *Acta Cryst.*, 2009, **C65**, m317–m320.
2. O. Q. Munro, M. P. Akerman and K. Gillham, *Acta Cryst.*, 2009, **C65**, m343–m346.

List of Abbreviations

<i>A</i>	Absorbance or Arrhenius pre-exponential factor (as indicated)
AET	2-aminoethanethiol
bpma	bis(2-pyridylmethyl)amine
bzimpy	2,6-bis(benzimidazo-2-yl)pyridine
C	Intrinsic reactivity
CCD	Cambridge Structural Database
CMT	Caroethoxymethanethiol
COD	1,5-cyclooctadiene
DFT	Density Functional Theory
dien	diethylenetriamine
DIm	1,2-dimethylimidazole
DMSO	Dimethyl Sulfoxide
DMTU	1,3-dimethyl-2-thiourea
DNA	Deoxyribonucleic acid
E_a	Arrhenius activation energy
ΔE	Energy gap between the HOMO and LUMO
ε	Extinction coefficient
ESI	Electron spray ionisation
EtOH	Ethanol
FTIR	Fourier Transform Infrared
ΔG^\ddagger	Gibbs free energy of activation
h	Planck's constant
ΔH^\ddagger	Change in enthalpy of activation
HET	2-hydroxyethanethiol
HOMO	Highest Occupied Molecular Orbital
HPLC	High performance liquid chromatography
<i>I</i>	Intensity
Im	Imidazole
IR	Infrared
IUCR	International Union of Crystallography
<i>k</i>	Rate constant
k_b	Boltzmann's constant

K_{eqm}	Equilibrium constant
k_{obs}	Observed rate constant
l	Pathlength
LC-MS	Liquid Chromatography Mass Spectrometry
LUMO	Lowest Unoccupied Molecular Orbital
MeOH	Methanol
MIIm	1-methylimidazole
n_{Pt}°	Nucleophilicity of the incoming group
NMR	Nuclear magnetic resonance
Nu	Nucleophile
py	Pyridine
Pyz	Pyrazole
R	Gas constant
RMS	Root Mean Squares
RMSD	Root Mean Squares Deviation
S	Nucleophilic discrimination factor
ΔS^{\ddagger}	Change in entropy of activation
T	Transmittance
Terpy	2,2':6',2''-terpyridine
TMTU	1,1,3,3-tetramethyl-2-thiourea
Trz	1,2,4-triazole
TU	Thiourea
ΔV^{\ddagger}	Change in partial molar volume change

List of Figures

Figure:	Title:	Page:
<i>Figure 1.1</i>	Section of periodic table highlighting Platinum-group metals.	2
<i>Figure 1.2</i>	Capped stick models of (a) $[\text{Pt}(\text{C}_2\text{H}_4)\text{Cl}_3]^-$ and (b) $[\text{Pt}(\text{C}_8\text{H}_{12})\text{Cl}_2]$. The dotted bond represents the η bonding.	3
<i>Figure 1.3</i>	A capped-stick model showing the simple structure of cisplatin.	7
<i>Figure 1.4</i>	Wire-frame models of the DNA nucleic bases; (a) thymine (b) cytosine (c) adenosine and (d) guanine.	10
<i>Figure 1.5</i>	Double helix structure of DNA.	10
<i>Figure 1.6</i>	X-ray Structure of <i>cis</i> - $[\text{Pt}(\text{NH}_3)_2(\text{d}(\text{pGG}))]$.	11
<i>Figure 1.7</i>	Structures of the various adducts produced in DNA by cisplatin (a) monofunctional adduct (b) intrastrand crosslinking (c) interstrand crosslinking and (d) intermolecular crosslinking with glutathione.	12
<i>Figure 1.8</i>	Structures of (a) carboplatin (b) oxaliplatin and (c) iproplatin.	13
<i>Figure 1.9</i>	Three different binding techniques (a) groove-binding (b) intercalation (c) insertion.	14
<i>Figure 1.10</i>	Structure of antitumour agent, doxorubicin, which can intercalate between DNA base pairs.	15
<i>Figure 1.11</i>	$\text{Pt}(\text{terpy})^{2+}$ covalently bound to guanosine.	17

Figure:	Title:	Page:
Figure 1.12	Structures of the complexes investigated by van Eldik <i>et al.</i> (the CF_3SO_3^- and ClO_4^- counterions are not shown).	19
Figure 1.13	The pH-dependent tautomeric forms of histidine.	24
Figure 1.14	Structure of (a) Fe^{2+} bound to protoporphyrin IX (heme) (b) mechanism of oxygen transport and storage by hemeproteins in mammals and (c) Protein diagram of myoglobin.	25
Figure 1.15	Variety of azoles and pyridines used in research studies.	26
Figure 1.16	X-ray structure of $[\text{Pt}(\text{terpy})(1\text{-methylimidazole})](\text{ClO}_4)_2 \cdot \text{MeCN}$ showing the dihedral angle between the least-squares Pt-terpy plane and the plane of the imidazole ring.	28
Figure 1.17	The series of platinum(II) terpy complexes and selected structural analogues and nucleophiles investigated in this study.	29
Figure 2.1	Energy profile diagram showing (a) dissociative, (b) associative and (c) interchange mechanisms.	37
Figure 2.2	Diagrams to illustrate a (a) dissociatively activated and (b) associatively activated intimate mechanism.	38
Figure 2.3	Diagram showing both associative k_2 and k_1 pathways for square planar complexes.	40
Figure 2.4	Formation of trigonal bipyramidal intermediate.	43
Figure 2.5	Diagrammatic representation of the ability of a ligand (T) to labilise the group <i>trans</i> to itself (X).	47

Figure:	Title:	Page:
Figure 2.6	Induced dipoles over T-Pt-X .	48
Figure 2.7	π -backdonation from full metal <i>d</i> -orbitals to vacant orbitals of the <i>trans</i> ligand.	48
Figure 2.8	Molecular orbital diagram of $[\text{PtCl}_4]^{2-}$.	50
Figure 2.9	The Langford and Gray model for the <i>trans</i> effect.	51
Figure 2.10	Donation of electrons into the empty <i>p</i> -orbital of the metal by the <i>trans</i> and leaving groups of the square planar metal complex.	51
Figure 3.1	(a) Photograph and (b) schematic diagram of a double-beam-in-space Varian Cary 100 Bio UV-Visible spectrophotometer.	72
Figure 3.2	Photograph of the Applied Photophysics SX.18MV (v4.33) stopped-flow system used by the University of KwaZulu Natal Physical Chemistry workgroup.	74
Figure 3.3	Modified schematic diagram of mechanistic action of stopped-flow apparatus.	75
Figure 4.1	(a) Pale yellow solution of PtL1 after the addition of the silver salt, (b) orange solution of PtL1-MIm and (c) darker yellow colour of PtL1-Pyz .	89
Figure 5.1	(a) Diffraction pattern, (b) Crystal, (c) Partially labeled thermal ellipsoid plot showing 50% probability surfaces of PtL1-MIm and (d) Unit cell of PtL1-MIm viewed down the <i>b</i> -axis.	99
Figure 5.2	(a) Interplanar spacing and (b) Top view of ring overlap between two PtL1-MIm molecules.	100

Figure:	Title:	Page:
<i>Figure 5.3</i>	Different views of RMS fit between X-ray and the geometry optimized DFT structure PtL1-MIm . The red structure is the X-ray structure and the green structure is the DFT structure.	101
<i>Figure 5.4</i>	Spacefill models of (a) PtL1-MIm(CH₃NO₂)(ClO₄)₂ (b) PtL1-MIm(CH₃CN)(ClO₄)₂ and (c) PtL1-MIm(ClO₄)₂ showing the effect of the solvent molecule on stacking.	102
<i>Figure 5.5</i>	Capped-stick diagrams of (a) PtL1-MIm(CH₃NO₂)(ClO₄)₂ viewed down the <i>b</i> -axis and (b) PtL1-MIm(ClO₄)₂ to show packing arrangement.	103
<i>Figure 5.6</i>	Diffraction pattern, crystal and partially labeled thermal ellipsoid plot showing 50% probability surfaces for (a) PtL1-DIm , (b) PtL1-Pyz and (c) PtL3-Pyz .	104
<i>Figure 5.7</i>	RMS fits between X-ray and the optimized DFT structures of (a) PtL1-DIm (b) PtL1-Pyz and (c) PtL3-Pyz . The red structure is the X-ray structure and the green structure is the DFT structure.	106
<i>Figure 5.8</i>	Spacefill models with and without the solvent molecules for (a) PtL1-DIm , (b) PtL1-Pyz and (c) PtL3-Pyz .	107
<i>Figure 5.9</i>	Capped stick models to show packing of (a) PtL1-DIm , (b) PtL1-Pyz viewed along <i>b</i> -axis and (c) PtL3-Pyz viewed along the <i>a</i> -axis.	108
<i>Figure 5.10</i>	Capped stick models showing short contacts between (a) PtL1-DIm and (b) PtL1-Pyz molecules.	108

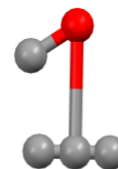
Figure:	Title:	Page:
<i>Figure 5.11</i>	(a) Diagram showing the more stable slipped ring conformation for dipole-dipole interactions compared to the less favoured direct overlap. (b) Top view of ring overlap between two PtL1-Pyz molecules showing the slipped conformation.	109
<i>Figure 5.12</i>	(a) Top view of two PtL3-Pyz molecules and (b) diagram showing the orientation of the Pt(II) terpy planes.	110
<i>Figure 5.13</i>	X-ray crystal structure of two Pt(II) terpys bridged by Pyz .	110
<i>Figure 6.1</i>	Labelled structure of PtL3 used for ^1H NMR.	116
<i>Figure 6.2</i>	Labelled structure of PtL4 used for ^1H NMR.	117
<i>Figure 6.3</i>	Labelled structure of PtL6 used for ^1H NMR.	118
<i>Figure 6.4</i>	Absorbance spectrum of PtL3 (2.43×10^{-5} M) and Im (2.43×10^{-4} M) at an ionic strength of 0.1 M (90 mM LiCF_3SO_3 and 10 mM NaCl) at 25 °C with the corresponding kinetic trace inset.	120
<i>Figure 6.5</i>	(a) Plot to determine rate constants from the slopes and y-intercepts for PtL3 and Im at varying temperatures. Eyring plot to determine ΔH^\ddagger and ΔS^\ddagger for the (b) forward reaction and (c) reverse reaction.	122
<i>Figure 6.6</i>	Graph showing a comparison of the variation of the rate of chloride substitution for the different Pt(II) terpy analogues with Im .	129
<i>Figure 6.7</i>	The electron withdrawing effect of the CF_3 group of PtL4 increases the overall π -backdonation effect onto the terpy ligand while the CH_3 group of PtL3 decreases this effect.	132

Figure:	Title:	Page:
<i>Figure 6.8</i>	The σ -donation ability of the carbon <i>cis</i> to the leaving group in PtL5 reduces the overall π -backdonation effect onto the terpy ligand.	134
<i>Figure 6.9</i>	Mesomeric shifts for Im and Pyz .	139
<i>Figure 6.10</i>	Tautomeric equilibria of (a) Im , (b) Pyz and (c) Trz .	140
<i>Figure 7.1</i>	Diagrams of (a) Ptbzimpy and (b) PtMe₂bzimpy .	154
<i>Figure 7.2</i>	Diagram of [Pt(1,3-bis(benzothiazol-2-yl)-benzene)Cl] ⁺ .	155
<i>Figure 7.3</i>	Absorbance spectrum of PtMe₂bzimpy (2.35x10 ⁻⁵ M) and TU (2.35x10 ⁻⁴ M) at an ionic strength of 0.1 M (NaCl) at 25 °C with the corresponding kinetic trace inset.	156
<i>Figure 7.4</i>	(a) Plot to determine rate constant from the slope for PtMe₂bzimpy and TU at 25 °C. (b) Eyring plot to determine ΔH^\ddagger and ΔS^\ddagger for the forward reaction.	157
<i>Figure 7.5</i>	Commercially available nitrogen- and sulfur-donor nucleophiles.	163

List of Tables

Table:	Title:	Page:
<i>Table 1.1</i>	Examples of anti-tumour agents and their mode of action.	6
<i>Table 1.2</i>	Activities of <i>cis</i> and <i>trans</i> complexes against the Sarcoma 180 tumour.	8
<i>Table 1.3</i>	Binding constants of Pt(II)terpy complexes to calf thymus DNA.	17
<i>Table 2.1</i>	Nucleophilicity scale of selected nucleophiles.	45
<i>Table 4.1</i>	Crystallographic Details for PtL1-MIm , PtL1-DIM , PtL1-Pyz and PtL3-Pyz .	95
<i>Table 5.1</i>	Bond lengths and angles for PtL1-MIm .	100
<i>Table 5.2</i>	Bond lengths and angles for PtL1-DIm , PtL1-Pyz and PtL3-Pyz .	105
<i>Table 6.1</i>	Experimentally measured reaction rates with associated errors and activation parameters for the substitution reactions of Pt(II) terpy and analogous complexes with Nu at 25 °C.	123
<i>Table 6.2</i>	Computational analysis of Pt(II) terpy analogues	127
<i>Table 6.3</i>	Summary of the HOMO and LUMO values for the Pt(II) terpy analogues from geometry optimisation studies.	128
<i>Table 6.4</i>	DFT calculated HOMOs for the Pt(II)terpy analogues.	136
<i>Table 6.5</i>	Second order rate constants, k_2 , at 25 °C for the substitution reactions involving Im , Pyz and Trz .	138

Table:	Title:	Page:
<i>Table 6.6</i>	DFT-calculated (Spartan '08) NBO charges for the azole nucleophiles without solvent present. Also shown are electron-density plots for these nucleophiles. Red represents the more electron-rich region whilst blue indicates the electron-deficient region.	141
<i>Table 6.7</i>	DFT-calculated NBO charges for the nucleophiles with and without solvent present using the computational software Gaussian 03.	142
<i>Table 6.8</i>	Rate constants for the forward reaction at 25 °C for the substitution reactions involving Im , MIm and DIm .	144
<i>Table 7.1</i>	Experimentally measured reaction rates with associated errors and activation parameters for the substitution reactions of PtMe₂bzimpy with TU and DMTU at 25 °C.	157



The discovery of the anti-tumour activity of *cis*-diaminedichloroplatinum, commonly known as cisplatin, by Barnett Rosenberg in 1969, catapulted platinum chemistry into the limelight.¹⁻⁸ This discovery has led to increased studies on anti-tumour platinum complexes which in turn has necessitated the need for mechanistic studies in order to explain the chemistry of these square planar d^8 transition metal complexes. This is confirmed by the number of publications in this field.²⁻⁸

The world today would not be the same without platinum chemistry. Every time a television or computer is switched on, when a car is driven or someone gets engaged, platinum has played a role either in the electronics, motor industry (as a catalyst) or as jewellery.⁹ These applications are important but also have far-reaching consequences as they provide jobs in these fields. Locally, platinum is significant as it forms the basis for the South African economy with South Africa producing 153 tons or 76.5% of the world total platinum production in 2008.¹⁰ Thus, the importance of platinum should not be underestimated, especially in South Africa, and studies in this area should be continued to get the most out of this very versatile metal.

1.1 Platinum(II) Chemistry

1.1.1 Chemical Properties of Platinum

Platinum forms part of the platinum-group metals, which also includes; ruthenium, rhodium, palladium, osmium and iridium, shown on the periodic table in *Figure 1.1*.¹¹ These metals are all found together in platinum-bearing ores.¹¹ The platinum metals are noble metals owing to their high sublimation energies and high ionization potentials.⁹ Platinum is usually found in the +2 and +4 oxidation states with the +1 and +3 states only being favoured by metal bonding in polymetallic species.¹¹

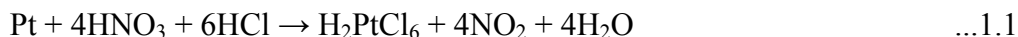
7	8	9	10	11	12	Al
Mn	Fe	Co	Ni	Cu	Zn	Ga
Tc	Ru	Rh	Pd	Ag	Cd	In
Re	Os	Ir	Pt	Au	Hg	Tl

Figure 1.1: Section of periodic table highlighting Platinum-group metals.¹¹

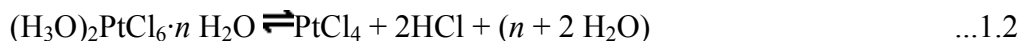
It has been shown to exhibit negative oxidation states ranging from -1 to -2 , when reacted with barium salts to form species such as: BaPt , Ba_3Pt_2 , and Ba_2Pt .¹²

In the $+2$ oxidation state, platinum has 8 d -orbital electrons and rigorously adopts a square planar geometry owing to vacant $d_{(x^2-y^2)}$ orbitals, an example being $[\text{Pt}(\text{NH}_3)_4]^{2+}$.¹¹ Characteristic reactions for these complexes are ligand substitution, reductive elimination and oxidative addition reactions.¹¹

Platinum does not oxidize at any temperature but can be attacked by halogens at room temperature and corroded by cyanides, sulfur and caustic alkalis.^{9,13} Platinum is unaffected by acids except for aqua regia in which it readily dissolves to form hexachloroplatinic acid, H_2PtCl_6 , as shown by *Equation 1.1*.¹⁴ The NO_3^- ions oxidize the metal while the Cl^- ions in aqua regia bind to the cation and stabilize it.¹¹



When hexachloroplatinic acid is heated, it decomposes to give platinum(IV) chloride and platinum(II) chloride which decomposes to elemental platinum as shown by *Equations 1.2-1.4*.¹⁵



Platinum can form various oxide compounds including platinum(IV) oxide, PtO_2 and the less common PtO , both of which decompose upon heating.¹⁶ Pt_3O_4 , can be formed in the following reaction:



One of the first organometallic compounds discovered was Zeise's salt, potassium trichloro(ethene)platinate(II), $\text{K}[\text{Pt}(\text{C}_2\text{H}_4)\text{Cl}_3]\text{H}_2\text{O}$, (*Figure 1.2 (a)*) which contains an η^2 -ethylene ligand.¹⁷ Dichloro(cycloocta-1,5-diene)platinum(II), $[\text{Pt}(\text{C}_8\text{H}_{12})\text{Cl}_2]$, (*Figure 1.2 (b)*), which contains easily displaceable 1,5-cyclooctadiene (COD) and halide ligands are convenient starting points for platinum chemistry. Platinum, being a soft Lewis acid, has a great affinity for sulfur and therefore readily forms complexes with sulfur compounds, such as DMSO.¹⁸

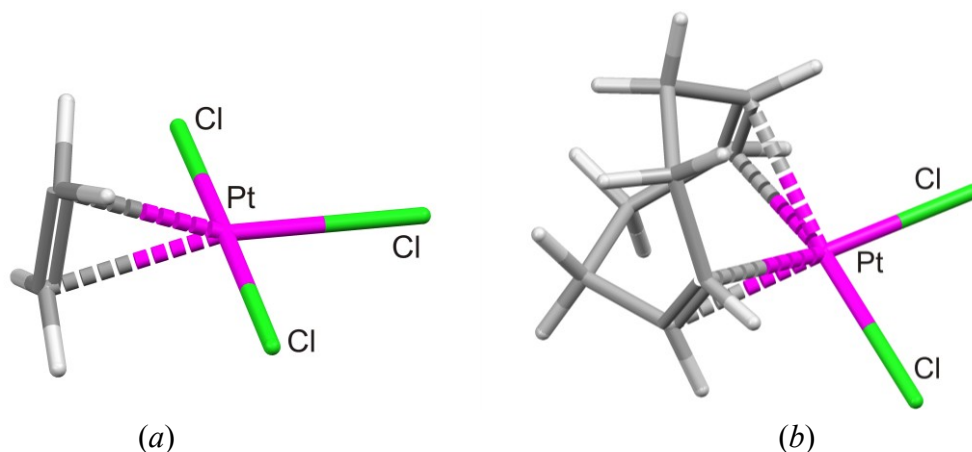
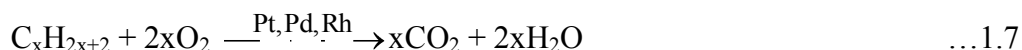
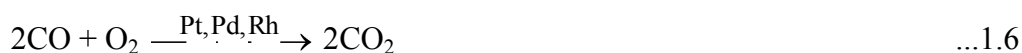


Figure 1.2: Capped stick models of (a) $[\text{Pt}(\text{C}_2\text{H}_4)\text{Cl}_3]^{-19}$ and (b) $[\text{Pt}(\text{C}_8\text{H}_{12})\text{Cl}_2]^{20}$ The dotted bond represents the η bonding.

1.1.2 Applications of Platinum

In the chemical industry, platinum is widely used as a catalyst: (i) in the oxidation of ammonia to nitric acid, (ii) for elective hydrogenation and (iii) as dehydrogenation catalysts for chemical intermediates in the plastics, synthetic fibres, rubber, pesticides and dyes.^{9,13}

Many countries around the world have awakened to the environmental problems caused by car exhaust emissions and have introduced new legislation to tackle this problem.⁹ Thus, with the automobile industry consuming 53% of platinum produced in 2007, platinum has found its single largest use as a component in autocatalysts, particularly in Japan and the US.^{9,10,13,21,22} The relatively new three-way catalysts based on platinum, palladium and rhodium do not only oxidise carbon monoxide (*Equation 1.6*), hydrogen and any unburnt hydrocarbons (*Equation 1.7*), but they also reduce the oxides of nitrogen (*Equation 1.8*).¹³



Platinum also has a large variety of applications in the electronics industry owing to its low, but temperature dependent, resistance.^{9,10,13,21,22} It can be used for temperature measurement and corrosion resistant electrical contacts for high and low voltage applications such as electrodes in fuel cells.^{9,13,21} Platinum also has applications both as a sensor for gas detection and as optical data storage disks and hybridised integrated circuits.^{9,11,13,21} Platinum metal is also used by the glass manufacturing sector in the vessels that channel molten glass in the production of fibre-glass, liquid crystal displays and flat-panel displays.^{13,21}

In recent times about 38% of the world's platinum has been used in jewellery manufacture.²² The use of platinum in jewellery is dominated by the Japanese who account for about 80% of all platinum jewellery.^{9,10,13,21,22} Pure platinum is too soft to work with so to increase its hardness and resistance to wear, it is alloyed with iridium or ruthenium.¹³ These jewellery alloys are easily workable and readily cast and melt.¹³

Platinum is also used in the medical field as another important application of platinum lies in anti-cancer drugs based on cisplatin (*cis*[Pt(NH₃)₂Cl₂]) and its derivatives.^{1,9,13} The compounds are particularly effective against testicular cancer as well as ovarian, head, neck, bladder, lung, prostate and cervical tumours.^{1,9,13} Although this is an important application of platinum, it is only responsible for a minor percentage of the total platinum consumption.⁹ The next section focuses in more detail on the role of platinum(II) in the medical field and more particularly in the design of anti-cancer drugs.

1.2 Cancer Chemotherapy Involving Platinum Complexes

1.2.1 Introduction to Cancer

When groups of cells divide more frequently or do not sustain as many losses as normal cells but do not invade surrounding tissues, they form benign tumours.²³ If the abnormal cells do spread to neighbouring tissues or distant regions of the body, they are called malignant tumours or cancers.²³ Cancer can thus be described as a disease in which one or more cells display uncontrolled growth leading to a solid mass known as a tumour.²⁴ The growth of a cancer must be viewed as the division of a single group of abnormal cells and not like an epidemic spreading among normal cells.²³

The initial cancer tumour that develops (primary tumour) can become life-threatening if it obstructs vessels or organs.^{23,24} However, the spread of the primary tumour to one or more regions in the body and establishing secondary tumours, known as metastasis, is the most common cause of death.^{23,24} Metastasis can occur when tumour cells directly invade blood vessels through thin-walled capillaries or penetrate walls of lymphatic vessels and move to draining lymph nodes.^{23,24} A tumour can also spread across body cavities via organs. It is this ability of cancer to spread to a number of far-reaching sites in the body that makes cancer such a dangerous disease as it is beyond the reach of local surgery.^{23,24}

Cancer accounts for 13% of deaths worldwide.²⁵ The main types of cancer leading to overall cancer mortality in the world are lung cancer with about 1.3 million deaths a year, stomach cancer with 803 000 deaths, colorectal cancer with 639 000 deaths, liver cancer with 610 000 deaths and breast cancer with 519 000 deaths per year.²⁵ Among men there are more deaths from lung, stomach, liver, colorectal, oesophageal and prostate cancers while woman die from breast, lung, stomach, colorectal and cervical cancers.²⁵

There are three ways in which cancer can be treated, namely: surgery, radiotherapy and chemotherapy.⁹ Surgery can be ineffectual against certain cancers and very traumatic for a patient.⁹ Chemo- and radiotherapy, are more effective against

leukemias, small tumours and metastases although treatment is accompanied by side effects such as anaemia, hair loss, nausea and vomiting.⁹

1.2.2 The Anti-Tumour Activity of Platinum Complexes

There are several anti-cancer drugs currently on the market, as shown in *Table 1.1*.⁹ All the groups, except one, contain organic compounds and require organic functionalities for their activity whereas the last group is based on the heavy metal, platinum, which is essential for anti-cancer activity.^{9,23,24}

Table 1.1: Examples of anti-tumour agents and their mode of action.⁹

Drug type	Examples	Mode of action
Antimetabolites	(a) Antifolates e.g. methotrexate	Inhibit synthesis of purines
	(b) Antipurine e.g. 6-mercaptopurine	Inhibit synthesis of purines
	(c) Antipyrimidines	Inhibit synthesis of pyrimidines
Alkylating Agents	(a) Bifunctional e.g. mustard gas	Inhibit DNA synthesis
	(b) Metabolised agents e.g. cyclophosphamide	Same as above
Natural Products	(a) Antibiotics e.g. Actinomycin D	Often inhibit m-RNA formation
	(b) Alkaloids e.g. Vincristine	May affect mitosis by reaction with –SH groups
Steroids and Hormones	Oestrogens, progesterone	Cancer cells are still subject to some degree of hormone control
Platinum Complexes	Cisplatin, paraplalin, iproplatin	Inhibit DNA synthesis, mainly by intrastrand crosslinking

Cisplatin, *cis*-diaminedichloroplatinum(II), as seen in *Figure 1.3*, is the original compound in the last group and is widely used for the treatment of testicular and ovarian cancers as well as head and neck tumours.^{1,2,9,23,24} Before the discovery of cisplatin, testicular cancer patients suffered a high mortality rate. However, today the prognosis for this treatment of testicular cancer is very good.^{1,2,9,24} The drug does have many unpleasant side-effects including nephrotoxicity, nausea and vomiting.^{1,2,9,24} Certain tumours have also developed a resistance to cisplatin.^{24,28} In the hope of developing a more potent, less toxic and resistant platinum analogue, much research has gone into determining the mechanism of action of cisplatin and its structure-activity relationships.^{1,2,9,24}

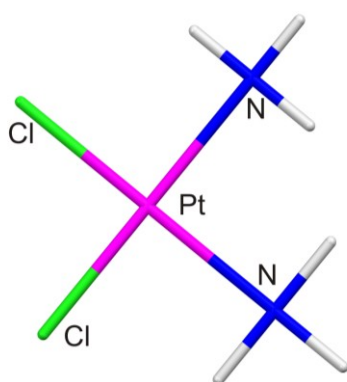


Figure 1.3: A capped-stick model showing the simple structure of cisplatin.

1.2.3 Structure-Activity Relationships of Platinum Complexes

Since the discovery of the anti-cancer properties of cisplatin, much research has gone into developing analogues of cisplatin with reduced toxicity and resistance.⁹ This involves the investigation of structure-activity relationships, including studies on *cis-trans* isomers and examining the effects of the labile and non-labile groups.²⁶

From very early on it was discovered that compounds with *cis* chlorides were more active than the *trans* isomers.^{9,26-28} Two factors have been suggested for the differing anti-cancer activities of the *cis* and *trans* isomers of platinum complexes. The *trans* chloro species react more rapidly than the *cis* isomers, reducing their selectivity and as a result this leads to undesired reactions.^{9,26-28} Cisplatin's main cytotoxic effect is through forming a 1,2-intrastrand cross-link between adjacent purines which is

stereochemically impossible for *trans* isomers.^{9,26-28} Table 1.2 shows the activities of *cis* and *trans* isomers of various complexes.⁹ There are several *trans* complexes which have shown anti-cancer activity.²⁶⁻²⁸ Examples of *trans* complexes which display cytotoxicity are of the general form [PtCl₂LL'] where L = L' = pyridine or thiazole or L = quinoline and L' = substituted sulfoxide.²⁶ Substituting the amine ligands with more bulky ligands has led to compounds with higher tumour growth inhibitory potential.²⁶ These bulky groups reduce the kinetic instability as they slow down the substitution reaction of the leaving groups. These anti-tumour transplatin complexes form different adducts to cisplatin indicating that cisplatin DNA adducts are not the only mechanism of inhibiting cancer growth.²⁶

Table 1.2: Activities of *cis* and *trans* complexes against the Sarcoma 180 tumour.^{29,30}

Complex	Dose range (mg/kg)	Toxic level* (mg/kg)	T/C**	Dose*** (mg/kg)
<i>cis</i> -[Pt(NH ₃) ₂ Cl ₂]	0.5-20	9	1	8
<i>trans</i> -[Pt(NH ₃) ₂ Cl ₂]	2.5-40	>40	85	2.5-40
<i>cis</i> -[Pt(CH ₃ NH ₂) ₂ Cl ₂]	10-30	12-20	25	15
<i>trans</i> -[Pt(CH ₃ NH ₂) ₂ Cl ₂]	5-100	25	100	5-20
<i>cis</i> -[Pt(EtNH ₂) ₂ Cl ₂]	5-50	45	14	40
<i>trans</i> -[Pt(EtNH ₂) ₂ Cl ₂]	5-20	20	105	5-20

*Toxic level – is the highest dose at which survivors are $\geq 83\%$

**Dose – refers to the amount of substance used in mg per kg of animal

***T/C – Wt of treated tumour/ Wt of control tumour x 100

On investigating the structure-activity relationships, studies were done on the labile groups. In cisplatin the labile groups are the chloride ligands, with the platinum amine linkage being stable to nucleophilic attack.^{9,29-31} Studies were carried out on a range of complexes of the type *cis*-[Pt(amine)₂X₂] where amine = NH₃, CH₃NH₂ or C₂H₅NH₂ and X = NO₃⁻, H₂O⁻, Cl⁻, Br⁻, I⁻, SCN⁻ or NO₂⁻.^{9,29-31} When X was a ligand such as water, which is very labile, the complexes showed little activity.²⁹⁻³¹ When X was a strongly bonded ligand such as I⁻, SCN⁻ and NO₂⁻, the complexes showed no anti-cancer activity while ligands similar to Cl⁻, which are of intermediate lability, had anti-cancer potential.²⁹⁻³¹

The non-labile ligands, specifically the amines, are ubiquitous to compounds with anti-tumour activity.^{9,26,27} Complexes containing different amine groups, *cis*-[Pt(amine)₂Cl₂] (where amine = NH₃, CH₃NH₂, n-C₂H₅NH₂, n-C₃H₇NH₂, (CH₃)₂NH₂ etc.), have been tested and show that complexes containing primary amines are still active, however, not as active as cisplatin whereas secondary amines show little activity.⁹ The properties of amines that appear to be important for anti-cancer activity include, water and lipid solubility and hydrogen bonding ability.⁹

1.2.4 Mechanisms of Action of Platinum Anti-Cancer Agents

Since the discovery of the structure of DNA, scientists have been interested in molecules that recognise and react at specific DNA sites.³² DNA is a nucleic acid macromolecule that contains the genetic instructions that allow living organisms to develop and function.³³ Molecules that can bind and interact with the DNA provide access to the genetic material, which allows the molecules to be used as diagnostic probes, reactive agents and therapeutics.³²

In order to understand how complexes bind to DNA, a basic understanding of the DNA molecule is required. DNA is a long polymer of simple units called nucleotides.³⁴ Each nucleotide is composed of a phosphate group, a five-carbon sugar (2-deoxyribose sugar) and a cyclic nitrogen-containing compound called a base.³³ The sugar and phosphate group atoms join by phosphodiester bonds to form the backbone of DNA. The bases are then attached to the sugar phosphate backbone to form the complete nucleotide.

The four different bases commonly found in DNA are adenine, guanine, thymine and cytosine, shown in *Figure 1.4*. Adenine and guanine are double-ring bases called purines, while cytosine and thymine are single aromatic bases called pyrimidines.³³

Green = carbon of the sugar group

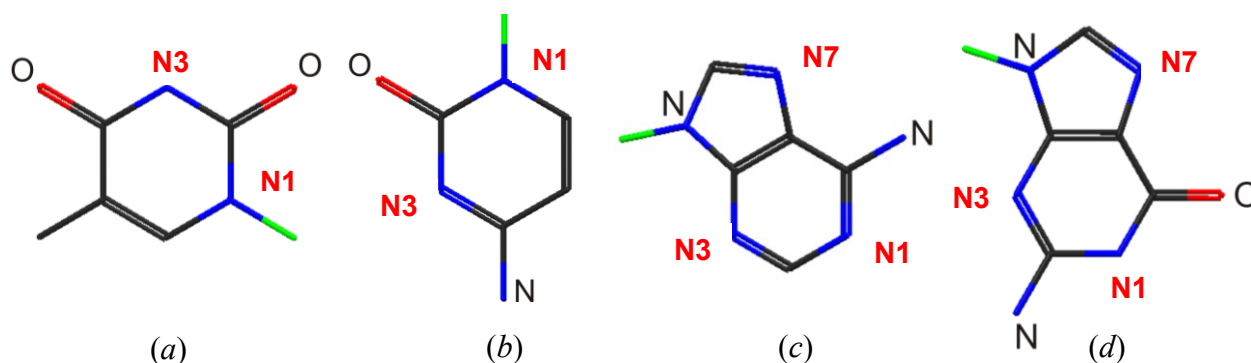


Figure 1.4: Wire-frame models of the DNA nucleic bases; (a) thymine (b) cytosine (c) adenosine and (d) guanine.

DNA is a double-stranded macromolecule. The two strands of DNA intertwine to form a double helix.³⁴ Thus, each nucleotide contains a backbone which holds the chain together and a base which interacts with the other DNA strand in the helix. The base pairs form a central hydrogen-bonded π stack.³² Each base forms hydrogen bonds with its complementary base on the opposite anti-parallel side, adenine with thymine and cytosine with guanine. The sugar phosphate backbone forms two grooves, a wide major groove and a narrow minor groove as shown in Figure 1.5.³²

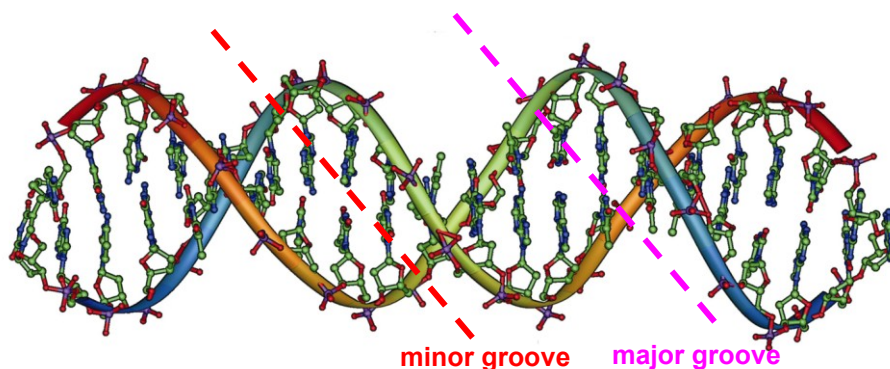


Figure 1.5: Double helix structure of DNA, adapted from reference 35.

DNA is the major target of platinum(II) anti-cancer drugs.^{1,2,9} These platinum(II) drugs predominantly react with purine and pyrimidine bases, with binding being dependent on pH.^{1,2,9} At neutral pH, the platinum prefers the binding sites; N(7) atoms of guanine and adenine, N(3) of cytosine and N(1) of adenine.^{1,2,9} The guanine N(7) has been shown to be the most likely coordination site for cisplatin.^{1,2,9} Hydrogen bonding between the O(6) group of guanine and the N–H of cisplatin

seems to stabilise binding to the guanine N(7) site.^{1,2,9} The guanine N(7) position is preferred over the adenine N(7) position as it is about 2.3 log units more basic than the corresponding adenine position.² It is not likely for binding to take place at the adenine N(1) and the cytosine N(3) sites as they are involved in DNA base pairing and less available for metal binding.^{1,2,9}

Cisplatin, when it binds to DNA causes the unwinding of the superhelix and shortening of the double helix.⁹ Cisplatin does this by forming various bifunctional adducts including intrastrand, interstrand and intermolecular crosslinks.^{1,9} The bifunctional intrastrand crosslinking involves the binding of the platinum(II) complex to two bases within the same strand of DNA and this type of lesion is the major type of adduct found.^{2,20,28} Intrastrand crosslinks between two neighbouring deoxyguanosines (GG) make up 65% of all DNA adducts.^{1,9} *Figure 1.6* shows an X-ray structure of cisplatin forming an intrastrand crosslink between two deoxyguanosine bases. About 20% of DNA adducts are formed by intrastrand crosslinks at an AG sequence; however, no adducts are formed at a GA sequence.¹ Crosslinks between two deoxyguanosines separated by a third nucleoside (GNG) makes up another 9% of all the DNA adducts formed.¹ *Figure 1.7 (a) and (b)* illustrates monofunctional and intrastrand crosslinks respectively.

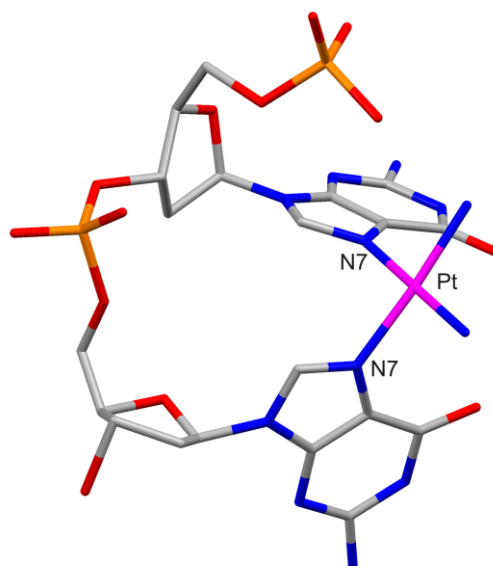


Figure 1.6: X-ray Structure of *cis*-[Pt(NH₃)₂(d(pGG))].³⁶

Bifunctional DNA interstrand cross-links (shown in *Figure 1.7 (c)*), involve the binding of platinum(II) complexes to bases on complementary strands. DNA

interstrand crosslinks have been found between two deoxyguanosines bases; however, these interstrand cross-links only account for less than 1% of the total platinum (II) adducts.^{1,2,9} This low level of occurrence is due to the fact that interstrand crosslinking causes a major contortion of the DNA structure and may only occur when an alternate purine is not in close proximity on the same strand.^{1,9}

Another type of adduct forms a crosslink between deoxyguanosine and glutathione (*Figure 1.7 (d)*).¹ At cellular concentrations of 1-5 mM, glutathione can reduce the amount of platinum bound to DNA as well as prevent the formation of cross-links after the DNA has been platinated.¹

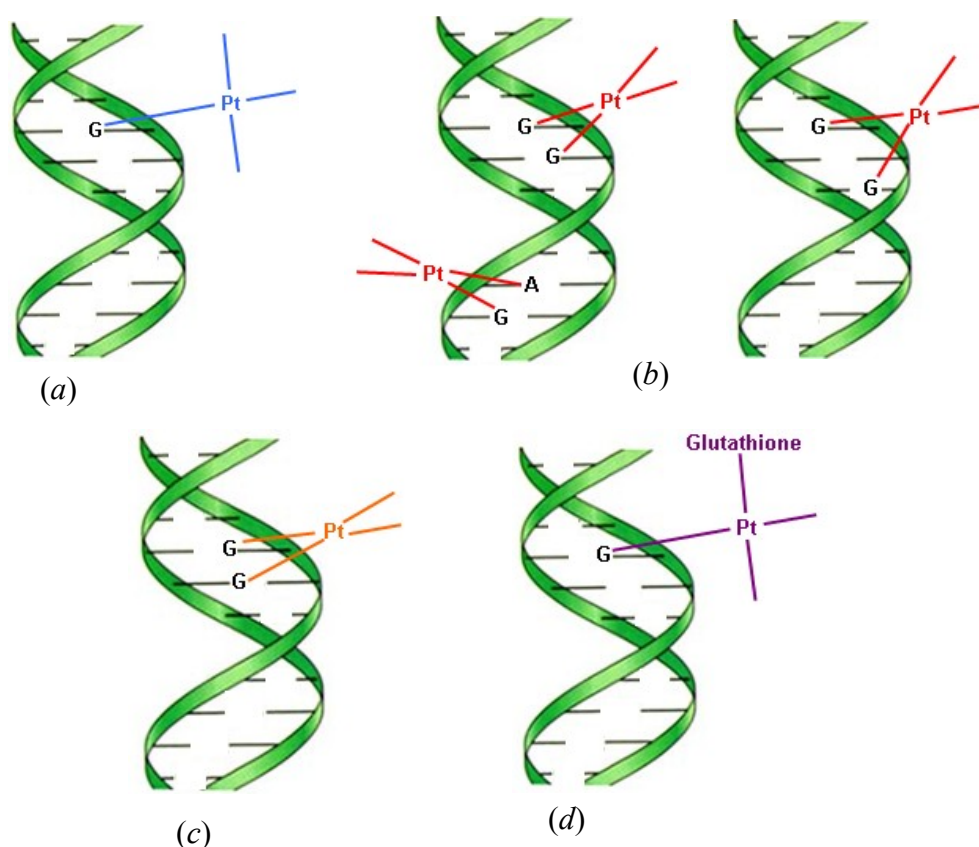


Figure 1.7: Structures of the various adducts produced in DNA by cisplatin (a) monofunctional adduct (b) intrastrand crosslinking (c) interstrand crosslinking and (d) intermolecular crosslinking with glutathione.¹

Although all of the structures of the DNA adducts are well studied, it is still unknown which are the most important adducts with respect to cytotoxicity.^{1,9} Research has; however, shown that the adducts inhibit DNA replication or transcription but the exact mechanism of toxicity still needs to be determined.^{1,9}

1.2.5 Development of New Platinum Anti-Cancer Complexes

In the last few decades many cisplatin analogues have been synthesised and screened against human cancer cell lines in an attempt to find compounds with the same or greater anti-tumour activity as cisplatin but with fewer associated side effects.^{2,9,26,37} When designing new platinum(II) anti-cancer drugs the following points should be considered:³⁷

- Although complexes which hydrolyse quickly can bind efficiently to biomolecules, these reactive platinum complexes can cause severe toxicity due to reactions with proteins.
- Stable, water soluble platinum complexes are less toxic but their tumour inhibiting properties are also reduced.
- Stable, lipophilic platinum complexes are moved quickly from the blood into the tissues and hence some of the typical side effects of chemotherapy are reduced.
- Varying the leaving groups alters the toxic side effects.
- Changing the non-leaving amine ligands will produce structurally different adducts with DNA, thereby changing the anti-cancer properties.³⁷

Research has led to the synthesis and production of a second set of compounds such as carboplatin, oxaliplatin and iproplatin whose structures are shown in *Figure 1.8*.^{2,9,24,26} Carboplatin is used to treat ovarian tumours and small lung carcinomas but with fewer side effects than cisplatin. Carboplatin is a myelosuppressive, causing reduced platelet levels in most patients.^{9,24} Oxaliplatin is used in the treatment of colorectal cancer, while Iproplatin is effective against ovarian cancer and small cell lung carcinoma.^{9,24}

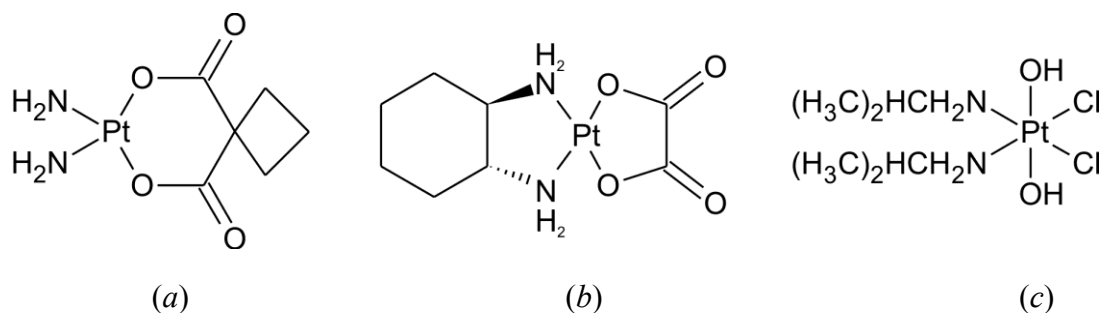


Figure 1.8: Structures of (a) carboplatin (b) oxaliplatin and (c) iproplatin.

There are three different ways in which molecules can bind to DNA, other than forming adducts, namely: groove binding, intercalation and insertion (*Figure 1.9*).³² Groove binding is where molecules bind into the minor groove of the DNA by hydrophobic interactions or by partial intercalation.³² Intercalators are molecules that partly unwind DNA and π -stack between two base pairs. Once in position, they are held in place by hydrogen bonding and van der Waals forces.³² Intercalators insert in the major groove of the double helix with the intercalating ligand acting as a new base.³² As no bases are removed the major groove widens. DNA insertion involves separation and displacement of a base-pair.³²

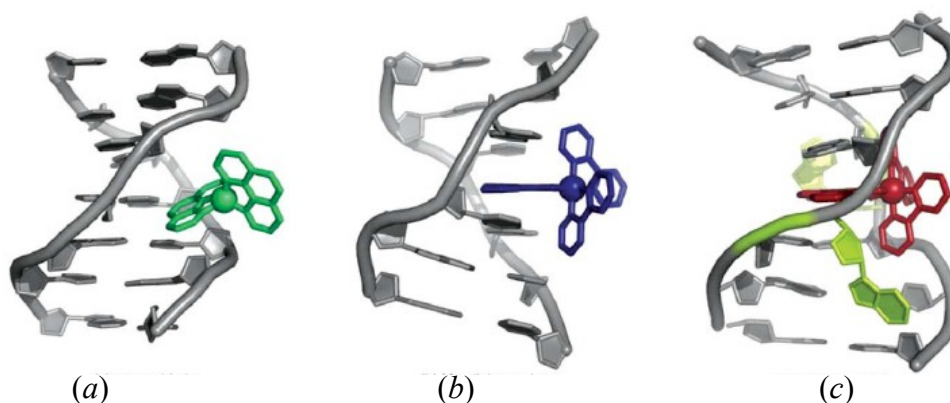


Figure 1.9: Three different binding techniques (a) groove-binding (b) intercalation (c) insertion.³²

In recent times, there has been a drive to produce drugs which are intercalators rather than drugs that bind to DNA directly. DNA intercalators usually have a few key features; they have an electrostatic attraction to the negatively charged phosphate groups of DNA and are planar in geometry, usually consisting of three or four fused aromatic rings. This gives them the ability to π -stack with the aromatic DNA.²⁴ Many intercalators also have side chains which have the ability to form hydrogen bonds with the DNA helix. DNA intercalators cause distortions in DNA and can inhibit DNA replication, by affecting DNA topoisomerase enzymes, which are important for forming the supercoils in DNA, and therefore are effective in the treatment of cancer.³³ Examples of DNA intercalators include the compounds such as Doxorubicin (*Figure 1.10*), Daunorubicin and Adriamycin which belong to a group of anti-tumour agents called the anthracyclines.^{24,38} These compounds consist of a planar anthraquinone centre attached to an amino-containing sugar.^{24,38}

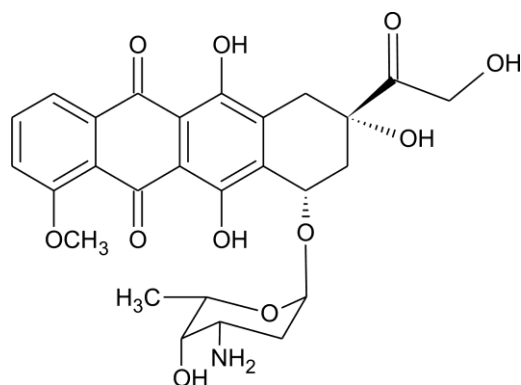


Figure 1.10: Structure of anti-tumour agent, doxorubicin, which can intercalate between DNA base pairs.

It is unusual to focus on transition metal DNA binding agents as traditionally organic molecules have been used as DNA intercalators. Even in nature, there is only one example of a group of transition metal complexes recognising and binding to DNA: the metallobleomycins.³² The bleomycins have a metal-binding region that can coordinate to a variety of metals including Zn(II), Cu(II) and Co(II) with the Fe(II) bleomycin complex being well studied.³² When the Fe-bleomycin complex is exposed to oxygen and a reducing agent, it becomes activated and can induce both single and double-stranded DNA cleavage.³² Another key feature is their positively charged tail, which allows them to bind through an electrostatic interaction to the negatively charged backbone of the DNA. Due to their ability to recognise and bind to specific sites in the DNA, bleomycins have been used successfully in the treatment of certain types of cancer.³²

Although there are few natural examples of transition metal-binding agents, there are definite advantages of using transition metals to intercalate DNA. Firstly, ligands can be bound to the metal centre, keeping a rigid structure;³² by substituting the ligands, the recognition properties of the complex may be changed. Another advantage is that the transition metal centres have photophysical and electrochemical properties that allow the metal complexes to have a wide range of applications from fluorescent markers to electrochemical probes.³² These obvious advantages of transition metal-binding agents have led to ever increasing interest in this field of research.

1.3 Platinum(II) Terpyridine Complexes

1.3.1 The Role of Platinum(II) Terpyridine Complexes in Modern Chemistry

Although the first report of the synthesis of Pt(II) terpy (where terpy = 2,2':6',2''-terpyridine) complexes was made in 1934, it took another 25 years for researchers to realise the full potential of these complexes.³⁹

One of the major areas of research of focus with these Pt(II) terpy complexes has been the bioinorganic field as these molecules have been shown to have interactions with biomolecules such as DNA and proteins.^{39,40} There are two explanations for the affinity of $[\text{Pt}(\text{YterpyX})]^+$ complexes (where X represents ligands at the fourth coordination site and Y represents substituents on the terpy chelate) for molecules such as DNA:³⁹

- Ability to stack with other π - systems
- The removal of the X ligand by nucleophiles

In 1974, Lippard and co-workers⁴¹ provided the first evidence that Pt(II) terpy complexes could bind to DNA when they studied the interactions of the complex $[\text{Pt}(\text{terpy})(\text{HET})]^+$ (HET=2-hydroxyethanethiol) with calf thymus DNA.⁴⁰ They proved that the complex intercalated between the base pairs by showing that the interaction resulted in competitive inhibition of ethidium fluorescence.⁴¹ Interestingly, McFayden *et al.*⁴² showed that the platinum in these complexes plays a role in the binding to DNA as the free terpy ligands do not intercalate at physiological pH.⁴⁰

Lippard and co-workers⁴³ investigated intercalative ability of a variety of Pt(II) terpy complex cations of the type $[\text{Pt}(\text{terpy})\text{X}]^{n+}$ where $n = 1$ and $\text{X} = \text{Cl}$, HET, cysteine or carboethoxymethanethiol (CMT) or where $n = 2$ and $\text{X} = 2\text{-aminoethanethiol (AET)}$.⁴⁰ Each of these complexes was shown to intercalate to the DNA by their ability to unwind closed circular DNA and inhibit ethidium bromide binding. They studied how strongly these complexes bound to DNA and it was discovered that the AET complex

has the highest binding constant. This is believed to be due to its dicationic charge which allows it to interact more strongly with the negatively charged DNA phosphate backbone.⁴⁰ Table 1.3 shows the binding constants for the Pt(II) terpy complexes.

Table 1.3: Binding constants of Pt(II)terpy complexes to calf thymus DNA.⁴⁰

Complex:	DNA; medium	K (M ⁻¹)	Reference
[Pt(terpy)Cl] ⁺	Ct-DNA; Tris buffer	3.9 x 10 ⁵	44
[Pt(terpy)(HET)] ⁺	Ct-DNA; pH 7.5 0.2 M NaCl	1.2 x 10 ⁵	43
[Pt(terpy)(AET)] ²⁺	Ct-DNA; pH 7.5 0.2 M NaCl	4.3 x 10 ⁵	43
[Pt(terpy)Cys] ⁺	Ct-DNA; pH 7.5 0.2 M NaCl	1.0 x 10 ⁵	43
[Pt(terpy)CMT] ⁺	Ct-DNA; pH 7.5 0.2 M NaCl	5 x 10 ⁴	43

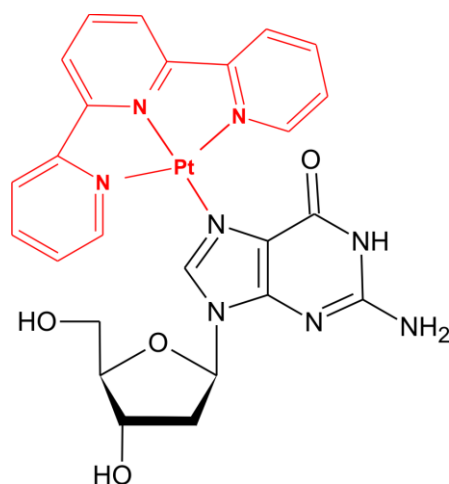


Figure 1.11: Pt(terpy)²⁺ covalently bound to guanosine.⁴⁰

This study showed that the binding affinity of Pt(II) terpy complexes seems to depend on several structural features including:⁴⁰ size and steric effect of the complex, hydrogen bonding and the charge of the complex.

[Pt(Yterpy)X]ⁿ⁺ complexes also have a labile X ligand which can undergo substitutions to bind covalently to nucleobases. Figure 1.11 illustrates this covalent interaction. Complexes where X = Cl⁻, H₂O, OH⁻ and pyridine derivatives have been proven to react with nucleobases.⁴⁰ Lowe and co-workers⁴⁵

characterised the first Pt(II) terpy nucleobase complexes by NMR spectroscopy when they studied the reaction of [Pt(terpy)Cl]⁺ and [Pt(terpy)(4-picoline)]²⁺ with nucleosides.⁴⁵

Pt(II) terpy are important molecules in the study of biomolecules as they often bind selectively to DNA and proteins. The attractiveness of using Pt(II) terpys in biological studies is due to the useful properties of Pt(II) terpy probes. These properties include: the spin-active ^{195}Pt nucleus for NMR spectroscopy, the large Pt nucleus leading to high-scattering for X-ray diffraction studies, and long wavelength light absorption and emission for studying binding modes.³⁹

Pt(II) terpy systems have not only been important from a biomedical view point but have been pivotal to the understanding of ligand substitution in square-planar d^8 metal complexes.³⁹ These studies include how electronic and steric factors within the metal complex affect the reactivity. The redox and photophysical properties of platinum terpy complexes have also been investigated to give a better understanding of how to create reagents with selective electron transfer and luminescent properties.³⁹

1.3.2 Previous Platinum(II) Terpyridine Investigations

Previous mechanistic studies on Pt(II) terpy complexes have been done in order to explain the substitution mechanism and behaviour of square planar d^8 transition metal complexes.⁴⁶⁻⁵² The basic terpy structure has been varied by the addition of substituents onto the chelate or by adjusting the chelate itself to investigate the different effects that sterics and electronics play on the reaction kinetics.

Van Eldik *et al.*^{46,47} have shown the importance of the three joined pyridine rings in a planar configuration to the reaction kinetics of Pt(II) terpy. Van Eldik *et al.*^{46,47} have investigated the effect of adding π -acceptor pyridine rings to the chelating ligand when they studied the aqua substitution from $[\text{Pt}(\text{diethylenetriamine})\text{OH}_2]^{2+}$ (**aaa**), $[\text{Pt}(2,6\text{-bis-aminomethylpyridine})\text{OH}_2]^{2+}$ (**apa**), $[\text{Pt}(\text{N-(pyridyl-2-methyl)-1,2-diamino-ethane})\text{OH}_2]^{2+}$ (**aap**), $[\text{Pt}(\text{bis(2-pyridylmethyl)amine})\text{OH}_2]^{2+}$ (**pap**), $[\text{Pt}(2,2'\text{-bipyridine})\text{-(NH}_3\text{)(OH}_2\text{)}]^{2+}$ (**app**), and $[\text{Pt}(\text{terpy})\text{OH}_2]^{2+}$ (**ppp**) by TU, DMTU and TMTU. The complexes are shown in *Figure 1.12*. For the reaction with TU, the rate of substitution increases by a factor of 4 by just the addition of a single pyridine ring in going from **aaa** to **aap**, there is a further increase in the reaction rate again by a factor of 4 on the addition of a second pyridine ring (**pap**). On going from **aaa** to **ppp** the rate of the substitution reaction increases by 4 orders of magnitude with a general

reactivity series of **aaa** < **apa** < **aap** < **pap** < **app** < **ppp**.^{46,47} The authors explained that the reactivity of the complexes is mainly due to the electrophilicity of the metal centre which is due to the electron back-donation to the ligand orbitals. The drastic increase in reactivity is that electronic communication between the π -acceptor ligands increases on going from **aaa** to **ppp**. They also showed that π -acceptor on its own (i.e. in the *cis* or *trans* position) has only a minor impact on the rate of the substitution reaction because of the lack of direct electronic communication. Breaking this electronic communication between π -acceptor groups has recently been shown to slow the substitution reaction rate by a factor of 60.⁴⁸

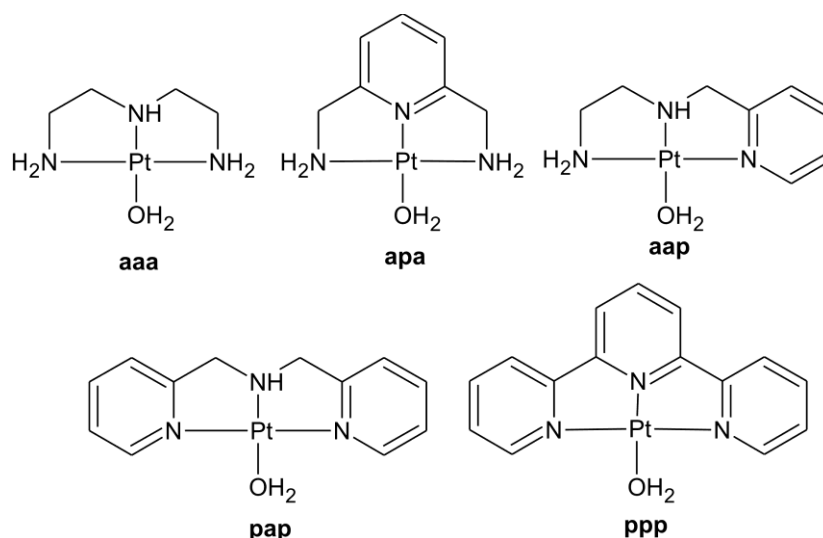


Figure 1.12: Structures of the complexes investigated by van Eldik *et al.*^{46,47} (the CF_3SO_3^- and ClO_4^- counterions are not shown).

Thus, studies by van Eldik *et al.*^{46,47} have shown that by adding π -acceptor pyridine rings to the chelating ligand, the reactivity of the metal centre is increased due to increased π -backdonation and increased electronic communication between the π -accepting ligands.

Jaganyi *et al.*⁴⁹ have extended the study on factors effecting the π -backdonation effect of Pt(II) terpy complexes by adding a 4' substituent on the chelate. Jaganyi *et al.*⁴⁹ studied the substitution kinetics of the complexes $[\text{Pt}\{4'-(2'''\text{-CH}_3\text{-Ph})\text{-terpy}\}\text{Cl}]^+$ (**CH₃PhPtCl**), $[\text{Pt}\{4'\text{-Ph}\}\text{-terpy}\}\text{Cl}]^+$ (**PhPtCl**), $[\text{Pt}(\text{terpy})\text{Cl}]^+$ (**PtCl**), $[\text{Pt}\{4'-(2'''\text{-Cl-Ph})\text{-terpy}\}\text{Cl}]^+$ (**ClPhPtCl**) and $[\text{Pt}\{4'-(2'''\text{-CF}_3\text{-Ph})\text{-terpy}\}\text{Cl}]^+$ (**CF₃PhPtCl**) with the nucleophiles TU, DMTU and TMTU. The

reactivity trend with TU was found to be **CF₃PhPtCl** > **ClPhPtCl** > **PtCl** > **PhPtCl** > **CH₃PhPtCl** with **PtCl** reacting 1.2x faster than **PhPtCl**. It has been argued that an extended π -interaction exists between the terpy moiety and the phenyl group. Jaganyi *et al.*⁴⁹ showed that due to a relatively large dihedral angle between the plane of the central pyridine ligand and phenyl ligand (37, 33, 49 and 65° for the calculated structure of **PhPtCl**, X-ray structure of [**PhPtCl**]BF₄·CH₃CN, calculated structure of **CH₃PhPtCl** and X-ray structure of [**CH₃PhPtCl**]SbF₄ respectively), any extension of π -interaction between the terpy moiety and the phenyl group is reduced. The difference in reactivity between **PtCl** and **PhPtCl** was thus ascribed to the phenyl group acting as a σ -donor group, pushing electron density towards the metal centre. This reduces the π -backdonation effect of the terpy moiety, making the metal centre less electropositive, repelling incoming nucleophiles.

Jaganyi *et al.*⁴⁹ also found that the effectiveness of the σ -donor phenyl group in the 4' position was controlled by the *ortho* substituent on this phenyl ring. They found that **CF₃PhPtCl** and **ClPhPtCl** reacted 1.6 and 1.4x, respectively, faster than the least reactive compound, **CH₃PhPtCl**.⁴⁹ The electron-withdrawing groups, CF₃ and chloro, withdraw electrons from the phenyl ring which reduces the σ -donation ability of the phenyl ring. This increases the π -acceptor effect of the terpy moiety, resulting in a more electropositive metal centre and hence more reactive complex. This effect causes the reactivity of the complexes to increase with an increase in the strength of the electron-withdrawing ability. Electron-donating groups, on the other hand, enhance the σ -donation ability of the phenyl ring, which reduces the π -acceptor effect of the terpy moiety resulting in a less electropositive metal centre.

The authors⁴⁹ supported these experimental results with computational calculations. These calculations showed that the complex with the strongest electron-withdrawing group, **CF₃PhPtCl**, had most of the electron density from the HOMO over the 2'''-CF₃-phenyl ligand rather than the metal centre. This indicates a more electropositive metal centre. The **CH₃PhPtCl** complex has no electron density situated over the 2'''-CH₃-phenyl ligand, illustrating the electron-donation effect. Electron-donating groups are also known to increase the HOMO-LUMO energy gap, resulting in slower reactions.⁴⁹

Variation of the Pt(II) terpy structure can be further achieved by the addition of substituents to the 4, 4', 4'' positions of the terpy backbone. Jaganyi *et al.*⁵⁰ have studied the substitution kinetics of $[\text{Pt}(\text{terpy})\text{Cl}]^+$ and $[\text{Pt}(\text{}^t\text{Bu}_3\text{terpy})\text{Cl}]^+$ with the nucleophiles; TU, DMTU, TMTU, iodide and thiocyanate, showing that the extent of π -backbonding can be controlled by the introduction of an electron-donating group at the 4, 4' and 4'' positions of the terpyridyl backbone.⁵⁰ Their results showed that the reaction rate decreases by a factor of 3.3 with TU on addition of ${}^t\text{Bu}$ groups to the 4, 4', 4'' positions of the chelate on going from $[\text{Pt}(\text{terpy})\text{Cl}]^+$ to $[\text{Pt}(\text{}^t\text{Bu}_3\text{terpy})\text{Cl}]^+$. They attributed this decrease in the rate of the substitution to the electron-donating groups in $[\text{Pt}(\text{}^t\text{Bu}_3\text{terpy})\text{Cl}]^+$ which leads to the reduction of π -acceptor effect of the terpy ligand, resulting in a less electrophilic complex.

Jaganyi *et al.*⁵⁰ also conducted computational calculations using complexes containing either electron-donating or electron-withdrawing groups in 4, 4', 4'' positions. These calculations showed that the introduction of electron-donating groups has the effect of decreasing the positive charge on the metal centre, as well as increasing the HOMO-LUMO gap of the ground state, making the complex less reactive. Introducing electron-withdrawing groups increases the positive charge on the metal centre and decreases the HOMO-LUMO gap of the ground state, enhancing the reactivity of the complex. The authors concluded that by placing these substituents in both the *cis* and *trans* positions that⁵⁰:

- the overall *trans*-influence is greater than the overall *trans*-effect and
- the overall π *cis*-effect is greater than the overall π *trans*-effect.

Various groups have also attempted to understand the *cis* and *trans* effects by varying these groups in Pt(II) terpy complexes.^{51,52,53} Kinetic studies involving a Pt–C bond (as opposed to the Pt–N bond) are of considerable interest with most of the studied complexes having a single Pt–C bond that is located *trans* to the leaving group. These studies generally focus on the ability of the metal-carbon bond to labilise square-planar d^8 metal complexes through the kinetic *trans* effect.^{4,54,55} The reports show that these complexes had a six fold increase in substitution reactivity. This is due to the σ -

bound carbon ligands such as alkyl and aryl groups having a large kinetic *trans* effect.⁵⁶⁻⁵⁸

There are few reports on the *cis* effect with results often being contradictory.^{46,47,59} This is attributed to the fact that Pt(II) complexes react at different rates depending on the σ -donor, π -acceptor and steric properties of the *cis* ligand. The general consensus is that the electronic effects of *cis* ligands is usually small when compared to that of the *trans* ligands in Pt(II) complexes.⁵

Van Eldik *et al.*⁵¹ studied the reaction kinetics of the complexes [Pt(6-phenyl-2,2'-bipyridine)Cl] (**PtNNC**), [Pt(1,3-di(2-pyridyl)benzene)Cl] (**PtNCN**) and [Pt(terpy)Cl] (**PtNNN**) with TU, DMTU and TMTU in order to get a better understanding of the different *cis*- and *trans* effects. For TU, the **PtNCN** complex reacted 30x faster than **PtNNN** and 455x faster than the **PtNNC** complexes.⁵¹ The σ -*cis* effect is, therefore, larger than the corresponding σ -*trans* effect. When the Pt–C bond is *trans* to the leaving group, the π -acceptor effect from the pyridyl/phenyl rings is small but still significant. The reactivity of this complex is thus the highest due to the highly destabilized ground state (labilisation of Pt–Cl by *trans* influence).⁵¹ When the Pt–C bond is *cis* to the leaving group the σ -donor effect of the carbon weakens the π -acceptor effect significantly. The σ -donor ability of the carbon counteracts the electron withdrawing affect of the π -acceptors.

Jaganyi *et al.*⁵² studied the substitution reactions of [Pt(terpy)Cl]⁺, (**Pt1**) [Pt(4'-Ph-terpy)Cl]⁺(**Pt2**), [Pt(4'-(2'''-CF₃-Ph)-terpy)]⁺ (**Pt3**) and [Pt(4'-(2'''-CF₃-Ph)-6-Ph-2,2'-bipy)](**Pt4**) with TU, DMTU and TMTU. Their results indicated that there were only minor differences in reactivity between the first three complexes with **Pt3** reacting the fastest.⁵² They put these minor differences down to electronic effects with the electron-donating phenyl ring reducing the π -acceptor abilities of the terpy ligand in **Pt2** and the electron-withdrawing CF₃-group increasing them in **Pt3**, as previously described.⁵²

When comparing **Pt3** with **Pt4**, the introduction of the Pt–C bond in the *cis*-position to the chloride atom decreases the reactivity of the substitution reaction by a factor of

16 with TU.⁵² This decrease in reactivity was attributed to the increase in electron density at the metal centre due to the σ -donating ability of the carbon atom, causing it to be less electrophilic than **Pt3**. This reduces the reaction rate because the incoming nucleophile is repelled by the increase of electron density.⁵² The authors explain that their results indicate that the *cis* and *trans* carbon σ -donors influence the lability of the leaving group differently. When the σ -donor is *trans* to the leaving group, the *trans* effect takes control due to ground state labilisation and transition state stabilization. This results in an elongation of the Pt–X bond (where X represents the leaving group) leading to an increase in the reaction rate. The decrease in the reaction rate when Pt–C is *cis* to the leaving group is due to the accumulation of electron density at the metal centre. This has less of an effect on the Pt–X bond length as there is no direct overlap of the orbitals of the two atoms *cis* to one another. This indicates that the Pt–C *cis* effect, unlike the *trans* effect, does not increase ground state destabilization of Pt(II) complexes.⁵²

The idea of a strong σ -donor carbon group decreasing the rate of ligand substitution because of the accumulation of electron density at the metal centre had already been explored by Romeo and co-workers⁵³ in their study on the effect of cyclometalation where the metal-carbon bond was located in the *cis* position.

1.4 Azoles

1.4.1 Azoles in Biological Systems

Some anti-cancer drugs use intercalation as their mode of action; however, other modes of interaction with DNA also involve direct covalent binding.⁶⁰ As azoles are similar in structure to the DNA nucleic bases, further studies of these Pt²⁺ complexes with azoles should bring about a link to how these complexes may react with the DNA base pairs. It has also been observed that derivatives of imidazole have shown antineoplastic properties.⁶¹ Antineoplasics are drugs that prevent the development of neoplasms which can cause tumours.

The study of substitution kinetics of azoles with platinum complexes was chosen for this study not only to help in the designing of future platinum-based drugs but also from a bioinorganic viewpoint to gain further understanding on other important reactions occurring in the body. The chemistry of five-membered azole rings and their mechanism of binding to transition metal centres are of great interest as many important reactions in biological systems involve the coordination of some form of azole to a metal centre.⁶²⁻⁶⁴

An important amino acid in nature is histidine, which is essentially an imidazole derivative. Histidine forms a crucial part of many biological systems through binding to hemeproteins.⁶²⁻⁶⁴ The coordination of histidine to metal complexes can change, depending on the pH as shown in *Figure 1.13*.

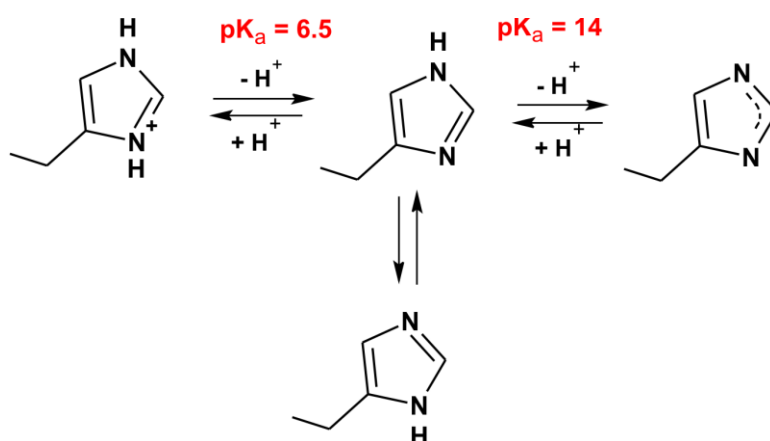


Figure 1.13: The pH-dependent tautomeric forms of histidine.⁶⁴

Hemeproteins usually consist of the iron(II) complex of protoporphyrin IX with an axially bound histidine, shown in *Figure 1.14*. These hemeproteins are responsible for the uptake, storage and transport of oxygen.⁶⁴ Hemoglobin is the hemeprotein which is responsible for oxygen transport and myoglobin is responsible for oxygen storage.⁶⁴ Hemeproteins are also responsible for electron transfer through cytochromes in both animals and plants.⁶⁴

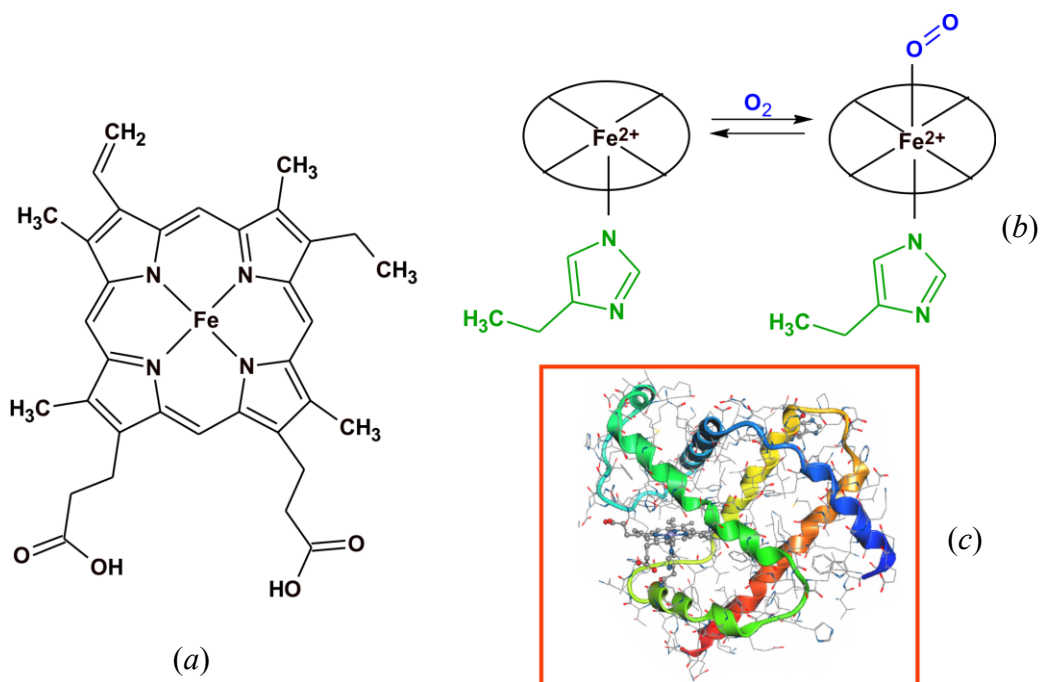


Figure 1.14: Structure of (a) Fe²⁺ bound to protoporphyrin IX (heme) (b) mechanism of oxygen transport and storage by heme proteins in mammals and (c) Protein diagram of myoglobin.⁶⁴

Thus, it can be seen that the reactions of hemeproteins form part of many life-giving reactions in biological systems and azoles play an important role in the functioning of these hemeproteins.

Azoles have also been found to inhibit the binding of CO to the sodium dithionite reduced cytochrome as well as inhibiting the activity of cytochrome P450, which is responsible for the oxidation of organic substrates, by binding to the cytochrome.^{62,63,65} Without the activity of cytochrome P450, the human liver would no longer be able to metabolise endogenous substances.⁶⁴ Again, a study of azoles would be important to understand this mechanism of action.

The kinetic study of the azoles may also be used to link computational data on metal binding properties of nitrogen bases with that gained from experimental research.^{62,63} Azoles can also be used as building blocks in the synthesis of more complicated structures, as they not only make good ligands but can also serve to bridge complexes.⁶¹

The importance of the further study of the reactions of azoles with metal complexes must not be underestimated. As has been discussed, azoles not only form part of crucial bioinorganic complexes but also may provide the building blocks for novel anti-cancer drugs.

1.4.2 Previous Azole Studies

A number of different studies involving substitution reactions with azoles and pyridine derivatives have been reported with the popularity of these reactions increasing over the last decade. The results of some of these studies are discussed below with *Figure 1.15* illustrating some of the azoles and pyridines used in these studies.

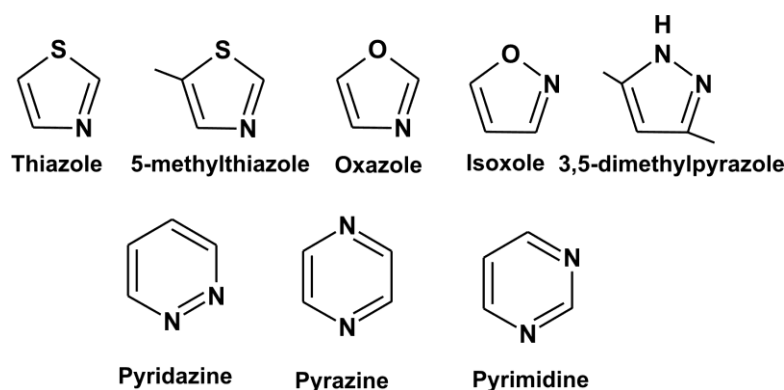


Figure 1.15: Variety of azoles and pyridines used in research studies.

Pitteri *et al.*^{66,67} have studied the nucleophilicity of a range of different nitrogen donor heterocycles and pyridines towards $[\text{Pt}(\text{terpy})\text{Cl}]^+$ in methanol. They reported that imidazole displaced the Cl^- in this complex faster than thiazole, 5-methylthiazole, oxazole, isoxazole, 3,5-dimethylpyrazole and 4,5-dimethylthiazole (see *Figure 1.15*) with imidazole substituting 14x faster than pyrazole.⁶⁶ They explained their results by saying that the kinetic data supports a reaction profile involving a transition state where the $\text{Pt}-\text{N}$ bond is significantly weaker than the fully formed $\text{Pt}-\text{Cl}$ bond, thus leading to a situation where the reactivity of the entering group depends linearly on the basicity of the nucleophile.^{66,67}

Rosic *et al.*⁶² studied the substitution reactions of the replacement of H_2O and Cl^- in the complexes of $[\text{Pt}(\text{dien})\text{H}_2\text{O}]^{2+}$ and $[\text{Pt}(\text{dien})\text{Cl}]^+$ respectively (where dien = diethylenetriamine) with nitrogen-donor ligands such as 1,2,4-triazole, pyrazole and

pyridazine. For both complexes they reported the order of reactivity as 1,2,4-triazole > pyridazine > pyrazole with the aqua complex being more reactive than the chloro complex. Rosic *et al.*⁶² like Pitteri *et al.*^{66,67}, explained their results in terms of basicity of the nucleophile.

Bugarcic *et al.*⁶³ have studied the reaction kinetics of $[\text{Pd}(\text{dien})\text{H}_2\text{O}]^{2+}$, $[\text{Pd}(\text{dienCl})]^+$, $[\text{Pd}(\text{bpma})\text{H}_2\text{O}]^{2+}$ and $[\text{Pd}(\text{bpma})\text{Cl}]^+$ where (bpma = bis(2-pyridylmethyl)amine) with 1,2,4-triazole, pyrazole, pyrimidine, pyrazine and pyridazine in aqueous solution. The authors reported an associative mechanism whereby the reactivity is linearly related to the basicity of the entering nucleophiles with triazole being more reactive than pyrazole in all cases.⁶³ Pyridazine was the most reactive of the six-membered rings which is because when the nitrogen atoms are in the 1,2 positions (pyridazine) the molecule is a better nucleophile than when the nitrogen atoms are in the 1,3 (pyrimidine) or 1,4 positions (pyrazine).⁶³ As expected the bpma complexes were faster than the dien complexes due to the stronger π effect of the bpma ligand.

Some workgroups have also grown crystals of azole-substituted complexes in order to infer the nature of the complex bound to the DNA nucleobases. This understanding is important as certain modes of interaction with DNA by Pt-based drugs involve direct covalent binding.

Both Roszak *et al.*⁶⁰ and Muller *et al.*⁶⁸ have crystallised the complex $[\text{Pt}(\text{terpy})(1\text{-methylimidazole})](\text{ClO}_4)_2 \cdot \text{MeCN}$ and both groups interpret the structures differently. Roszak *et al.*⁶⁰ found that the dihedral angle between the least-squares Pt-terpy plane and the plane of the imidazole ring was $66.5(2)^\circ$, as shown in *Figure 1.16*.⁶⁰ The authors suggest that this almost perpendicular orientation of the 1-methylimidazole ligand with respect to the Pt-terpy plane means that the Pt-terpy complex would form a similar orientation with the DNA bases on binding.⁶⁰ This arrangement would probably disrupt the DNA helix in a different mode to intercalation.⁶⁰ Muller *et al.*⁶⁸ crystallised the same complex with and without the solvent molecule, acetonitrile. For the crystal structure without the solvent, the dihedral angle between the least-squares Pt-terpy plane and the plane of the imidazole ring is $74.0(2)^\circ$.⁶⁸ They believe that the entire complex does not exhibit sufficient planarity for interaction with the DNA base pairs. On the other hand, they noticed that

by the addition of solvent the dihedral angle decreased by $7.5(3)^{\circ}$ implying that it might be possible to create a more planar system.⁶⁸

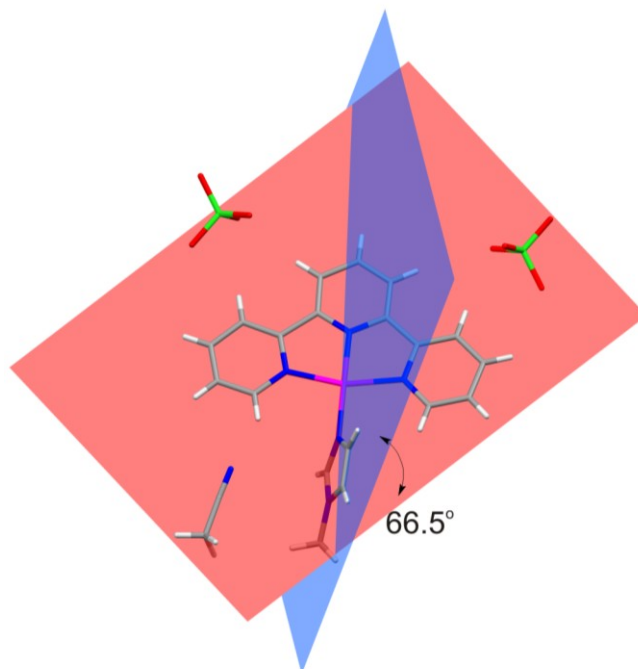


Figure 1.16: X-ray structure of $[\text{Pt}(\text{terpy})(1\text{-methylimidazole})](\text{ClO}_4)_2 \cdot \text{MeCN}$ showing the dihedral angle between the least-squares Pt-terpy plane and the plane of the imidazole ring.⁶⁰

1.5 Aims of the Current Study

This study involves the investigation of the substitution kinetics of chloride from the $[\text{Pt}(\text{terpy})\text{Cl}]^+$ (where terpy = 2,2':6',2''-terpyridine) and several structural analogues with a variety of azoles shown in *Figure 1.17*. The structural differences between the complexes were carefully selected in order to study the manner in which varying steric and electronic effects affect ligand substitution. These effects include (i) controlling the π -acceptor properties of the surrounding ligand structure by substituting either electron-donating or -withdrawing on the ligand periphery and (ii) modifying the π -acceptor properties of the surrounding ligand structure by substitution of the *cis* donor ligand. In addition the azoles chosen as nucleophiles for the current study allowed for a brief investigation into the nucleophilicity of these

based on the number and position of the nitrogen atoms in the ring as well as substituents present.

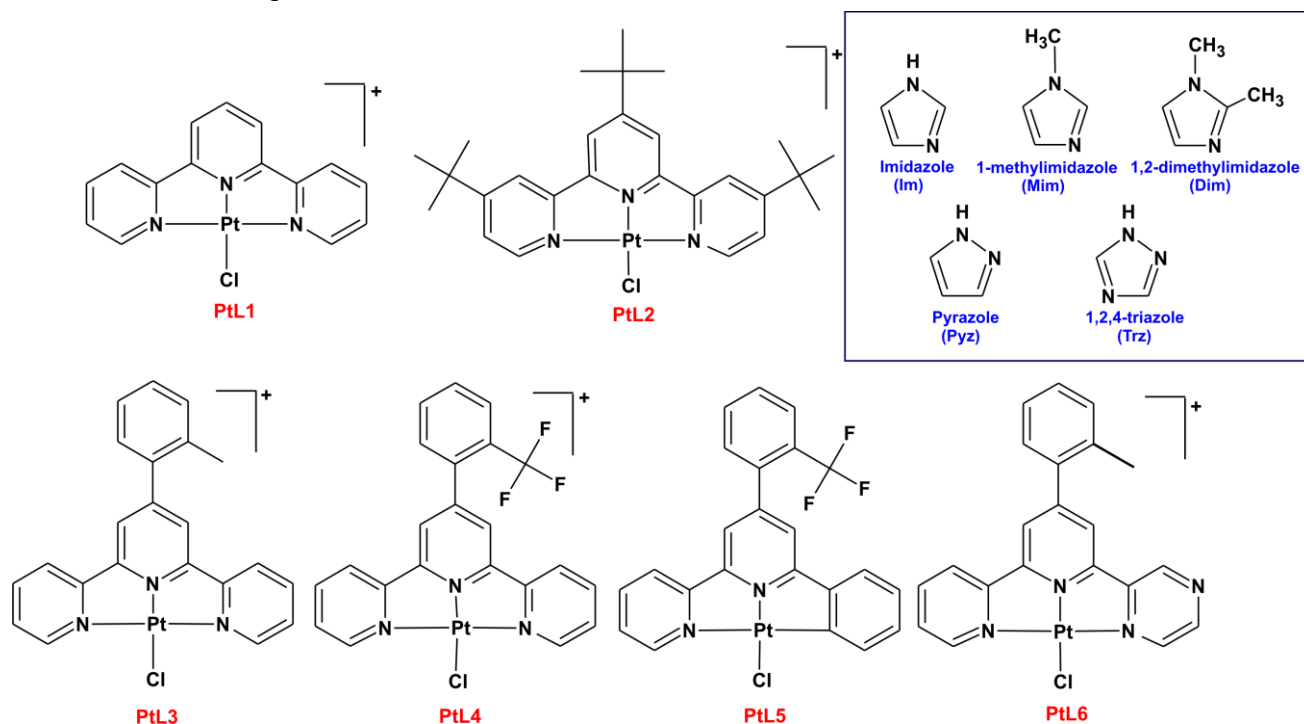


Figure 1.17: The series of Pt(II) terpy complexes and selected structural analogues and nucleophiles investigated in this study.

The aims of this research were to:

1. Synthesise model compounds which mimic metal ion interaction with proteins.
2. Observe the kinetic effect and deduce the mechanism of the square-planar substitution reactions of these complexes with azoles, which represent nuclear bases and amino acids in biological systems.
3. Determine the effect of structural modification of the terpy backbone and the azole nucleophiles on the reaction kinetics in order to investigate how electronic and steric factors within the metal complex affect its reactivity.
4. Use the conclusions from the study to help in the future designing of new types of anti-cancer drugs.

1.6 References

1. B. Lippert, *Cisplatin. Chemistry and Biochemistry of a Leading Anti-cancer Drug*, Wiley-VCH, Weinheim, 1999, pgs 3-27,111-131,159-177.
2. A. Sigel and H. Sigel, *Metal Ions in Biological Systems*, Marcel Dekker Inc., NY, 1996, 339.
3. D. T. Richens, *Chem. Rev.*, 2005, **105**, 1961.
4. M. L. Tobe and J. Burgess, *Inorganic Reaction Mechanisms*, Addison Wesley Longman Ltd., Essex, 1999, pgs 30-43, 70-112.
5. J. D. Atwood, *Inorganic and Organometallic Reaction Mechanisms*, Wiley-VCH Inc., NY, 2nd edition, 1997, pgs 43-61.
6. R. B. Jordan, *Reaction Mechanisms of Inorganic and Organometallic Systems*, Oxford University Press Inc., 1991, pgs 29-74.
7. R. G. Wilkins, *Kinetics and Mechanism of Reactions Transition Metal Complexes*, VCH, Weinheim, 2nd edn, 1991, pgs 199-201, 221, 232-242.
8. R. J. Cross, *Adv. Inorg. Chem.* 1989, **34**, 219.
9. F. R. Hartley, *Chemistry of the Platinum Group Metals Recent Developments*, Elsevier, Amsterdam, 1991, pgs 9, 23-30, 547-570.
10. P. J. Loferski, *Platinum-Group Metals*, United States Geological Survey, 2009.
11. D. F. Shriver and P. W. Atkins, *Inorganic Chemistry*, 3rd ed., Oxford University Press, New York, 2002, pgs 285, 308-309, 490, 627.
12. A. Karpov, M. Konuma and M. Jansen, *Chem. Comm.*, 2006, **8**, 838-40.
13. R. J. Seymour and J. I. O'Farrelly, *Kirk Othmer Encyclopedia of Chemical Technology, Platinum-group metals*, Wiley, 2001.
14. G. B. Kauffman, *Inorg. Syn.*, 1967, **9**, 182.
15. A. E. Schweizer, G. T. Kerr, *Inorg. Chem.*, 1978, **17**, 8, 2326.
16. D. L. Perry, *Handbook of Inorganic Compounds*, CRC Press, 1995, pgs 296-298.
17. F. A Cotton, G. Wilkinson and P. L Gaus, *Basic Inorganic Chemistry*, 3rd ed., John Wiley & Sons, Inc, New York, 1995, pgs 682-683.
18. Y. Han, H. V. Huynh and G. K. Tan, *Organometallics*, 2007, **26**, 4612.
19. P. G. Eller, R. R. Ryan, R. O. Schaeffer, *Cryst. Struct. Commun.*, 1977, **6**, 163.

20. A. Syed, E. D. Stevens and S. G. Cruz, *Inorg.Chem.*, 1984, **23**, 3673.
21. Z. Xiao and A. R. Laplante, *Minerals Engineering*, 2004, **17**, 961.
22. P. J. Loferski, *2007 Minerals Yearbook: Platinum-Group Metals*, United States Geological Survey, 2007.
23. J. Cairns, *Cancer Science and Society*, W. H. Freeman and Company, US, 1978, pgs 15-31, 35-39.
24. D. E. Thurston, *Chemistry and Pharmacology of Anti-cancer Drugs*, CRC Press Taylor & Francis Group, USA, 2007, pgs 1-27, 61-63, 69-73.
25. World Health Organisation, *Cancer*, <http://www.who.int/cancer/en/>, 2009, Date accessed 13/07/09.
26. T. Hambley, *Coord. Chem. Rev.*, 1997, **166**, 181.
27. M. Coluccia and G. Natile, *Anti-Cancer Agents in Medicinal Chemistry*, 2007, **7**, 111.
28. G. Natile and M. Coluccia, *Coord. Chem. Rev.*, 2001, **216–217**, 383.
29. M. Cleare and J. Hoeschele, *Platinum Met. Rev.*, 1973, 17.
30. M. Cleare, *Co-ordination Chemistry Rev.*, 1974, **12**, 349.
31. M. Cleare and J. Hoeschele, *Bioing. Chem.*, 1973, **2**, 187.
32. B. M. Zeglis, V. C. Pierre and J. K. Barton, *Chem.Commun.*, 2007, 4565-4579.
33. D. P. Snustad and M. J. Simmons, *Principles of Genetics*, 4th ed., John Wiley & Sons, Inc., 2006, USA, pgs 210-219.
34. S. Kar, B. Sarkar, S. Ghumaan, M. Leboschka, J. Fielder, W. Kaim and G. Lahiri, *Dalton Trans.*, 2007, 1934.
35. DNA, <http://www.lmusd.tehama.k12.ca.us/>, Date accessed: 16/02/08.
36. S. Sherman, D. Gibson, A. Wang and S. Lippard, *Science*, 1985, **230**, 412.
37. M. Galanski and B. K. Keppler, *Anti-Cancer Agents in Medicinal Chemistry*, 2007, **7**, 55.
38. L. A. Lipscomb, M. E. Peek, F. Xiao Zhou, J. A. Bertrand, D. Van Derveer, and L. D Williams, *Biochem.*, 1994, **33**, 3649.
39. S. D. Cummings, *Coord. Chem. Rev.*, 2009, **253**, 449.
40. S. D. Cummings, *Coord. Chem. Rev.*, 2009, **253**, 1495.
41. K. W. Jennette, S. J. Lippard, G. A Vassiliades and W. R. Bauer, *Proc. Natl. Acad. Sci. U.S.A.*, 1974, **71**, 3839.

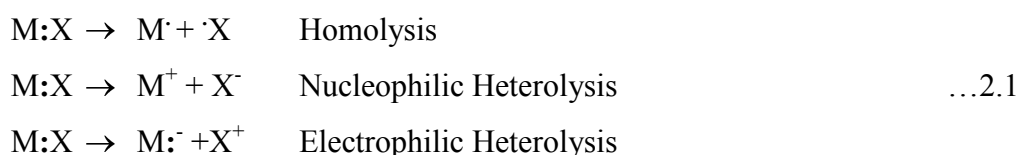
42. W. D. McFadyen, L. P. Wakelin, I. A. Roos and V. A. Leopold, *J. Med. Chem.*, **28**, 1985, 1113.
43. M. Howe-Grant, K. C. Wu, W. R. Bauer and S. J. Lippard, *Biochem.*, **15**, 1976, 4339.
44. W. D. McFadyen, L. P. Wakelin, I. A. Roos and B. L. Hillcoat, *Biochem. J.* **242**, 1987, 177.
45. G. Lowe and T. Vilaivan, *J. Chem. Soc., Perkin Trans*, **1**, 1996, 1499.
46. D. Jaganyi, A. Hofmann, and R. van Eldik, *Angew. Chem. Int. Ed.*, 2001, **40**, 1680.
47. A. Hofmann, D. Jaganyi, O. Q. Munro, G. Liehr, and R. van Eldik, *Inorg. Chem.*, 2003, **42**, 1688.
48. R. Romeo, M. R. Plutino, L. M. Scolaro, S. Stoccoro and G. Minghetti, *Inorg. Chem.* 2000, **39**, 4749.
49. D. Jaganyi, K-L. De Boer, J. Gertenbach and J. Perils, *Int. J. Chem. Kinetics*, 2008, 808.
50. D. Reddy and D. Jaganyi, *Dalton Trans.*, 2008, 6724.
51. A. Hofmann, L. Dahlenburg and R. van Eldik, *Inorg. Chem.*, 2003, **42**, 6528.
52. D. Jaganyi, D. Reddy, J. A. Gertenbach, A. Hofmann and R. van Eldik, *Dalton Trans.*, 2004, 299.
53. R. Romeo, M. R. Plutino, L. M. Scolaro, S. Stoccoro and G. Minghetti, *Inorg. Chem.*, 2000, **39**, 4749.
54. F. Basolo, J. Chatt, H.B. Gray, R. G. Pearson and B. L. Shaw., *J. Chem. Soc.*, 1961, 2207.
55. G. Alibrandi, D. Minniti, L. M Scolaro and R. Romeo, *Inorg. Chem.*, 1988, **27**, 318.
56. R. Gosling and M. L Tobe, *Inorg Chem.*, 1983, **22**, 1235.
57. L. Canovese and M. L. Tobe, *Dalton Trans.*, 1985, 27.
58. O. F. Wendt and L. I Elding, *Dalton Trans.*, 1997, 4725.
59. J. K. Burdett, *Inorg. Chem.*, 1977, **16**, 3013.
60. A. W. Roszak, O. Clement and E. Buncel, *Acta. Cryst.*, 1996, **C52**, 1654.
61. R. Conteras, A. Flores-Parra, E. Mijangos, F. Tellez, H. Lopez-Sandoval and N. Barba-Behrens, *Coord. Chem. Rev.*, 2009, **253**, 1979.
62. J. Rosic, B. Petrovic, M. Djuran and Z.D Bugarcic, *Chemical Monthly*, 2007, **138**, 1.

63. Z. D. Bugarcic, S. T. Nandibewoor, M. S. A. Hamza, F. Heinemann and R. van Eldik, *Dalton Trans.*, 2006, 2984.
64. W. Kaim and B. Schwederski, *Bioinorganic Chemistry: Inorganic Elements in the Chemistry of Life*, 1st ed, John Wiley & Sons, New York, 1994, pgs 16-35, 106-123.
65. P. R. Balding, C. S. Porro, K. J. McLean, M. J. Sutcliffe, J-D Mare'chal, A. W. Munro and S. P. de Visser, *J. Phys. Chem. A*, 2008, **112**, 12911.
66. B. Pitteri and M. Bortoluzzi, *Polyhedron*, 2006, **25**, 2698.
67. B. Pitteri, G. Marangoni, F. V. Visentini, L. Cattalini and T. Bobbo, *Polyhedron*, 1998, **17**, 475.
68. J. Muller, E. Freisinger, P. Lax, D. A. Megger and F. Polonius, *Inorg. Chim. Acta*, 2007, **360**, 255.

Substitution Reactions

A substitution reaction is a process whereby a ligand in the coordination shell is replaced by another from the environment.^{1,2} A simple substitution is where the replacement of the ligand involves no temporary change in the oxidation state, only a change in coordination number, of the reaction centre.^{1,2}

The modes of bond breaking have been classified as either homolytic or heterolytic,^{1,2,3}

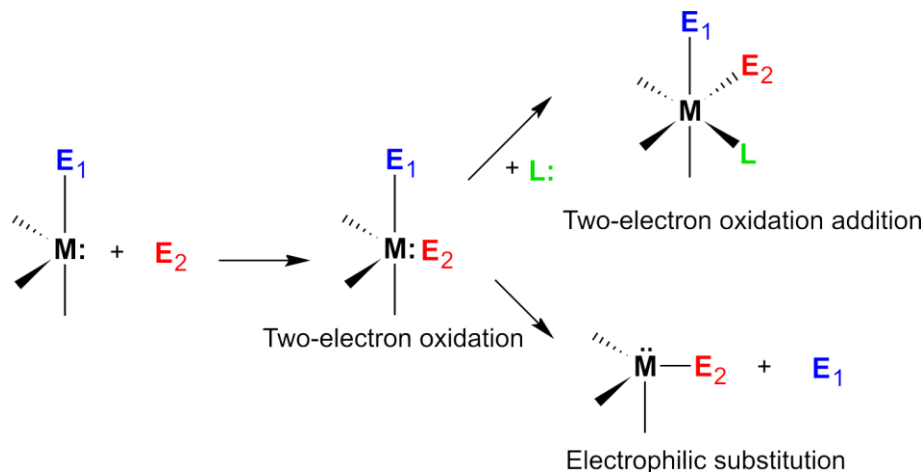


In a homolytic process, each member of the former bond takes one of the electrons.^{1,2} In non-transition elements this will lead to unstable, odd-electron free radicals; however, with transition metals this leads to the transfer of one electron formerly involved in bonding from the ligand to the metal.^{1,2}

The heterocyclic process can be nucleophilic where the electrons of the bond may remain with the leaving group and the incoming ligand needs to provide a replacing pair of electrons.^{1,2} The heterocyclic process can also be electrophilic where the electrons of the bond remain with the reaction centre and the incoming ligand acts as an electron pair acceptor.^{1,2}

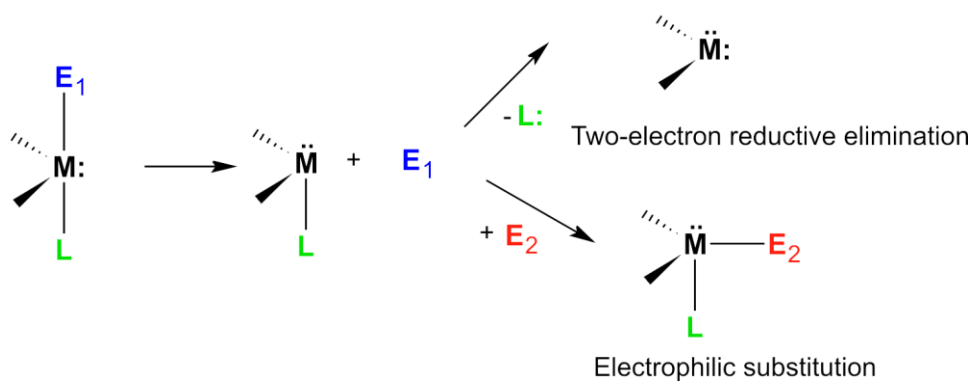
In a nucleophilic process, the reaction centre acts as a Lewis acid (species that accepts a pair of electrons from Lewis base).^{1,2} The change in the number of ligands does not lead to a temporary change in oxidation state of the reaction centre.¹ The addition of an electrophile results in a two-electron oxidation.¹ If a ligand then leaves as a Lewis acid, the reaction is an electrophilic substitution; however, an oxidative addition

reaction may also occur where a ligand acting as a Lewis base (species that donates a pair of electrons to a Lewis acid) attaches itself to the metal centre.¹ *Scheme 2.1* illustrates this concept. Most coordination complexes, except some organometallic compounds, undergo nucleophilic substitution reactions.



Scheme 2.1: The bond-making process.^{1,2}

In an electrophilic reaction, the reaction centre acts as a base.^{1,2} A two-electron reduction is a dissociative electrophilic process whereby a bonding pair of electrons becomes non-bonding.¹ The loss of a Lewis base leads to reductive elimination whereas the gain of an electron pair acceptor completes the substitution¹, as shown in *Scheme 2.2*.



Scheme 2.2: The bond-breaking process.^{1,2}

2.1 Stoichiometric and Intimate Mechanisms

Langford and Gray⁴ attempted to classify inorganic reactions according to simple mechanistic schemes. They introduced the stoichiometric mechanism which exists in one of three forms: ^{1,3}

- A dissociative process (**D** mechanism) involves a reaction where an intermediate with a reduced coordination number is formed.^{1,2,5-8} This type of intermediate is produced when bond breaking of the leaving group occurs before the attachment of the entering group.^{1,2,5-8} As the bond breaking step is the rate determining step of the reaction, the rate of the reaction is insensitive to the entering group.^{1,2,5-8} The rate is; however, dependent on the nature of the leaving group.^{1,2,5-8}
- An associative process (**A** mechanism) involves a reaction where an intermediate of increased coordination number is formed.^{1,2,5-8} This happens when there is bond formation between the entering group and the metal centre before the bond between the leaving group and the metal centre breaks.^{1,2,5-8} As the bond formation is the rate determining step, the rate of the reaction is dependent on the entering group.^{1,2,5-8}
- An interchange process (**I** mechanism) involves a reaction where bond making and breaking occur at the same time and no intermediate is formed.^{1,2,5-8}

The energy profile diagrams for the dissociative, associative and interchange mechanisms are shown in *Figure 2.1*, where X represents the leaving group and Y represents the incoming group.

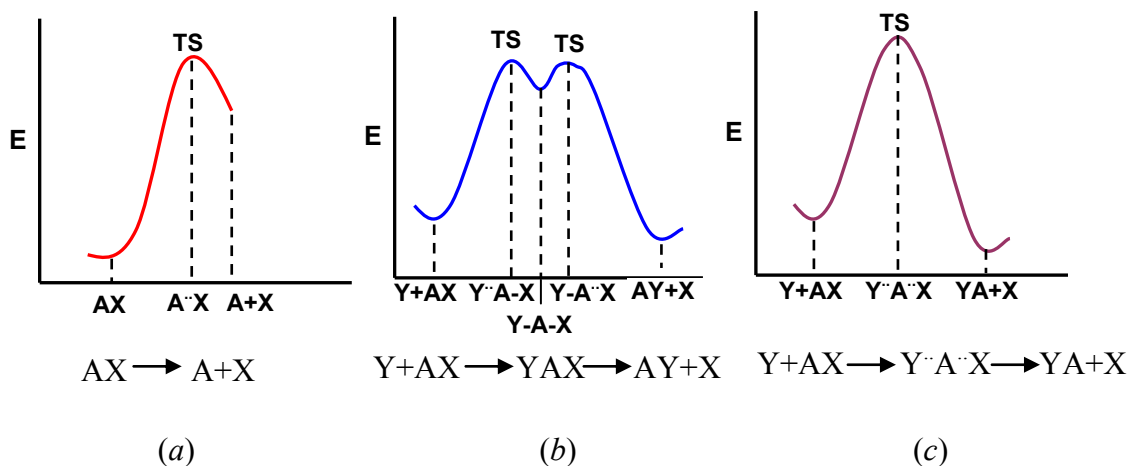


Figure 2.1: Energy profile diagram showing (a) dissociative, (b) associative and (c) interchange mechanisms.^{1,2}

Stoichiometric mechanisms depend on the identification of an intermediate species.¹ The intermediate can be characterised through its influence on the kinetics of a reaction and does not have to be isolated.¹

The stoichiometric interchange mechanism has a variety of transition states:

- The dissociatively activated intimate mechanism (I_d mechanism) involves a transition state in which there is only very weak bonding of the metal centre to the entering and leaving group in the transition state.^{1,2,5-8} The entering group only has a small effect on the reaction rate.^{1,2,5-8} Both bond breaking and formation take place but to different degrees. In a dissociatively activated intimate mechanism bond breaking is more dominant, *Figure 2.2(a)*.
- The associatively activated intimate mechanism (I_a mechanism) has a transition state in which there is substantial bonding of the metal to both the entering and leaving groups.^{1,2,5-8} The reaction rate will show some dependence on the entering group.^{1,2,5-8} Bond formation is more dominant, *Figure 2.2(b)*.

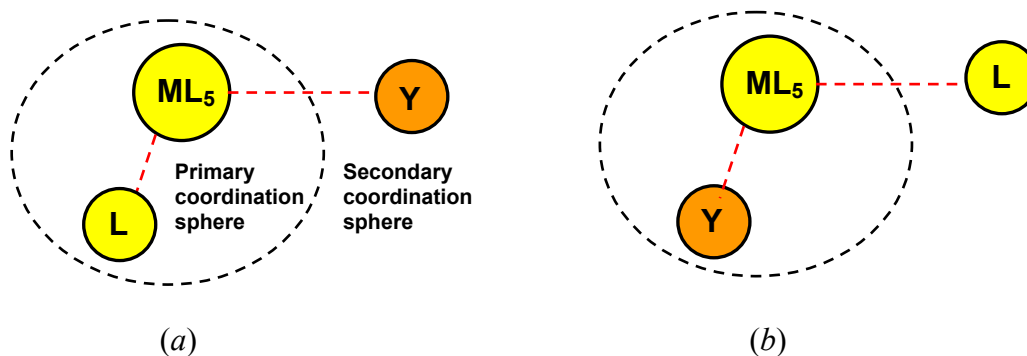


Figure 2.2: Diagrams to illustrate a (a) dissociatively activated and (b) associatively activated intimate mechanism.

2.2 Coordination Number and Substitution Mechanism

Logically, more ligands surrounding a central atom should make it more difficult for a further ligand to bind. Thus, centres with high coordination numbers should undergo a dissociative mechanism while centres with lower coordination numbers should favour an associative mechanism. However, the connection between coordination and substitution mechanism is not so simple.¹

Electronic and steric factors of the central atom and its ligands control the ground-state geometry and thus the change on going to the transition state is also determined by a number of factors.¹ Tetrahedral *sp*-block elements and the first-row *d*-block M^{2+} and M^{3+} centres have been shown to follow I_d and I_a pathways.¹ As *f*-block elements can form seven and eight coordinate species of differing geometries, they can react by either associative or dissociative pathways.¹ Square-planar *d*-block complexes generally follow an associative mechanism^{1,2,5-12}; however, examples of dissociative substitution have been reported.^{13,14}

2.3 Substitution in Square-Planar Complexes

Square-planar geometry is not the lowest energy arrangement of four ligands in an electrostatically bonded system. Thus, in order for this geometry to occur special circumstances are necessary.^{1,2} The three major areas where this geometry may occur are as follows: (a) complexes of *p*-block elements such as XeF_4 , $[\text{ClF}_4]^-$, $[\text{ICl}_4]^-$, which

have four bonding and two non-bonding pairs of electrons, (b) transition metal complexes where the ligands require a four-coordinate planar arrangement such as complexes of the planar quadridentate phthalocyanin, porphyrin and corrin ligands and (c) complexes of metal ions with d^4 , d^9 and low spin d^8 configuration.^{1,2}

Of the three circumstances where square-planar geometry occurs, the first category of complexes are highly reactive materials undergoing side reactions rather than substitution reactions.^{1,2} These complexes also undergo decomposition after substitution of the labile ligand and as a result they have not been fully investigated.^{1,2} Substitution reactions of the second category of complexes are either complicated or destroy the geometry of the complex.^{1,2} The third category containing d^4 and d^9 complexes are better considered as octahedral species with a tetragonal distortion and therefore are not relevant to the study of substitution reactions of square-planar complexes.² Most of the information garnered on substitution reactions of square-planar complexes is from the study of complexes whose central ion has the low-spin d^8 electron configuration.^{1,2}

Not all reaction centres with a d^8 configuration are suitable for square planar substitution reactions. From the metal centres with +1 oxidation state, Co(I) prefers to form five-coordinate species and whilst Rh(I) and Ir(I) form square-planar complexes with certain ligands they are sensitive to oxidative addition.¹ This has led to very few studies on substitution reactions of the d^8 reaction centres with +1 oxidation state. Cu(III) and Ag(III) are often reduced while only Au(III) can form square-planar complexes that can be studied; however, these complexes are still sensitive to reduction.¹ Most d^8 square-planar complexes have a metal centre with a +2 oxidation state.¹ Complexes of Ni(II) can be found with a variety of geometries, coordination numbers and spin multiplicities with square-planar geometry not being favoured.^{1,2} Pt(II) is the favoured metal when studying square-planar substitution reactions as it is stable to redox reactions, has low reactivity which leads to the synthesis of a variety of complexes and reactions lead to kinetics which are simple and easy to interpret.^{1,2,6} Pd(II) complexes are less favourable to study as they are much more reactive than Pt(II) complexes.^{1,2} In some cases, changing a Pt(II) centre to a Pd(II) centre can increase the rate constant by a factor of 10^5 .^{1,2}

2.3.1 The Kinetics and Mechanisms of Substitution

The following reaction,



has the rate law:

$$\frac{-d[\text{L}_3\text{MX}]}{dt} = (k_1 + k_2[\text{Y}])[\text{L}_3\text{MX}] \quad \dots 2.3$$

where k_1 is the rate constant that is independent of the incoming nucleophile, Y and k_2 is the rate constant that is very sensitive to Y (for a given solvent at a fixed temperature).^{1,2,6,15}

Evidence strongly suggests that short-lived five-coordinate intermediate is involved in the k_2 path indicating an associative intimate mechanism.^{1,2,6,15} There have been two possible mechanisms proposed to describe the k_1 term, namely dissociative and associative mechanisms.^{1,2,6,15} The associative k_1 pathway is shown in *Figures 2.3*.

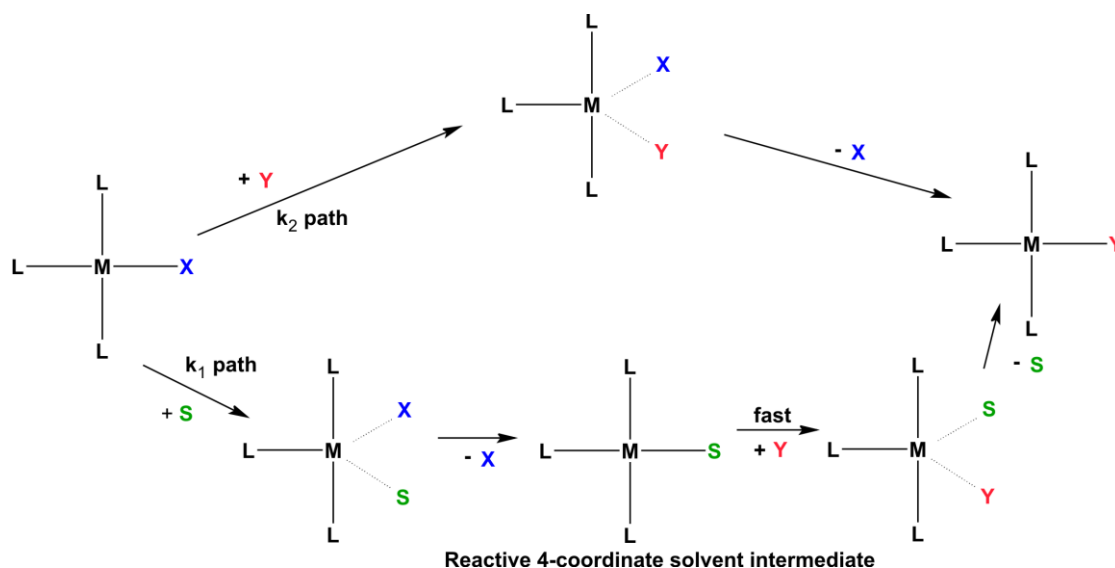
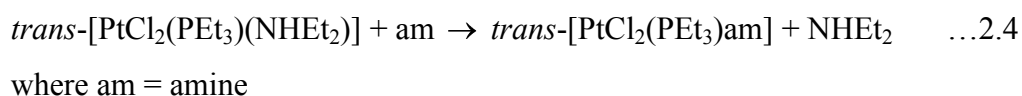


Figure 2.3: Diagram showing both associative k_2 and k_1 pathways for square planar complexes.²

The mechanism in *Figure 2.3*, shows associative solvolysis and direct substitution. In the associative path of this mechanism there is the formation of the reactive intermediate, L_3MS .

The following evidence is in favour of an associative mechanism for the k_1 pathway.^{1,2}

- a) According to the 18-electron rule for stability, four coordinate d^8 metals with only sixteen valence electrons are coordinatively unsaturated.^{1,2} As an associatively activated substitution would involve the formation of a five-coordinate transition state with an eighteen electron valence shell, it is believed that this substitution mechanism is favoured to dissociatively activated substitution involving the formation of three-coordinate intermediates with a fourteen-electron valence shell.^{1,2} Stable five- and six-coordinate complexes for d^8 metals have been seen such as $[\text{Pt}(\text{SnCl}_3)_5]^{3-}$.^{1,2,15} This favours the formation of five-coordinate intermediates in the associative mechanism.
- b) Steric hindrance affects both k_1 and k_2 , which implies that both pathways follow an associative mechanism.^{1,2,15} For example, in the pyridine substitution into $\text{cis}-[\text{PtCl}(\text{PEt}_3)_2]$, when $\text{L} = \text{phenyl}$ the rate constant was about $8 \times 10^{-2} \text{ s}^{-1}$ but with an increase in steric bulk, i.e. $\text{L} = 2\text{-tolyl}$, the rate drops to $2 \times 10^{-4} \text{ s}^{-1}$.¹⁶
- c) The k_1 term is very sensitive to the solvent and is not evident in non-coordinating solvents.^{1,2,6,15} Raethel and Odell¹⁷ studied the following reaction in a range of coordinating and non-coordinating solvents.

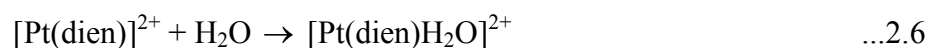


Their results showed that in non-coordinating solvents such as hexane and benzene, the k_1 term disappears, while in a coordinating solvent such as methanol the rate takes on the form $\text{rate} = (k_1 + k_2[\text{amine}])[\text{complex}]$.¹⁷

- d) Olcott and Gray¹⁸ have been able to isolate the solvent containing intermediate, thus proving an associative mechanism for k_1 in the reactions of $[\text{Pt}(\text{dien})\text{I}]^+$ in water. Hence the solvent intermediate would be $[\text{Pt}(\text{dien})\text{H}_2\text{O}]^{2+}$

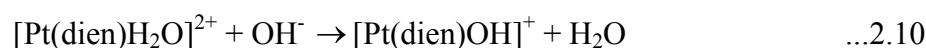
which is extremely labile species and the H_2O is readily replaced.¹⁸ The removal of a proton from the complex is, however, much faster than breaking the $\text{Pt}-\text{OH}_2$ bond and the resultant $[\text{Pt}(\text{dien})\text{OH}]^+$ complex is inert to substitution. As OH^- is a weak nucleophile, this system has no k_2 pathway.¹⁸ Thus any solvent complex formed, would be trapped before the water is replaced by the incoming nucleophile.^{1,2} Based on these facts Olcott and Gray¹⁸ monitored the formation of $[\text{Pt}(\text{dien})\text{OH}]^+$ from $[\text{Pt}(\text{dien})\text{I}]^+$ with varying concentrations of OH^- and I^- .

If the k_1 path is dissociative:



then iodide would affect the rate of formation of $[\text{Pt}(\text{dien})\text{OH}]^+$ and varying $[\text{I}^-]$ should change the rate.¹⁸

If the k_1 path is associative:



then the rate of formation of $[\text{Pt}(\text{dien})\text{OH}]^+$ should not show a dependence on $[\text{OH}^-]$ or $[\text{I}^-]$.¹⁸

Experimentally it was found that $[\text{I}^-]$ and $[\text{OH}^-]$ do not play a role in the rate of reaction indicating that k_1 follows an associative mechanism.¹⁸

- e) Practically all k_1 values in square-planar substitution reactions increase when the pressure is raised, indicating a negative volume of activation which signifies an associative mechanism.^{1,19,20}

All the evidence is in agreement with an associative mechanism for both the k_1 and k_2 paths in a low spin d^8 square-planar complex.^{1,2,6,15} The dissociative mechanism is possible but only under very specific conditions (see Section 2.3.4).

2.3.2 Geometries of the Transition States and Intermediates

As the major pathway for substitution in square planar complexes is associative, then the intermediates and transition states must be five coordinate.^{1,2,6} The geometry of the intermediate has been characterized as trigonal bipyramidal with the entering and leaving groups, as well as the *trans* ligand in the trigonal plane, see Figure 2.4.^{1,2}

Substitution takes place with complete retention of configuration, implying that the three spectator groups must retain the same positions relative to one another throughout the reaction.^{1,2,6}

Although the square-pyramidal geometry, which is found in five-coordinate d^8 metal-ion complexes, may occur during substitution, it is a structure that is below the energy maxima of the transition states.^{1,2}

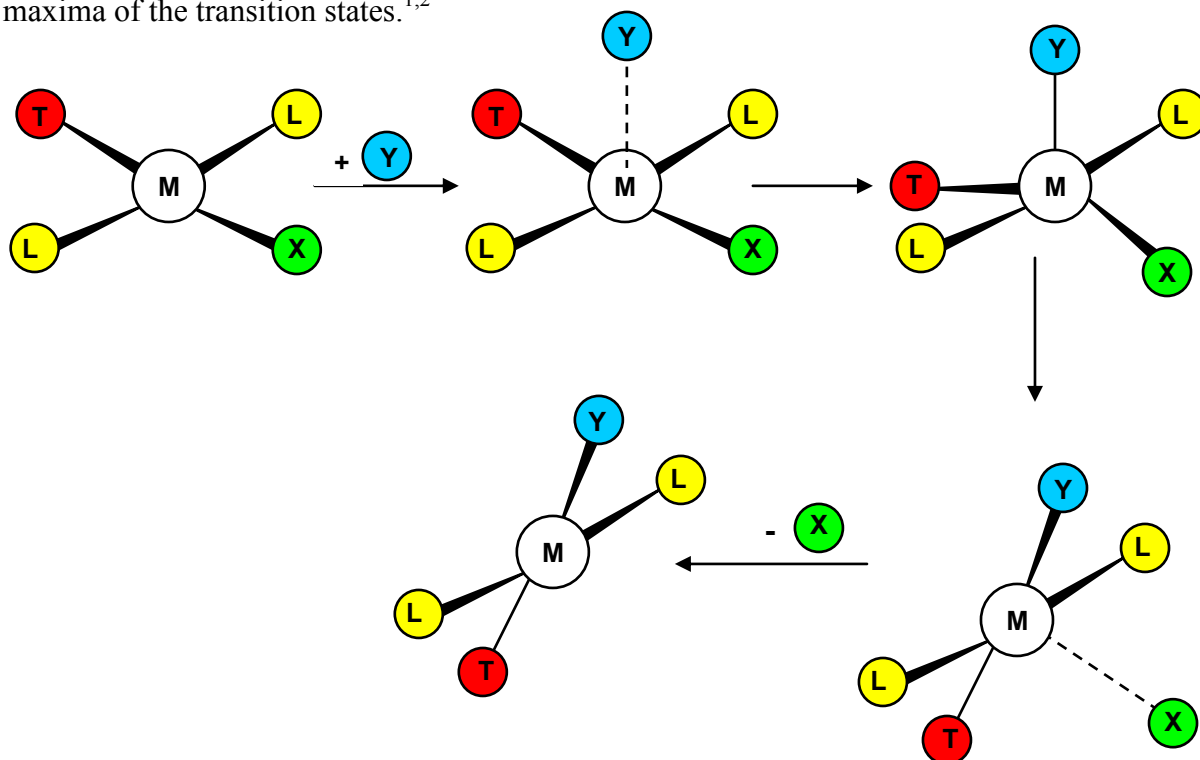


Figure 2.4: Formation of trigonal bipyramidal intermediate.¹

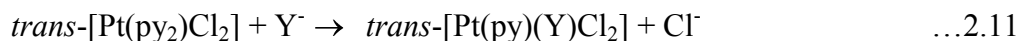
2.3.3 Factors Controlling the Reactivity of Square-Planar Complexes

The following factors all play a role in the reactivity of a four coordinate complex:

- Nature of the incoming group
- Nature of the *trans* ligand
- Nature of the *cis* ligand
- Nature of the leaving group
- Nature of the metal centre

Nature of the Incoming Group

In an associative mechanism, the incoming group is an important factor in determining the rate of a reaction. The size of the rate constant, k_2 , is a measure of the effectiveness of the incoming group.^{1,2} The quantitative measure of the effectiveness or reactivity of the incoming group is termed nucleophilicity.^{1,2} In order to correlate an empirical scale of nucleophilicity a standard reaction was used:^{21,22}



$$\text{Rate} = (k_1 + k_2[\text{Y}^-])[\text{Pt}(\text{py}_2)\text{Cl}_2] \quad \dots 2.12$$

And the nucleophilicity of the incoming group, n_{Pt} , is determined by $n_{Pt} = \log(k_2/k_1)$.^{1,2,23} Since k_2 has the units of $\text{L mol}^{-1} \text{s}^{-1}$ and k_1 has units s^{-1} , it is necessary to change k_1 to a second-order constant by using the equation $k_1^0 = k_1/[\text{CH}_3\text{OH}]$.^{1,2,23} This produces a unitless nucleophilicity and hence, $n_{Pt}^0 = \log(k_2/k_1^0) = \log(k_2[\text{CH}_3\text{OH}]/k_1)$.^{1,2,23} The concentration of methanol at 30 °C is 24.90 mol L^{-1} and so $n_{Pt}^0 = n_{Pt} + 1.40$. Table 2.1 below shows a number of important n_{Pt}^0 values.²

Table 2.1: Nucleophilicity scale of selected nucleophiles.²

Nucleophile	Donor atom	η
CH ₃ OH	O	0
F ⁻	F	2.2
Cl ⁻	Cl	3.04
NH ₃	N	3.07
Pyridine	N	3.19
NO ₂ ⁻	N	3.22
N ₃ ⁻	N	23.58
Br ⁻	Br	4.18
(CH ₃) ₄ S	S	5.14
Ph ₃ Sb	Sb	6.79
Ph ₃ As	As	6.89
CN ⁻	C	7.14
Ph ₃ P	P	8.93

From this table a number of interesting trends can be observed. It can be seen from the table that the nucleophilicity of halides decreases down the order, $\text{I}^- > \text{Br}^- > \text{Cl}^- > \text{F}^-$ (values are highlighted in yellow).^{1,2} It is also important to note that the Group 15 bases (except amines) are all excellent nucleophiles towards Pt(II) but nucleophilicity does decrease in the order phosphines > arsines > stibines > amines (values highlighted in green) while hydroxides are too weak to produce a k_2 term.^{1,2} No relationship can be found between n_{Pt}^0 (kinetic) and $\text{p}K_{\text{a}}$ (thermodynamic).^{1,2} In general, the most reactive nucleophiles are “soft” (this refers to species which are large, have low charge states and are strongly polarizable) which is why sulfur is a better donor than oxygen.^{1,2,24-27}

The nucleophilicity reaction sequence does not only apply to the standard reaction but can be quantitatively used to describe a wide range of platinum(II) complexes.^{1,2}

There is a linear relationship between $\log k_2$ and n_{Pt}^0 for a specific nucleophile which can be described as,



$$\log k_2 = S. n_{Pt}^0 + C \quad \dots 2.14$$

where k_2 = second-order rate constant for the nucleophile, Y

S = nucleophilic discrimination factor

C = intrinsic reactivity and $C = \log k_1 - 1.40$ (intrinsic reactivity can only be used effectively in reactions carried out in methanol.)^{1,2}

Certain nucleophiles, viz NO_2^- and $SeCN^-$, do not follow the linear relationship described above as their nucleophilicity changes depending on the substrate.^{1,2} For example, the nucleophile might be less effective than expected from the n_{Pt}^0 value when the effective nuclear charge of platinum is high while it might be more effective than expected if the nuclear charge of platinum is low.^{1,2} Another reason for a change in the nucleophilicity sequence is due to increases in steric influence where the size and shape of the nucleophile is, the more dominant the n_{Pt}^0 value.^{1,2}

Nature of the *Trans* Ligand

Another factor that is important in determining the rate of substitution in a square planar complex is the effect of the *trans* ligand. In synthetic chemistry, it was discovered that some ligands could encourage substitution *trans* to themselves in square planar platinum(II) complexes.^{1,2,6,15} This enabled synthetic chemists to set up an order of effectiveness of these *trans* ligands which was maintained irrespective of the nature of the reaction.^{1,2,6,15} This phenomenon was introduced by Chernayev as the *trans* effect and is defined as ‘the effect of a coordinated ligand on the rate of replacement of a ligand *trans* to itself’.^{1,15} These groups labilise a ligand *trans* to themselves in order to facilitate substitution, *Figure 2.5*. Thus, complexes in which the *trans* group influences the rate far more than the *cis* groups are considered to show the *trans* effect.¹⁵

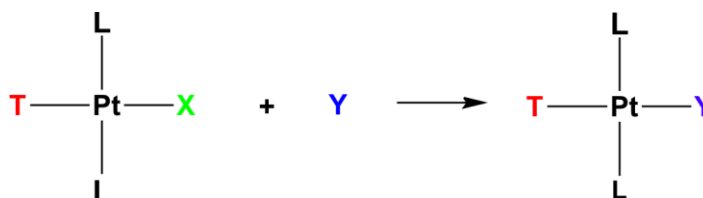
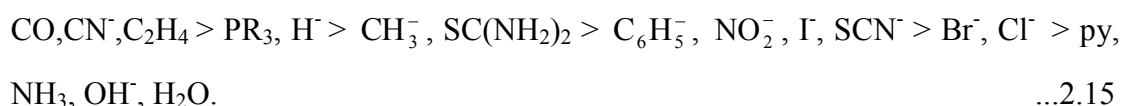


Figure 2.5: Diagrammatic representation of the ability of a ligand (**T**) to labilise the group *trans* to itself (**X**).¹⁵

The approximate order of decreasing *trans* effect is:^{1,2,4,15,28-32}



Kinetically, the *trans* effect can be large; a difference in rate of reaction of a factor of 10^6 can be found between a complex containing a good *trans* ligand and a poor *trans* ligand.¹⁵

It is important to differentiate between the *trans* effect and the *trans* influence of a ligand. The *trans* effect involves the effect of the ligand on the rate of substitution of the *trans* ligand, this involves both the ground and transition state.⁶ The *trans* influence is the effect of the *trans* ligand only on the ground state properties such as bond lengths or infrared stretching frequencies.⁶

There have been many theories to try and explain the *trans* effect. One such theory, postulated by Grinberg³³, is based on polarization and focuses on bond weakening. Grinberg's theory states that the primary charge on the Pt(II) induces a dipole in the *trans* ligand, which then induces a dipole in the metal.³³ This second dipole repels the negative charge in the leaving group, **X**, which causes the **Pt–X** bond to lengthen and weaken. Figure 2.6 shows the arrangement of the induced dipoles. There is indeed a link between the *trans* influence of **T** and its polarizability e.g. $\text{H}^- \sim \text{I}^- > \text{Cl}^-$.¹⁵ There are, however, objections to this electrostatic theory which include the fact that the induced dipole on Pt(II) should depend on the distance from **T** (greater for a smaller distance) and should depend on the net charge of **T** more strongly than on its induced dipole moment.¹⁵ This would lead to Cl^- having a greater *trans* effect than I^- which is not true. However, this objection can be removed if covalent bonding is taken into account as highly polarizing ligands will also form more covalent bonds to Pt(II).¹⁵

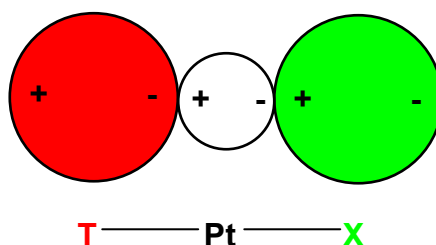


Figure 2.6: Induced dipoles over **T-Pt-X**.¹⁵

Another attempt to explain the *trans* effect is the π -bonding theory. This theory states that ligands with π -bonds such as C_2H_4 , PR_3 and CO stabilize the transition state for a reaction and are therefore high in the *trans* effect series.^{1,2,6,15} A σ bond is formed between the ligand and metal by the donation of a pair of electrons from the ligand to the metal centre and the π bond by the overlap of a filled d orbital of the platinum and a vacant orbital of the ligand.¹⁵ In the ground state, it would appear that the removal of electrons from the metal by the π bonding would actually strengthen bonds of the other ligands instead of weakening the **Pt-X** bond.¹⁵ Chatt *et al.*³⁴ and later Orgel^{35,36} proposed π bonding stabilization of the trigonal bipyramidal intermediate in the transition state to explain the *trans* effect. Chatt stated that in the transition state, the incoming group brings in extra electron density and the removal of this added charge from Pt(II) by π bonding of **T** will enhance the addition of **Y** and the reaction will happen more rapidly as the activation energy is lowered, Figure 2.7.^{1,2} Orgell supports this, stating that π bonding reduces the electron density on Pt(II) along the **Pt-X** and **Pt-Y** direction which will lead to a retention of configuration.¹⁵ This is known as the π -*trans* effect.

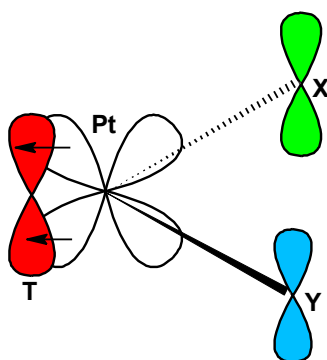


Figure 2.7: π -backdonation from full metal d -orbitals to vacant orbitals of the *trans* ligand.¹⁵

Molecular orbital (MO) theory supports the π -*trans* effect. A simplified MO diagram of $[\text{PtCl}_4]^{2-}$ is shown in Figure 2.8^{15,37} The most stable orbitals are the σ bonding orbitals and the next most stable orbitals are the π bonding molecular orbitals, all of

which are mainly located on the four chlorines.^{15,37} The next orbitals are the relatively stable antibonding orbitals, π_{xz}^* , π_{yz}^* , $\pi_{z^2}^*$, $\sigma_{z^2}^*$ and π_{xy}^* and the comparatively unstable $\sigma_{x^2-y^2}^*$ which come from the $5d$ atomic orbitals of Pt(II).^{15,37} At higher energy are the antibonding orbitals σ_s^* , σ_x^* , σ_y^* and σ_z^* .^{15,37} In a square planar complex, π_{xz}^* , π_{yz}^* and π_{xy}^* are the only orbitals with the correct orientation for π bonding.⁴⁵ With the formation of the trigonal bipyramidal intermediate on the addition of **Y**, π_{xz}^* , π_{yz}^* , π_{xy}^* and $\pi_{x^2-y^2}^*$ are now in the correct orientation for π interactions and are shared in π bonding with the three ligands, **T**, **X** and **Y** in the trigonal plane.¹⁵ The *trans* ligand can thus greatly stabilize the transition state if it is capable of bonding to the π^* orbitals and delocalize the electronic charge to lower the energy.¹⁵ It is the transition state that is stabilized as there are more filled π^* orbitals in the transition state than in the ground state. Thus a good *trans* π -acceptor ligand will lower the activation energy for the reaction.

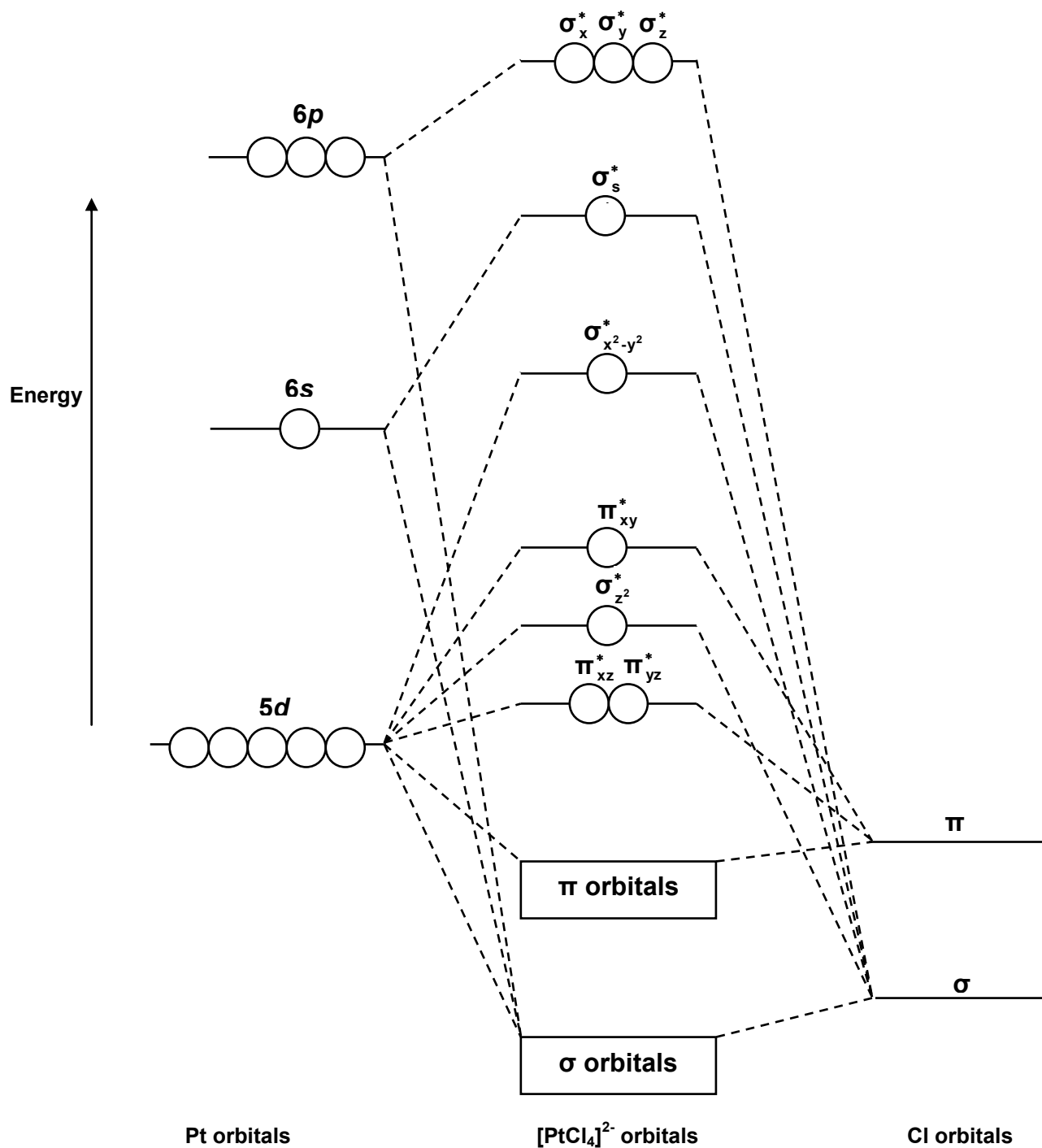


Figure 2.8: Molecular orbital diagram of $[\text{PtCl}_4]^{2-}$.^{15,37}

Langford and Gray⁴ have given an explanation for the increased stabilization of the trigonal bipyramidal intermediate using σ bonding.^{1,15} In the ground state of a square planar complex, there is only one p -orbital (p_x) used to bond T-Pt-X , addition of the entering group, causes X to move out of the x -axis into the trigonal plane.^{1,15} This

trigonal plane has two p -orbitals, p_x and p_z increasing the number of orbitals available for bonding. Thus, in the ground state there was only one p -orbital bonding two ligands but in the transition state there are two orbitals bonding three ligands, leading to increased stability of the transition state, *Figure 2.9*.^{1,15} This means that good σ -bonding ligands which can donate into the extra p -orbitals can stabilize the σ structure in the transition state.^{1,15} This effect is known as the σ trans effect.⁴

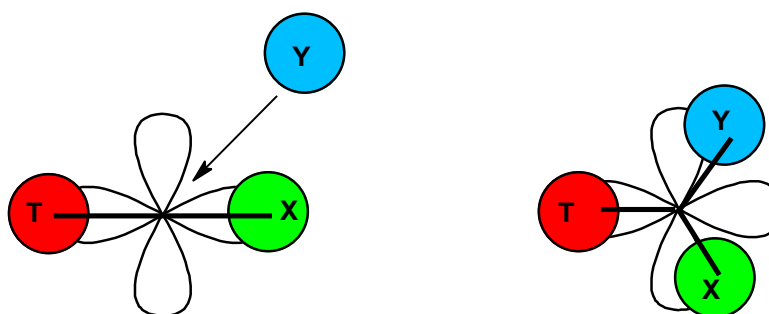


Figure 2.9: The Langford and Gray model for the *trans* effect.¹

The ground state stability of a complex can also be affected by σ bonding.¹⁵ As previously discussed, in the ground state, the *trans* ligand and the leaving group share the same p_x orbital, *Figure 2.10*. A strong σ donor *trans* ligand, such as H^- and CH_3^- , would donate more electron density to the shared p -orbital, thus strengthening the $T-Pt$ bond and weakening the $Pt-X$ bond which increases the rate of the reaction.¹⁵

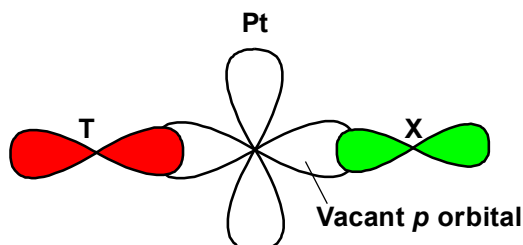


Figure 2.10: Donation of electrons into the empty p -orbital of the metal by the *trans* and leaving groups of the square planar metal complex.¹⁵

Nature of the *cis* Ligand

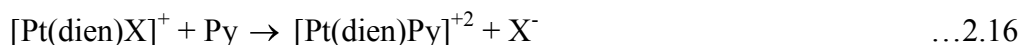
There are few reports on the *cis* effect with results often being contradictory³⁸⁻⁴⁰; however, the general consensus is that in comparison to the *trans* effect, the effect of the *cis* ligand is very weak.^{1,2,6} The only time the *cis* effect becomes significant is when steric factors are involved as steric hindrance will have a greater effect from the *cis* position than from the *trans* position.¹ This becomes more pronounced in the

trigonal bipyramidal transition state as the *trans* group is in the equatorial plane with an angle of 120° between it and the incoming and leaving groups while the axial *cis* ligands are separated from the incoming and leaving groups by only 90°. The increase of steric size causes a decrease in the rate of substitution for an associative reaction.¹

Van Eldik and co-workers⁴¹ studied the reaction kinetics of the complexes [Pt(6-phenyl-2,2'-bipy)Cl], [Pt(1,3-di(2-pyridyl)benzene)Cl] and [Pt(terpy)Cl] with TU, DMTU and TMTU. When the Pt–C bond was in the *trans* position the complex reacted much faster than the standard terpy complex and when the Pt–C bond was in the *cis* position to the leaving group the complex reacted much slower than the terpy complex. This suggests that the Pt–C bond in the *cis* position activates the metal centre in a different way to that in the *trans* position. Janganyi *et al.*⁴² obtained similar results.

Nature of the Leaving Group

The effect of the leaving group is very difficult to qualify as it is very closely connected with the nature of the incoming nucleophile and the *trans* ligand.² In a dissociative reaction the bond between the leaving group and the metal breaks in the transition state and therefore in these reactions there is a large dependence on the nature of the leaving group.^{2,6} However, for an associative reaction, the effect of the leaving group is dependent on the degree to which bond breaking occurs in the transition state.^{2,6} Each reaction differs in the extent to which bond breaking occurs in the transition. The effect of the leaving group on the following reaction has been studied in depth,^{10,43}



where the rate of substitution of **X** decreases in the order^{2,6}



This series is similar to the inverse of the *trans* effect which highlights the fact that as the *trans* effect depends on the strength of bonding, the more strongly bound ligands dissociate more slowly from the five-coordinate intermediate.⁶

Nature of the Metal Centre

The nature of the reaction centre also affects the rate of substitution of square planar complexes. To ensure that effects are due only to a change in metal centre, only the reactivities of isovalent ions can be compared.² Thus, the only d^8 isovalent ions that can be compared are Ni(II), Pd(II), Pt(II) and Co(I), Rh(I) and Ir(I). The general sequence that has been determined is Ni > Pd > Pt in the ratio 10^7 - 10^8 : 10^5 - 10^6 :1.^{2,44} There have been no other adequate comparisons made although Tobe² predicts that the smaller the effective nuclear charge on the metal, the greater the relative stability of the five-coordinate intermediate and thus Ir(I) > Pt(II) > Au(III).²

2.3.4 The Dissociative Mechanism in Square Planar Complexes

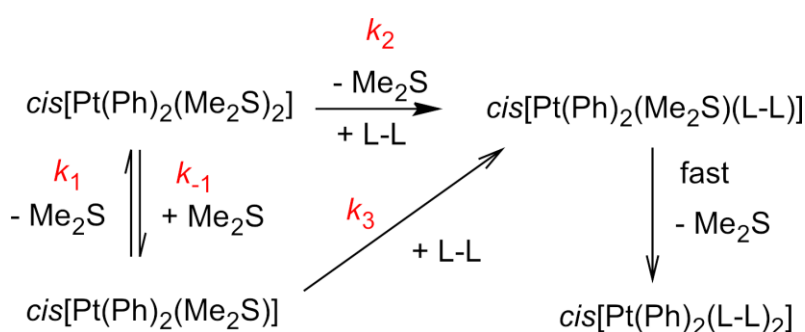
As it has already been discussed, a dissociative mechanism is not the favoured pathway for substitution of square planar complexes; however, it can be encouraged by following one or more of the following methods: promote bond weakening, stabilize the intermediate of lower coordination number or prevent bond formation.^{2,45} In theory this can be done by using either electronic or steric effects.^{2,45}

Weakly electronegative ligands can cause bond weakening of the *trans* metal-ligand bond by forming very strong bonds to the metal.² However, there is no evidence that this causes a change in mechanism.²

Much investigation has gone into the use of steric hindrance to disfavour the associative mechanism. As the transition state for an associative reaction is more crowded than the ground state, if sterically bulky ligands were chosen in the ground state, then the associative mechanism will be hindered.^{1,2} The transition state for the dissociative mechanism is less crowded than the ground state; therefore the choice of bulky ligands in the ground state should speed up the reaction to relieve the strain.^{1,2}

There has been some success when using *N*-substituted diethylenetriamine.² The ethyl groups in $[M(\text{Et}_4\text{dien})\text{X}]^+$ block the metal making an associative mechanism difficult to follow.² It is believed that the steric hindrance has allowed the reaction to follow the less favourable dissociative mechanism.² There is not a complete mechanism changeover as five-coordinate complexes of Co(II) and Ni(II) with Et₄dien have been reported.²

Romeo *et al.*^{46,47} have reported a dissociative mechanism. They studied the substitution reactions of *cis*-PtR₂S₂ (R = Me, Ph; S = SMe₂, S(O)Me₂) with L-L (L-L = 2,2'-bipyridine, 2,2'-bipyrimidine, 1,10-phenanthroline, 1,2-bis(diphenylphosphino)ethane) in aprotic solvents such as benzene and chloroform. Scheme 2.3 illustrates the reaction mechanism that is occurring in these reactions. There is the dissociative loss of Me₂S in the k_1 path to yield a 3-coordinate 14-electron intermediate. This can either be converted back to the original species with the readdition of the Me₂S group or it can react with L-L via k_3 pathway to form an open-ring sulfide species. This species can also be formed by a parallel associative attack of L-L on the starting complex (k_2 , path). The dissociative pathway is supported by the positive volumes of activation obtained. These complexes fulfil two important criteria to produce a dissociative mechanism: they prevent bond formation by means of sterically hindered ligands and they promote bond weakening by making use of strong σ -donor *trans* activating ligands.

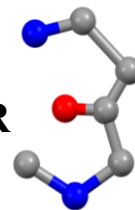


Scheme 2.3: Predicted mechanism for the substitution reaction of *cis*[Pt(Ph)₂(Me₂S)₂] with L-L.^{46,47}

2. 4 References

1. M. L. Tobe and J. Burgess, *Inorganic Reaction Mechanisms*, Addison Wesley Longman Limited, New York, 1999, pgs 30-43, 70-112.
2. M. L. Tobe, *Inorganic Reaction Mechanisms Studies in Modern Chemistry*, Nelson, London, 1972, pgs 17-23, 42-68.
3. C. K. Ingold, *Structure and Mechanism in Organic Chemistry*, Bell, London, and Cornell University Press, Ithaca, NY, 1953, 315.
4. C. H. Langford and H. B. Gray, *Ligand Substitution Processes*, Benjamin, New York, 1966.
5. S. Ašperger, *Chemical Kinetics and Inorganic Reaction mechanisms* 2nd edition, Kluwer Academic/Plenum Publishers, New York, 2003, pgs 28-35.
6. J. D. Atwood, *Inorganic and Organometallic Reaction Mechanisms* 2nd edition, Wiley-VCH, Inc., Canada, 1997, pgs 43-62.
7. R. B. Jordan, *Reaction Mechanisms of Inorganic and Organometallic Systems*, Oxford University Press Inc., 1991, pgs 29-74.
8. R. G. Wilkins, *Kinetics and Mechanism of Reactions Transition Metal Complexes* 2nd edition, VCH, Weinheim, , 1991, pgs 199-201, 221, 232-242.
9. F. Basolo, *Coord. Chem. Rev.*, 1996, 151.
10. F. Basolo, H. B. Gray, R.G. Pearson, *Dalton Trans.*, 1960, **82**, 4200.
11. B. V. Petrovic, M. I. Djuran, Z. D. Bugarcic, *Metal-Based Drugs*, 1999, **6**, 355.
12. S. D. Cummings, *Coord. Chem. Rev.*, 2009, 253, 449.
13. R. Romeo, *Comment Inorg. Chem.*, 1990, **11**, 21.
14. G. Faraone, V. Ricevuto, R. Romeo, M. Trozzi, *J. Chem. Soc.*, 1971, 1877.
15. F. Basolo and R.G. Pearson, 'Mechanisms of Inorganic Reactions. A Study of Metal Complexes in Solution' 2nd edition', John Wiley and Sons, Inc, 1967 USA, pgs 351-410.
16. F. Basolo, J. Chatt, H. B. Gray, R. G. Pearson and B. L. Shaw, *J. Chem. Soc.*, 1961, 2207.
17. A. L. Odell and H. A. Raethel, *J. Chem. Soc., Chem Commun*, 1968, 1323.
18. H. B. Gray and R. J. Olcott, *Inorg. Chem.*, 1962, **1**, 481.
19. R. van Eldik, *Mech. Inorg. Organomet. Reactions*, 1994, **8**, 399.
20. D. A. Palmer and H. Kelm, *Inorg. Chim. Acta.*, 1976, **19**, 117.
21. C. G. Swain and C. B. Scott, *J. Am. Chem. Soc.*, 1953, **85**, 141.

22. U. Belluco, L. Cattalini, F. Basolo, R. G. Pearson and A. Turco, *J. Am. Chem. Soc.*, 1965, **87**, 241.
23. D. K. Lin and C. S. Garner, *J. Am. Chem. Soc.*, 1969, **91**, 6637.
24. F. A. Cotton, G. Wilkinson and P. L. Gaus, *Basic Inorganic Chemistry* 3rd edition, John Wiley & Sons, New York, 1995, pgs 228-229.
25. R. G. Pearson, *J. Am. Chem. Soc.*, 1963, **85**, 3533.
26. R. G. Pearson, *J. Chem. Edu.*, 1968, **45**, 643.
27. R. G. Pearson, *J. Chem. Edu.*, 1987, **64**, 561.
28. F. A. Cotton, L. M. Daniels, C. A. Murillo and J. F. Quesada, *Inorg. Chem.*, 1993, **32**, 4861.
29. I. I. Chernyaev, *Ann. inst. platine USSR*, 1926, **4**, 261.
30. I. I. Chernyaev, *Ann. inst. platine. USSR*, 1926, **4**, 243.
31. I. I. Chernyaev, *Ann. inst. platine. USSR*, 1927, **5**, 102.
32. I. I. Chernyaev, *Ann. inst. platine. USSR*, 1928, **6**, 55.
33. A. A. Grinberg, *Acta Physicochim*, 1935, **3**, 573.
34. J. Chatt, L. A. Duncanson and L. M. Venanzi, *J. Chem. Soc.*, 1955, 1955.
35. L. E. Orgel, *J. Inorg. Nucl. Chem*, 1956, **2**, 137.
36. J. Chatt, G. A. Gamlen and L. E Orgel, *J. Am. Chem. Soc.*, 1959, 486.
37. C. W. Schwietert and J. P. McCue, *Coord. Chem. Rev.* 1999, **184**, 89.
38. D. Jaganyi, A. Hofmann and R. van Eldik, *Angew. Chem., Int. Ed.*, 2001, **40**, 1680.
39. A. Hofmann, D. Jaganyi, O. Q. Munro, G. Liehr and R. van Eldik, *Inorg. Chem*, 2003, **42**, 1688.
40. J. K. Burdett, *Inorg. Chem.*, 1977, **16**, 3013.
41. A. Hofmann, L. Dahlenburg and R. van Eldik, *Inorg. Chem.*, 2003, **42**, 6528.
42. D. Jaganyi, D. Reddy, J. A. Gertenbach, A. Hofmann and R. van Eldik, *Dalton Trans.*, 2004, 299.
43. H. G. Gray and R. J. Olcott, *Inorg Chem*, 1962, **1**, 481.
44. J. J. Pesek and W. R. Mason, *Inorg. Chem*, 1983, **22**, 2958.
45. R. Romeo, *Comments Inorg. Chem.*, 1990, **11**, 21.
46. G. Alibrandi, G. Bruno, S. Lanza, R. Romeo and M. L. Tobe, *Inorg. Chem.*, 1987, **26**, 185.
47. U. Frey, L. Helm, A. E. Merbach and R. Romeo, *J. Am. Chem. Soc.*, 1989, 8161.



3.1 Introduction

One of the cornerstones in chemistry is the chemical reaction, whereby reactants are converted to products and a balanced or stoichiometric equation can be written for the reaction.¹ Quantitative studies of chemical reactions may fall into one of two groups:

- i) The first group involves studies related to the actual occurrence of the reaction.¹ These studies are known as thermodynamic methods and are performed on systems that are at a steady state with static concentrations. This study does not take into account how quickly or how slowly a chemical reaction takes place but rather the direction a reaction will proceed.^{1,2} Thermodynamic methods measure quantities such as the standard enthalpy change or the standard Gibbs energy change of a reaction.^{1,3}
- ii) The second group involves studies related to how fast a chemical reaction occurs and, unlike thermodynamic studies, uses time as a variable.^{1,2} These studies are known as chemical kinetics where measurements are made under dynamic conditions in which the concentrations of the reactants and products are changing as a function of time.^{1,2} These measurements lead to the determination of the reaction rate.

This second group of studies, chemical kinetics, is the focus of this chapter and in fact the focus of this thesis. Chemists not only use the term kinetics to explain the studies of a reaction and its parameters but also to understand the factors that influence how quickly a reaction will take place.¹ Thus, kinetics involves not only experimental measurements but empirical and theoretical methods to interpret these measurements.¹

Using kinetic methods has many advantages and its importance must not be underestimated. Kinetic studies of the rate of a reaction using a range of factors can allow for the prediction of how rapidly a reaction would proceed under hypothetical conditions.¹ Another important aspect of kinetic methods is that it provides some of the information needed to determine the mechanism of a reaction.^{1,4} Kinetic methods allow many more chemical reactions to be used for analytical purposes because it can make use of reactions that are too slow for thermodynamic studies.² Kinetic methods encompass many systems such as: complexation reactions, acid-base reactions, redox reactions.²

There are many factors that influence the rate of a chemical reaction and these include: concentration of reactants, ionic strength of a solution, pH, solvent, temperature and pressure.⁵

- An increase in concentration of a reagent will lead to an increase in the rate of the reaction. Thus, controlling and understanding the effect that the concentration has on a reaction is very important in a kinetic study.
- Maintaining the ionic strength of a solution ensures that the total concentration of ions and the charge in the solution is constant when a reaction takes place.
- A pH study of a reaction will allow for the determination of the pK_a of a molecule. Below their pK_a , molecules remain aquated but will lose a proton at a pH above the pK_a . The two forms of the molecule at different pH may react differently.
- Solvents play a role in a chemical reaction in that they can either directly affect a reaction by acting as a reactant or the solvent may form a solvent cage around the molecule thereby changing the kinetics of a reaction.
- From temperature dependent studies the entropy and enthalpy of a reaction gets determined. The enthalpy and entropy can give an indication of the substitution mechanism for the reaction.
- From pressure dependent studies the volume of activation is determined, leading to the assignment of a mechanism for the reaction.

Thus, in order to study the kinetics of a chemical reaction, these factors need to be controlled and their effects on the reaction needs to be quantified.

3.2 The Rate Law

The rate of reaction can be defined as the amount of reactant converted to product in a specified period of time. The units of rate are generally stated as molarity per second (M s^{-1}).^{6,7}

$$\text{Rate} = -\frac{d[\text{reactant}]}{dt} = \frac{d[\text{product}]}{dt} \quad \dots 3.1$$

The rate law describes the dependence of the reaction rate on the reagent concentrations.^{6,7} The rate law has the general form:

$$\text{Rate} = k[X]^m[Y]^n \quad \dots 3.2$$

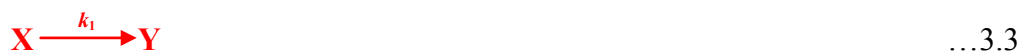
where k is the rate constant whose units depend on the rate law and the exponents m and n are experimentally determined. The exponents in the rate law are not necessarily linked to stoichiometric coefficients in balanced reactions.^{6,7} The rate law is important as it gives information on the concentrations of reagents needed to get to the product by the lowest energy pathway.^{6,7}

The order of a rate law is described as the sum of the exponents in the rate law.^{6,7}

3.3 Integrated Rate Laws

3.3.1 First Order Reactions

First order reactions are the least complicated type of reaction to interpret and therefore most reaction conditions are manipulated in order to allow reactions to follow first order reaction kinetics.^{6,7} A first-order reaction,



will have the following rate law:

$$\text{Rate} = -\frac{d[X]}{dt} = k_1[X] \quad \dots 3.4$$

which can be rearranged to give:

$$\frac{-d[X]}{[X]} = k_1 dt \quad \dots 3.5$$

Equation 3.5 can be integrated from time at 0 ($t = 0$) to any time, t ($t = t$)

$$\int_{[X]_0}^{[X]_t} \frac{d[X]}{[X]} = -k_1 \int_0^t dt \quad \dots 3.6$$

$$\ln \frac{[X]_t}{[X]_0} = -k_1 t \quad \dots 3.7$$

$$\ln [X]_t = -k_1 t + \ln [X]_0 \quad \dots 3.8$$

Hence, as Equation 3.8 represents a straight line, a plot of $\ln[X]_t$ versus t gives a straight line with a slope of $-k_1$ (rate constant).^{6,7}

In a first-order rate law any factor that is proportional to concentration, such as absorbance, volume, pressure and conductivity can be used directly to measure the first order rate constant.⁵⁻⁷ For example when a reaction is characterized by a change in absorbance from A_0 to A_∞ during the reaction then,

$$\ln \frac{[X]_t}{[X]_0} = \ln \frac{A_t}{A_0} = -k_1 t \quad \dots 3.9$$

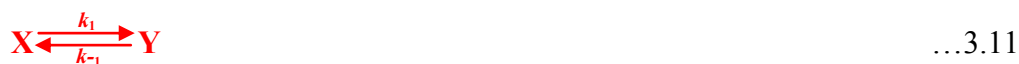
$$\ln A_t = -k_1 t + \ln(A_0) \quad \dots 3.10$$

Where A_0 , A_t and A_∞ are the absorbance measurements for the reactant X at time $t = 0$, t and ∞ respectively.

Thus, a plot of $\ln(A_t)$ versus t can be used to determine k_1 .

3.3.2 Reversible First Order Reactions

Certain reactions form an equilibrium where some of the product formed is converted back into starting material and the reaction is described as reversible^{6,7}, such as *Equation 3.11*.



The rate law for the above reaction would be in the form of:

$$\begin{aligned} \text{Rate} &= \frac{d[Y]}{dt} = \frac{d[X]}{dt} \\ &= k_1[X] - k_{-1}[Y] \end{aligned} \quad \dots 3.12$$

At time $t = 0$, no product has formed, hence $[Y]_0 = 0$ and $[X]_t = [X]_0$, therefore at any time during the reaction:

$$[X] = [X]_0 - [Y] \quad \dots 3.13$$

The substitution of *Equation 3.13* into *Equation 3.12* yields:

$$-\frac{d[X]}{dt} = k_1[X] - k_{-1}([X]_0 - [X]) \quad \dots 3.14$$

As no net reaction occurs at equilibrium:

$$-\frac{d[X]}{dt} = 0 \quad \dots 3.15$$

Substituting *Equation 3.14* into *Equation 3.12* and applying *Equation 3.15*, results in:

$$k_1[X]_{eqm} = k_{-1}[Y]_{eqm} = k_{-1}([X]_0 - [X]_{eqm}) \quad \dots 3.16$$

which can also be written as:

$$[X]_0 = \frac{k_1 + k_{-1}}{k_{-1}} [X]_{eqm} \quad \dots 3.17$$

The substitution of Equation 3.17 into 3.14, gives the following:

$$-\frac{d[X]}{dt} = k_1 + k_{-1}[X] - k_1 + k_{-1}[X]_{eqm} \quad \dots 3.18$$

Separation of the variables, results in the following expression:

$$\frac{d[X]}{[X] - [X]_{eqm}} = -(k_1 + k_{-1})dt \quad \dots 3.19$$

Integrating this equation from $t = 0$ to $t = t$:

$$\int_{[X]_0}^{[X]_t} \frac{d[X]}{[X] - [X]_{eqm}} = -(k_1 + k_{-1}) \int_0^t dt \quad \dots 3.20$$

$$\ln \left(\frac{[X]_t - [X]_{eqm}}{[X]_0 - [X]_{eqm}} \right) = -(k_1 + k_{-1})t \quad \dots 3.21$$

Rearrangement of Equation 3.21 results in:

$$\ln([X]_t - [X]_{eqm}) = -(k_1 + k_{-1})t + \ln([X]_0 - [X]_{eqm}) \quad \dots 3.22$$

As Equation 3.22 is in the form of the linear equation $y = mx + c$, a plot of $\ln([X]_t - [X]_{eqm})$ versus t is a straight line with a slope of $-(k_1 + k_{-1})$.^{6,7} A problem of first-order reversible reactions is that it is difficult to measure $[X]_{eqm}$ accurately.⁵⁻⁷

The equilibrium constant is a ratio of the concentration of products formed and starting material left at equilibrium and therefore the equilibrium constant can be related to the individual rate constants in the following manner:

$$K_{eqm} = \frac{k_1}{k_{-1}} \quad \dots 3.23$$

The observed rate constant, k_{obs} , is the sum of the two individual rate constants:

$$k_{obs} = k_1 + k_{-1} \quad \dots 3.24$$

3.3.3 Second Order Reactions

Second order kinetics is widely used for interpreting the reactions of complexes.^{6,7} A second order reaction which is first order with respect to each of the two starting materials in a bimolecular reaction is described in the reaction equation below:



The above second order reaction has the following rate law:

$$\frac{d[Z]}{dt} = - \frac{d[X]}{dt} = - \frac{d[Y]}{dt} = k_2[X]_t[Y]_t \quad \dots 3.26$$

Equation 3.26 can be rewritten as follows:

$$\frac{d[X]}{[X]_t[Y]_t} = - k_2 dt \quad \dots 3.27$$

Following reaction stoichiometry, if the initial concentrations of X and Y are $[X]_0$ and $[Y]_0$, then when the concentration of X drops to $[X]_0 - x$, where x refers to the amount of Z produced at time t , the concentration of Y must drop to $[Y]_0 - x$. The rate equation for the reaction can thus be rewritten⁸:

$$- \frac{d[X]}{dt} = k_2([X]_0 - x)([Y]_0 - x) \quad \dots 3.28$$

As $[X]_t = [X]_0 - x$, it means that $-\frac{d[X]}{dt} = \frac{dx}{dt}$ and hence Equation 3.28 can be expressed as:

$$\frac{dx}{dt} = k_2([X]_0 - x)([Y]_0 - x) \quad \dots 3.29$$

or

$$\frac{dx}{([X]_0 - x)([Y]_0 - x)} = k_2 dt \quad \dots 3.30$$

Integrating *Equation 3.30* between the limits $x = 0$ and $x = x$ gives the following equation:

$$\int_0^x \frac{dx}{([X]_0 - x)([Y]_0 - x)} = k_2 \int_0^t dt \quad \dots 3.31$$

which affords *Equation 3.32* (as long as $[X]_0$ not equal to $[Y]_0$):

$$\frac{1}{[X]_0 - [Y]_0} \ln \frac{[Y]_0([X]_0 - x)}{[X]_0([Y]_0 - x)} = k_2 t \quad \dots 3.32$$

Equation 3.32 can be simplified to:

$$\frac{1}{[X]_0 - [Y]_0} \ln \frac{[Y]_0[X]_t}{[X]_0[Y]_t} = k_2 t \quad \dots 3.33$$

This equation is in the form $y = mx + c$ with a slope of k_2 ($M^{-1}s^{-1}$) and y-intercept = 0 i.e. line passes through the origin. However, in order to plot the graph $[X]_0$, $[Y]_0$, $[X]_t$ and $[Y]_t$ must be known which can make the kinetic experiment time-consuming and unnecessarily involving and complicated.^{6,7} The experiments can be optimised by using the first-order rate law as it has fewer variables to determine, leading to a more reliable rate constant. This can be achieved by using *pseudo* first-order conditions.⁵⁻⁸ The *pseudo* first-order condition is whereby one of the reactants is in large excess, i.e. $[Y]_0 \gg [X]_0$ (at least 10-fold excess). Thus the concentration of Y remains essentially constant during the reaction. Under *pseudo* first-order conditions the rate law simplifies to a first order rate law.⁵⁻⁸

Using *pseudo* first-order conditions, *Equation 3.26* can be expressed as:

$$\begin{aligned} -\frac{d[X]}{dt} &= k_2[X]_t[Y]_t = k_2[Y]_0[X]_t \\ &= k_{obs}[X]_t \end{aligned} \quad \dots 3.34$$

with $k_{obs} = k_2[Y]_0$

Plotting $\ln[X]$ versus time gives a straight line with a slope of k_{obs} . A series of k_{obs} values can be determined by varying the concentration of Y .⁵⁻⁸ Then using $k_{\text{obs}} = k_2[Y]_0$, a plot of k_{obs} vs $[Y]_0$ will give a straight line with a slope of k_2 .⁵⁻⁸

3.3.4 Reversible Second Order Reactions

Some second order reactions may not go to completion leading to the formation of an equilibrium:



The reaction exhibits mixed order behaviour as the forward reaction is second order while the reverse reaction is first order. By selecting *pseudo* first-order conditions for the forward reaction, $[Y]_0 \gg [X]_0$, this problem of mixed orders can be avoided.^{6,7} Thus the equation can be simplified to a reversible first order reaction.

Using *pseudo* first-order conditions, the rate law can be written as follows:

$$-\frac{d[X]}{dt} = -\frac{d[Y]}{dt} = \frac{d[Z]}{dt} = k_2[X]_t[Y]_t - k_{-2}[Z]_t \quad \dots 3.36$$

To simplify this equation, it can be assumed that there is no product present initially and that the stoichiometry is 1:1:1, so that at any time, t , the mass balance must be:

$$[X]_t = [X]_0 - [Z]_t$$

and $[Y]_t = [Y]_0 - [Z]_t \quad \dots 3.37$

At equilibrium:

$$[X]_{\text{eqm}} = [X]_0 - [Z]_{\text{eqm}}$$

and $[Y]_{\text{eqm}} = [Y]_0 - [Z]_{\text{eqm}} \quad \dots 3.38$

From *Equations 3.37 and 3.38*,

$$[Z]_t = [X]_0 - [X]_t$$

and $[Z]_{eqm} = [X]_0 - [X]_{eqm}$...3.39

If the stoichiometry is not 1:1:1 then the appropriate stoichiometric coefficients must be used in the mass balance equations and in the rate law.

It is convenient to note that the forward and reverse rates are equal at equilibrium, which means that:

$$-\frac{d[X]}{dt} = k_2[X]_{eqm}[Y]_{eqm} - k_{-1}[Z]_{eqm} = 0$$
 ...3.40

And hence,

$$k_2[X]_{eqm}[Y]_{eqm} = k_{-1}[Z]_{eqm}$$
 ...3.41

Using *Equation 3.39*, *Equation 3.41* can be re-written as:

$$k_2[X]_{eqm}[Y]_{eqm} = k_{-1}([X]_0 - [X]_{eqm})$$
 ...3.42

Rearranging *Equation 3.42* leads to:

$$k_{-1}[X]_0 = k_2[X]_{eqm}[Y]_{eqm} + k_{-1}[X]_{eqm}$$
 ...3.43

Substitution for $[Z]_t$ of *Equation 3.36* using expression of *Equation 3.39* and the replacement of the $k_2[X]_0$ term from *Equation 3.43* into *Equation 3.36* allows the rate equation to be written as:

$$-\frac{d[X]}{dt} = k_2[X]_t[Y]_t - k_2[X]_{eqm}[Y]_{eqm} - k_{-1}[X]_{eqm} + k_{-1}[X]_t$$
 ...3.44

Substituting $[Y]_t$ and $[Y]_{eqm}$ from *Equations 3.37 and 3.38* into *Equation 3.44* and using the approximations $k_2[X]_t[X]_0 \approx k_2[X]_{eqm}[X]_0$ and $k_2[A]_t^2 \approx k_2[X]_{eqm}^2$ gives:

$$\begin{aligned} -\frac{d[X]}{dt} &= k_2[X]_t[Y]_0 - k_2[X]_{eqm}[Y]_0 - k_{-1}[X]_{eqm} + k_{-1}[X]_t \\ &= (k_2[Y]_0 + k_{-1})([X]_t - [X]_{eqm}) \end{aligned}$$
 ...3.45

Rewriting Equation 3.45 in terms of X and integrating gives:

$$\int_{[X]_0}^{[X]_t} \frac{d[X]}{([X]_t - [X]_{eqm})} = -(k_2[Y]_0 + k_{-2}) \int_0^t dt \quad \dots 3.46$$

and hence

$$\ln \left(\frac{[X]_t - [X]_{eqm}}{[X]_0 - [X]_{eqm}} \right) = -(k_2[Y]_0 + k_{-2})t$$

$$= -k_{obs}t \quad \dots 3.47$$

$$\text{where } k_{obs} = k_2[Y]_0 + k_{-2}$$

Thus, plotting k_{obs} vs $[Y]_0$ gives a straight line with a slope k_2 and intercept k_{-2} .

The equilibrium constant can be calculated by determining the ratio:

$$K_{eqm} = \frac{k_2}{k_{-2}} \quad \dots 3.48$$

A reversible process as described leads to a two termed rate law. Another process which leads to this type of rate law is two parallel reaction paths where one is independent of $[Y]_0$.⁵⁻⁷

3.4 Temperature Dependence and Activation Parameters

A rate law is important in assigning a mechanism for a reaction. However, to gain more information about the energetics of a reaction, the temperature dependence of the rate constant is often studied.^{6,7} This results in the determination of a reaction's activation parameters. This may also involve, for more complex rate laws, a study of concentration dependence of the rate at various temperatures, to determine the temperature dependence of different species in the rate law.^{6,7} The experimental data for the rate constants can be analyzed in terms of the Arrhenius equation or transition state theory as described below.

3.4.1 Arrhenius Equation

Arrhenius discovered that rate constants have a temperature dependence comparable to that of equilibrium constants,^{6,7} stated as follows:

$$k = Ae^{\left(-\frac{E_a}{RT}\right)} \quad \dots 3.49$$

Where A is the Arrhenius pre-exponential factor, E_a is the Arrhenius activation energy (with units J mol^{-1}), R is the gas constant ($8.315 \text{ J K}^{-1} \text{ mol}^{-1}$) and T is absolute temperature (with units in Kelvin).

The rate constant, k , is determined by carrying out experiments at varying temperatures and it is always expected to increase with increasing temperature.^{6,7} A plot of $\ln k$ versus $\left(\frac{1}{T}\right)$ according to the following equation, which is the natural log of Equation 3.49,

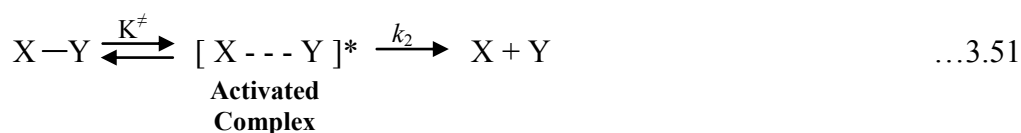
$$\ln k = \ln A - \frac{E_a}{RT} \left(\frac{1}{T}\right) \quad \dots 3.50$$

will be linear with a slope of $-\frac{E_a}{R}$ and intercept of $\ln A$. The Arrhenius equation is useful in systems where the experimental rate constant is thought to be a combination of rate constants.⁷

3.4.2 Transition State Theory

A similar relationship to that determined by Arrhenius is derived by the transition state theory. It is used exclusively in considering and understanding the kinetics of reactions in solution with concentration on the activated complex in the transition state.^{6,7}

Originally the transition state theory was developed for a simple dissociation process in the gas phase, assuming the reaction follows the mechanism shown below,^{7,9,10}



with a reaction rate as follows,

$$-\frac{d[X]}{dt} = \frac{k_b T}{h} [X \cdots Y]^\ddagger = \frac{k_b T}{h} K^\ddagger [X][Y] \quad \dots 3.52$$

where k_b is Boltzmann's constant ($1.38 \times 10^{-23} \text{ J K}^{-1}$), T is temperature (kelvin), h is Planck's constant ($6.626 \times 10^{-34} \text{ J s}^{-1}$) and K^\ddagger is the equilibrium constant.

The experimental second order rate constant k_2 can be written as:

$$k_2 = \frac{k_b T K^\ddagger}{h} \quad \dots 3.53$$

The free energy of activation, ΔG^\ddagger , can be written as:

$$\Delta G^\ddagger = -RT \ln K^\ddagger = \Delta H^\ddagger - T\Delta S^\ddagger \quad \dots 3.54$$

Where ΔH^\ddagger and ΔS^\ddagger are the changes in enthalpy and entropy of activation respectively.

Substitution of *Equation 3.54* into 3.53 gives the following expression:

$$k_2 = \frac{k_b T}{h} \exp\left(-\frac{\Delta G^\ddagger}{RT}\right) = \frac{k_b T}{h} \exp\left(-\frac{\Delta H^\ddagger}{RT}\right) \exp\left(\frac{\Delta S^\ddagger}{R}\right) \quad \dots 3.55$$

Taking the natural log of *Equation 3.55* results in *Equation 3.56*:

$$\ln\left(\frac{k_2}{T}\right) = \ln\left(\frac{k_b}{h}\right) - \frac{\Delta H^\ddagger}{RT} + \frac{\Delta S^\ddagger}{R} \quad \dots 3.56$$

Subsequent linearization gives:

$$\ln\left(\frac{k_2}{T}\right) = -\frac{\Delta H^\ddagger}{R} \cdot \frac{1}{T} + \left(\ln \frac{k_b}{h} + \frac{\Delta S^\ddagger}{R}\right) \quad \dots 3.57$$

where $\ln \frac{k_b}{h} = 23.8$.

A plot of $\ln\left(\frac{k_2}{T}\right)$ versus $\frac{1}{T}$ is called an Eyring plot.^{1,7,9} The slope of such a graph gives the enthalpy of activation, ΔH^\ddagger and the entropy, ΔS^\ddagger , can be calculated from the y-intercept.^{1,7,9}

Values for the activation parameters determined by different workers on the same system may not always agree. This is because in order to determine the entropy of activation there has to be a long extrapolation of Eyring plots to $\frac{1}{T} = 0$ which compromises the accuracy of the values obtained.^{6,7} This can be solved by using a wide range of temperatures or by determining the volume of activation (see *Section 3.4.3*) which is more accurate.^{6,7}

The enthalpy and entropy of activation are important for determining ‘extreme’ mechanisms of reactions in solution. A negative or very small enthalpy of activation indicates a multistep process that includes a pre-equilibrium.^{6,7,11} Large negative values of the activation parameters indicate an associative mechanism whereas large positive values are indicative of a dissociative mechanism as chaos increases due to bond breaking before complex formation.^{6,7,11}

3.4.3 Pressure Dependence and Volumes of Activation

In some cases the entropy and enthalpy of activation may be neither large and positive nor large and negative, making it difficult to infer a mechanism. A more decisive parameter for mechanistic assignment is the volume of activation.^{6,7,11} In order to determine the volume of activation, the effect of pressure on the rate of reaction needs to be determined.^{6,7,11} This effect can be summarized as:

$$\left(\frac{\partial \ln k_2}{\partial P}\right) = -\frac{\Delta V^\ddagger}{RT} \quad \dots 3.58$$

where ΔV^\ddagger is the partial molar volume change when reactants are converted to the activated complex. A plot of $\ln k_2$ vs P is linear with a slope of $-\frac{\Delta V^\ddagger}{RT}$.^{6,7} A positive volume of activation indicates a dissociative mechanism while a negative value is indicative of an associative substitution reaction.

3.5 Experimental Kinetic Techniques

Reactions in solutions make up a very large number of the chemical reactions whose kinetics have been studied in detail.¹ There are many different methods by which reaction rates are measured and the choice of method depends on whether the reaction of interest is fast or slow.² A reaction is generally regarded as rapid if it proceeds to 50 % of completion in 10 s or less.² Fast reactions require special equipment that allows rapid mixing and rapid data recording.

A sufficiently slow reaction can be studied by conventional methods of analysis to determine the concentration of a reactant or product as a function of time. However, most reactions are too rapid with the concentrations of the species changing appreciably during the measurement process.² Under these conditions, the reaction has to be stopped while the measurement is made (quenching) or an instrumental technique that continuously records concentration as the reaction proceeds must be used.^{1,2}

- Quenching occurs when the temperature is lowered to slow the reaction to allow a measurement to be taken. This is a very slow and time-consuming technique.^{1,2}
- A more convenient technique is to monitor the progress of the reaction continuously by spectrophotometry, conductometry, potentiometry or some other instrumental technique.²

As laboratory instrumentation has become increasingly more available since the 1930s, an increasing number of kinetic studies have been carried out by monitoring a physical property of a reaction mixture.^{1,2}

Although there are many techniques available for kinetic studies such as pulse methods, infrared spectroscopy (IR) and nuclear magnetic resonance spectroscopy (NMR), only the methods used in this study, namely UV/Visible absorption spectroscopy and stopped-flow analysis are discussed below.

3.5.1 UV/Visible Spectrophotometry

In a UV/Visible spectrophotometer, light from a continuous light source is passed through a monochromator (a prism, grating or even a filter) to select a single wavelength.¹²⁻¹⁶ The light of the selected wavelength with an intensity, I_0 , strikes a sample in a cell called a cuvette of length, l . The intensity of the beam exiting the sample is I where $I \leq I_0$ as the sample absorbs the light.¹²⁻¹⁶ In a double-beam spectrophotometer, light passes alternately through the sample and reference cuvettes. Using a reference cuvette containing pure solvent is important as it compensates for absorption due to the cuvette and solvent or light scattering.¹²⁻¹⁶ A double-beam spectrophotometer, as shown in *Figure 3.1*, manages to alternate between cuvettes by using a chopper which is a motor that rotates a mirror into and out of the light path. When the chopper is not deflecting the beam, the light passes through the sample and the detector measures the intensity; however, when the chopper deflects the beam through the reference cuvette, the detector reads the reference value.¹²⁻¹⁶ The beam is chopped several times per second.

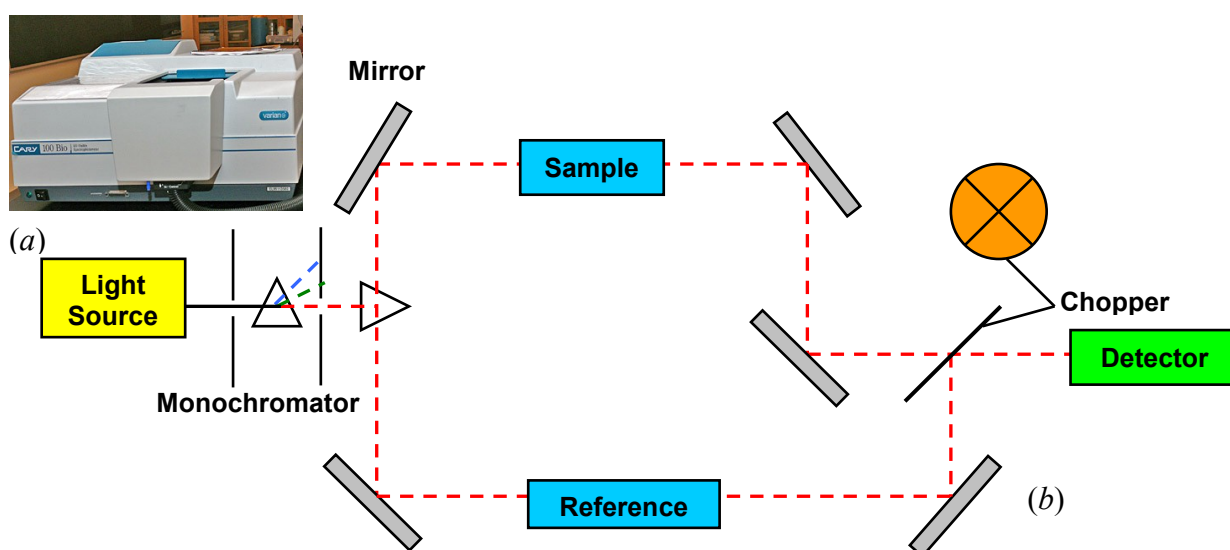


Figure 3.1: (a) Photograph and (b) schematic diagram¹⁵ of a double-beam-in-space Varian Cary 100 Bio UV-Visible spectrophotometer.

A spectrophotometer can measure the transmittance, T , which is defined as the fraction of the original light passing through the sample.¹²⁻¹⁶

$$T = \frac{I}{I_0} \quad \dots 3.59$$

However, absorbance is a more useful quantity and can be easily converted from transmittance.¹²⁻¹⁶

$$A = -\log\left(\frac{I}{I_0}\right) = -\log T \quad \dots 3.60$$

Absorbance is important because according to Beer's law given in *Equation 3.61*¹²⁻¹⁶, it is directly proportional to the concentration of the sample:

$$A = \epsilon c l \quad \dots 3.61$$

Where A is the absorbance (it is dimensionless), c is the concentration of the sample (in units mol dm^{-3}), l is the pathlength (with units of cm) and ϵ is the extinction coefficient (with the units $\text{M}^{-1}\text{cm}^{-1}$).

For a first order reaction, *Equation 3.3*:



The absorbance at any time t is²

$$A_t = \epsilon_X [X]_t + \epsilon_Y [Y]_t \quad \dots 3.62$$

where ϵ_X , ϵ_Y is the molar absorptivity of X and Y respectively.

At completion of the reaction, the absorbance will be²

$$A_\infty = \epsilon_X [X]_\infty + \epsilon_Y [Y]_\infty \quad \dots 3.63$$

Thus in kinetic analysis the following equation is used based on absorbances:

$$\ln \frac{[X]_0}{[X]_t} = \ln \left(\frac{A_0}{A_t} \right) = k_1 t \quad \dots 3.64$$

where A_t is defined as absorbance of the reactant X at any time t .

The absorbance of a reaction is measured over time over a specific wavelength range. The observed rate constant for the reaction is determined by a least squares fit of an absorbance versus time plot at a specific wavelength. By monitoring the reaction at different concentrations of the reactant, the rate constant for the reaction at that temperature can be determined.

3.5.2 Stopped-flow Techniques

Many reactions happen too quickly to be monitored by standard absorption spectroscopy.^{2,4,6} In the time taken to mix the samples and take a reading, the reaction would have already occurred. A popular and reliable method to monitor these rapid reactions is stopped-flow mixing.^{2,4,6} This method involves mixing reagents rapidly and stopping the flow of the mixed solution suddenly. The progress of the reaction is analysed near the mixer.^{2,4,6,13} The apparatus can be seen in *Figure 3.2*.

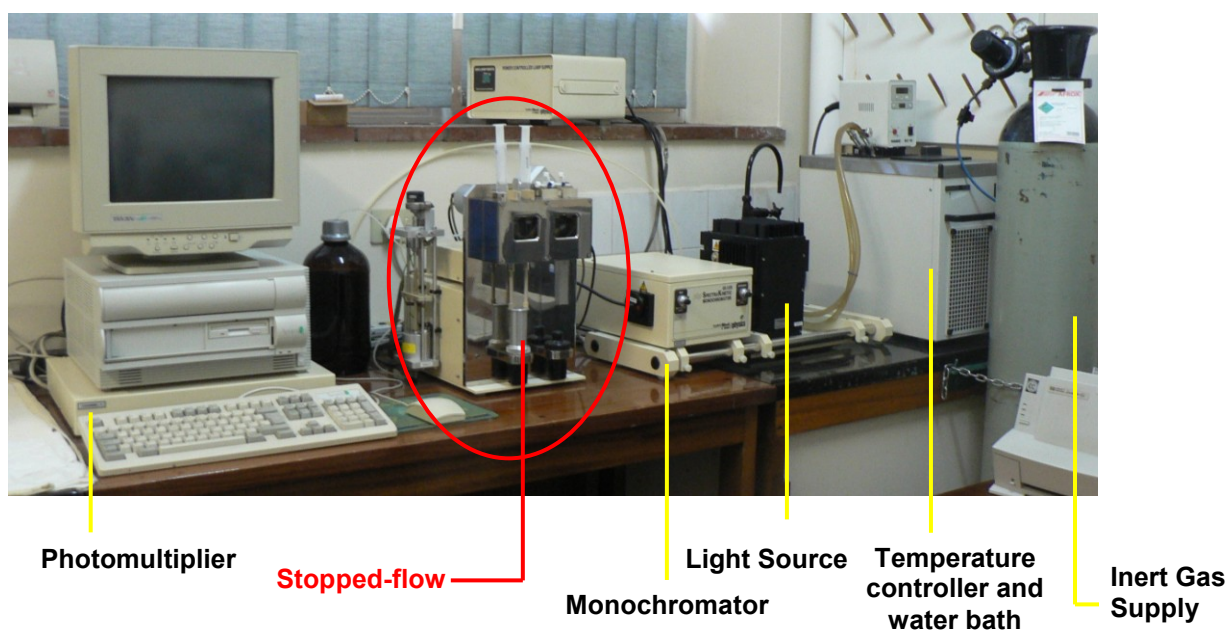


Figure 3.2: Photograph of the Applied Photophysics SX.18MV (v4.33) stopped-flow system coupled to an online data acquisition system setup used by the University of KwaZulu Natal Physical Chemistry workgroup.

The drive syringes are filled separately with different reagents.^{2,4,13} When the drive mechanism, which is usually piston driven, is activated, it causes the drive syringe plungers to go forward rapidly. The reagents move into the mixer where there is rapid

mixing within 0.001 s and the solution passes into the observation cell.^{2,4,13} The reaction solution then passes into the stop syringe. The stop syringe will eventually fill, causing the plunger to strike the stop block instantly ceasing the flow, but leaving a recently mixed plug of solution in the observation cell.^{2,4,13}

When the mixed solution is stationary in the observation cell a recording device (e.g. oscilloscope) starts taking readings. The usual method of detection is UV/visible spectrophotometry and once the recording device starts, the amount of light transmitted through the observation chamber at a specific wavelength will change as the reaction goes to completion.^{2,4,13} A photomultiplier converts transmitted light into electric current and a computer interprets the data as an absorption versus time spectrum. The data is then analysed normally.^{2,4,13} Figure 3.3 illustrates the inner workings of the stopped-flow apparatus.

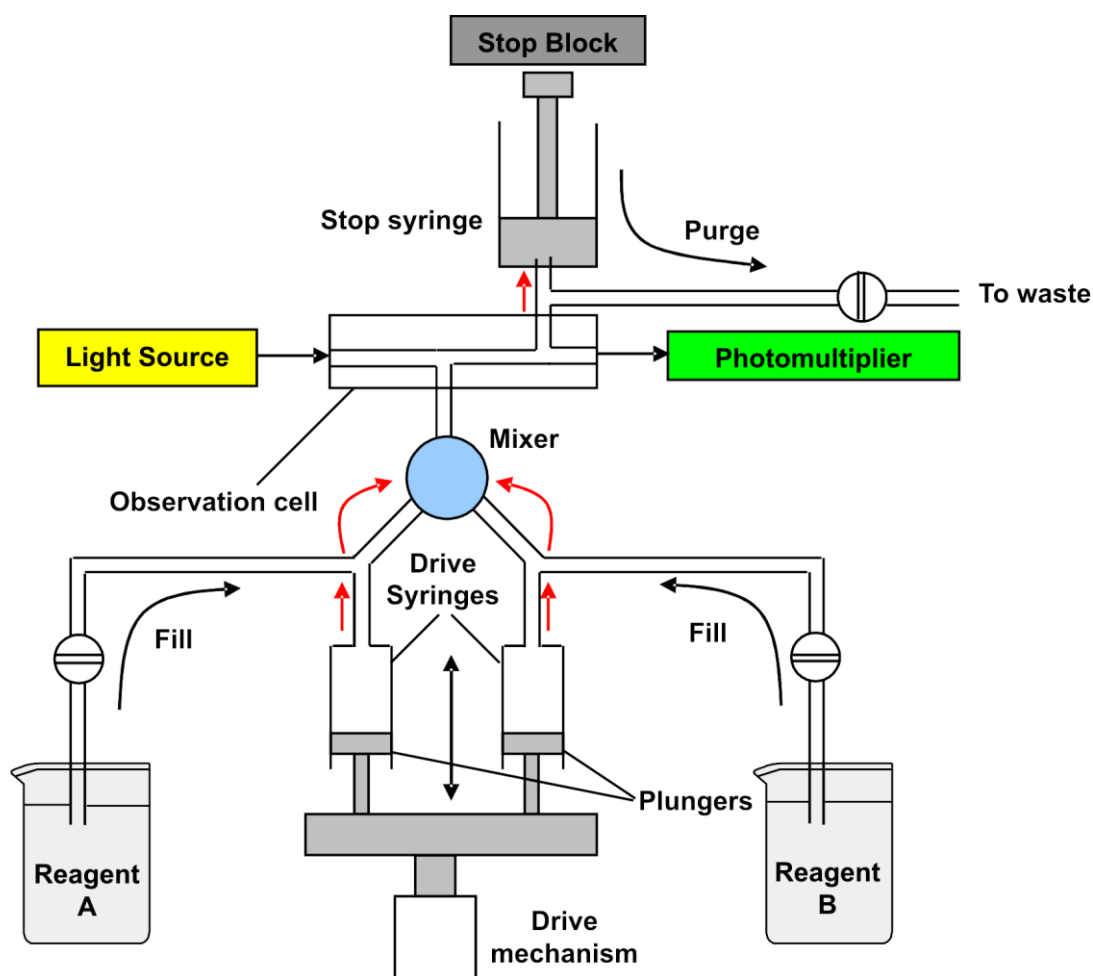


Figure 3.3: Modified schematic diagram of mechanistic action of stopped-flow apparatus.²

Stopped-flow analysis is a simple technique with many advantages. It allows very rapid first order reaction constants to be measured, $k \approx 40 \text{ s}^{-1}$.² The analysis is easy and only uses small ($\approx 0.2 \text{ ml}$) volumes of solutions.¹³ There are a number of different monitoring methods that can be used in conjunction with this technique.

3.6 References

1. S. R. Logan, *Fundamentals of Chemical Kinetics*, Longman, Essex, 1996, pgs 1-30.
2. D. A. Skoog, D. M. West, F. J. Holler and S. R. Crouch, *Fundamentals of Analytical Chemistry*, 8th Ed., Brooks/Cole – Thomson Learning, Inc., United States, 2004, pgs 718-734, 771-775, 878-894.
3. M. S. Silberberg, *Chemistry. The Molecular Nature of Matter and Change*, 2nd edition., McGraw-Hill, United States, 2000, pgs 664-684.
4. K. J. Laidler, J. H. Meiser and B. C. Sanctuary, *Physical Chemistry*, Houghton Mifflin Company, United States, 2003, pgs 363-376.
5. J. H. Espenson, *Chemical Kinetics and Reaction Mechanisms*, 2nd edition, McGraw-Hill, New York, 1995, pgs 1-86.
6. J. D. Atwood, *Inorganic and Organometallic Reaction Mechanisms*, 2nd edition, Wiley-VCH, New York, 1997, pgs 1-32.
7. R. B. Jordan, *Reaction Mechanisms of Inorganic and Organometallic Systems*, Oxford University Press, New York, 1991, pgs 1-17.
8. P. Atkins and J. de Paula, *Atkins' Physical Chemistry*, 8th edition., Oxford University Press, Oxford, 2006, pgs 791-829.
9. S. Ašperger, *Chemical Kinetics and Inorganic Reaction Mechanisms*, 2nd edition., Kluwer Academic/Plenum Publishers, New York, 2003, pgs 3, 14-23.
10. H. Eyring, *J. Chem. Phys*, 1935, **3**, 107.
11. L. Helm and A. E. Merbach, *Dalton. Trans.*, 2002, 633.
12. D. C. Harris, *Quantitative Chemical Analysis*, W.H Freeman and Company, San Francisco, 1982, pgs 468-485.
13. R. G. Wilkins, *Kinetics and Mechanism of Reactions of Transition Metal Complexes*, 2nd Ed., VCH Verlagsgesellschaft mbH, Weinheim, 1991, pgs 136-140.
14. H. H. Willard, L. L. Merritt, Jr., J. A. Dean and F. A. Settle, Jr., *Instrumental Methods of Analysis*, 7th edition., Wadsworth Publishing Company, California, 1988, pgs 118-156, 159-162.
15. H. H. Bauer, G. D. Christian and J. E. O'Reilly, *Instrumental Analysis*, Allyn and Bacon, Inc., Boston, 1978, pgs 167-188.

16. D.A. Skoog and D. M. West, *Principles of Instrumental Analysis*, 2nd edition, Saunders College, 1980, pgs 180-186.

CHAPTER

Experimental

4.1 General Methods

All reactions that required inert conditions were carried out using a double manifold vacuum line, Schlenkware and cannula techniques. Organic solvents used in the syntheses were purchased from Aldrich and used as received, except for acetonitrile which was distilled by the method of Carlsen *et al.*¹ The metal salts K₂PtCl₄ (99.9%) and [Pt(PhCN)₂Cl₂] (99.9%) (Strem), AgCF₃SO₃ (99%), AgBF₄ (98%), LiCF₃SO₃ (96%), and NaClO₄·H₂O (98%) (Aldrich) were used as supplied. The ligands, 1,5-cyclooctadiene (COD), 2,2':6',2''-terpyridine (**L1**) and 4,4',4''-tri-*tert*-butyl-2,2':6',2''-terpyridine (**L2**) were purchased from Aldrich and also used as supplied.

The remaining ligands namely: 4'-(2'''-CH₃-Phenyl)-2,2':6',2''terpyridine (**L3**), 4'-(2'''-CF₃-Phenyl)-2,2':6',2''terpyridine (**L4**), 4'-(2'''-CF₃-Phenyl)-6-Phenyl-2,2'-bipyridine (**L5**) and 4'-(2'''-CH₃-Phenyl)-6-pyrazin-2-yl-2,2'-bipyridine (**L6**) were synthesised using the method of Kröhnke² and supplied by G. C. Summerton³ and J. A. Gertenbach⁴. These ligands were used without any further purification. All other chemicals were of analytical quality.

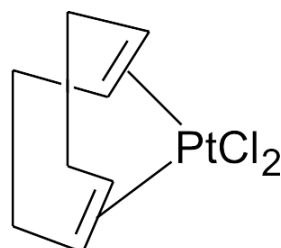
The Pt(II) precursor, dichloro(1,5-cyclooctadiene)platinum(II) [(Pt(COD)Cl₂)]⁵ as well as the complexes: [Pt(terpy)Cl]Cl·2H₂O (**PtL1**)⁶, [Pt(*t*Bu₃terpy)Cl]ClO₄ (**PtL2**)⁷, [Pt{4'-(2'''-CH₃-Ph)terpy}Cl]BF₄ (**PtL3**)^{3,8}, [Pt{4'-(2'''-CF₃-Ph)terpy}Cl]CF₃SO₃ (**PtL4**)³, [Pt{4'-(2'''-CF₃-Ph)-6-Ph-bipy}Cl] (**PtL5**)⁹ and [Pt{4'-(2'''-CH₃-Ph)-6-pyrazin-2-yl-2,2'-bipyridine}Cl]CF₃SO₃ (**PtL6**)⁴ were all synthesised according to known literature procedures.

HPLC grade methanol used for the kinetic measurements was purchased from Aldrich. The nucleophiles: imidazole (**Im**, 99.5%), 1-methylimidazole (**MIm**, 99%),

1,2-dimethylimidazole (**DIm**, 98%), pyrazole (**Pyz**, 98%) and 1,2,4-triazole (**Trz**, 98%) were also purchased from Aldrich and used as received.

4.2 Synthesis of Complexes

4.2.1 Synthesis of Dichloro(1,5-cyclooctadiene)platinum(II)



A solution of potassium tetrachloroplatinate (K_2PtCl_4) (2.18 g, 5.23 mmol) in water (55 ml) was filtered to remove reduced platinum particles. To this solution, glacial acetic acid (35 ml) and 1,5-cyclooctadiene (COD) (2.1 ml, 17 mmol) were added and the mixture was heated with vigorous stirring to 90 °C for about 30 minutes. The mixture changed from a red to a pale-yellow colour and the product, $[(\text{PtCOD})\text{Cl}_2]$, precipitated as pale-yellow crystals during this time. Further precipitation occurred when the solution was further concentrated under reduced pressure to a final volume of about 10 ml. The crystalline product was filtered off and washed with consecutive 50 ml portions of water, ethanol and diethyl ether. This pale-yellow product was then dried in the oven at 100 °C for 1 hour to produce a sufficiently high purity complex of the precursor, dichloro(1,5-cyclooctadiene)platinum(II) $[(\text{PtCOD})\text{Cl}_2]$.

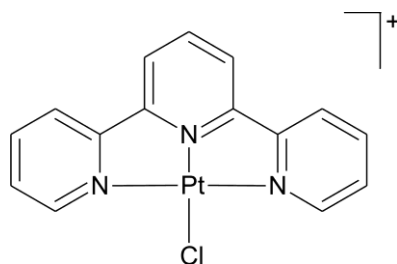
Yield: 1.67 g (84 %)

Elemental Analysis

Calc. for $\text{PtC}_8\text{H}_{12}\text{Cl}_2$: C = 25.7; H = 3.2 ; N = 0.0 %.

Found for $\text{PtC}_8\text{H}_{12}\text{Cl}_2$: C = 26.2; H = 3.5; N = 0.0 %.

4.2.2 Synthesis of [Pt(terpy)Cl]Cl·2H₂O (PtL1)



The ligand 2,2':6',2''-terpyridine (**L1**) (313 mg, 1.34 mmol) was added to a stirred suspension of [Pt(COD)Cl₂] (500 mg, 1.34 mmol) in water and the mixture was heated to between 45 and 50 °C. The suspended [Pt(COD)Cl₂] complex completely dissolved to give an orange-red solution after about 20 minutes. The solution was then allowed to cool to room temperature and filtered to remove any unreacted material. A red solid was obtained by concentrating the filtrate under reduced pressure. This red product, [Pt(terpy)Cl]Cl·2H₂O (**PtL1**), was filtered, washed with diethyl ether and air-dried.

Yield: 0.61g (85 %)

Elemental Analysis.

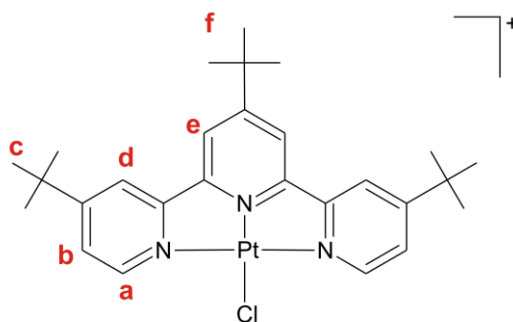
Calc. for PtCl₂O₂C₁₅H₁₅N₃: C = 33.7; H = 2.8; N = 7.9 %.

Found for PtCl₂O₂C₁₅H₁₅N₃: C = 33.5; H = 2.7; N = 7.7 %.

IR cm⁻¹: 460(m), 519(m), 720(m), 779(vs), 1029(m), 1091(w), 1246(m), 1283(m), 1312(m), 1400(m), 1451(m), 1604(s), 3037(mb), 3301 (sb)*.

m/z: 463.0289 (M⁺) C₁₅H₁₁N₃ClPt

4.2.3 Synthesis of [Pt(tBu₃terpy)Cl]ClO₄ (PtL2)



K₂PtCl₄ (415 mg, 1.00 mmol) was added to a 50% aqueous acetonitrile (30 ml) solution. It was then filtered to remove any reduced platinum particles. The ligand, 4,4',4''-tri-*tert*-butyl-2,2':6',2''-terpyridine (**L2**) (402 mg, 1.00 mmol), was added to the stirring platinum solution and this mixture was heated to reflux for 24 hours. Over this time 4,4',4''-tri-*tert*-butyl-2,2':6',2''-terpyridine (**L2**) mostly dissolved to afford a yellow solution which was then filtered into a 0.50 M aqueous solution of NaClO₄. The filtrate was allowed to cool slowly, following which, a yellow precipitate formed. This precipitate was filtered and washed with hydrochloric acid (0.1 M). The purified product of [Pt(^tBu₃terpy)Cl]ClO₄ (**PtL2**) was obtained as yellow needle-like crystals by recrystallisation of this yellow powder by vapour diffusion of diethyl ether into acetonitrile containing the product.

Yield: 0.41 g (55 %)

Elemental Analysis:

Calc. for PtCl₂O₄C₂₇H₃₅N₃: C = 44.3; H = 4.8; N = 5.7 %.

Found for PtCl₂O₄C₂₇H₃₅N₃: C = 44.4; H = 4.8; N = 5.7 %.

IR cm⁻¹: 432(m), 607(m), 622(s), 738(w), 848(m), 865(m), 917(m), 1032(m), 1086(vs), 1256(m), 1370(m), 1422(m), 1479(m), 1553(m), 1616(s), 2922(m), 2967(s).

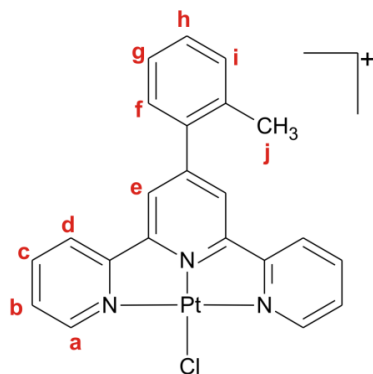
m/z: 631.2167 (M⁺) C₂₇H₃₅N₃ClPt

¹⁹⁵Pt NMR: (CD₃CN) -2731.7 ppm

¹H NMR: (DMSO-d₆)

Shift: (ppm)	Multiplicity:	Integration:	Coupling: (Hz)	Assignment:
1.44	s	18		c
1.53	s	9		f
7.72	dd	2	⁴ J _{HH} =2.11, ³ J _{HH} =6.05	b
8.25	s	4		d,e
8.64	d	2	³ J _{HH} =6.05	a

4.2.4 Synthesis of [Pt{4'-(2'''-CH₃-Ph)terpy}Cl]BF₄ (PtL3)



AgBF₄ (41 mg, 0.21 mmol) dissolved in acetonitrile (5 ml) was added to a suspension of [Pt(PhCN)₂Cl₂] (100 mg, 0.21 mmol) in acetonitrile (10 ml). The reaction mixture was heated under reflux for 16 hours under nitrogen and over this time AgCl precipitated out of the solution. This fine precipitate was removed by filtration through a 0.45 μm nylon membrane. The ligand 4'-(2'''-CH₃-phenyl)-2,2':6',2''-terpyridine (**L3**) (60 mg, 0.20 mmol) was added to the filtrate. The mixture was then heated under reflux for another 24 hours and then the solution was concentrated under reduced pressure. The solution was allowed to cool to room temperature and was left to stand for a further 24 hours. This led to the precipitation of a yellow powder, [Pt{4'-(2'''-CH₃-Ph)terpy}Cl]BF₄ (**PtL3**) which was filtered and washed with cold acetonitrile and diethyl ether and dried *in vacuo*.

Yield: 96 mg (75 %)

Elemental Analysis:

Calc. for C₂₂H₁₇BClF₄ N₃Pt: C = 41.8; H = 2.9; N = 6.7 %.

Found for C₂₂H₁₇BClF₄ N₃Pt: C = 41.6; H = 2.9; N = 6.6 %.

IR cm^{-1} : polypyridine: 881(m), 1414(m), 1477 (m), 1555 (w), 1606 (s)
counterion: 1051 (vs,br).

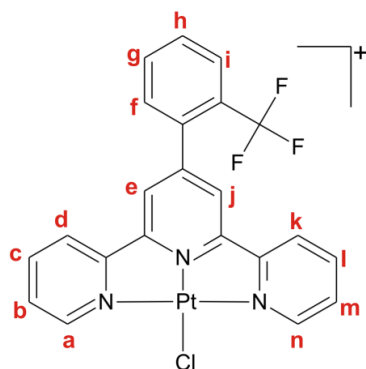
m/z: 553.0759 (M^+) $\text{C}_{22}\text{H}_{17}\text{N}_3\text{ClPt}$

^{195}Pt NMR: (DMSO- d_6) -2721.8 ppm

^1H NMR: (DMSO- d_6)

Shift: (ppm)	Multiplicity:	Integration:	Coupling: (Hz)	Assignment:
2.47	s	3		j
7.50	m	4		f, g, h, i
7.80	m	2		b
8.40	m	2		c
8.66	m	4		a, d
8.71	s	2		e

4.2.5 Synthesis of $[\text{Pt}\{4'-(2'''-\text{CF}_3-\text{Ph})\text{terpy}\}\text{Cl}]\text{CF}_3\text{SO}_4$ (PtL4)



$[\text{Pt}(\text{PhCN})_2\text{Cl}_2]$ (100 mg, 0.21 mmol) was suspended in acetonitrile (10 ml) and AgCF_3SO_3 (41 mg, 0.21 mmol) in acetonitrile (5 ml) was added to this suspension. The mixture was heated under reflux for 16 hours under inert conditions and the AgCl precipitate was removed by filtration. The ligand 4'-(2'''- CF_3 -phenyl)-2,2':6',2''terpyridine (**L4**) (80 mg, 0.21 mmol) was added to the solution which was then refluxed again overnight. After this time, the volume of the solution was decreased under reduced pressure causing the precipitation of

Designation: vs = very strong, s = strong, sb = strong broad, ms = medium strong, m = medium
mb = medium broad, w = weak, br = broad.

Multiplicity: s = singlet, d = doublet, dd = doublet of doublets, t = triplet, td = triplet of doublets
m = multiplet

[Pt{4'-(2'''-CF₃-Ph)terpy}Cl]CF₃SO₄ (**PtL4**). The orange powder was washed with a minimum amount of acetonitrile and diethyl and dried *in vacuo*.

Yield: 112 mg (70%)

Elemental Analysis:

Calc. for C₂₃H₁₄ClF₆N₃O₃PtS: C = 36.5; H = 2.0; N = 5.5 %.

Found for C₂₃H₁₄ClF₆N₃O₃PtS: C = 36.4; H = 1.8; N 5.4 %.

IR cm⁻¹: polypyridine: 879(w), 1072(m), 1135(m), 1420(m), 1477(m), 1609(m)
counterions: 1029(s), 1263(vs), 1316(ms).

m/z: 607.0476 (M⁺) C₂₂H₁₄N₃F₃ClPt

¹⁹⁵Pt NMR: (DMSO-d₆) -2724.1 ppm

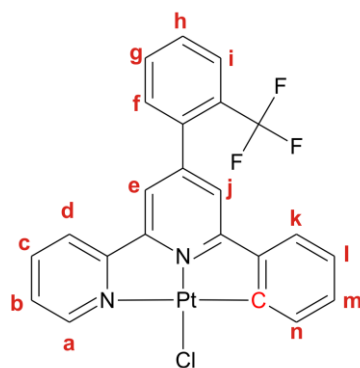
¹H NMR: (DMSO-d₆)

Shift: (ppm)	Multiplicity:	Integration:	Coupling: (Hz)	Assignment:
7.70	d	1	³ J _{HH} =7.75	f
7.85-7.97	m	4		g, h, b, m
8.06	d	1	³ J _{HH} =7.75	i
8.48	td	2	⁴ J _{HH} =1.54, ³ J _{HH} =7.88	c, l
8.65	d	2	³ J _{HH} =7.88	d, k
8.78	s	2		e, j
8.85	dd	2	⁴ J _{HH} =0.95, ³ J _{HH} =5.69	a

Designation: vs = very strong, s = strong, sb = strong broad, ms = medium strong, m = medium
mb = medium broad, w = weak, br = broad.

Multiplicity: s = singlet, d = doublet, dd = doublet of doublets, t = triplet, td = triplet of doublets
m = multiplet

4.2.6 Synthesis of [Pt{4'-(2'''-CF₃-Ph)-6-Ph-bipy}Cl] (PtL5)



K₂PtCl₄ (100 mg, 0.24 mmol) and the ligand, 4'-(2'''-CF₃-phenyl)-6-phenyl-bipyridine (**L5**) (90 mg, 0.24 mmol) was refluxed in a 50 % aqueous acetonitrile solution (10 ml) for 2 days under an atmosphere of nitrogen over which time an orange powder precipitated out of solution. This precipitate was filtered and washed with copious amounts of diethyl ether and then a smaller amount of acetonitrile. The resulting powder was extracted using the sohxlet method with dichloromethane and the solution was concentrated under reduced pressure. The purified product, [Pt{4'-(2'''-CF₃-Ph)-6-Ph-bipy}Cl], was obtained by recrystallisation through slow diffusion of diethyl ether into dimethylformamide solution containing the crude product.

Yield: 85 mg (91 %)

Elemental Analysis:

Calc. for C₂₃H₁₄ClF₃N₂Pt: C = 45.6; H = 2.3; N = 4.6 %.

Found for C₂₃H₁₄ClF₃N₂Pt: C = 45.7; H = 2.0; N = 4.9 %.

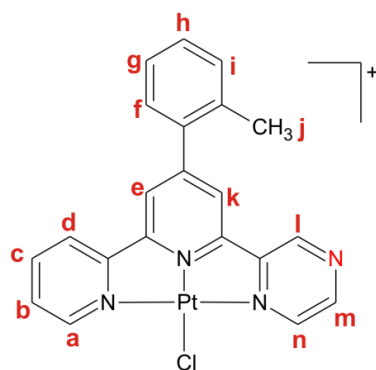
IR cm⁻¹: polypyridine: 1603(m), 1582(w), 1533(m), 1478(w), 1463(w), 1402(m), 1310(ms), 1162(ms), 1112(vs), 1033(ms), 783(m), 766(ms), 750(ms), 727(ms).

m/z: 628.0343 (M⁺) C₂₃H₁₄N₂F₃NaClPt

¹H NMR: (DMSO-d₆)

Shift: (ppm)	Multiplicity:	Integration:	Coupling: (Hz)	Assignment:
7.06	t	1	³ J _{HH} = 7.43	l
7.16	t	1	³ J _{HH} = 7.43	m
7.53	d	1	³ J _{HH} = 7.62	n
7.64	d	1	³ J _{HH} = 7.62	k
7.70	d	1	³ J _{HH} = 7.37	f
7.78	t	1	³ J _{HH} = 7.62	h
7.88	t	1	³ J _{HH} = 7.37	g
7.94	t	1	³ J _{HH} = 6.61	b
7.97	d	2	³ J _{HH} = 6.01	i,j
8.25	s	1		e
8.33	t	1	³ J _{HH} = 92	c
8.58	d	1	³ J _{HH} = 7.99	d
8.94	d	1	³ J _{HH} = 5.06	a

4.2.7 Synthesis of [Pt{4'-(2''-CH₃-Ph)-6-2''pyraz-2,2' bipy}Cl]CF₃SO₃ (PtL6)



AgCF₃SO₃ (54 mg, 0.21 mmol) was dissolved in acetonitrile (5 ml) and added to a suspension of [Pt(PhCN)₂Cl₂] (100 mg, 0.21 mmol) in acetonitrile (10 ml). This mixture was then refluxed for 24 hours under inert conditions over which time a white precipitate of AgCl formed. This precipitate was removed by filtration through a 0.45 μm nylon membrane. The ligand, 4'-(2''-CH₃-Ph)-6-pyrazin-2-yl-2,2'-bipyridine (**L6**) (65 mg, 0.20 mmol), was added to the solution and the mixture was refluxed for

an additional 24 hours. The mixture was then filtered while it was still hot, to remove unreacted reactants. The solution was concentrated under reduced pressure resulting in the precipitation of $[\text{Pt}\{4'-(2'''-\text{CH}_3-\text{Ph})_6\text{-pyrazin-2-yl-2,2'-bipyridine}\}\text{Cl}]\text{CF}_3\text{SO}_3$ (**PtL6**), which was filtered and washed thoroughly with diethyl ether and acetonitrile. The resulting red powder was recrystallised from hot acetonitrile.

Yield: 63 mg (45 %)

Elemental Analysis:

Calc. for $\text{C}_{22}\text{H}_{16}\text{ClF}_3\text{N}_4\text{O}_3\text{PtS}$: C = 37.5; H = 2.3; N = 8.0 %.

Found for $\text{C}_{22}\text{H}_{16}\text{ClF}_3\text{N}_4\text{O}_3\text{PtS}$: C = 37.8 H = 1.8; N = 7.9 %.

IR cm^{-1} : polypyridine: 1609(m), 1466(m), 1417(m), 884(w), 765(s).
Counterion: 1261(vs), 1142(s), 1030(s).

m/z: 554.0711 (M^+) $\text{C}_{21}\text{H}_{16}\text{N}_4\text{ClPt}$

^{195}Pt NMR: (DMSO- d_6) -2724.1 ppm

^1H NMR: (DMSO- d_6)

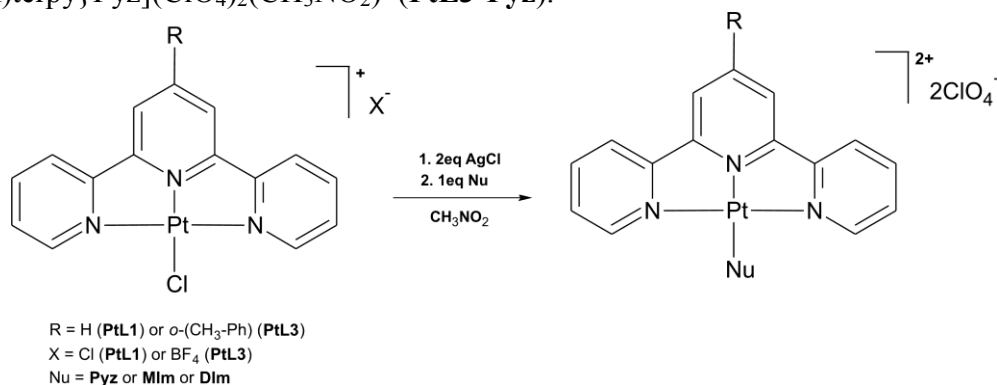
Shift: (ppm)	Multiplicity:	Integration:	Coupling: (Hz)	Assignment:
2.45	s	3		j
7.49-7.55	m	4		f,g,h,i
7.96	m	1		b
8.54	td	1	$^4J_{\text{HH}}=1.59, ^3J_{\text{HH}}=7.90$	c
8.75	dd	1	$^4J_{\text{HH}}=0.66, ^3J_{\text{HH}}=8.16$	d
8.81	d	1	$^3J_{\text{HH}}=1.23$	e
8.86	d	1	$^3J_{\text{HH}}=1.23$	k
8.89	dd	1	$^4J_{\text{HH}}=1.23, ^3J_{\text{HH}}=5.69$	a
8.93	dd	1	$^4J_{\text{HH}}=1.23, ^3J_{\text{HH}}=3.14$	m
9.16	d	1	$^3J_{\text{HH}}=3.14$	n
9.91	d	1	$^3J_{\text{HH}}=0.94$	l

Designation: vs = very strong, s = strong, sb = strong broad, ms = medium strong, m = medium
mb = medium broad, w = weak, br = broad.

Multiplicity: s = singlet, d = doublet, dd = doublet of doublets, t = triplet, td = triplet of doublets
m = multiplet

4.3 X-ray Crystal Structures

The following method, shown in *Scheme 4.1*, was used to form the complexes: [Pt(terpy)Pyz](ClO₄)₂(CH₃NO₂) (**PtL1-Pyz**), [Pt(terpy)MIm](ClO₄)₂(CH₃NO₂) (**PtL1-MIm**), [Pt(terpy)DIm](ClO₄)₂(CH₃NO₂) (**PtL1-DIm**) and [Pt{4'-(2'''-CH₃-Ph)terpy}Pyz](ClO₄)₂(CH₃NO₂) (**PtL3-Pyz**).



Scheme 4.1: Reaction scheme for the synthesis of the substituted complexes.

The respective platinum salts (**PtL1** or **PtL3**, 0.13 mmol) were dissolved in nitromethane (4 ml) and AgClO₄ (54 mg, 0.26 mmol) was added to the stirred platinum solution at ca. 50 °C. The respective solutions were stirred for 1 hour over which time they both turned a paler yellow colour (see *Figure 4.1(a)*) and a white silver precipitate formed which was filtered off, using a 0.45 µm nylon membrane. One equivalent of the respective nucleophile (0.13 mmol) was then added to the filtrate. The solution turned either an orange colour (see *Figure 4.1(b)*) or darker yellow (see *Figure 4.1(c)*) depending on the nucleophile and complex. All crystals were grown via vapour diffusion of ether into the nitromethane solution of the desired product.

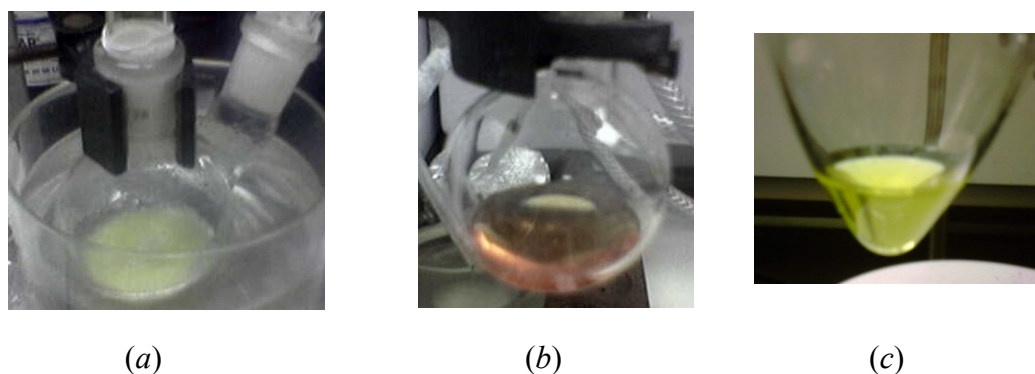


Figure 4.1: (a) Pale yellow solution of **PtL1** after the addition of the silver salt, (b) orange solution of **PtL1-MIm** and (c) darker yellow colour of **PtL1-Pyz**.

4.4 Preparation of Complex and Nucleophile Solutions for Kinetic Analysis

The 0.1 M ionic strength solution used in the preparation of the complex and neutral nucleophile solutions was made up by dissolving the required amount of LiCF_3SO_3 or NaClO_4 (0.09M) and NaCl (0.01M) in HPLC grade methanol. Neither CF_3SO_3^- nor ClO_4^- coordinates to Pt(II)^{10} and hence the substitution reactions could be studied in this media. The salts were chosen depending on the interaction of the metal complex when reacted with solutions of the nucleophile i.e. certain salt solutions led to precipitation of the complex on addition of the nucleophile. The NaCl was added to prevent solvolysis.

Metal complex solutions were prepared by dissolving the required amount of metal complex in 100 ml of the ionic strength solution (either the methanolic $\text{LiCF}_3\text{SO}_3+\text{NaCl}$ or the $\text{NaClO}_4+\text{NaCl}$ solution) described above. The nucleophile solutions: **Im**, **MIm**, **DIm**, **Pyz** and **Trz**, of 50 times the concentration of the metal complex solution was prepared by dissolving a known amount of a select nucleophile in 100 ml of the ionic strength solution. Subsequent dilutions of the 50 times nucleophile solution affords solutions of concentrations 10, 20, 30 and 40 times the concentration of the metal complex.

4.5 Instrumentation and Measurements

Supporting documentation relating to the analysis of the complexes is attached as **Appendix A**. These include infrared and mass spectra as well as ^1H NMR and ^{195}Pt NMR spectra for the complexes.

4.5.1 Microanalysis

Microanalyses for % C, H and N were performed by Galbraith laboratories Inc., Knoxville, Tennessee, USA and at the Institute for Inorganic Chemistry, University of Erlangen-Nürnberg, Egerlandstr. 1, Erlangen, Germany.

4.5.2 NMR Spectroscopy

NMR spectra were recorded with either a 500 MHz Varian Unity Inova spectrometer, equipped with an Oxford magnet (11.744 T) or a 400 MHz Bruker Avance spectrometer equipped with a Bruker magnet (9.395 T). The spectra were run at 25 °C, with chemical shifts referenced to Si(CH₃)₄ and the solvents used included: deuterated DMSO and acetonitrile.

4.5.3 Infrared Spectroscopy

FTIR spectra were recorded using the Bruker Alpha FTIR spectrometer with ATR platinum Diamond 1 Repl accessory. Spectra were recorded by placing a single crystal on the platform and crushing the crystal between the platform and the diamond head. The machine acquired the information in 25 scans. For this study the most relevant portion of the infrared region is in the frequency range 4 000 to 400 cm⁻¹.

4.5.4 Mass Spectrometry

An LCT premiera LC-MS was used with a time of flight mass analyser to obtain mass spectra. The method of ionization is electron spray ionisation (ESI) and the samples were run in the positive mode (ES⁺). Terfenadine was used as the lockmass for **PtL1** while reserpine was used for **PtL2** and **PtL5** while raffinose was the lockmass used for **PtL3**, **PtL4** and **PtL6**. In the sample **PtL5**, sodium has been picked up from the glass to form (M+Na)⁺ which is quite common in ES⁺. This simply means that Na⁺ charges the species rather than H⁺.

4.5.5 Computational Modelling

Computational modelling of the complexes was performed using the computational software package Spartan '08 for Windows^{11,12} using the B3LYP¹³ density functional method^{14,15} and the LACVP+** (Los Alamos core valence potentials)¹⁶ basis set. B3LYP relates to the hybrid functional Becke's three parameter formulation¹³ and has been proven to be more effective than the usual functionals. The LACVP basis set

employs effective core potentials for K-Cu, Pb-Ag, Cs-La and Hf-Au while Pople's 6-31G** basis set describes second and third row *s*- and *p*-block elements.^{17,18} The performance of the DFT (Density Functional Theory) calculations at the chosen level of theory was gauged by comparison of the calculated structures to X-ray structure of [Pt(^tBu₃terpy)Cl]⁺ and of similar terpy analogues of platinum(II).^{7-9,19}

Further computational modelling of the nucleophiles in a methanol solvent was done using the computational software package Gaussian²⁰. The density functional used for all our calculations is PBE1PBE.¹³ The basis set 6-311G was used and is restricted to atoms from H-Kr, but is considered to give more accurate results than the broader basis set 3-21G, which could also be used as it is applicable to atoms in the range H-Xe.^{17,18}

The RMS (Root Mean Squares) difference between the X-ray structures and the DFT-calculated structures was done using Mercury versions 2.2.²¹

4.5.6 X-ray Structure Determination

X-ray data was collected with an Oxford Diffraction Xcalibur 2 CCD Diffractometer. This instrument employs a CCD area detector and a 4-circle goniometer. It has an Enhance X-ray source and a 3 kW ceramic X-ray tube which emits Mo K α radiation ($\lambda = 0.71703\text{\AA}$). Data was collected and reduced using *CrysAlis CCD* and *CrysAlis RED*²² Version 1.7.1. The structures were solved by direct methods, using SHELXS-97²³ and refined using SHELXL-97²⁴. A semi-empirical Multiscan²⁵ absorption correction was applied to the data. Crystallographic details on each of the structures are given in *Table 4.1*. The IUCR²⁶ CIF check reports can be found in **Appendix B** while a complete set of atomic coordinates, anisotropic thermal parameters and fixed hydrogen atom coordinates are given in the electronic **Appendix F**.

Table 4.1: Crystallographic Details for **PtL1-MIm**, **PtL1-DIM**, **PtL1-Pyz** and **PtL3-Pyz**.

	PtL1-MIm	PtL1-DIM	PtL1-Pyz	PtL3-Pyz
Formula	C ₂₀ H ₂₀ Cl ₂ N ₆ O ₁₀ Pt	C ₂₁ H ₂₂ Cl ₂ N ₆ O ₁₀ Pt	C ₁₉ H ₁₈ C ₁₂ N ₆ O ₁₀ Pt	C ₂₆ H ₂₄ Cl ₂ N ₆ O ₁₀ Pt
Mr (gmol⁻¹)	770.41	784.44	756.38	846.50
a (Å)	16.389(5)	7.718(5)	16.351(5)	19.749(5)
b(Å)	11.582(5)	20.820(5)	11.534(5)	7.453(5)
c(Å)	14.538(5)	16.791(5)	14.075(5)	21.273(5)
α (deg)	90	90	90	90
β (deg)	110.147(5)	94.536(5)	111.311(5)	110.843(5)
γ (deg)	90	90	90	90
Volume (Å³)	2590.7(16)	2690(2)	2472.9(16)	2926(2)
Z	4	4	4	4
Space Group	P2 ₁ /c	P2 ₁ /c	P2 ₁ /c	P2 ₁ /n
Density (Mgcm⁻³)	1.975	1.937	2.032	1.921
F(000)	1496	1528	1464	1656
Crystal Dim. (mm³)	0.60x0.60x0.60	0.40x0.10x0.07	0.60x0.40x0.20	0.60x0.20x0.07
Radiation M_o				
K_α (Å)		0.71073		
T (K)	296(2)	296(2)	296(2)	296(2)
Total Data	17563	18837	16394	20049
Unique Data	5102 [R(int) = 0.0528]	5336 [R(int) = 0.1051]	4879 [R(int) = 0.0566]	5790 [R(int) = 0.0814]
Refinement		Full-matrix least-squares on F ²		
Final R indices [1>2σ(I)]	R1 = 0.0452, wR2 = 0.1123	R1 = 0.0856, wR2 = 0.2081	R1 = 0.0475, wR2 = 0.1240	R1 = 0.0736, wR2 = 0.1948
Final Indices	R1 = 0.0602, wR2 = 0.1178	R1 = 0.1200, wR2 = 0.2240	R1 = 0.0589, wR2 = 0.1296	R1 = 0.0984, wR2 = 0.2081

4.5.7 Kinetic Measurements

All kinetic measurements were performed under pseudo first-order conditions using at least a 10-fold excess of the entering nucleophile. The Varian Cary 100 Bio UV-Visible spectrophotometer with an attached Varian Peltier temperature control unit with online kinetics application was used to follow the ligand substitution in order to determine the suitable wavelength at which kinetic investigations could be performed. Most of the ligand substitutions reached completion in a time greater than sixteen minutes and thus the UV/visible spectrophotometer was used to monitor these reactions over time.

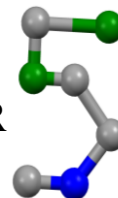
For those reactions that were complete in less than sixteen minutes (**PtL6** with **Im** and **MIm** at 25, 30 and 35 °C) an Applied Photophysics SX.18MV (v4.33) stopped-flow system coupled to an online data acquisition system was used to follow the reactions. All UV/visible and stopped-flow measurements were thermostatted to within *ca.* 0.1 °C. All data were graphically analysed using the software package, Origin 5.0.²⁷

4.6 References

1. L. Carlsen, H. Egsgaard and J. R. Anderson, *Anal. Chem.*, 1979, **51**, 1593.
2. F. Kröhnke, *Synthesis*, 1976, 1.
3. Summerton, G. C. PhD Thesis, *Solid State Structures and Photophysical Properties of Polypyridyl Complexes of Platinum(II)*, University of Natal, Pietermaritzburg, South Africa, 1997, pgs 51, 53, 71-77, 94-107, 150-156.
4. J. A. Gertenbach, PhD Thesis, *Synthesis and Emission Studies of Polypyridyl Complexes of Platinum (II)*, University of Natal, Pietermaritzburg, South Africa, 2002, pgs 220-230, 260-262.
5. J. X. McDermott, J. F. White and G. M. Whitesides, *J. Am. Chem. Soc.*, 1976, **98**, 6521.
6. G. Annibale, M. Brandolisio and B. Pitteri, *Polyhedron*, 1995, **14**, 451.
7. S.-W. Lai, M. C. W. Chan, K.-K. Cheung and C.-M. Che, *Inorg. Chem.*, 1998, **38**, 4262.
8. J. S. Field, R. J. Haines, D. R. McMillin, G. C. Summerton, *Dalton Trans.*, 2002, 1369.
9. D. Jaganyi, D. Reddy, J. A. Gertenbach, A. Hofmann and R. van Eldik, *Dalton Trans.*, 2004, 299.
10. T. G. Appleton, J. R. Hall, S. F. Ralph and C. S. M. Thompson, *Inorg. Chem.*, 1984, **23**, 3521.
11. *Spartan '08*, Wavefunction, Inc., 18401 Von Karman Avenue, Suite 370, Irvine, CA, 92612, USA; Q-Chem, Inc., The Design Center, Suite 690, 5001 Baum Blvd., Pittsburgh, PA, 15213, USA, 2008, <http://www.wavefun.com/>
12. J. Kong, C. A. White, A. I. Krylov, C. D. Sherrill, R. D. Adamson, T. R. Furlani, M. S. Lee, A. M. Lee, S. R. Gwaltney, T. R. Adams, C. Ochsenfeld, A. T. B. Gilbert, G. S. Kedziora, V. A. Rassolov, D. R. Maurice, N. Nair, Y. Shao, N. A. Besley, P. E. Maslen, J. P. Dombroski, H. Daschel, W. Zhang, P. P. Korambath, J. Baker, E. F. C. Byrd, T. Van Voorhuis, M. Oumi, S. Hirata, C.-P. Hsu, N. Ishikawa, J. Florian, A. Warshel, B. G. Johnson, P. M. W. Gill, M. Head-Gordon and J. A. Pople, *J. Comput. Chem.*, 2000, **21**, 1532.
13. A. D. Becke, *J. Chem. Phys.*, 1993, **98**, 5648.
14. R. A. Friesner, *Chem. Phys. Lett.*, 1985, **116**, 39.

15. R. A. Friesner, *Annual Rev. Phys. Chem.*, 1991, **42**, 341.
16. P. J. Hay and W. R. Wadt, *J. Chem. Phys.*, 1985, **82**, 299.
17. V. A. Rassolov, J. A. Pople, M. A. Ratner and T. L. Windus, *J. Chem. Phys.*, 1998, **109**, 1223.
18. M. M. Francel, W. J. Pietro, W. J. Hehre, J. S. Binkley, M. S. Gordon, D. J. DeFrees and J. A. Pople, *J. Chem. Phys.*, 1982, **77**, 3654.
19. D. Reddy and D. Jaganyi, *Dalton Trans.*, 2008, 6724.
20. Gaussian 03, Revision A.1, M. J. Frisch, G. W. Trucks, H. B. Schlegel, G. E. Scuseria, M. A. Robb, J. R. Cheeseman, J. A. Montgomery, Jr., T. Vreven, K. N. Kudin, J. C. Burant, J. M. Millam, S. S. Iyengar, J. Tomasi, V. Barone, B. Mennucci, M. Cossi, G. Scalmani, N. Rega, G. A. Petersson, H. Nakatsuji, M. Hada, M. Ehara, K. Toyota, R. Fukuda, J. Hasegawa, M. Ishida, T. Nakajima, Y. Honda, O. Kitao, H. Nakai, M. Klene, X. Li, J. E. Knox, H. P. Hratchian, J. B. Cross, C. Adamo, J. Jaramillo, R. Gomperts, R. E. Stratmann, O. Yazyev, A. J. Austin, R. Cammi, C. Pomelli, J. W. Ochterski, P. Y. Ayala, K. Morokuma, G. A. Voth, P. Salvador, J. J. Dannenberg, V. G. Zakrzewski, S. Dapprich, A. D. Daniels, M. C. Strain, O. Farkas, D. K. Malick, A. D. Rabuck, K. Raghavachari, J. B. Foresman, J. V. Ortiz, Q. Cui, A. G. Baboul, S. Clifford, J. Cioslowski, B. B. Stefanov, G. Liu, A. Liashenko, P. Piskorz, I. Komaromi, R. L. Martin, D. J. Fox, T. Keith, M. A. Al-Laham, C. Y. Peng, A. Nanayakkara, M. Challacombe, P. M. W. Gill, B. Johnson, W. Chen, M. W. Wong, C. Gonzalez, and J. A. Pople, Gaussian, Inc., Pittsburgh PA, 2003.
21. Mercury, Version 2.2, Cambridge Crystallographic Data Centre: Cambridge, UK, (2009).
22. *CrysAlis CCD* and *CrysAlis RED*, Version 170, Oxford Diffraction Ltd., Abingdon, UK, 2002.
23. Sheldrick, G.M. SHELXS-97, *Program for solution of crystal and structures*, University of Göttingen, Germany, 1997.
24. Sheldrick, G.M. SHELXL-97, *Program for refinement of crystal structures*, University of Göttingen, Germany, 1997.
25. R. H. Blessing, *Acta Cryst.*, 1995, **A51**, 33.
26. International Union of Crystallography, CheckCIF, [Online] URL: <http://www.iucr.org/>

27. *MicrocalTM OriginTM Version 5.0*, Microcal Software, Inc., One Roundhouse Plaza, Northampton, MA, 01060, USA, 1991–1997.



X-ray Crystallography

In an effort to understand the manner in which the azole nucleophiles bind to the metal centre in the platinum(II) terpyridyl systems and to allow for comparison with gas phase structures obtained from computational modelling, structural elucidation via X-ray diffraction was undertaken.

The substituted complexes were prepared as described in *Section 4.3*. Single-crystal growth was achieved by slow diffusion of diethyl ether into a nitromethane solution of the substituted complex. Single crystals of **PtL1-MIm(CH₃NO₂)(ClO₄)₂**, **PtL1-DIm(CH₃NO₂)(ClO₄)₂**, **PtL1-Pyz(CH₃NO₂)(ClO₄)₂** and **PtL3-Pyz(CH₃NO₂)(ClO₄)₂** were successfully prepared. From here on the X-ray structures elucidated from this study will be named without the solvent molecule or counteranions i.e. **PtL1-MIm(CH₃NO₂)(ClO₄)₂** will be referred to as **PtL1-MIm**.

A search of the Cambridge Structural Database (CSD)¹ showed that similar (but not identical) structures for some of these complexes have been elucidated previously. These will be discussed later in this monograph.

The full X-ray crystallographic data set can be found in the electronic appendix, **Appendix F**, while the IUCR² CIF check reports can be found in **Appendix B**.

5.2 X-ray structure of PtL1-MIm

The X-ray structure of **PtL1-MIm** at 296 K was obtained from a single clear yellow crystal of dimensions 0.60 x 0.60 x 0.60 mm. The X-ray structure of **PtL1-MIm** along with the crystal and diffraction pattern are shown in *Figure 5.1* overleaf.

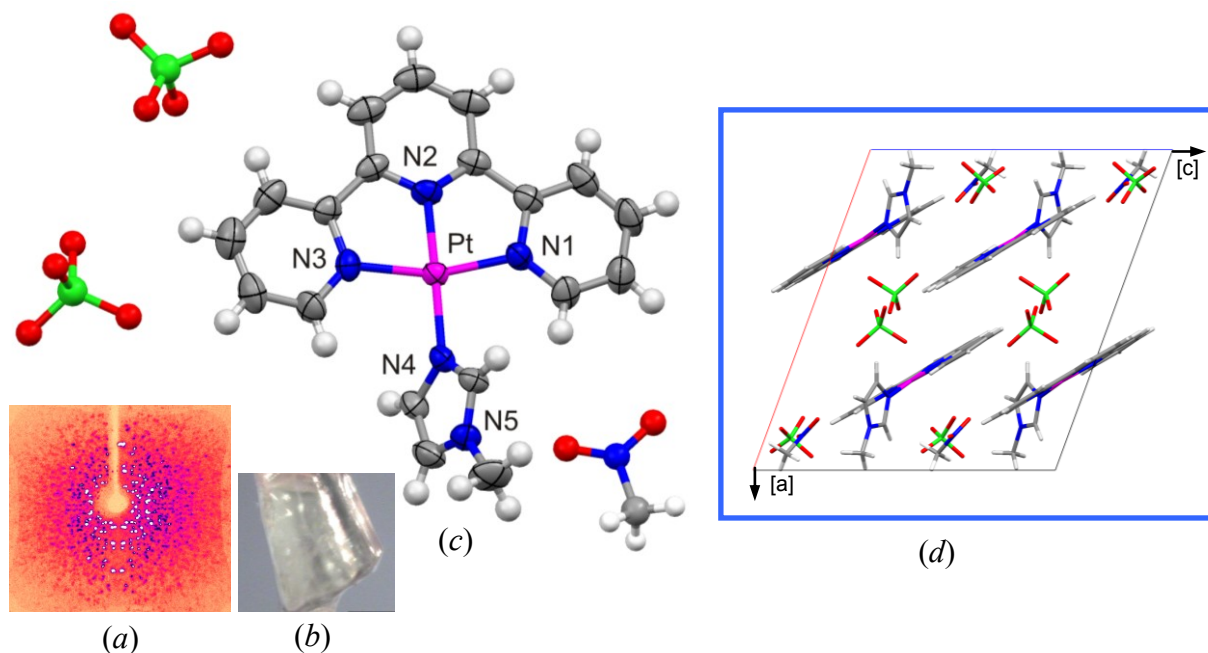


Figure 5.1: (a) Diffraction pattern, (b) Crystal, (c) Partially labelled thermal ellipsoid plot showing 50% probability surfaces of **PtL1-MIm** and (d) Unit cell of **PtL1-MIm** viewed down the *b*-axis.

The complex **PtL1-MIm**, **MIm** crystallised in the monoclinic space group $P2_1/c$. The asymmetric unit contains one complete molecule with $Z = 4$. Figure 5.1(d) shows packing in the unit cell viewed down the *b*-axis. The complex consists of **MIm** bound to **PtL1** with two perchlorate counterions present and a nitromethane solvent molecule trapped in the lattice. **MIm** binds through its second nitrogen atom to the Pt(II) terpy complex.

There is no hydrogen-bonding and no direct short contacts between adjacent Pt(II) complexes; however, the **PtL1-MIm** molecules exhibit weak long distance interactions between adjacent molecules and the counterions. The interplanar spacing between two **PtL1-MIm** molecules is 3.589 Å which is a large distance when compared to the interplanar spacing of graphite (3.35 Å).³ This large interplanar spacing is due to the steric hindrance of the bulky methyl group on the azole ligand which do not allow the **PtL1-MIm** molecules to pack closely. The solvent trapped in the lattice also plays a role in how closely the molecules pack and this is discussed later in more detail. Due to this large interplanar spacing, there are no interactions between stacked adjacent ring systems even though these ring systems appear to sit in a slipped conformation above each other, Figure 5.2.

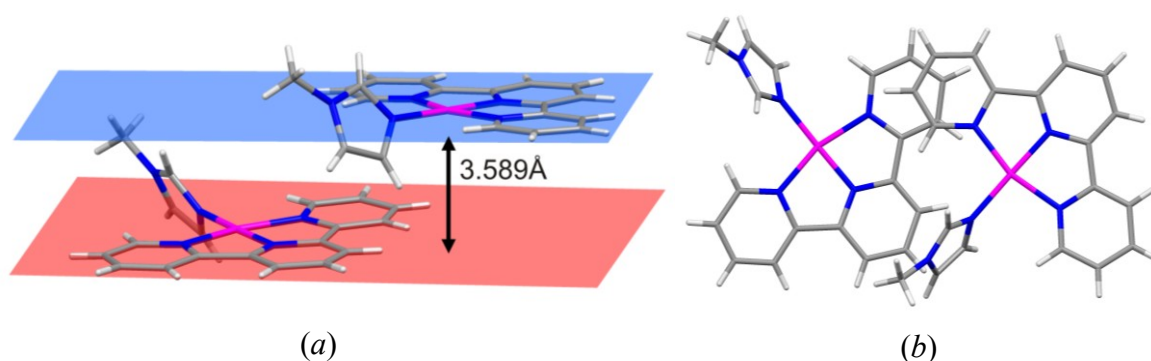


Figure 5.2: (a) Interplanar spacing and (b) Top view of ring overlap between two **PtL1-MIm** molecules.

As previously mentioned, the CSD revealed similar structures have been previously found. Roszak *et al.*⁴ have also crystallized PtL1-MIm but from acetonitrile solution and consequently has an acetonitrile molecule trapped in the lattice, **PtL1-MIm(CH₃CN)(ClO₄)₂**. J. Muller *et al.*⁵ have also managed to crystallize the **MIm** complex but with no solvent molecule trapped in the lattice, **PtL1-MIm(ClO₄)₂**. It is interesting to note (Table 5.1) the effect changing the solvent molecule can have on the bond lengths and angles of the complex.

Table 5.1: Bond lengths and angles for **PtL1-MIm**.

	X-ray*	A. Roszak <i>et al.</i> ⁴	J. Muller <i>et al.</i> ⁵	DFT
Bond distances / Å				
Pt-N4	2.013(6)	2.021(6)	2.029(5)	2.074
Pt-N1	2.021(6)	2.016(7)	2.026(5)	2.068
Pt-N3	2.025(6)	2.026(7)	2.032(5)	2.067
Pt-N2	1.925(5)	1.943(7)	1.943(4)	1.972
Bond angles / °				
N1-Pt-N3	162.2(2)	161.8(3)	162.6(2)	161.0
N2-Pt-N4	178.5(2)	179.4(3)	179.4(2)	180.0
N1-Pt-N2	80.7(3)	80.5(3)	81.5(2)	80.4
N2-Pt-N3	81.5(3)	81.3(3)	81.1(2)	80.5
Dihedral[#]	64.4(6)	66.5(2)	74.0(2)	85.6

* Present work, **PtL1-MIm(CH₃NO₂)(ClO₄)₂**.

[#] This refers to the dihedral angle between the least-squares Pt(II) terpy plane and the plane of theazole ring.

The RMS (Root Mean Squares) fit of the X-ray and DFT calculated structures is shown in *Figure 5.3*, and reflects slight structural differences between the two structures. The RMS fit supports the fact that the two structures are in relatively close agreement (RMSD (Root Mean Squares Deviation) = 0.248 Å).

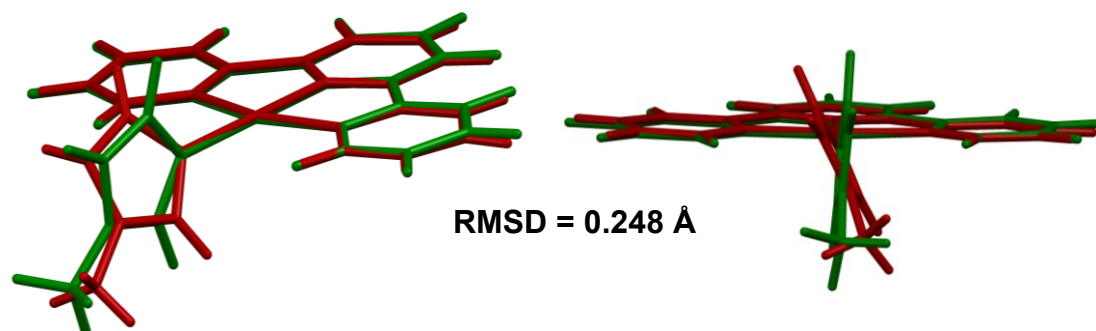


Figure 5.3: Different views of RMS fit between X-ray and the geometry optimised DFT structure **PtL1-MIm**. The red structure is the X-ray structure and the green structure is the DFT structure.

The DFT data and the experimental X-ray data vary mainly in the dihedral angle between the **MIm** ring and Pt-terpy backbone. For the gas phase calculation where there are no solvent or packing effects the **MIm** ring sits almost perpendicular to the Pt-terpy backbone with an angle of 85.6° while in the solid state the angle for the X-ray structure obtained in this study is $64.4(6)^\circ$. This is a remarkable difference and can be attributed to the cations and the role of the solvent as well as the arrangement of the molecules in the lattice.

The solvent effect can be further explored when looking at the dihedral angle for the other two reported structures. Muller's⁵ complex contains no solvent and has a dihedral angle of $74.0(2)^\circ$, differing from the DFT value by 14%, while Roszak's⁴ complex which contains acetonitrile has a smaller angle of $66.5(2)^\circ$ which differs from the calculated value by 22% and from Muller's⁵ value by 10%. When comparing Muller's⁵ complex to that of the DFT value, the 14% difference can only be due to the stacking of molecules in the solid state and the effect of the cations as neither complex contains any solvent molecules. It can be seen that by increasing the size of the solvent molecule in the lattice (from no solvent to nitromethane), the size of the dihedral angle decreases. This difference in angle size is, thus, believed to be partly due to the steric effects that the solvent molecule has on the stacking and

orientation of the complexes. *Figure 5.4* shows spacefill diagrams of the different complexes and the effect that this has on the stacking of the molecules. This figure shows the steric effect of the methyl groups on the imidazole ligand causing the large interplanar distance as already discussed.

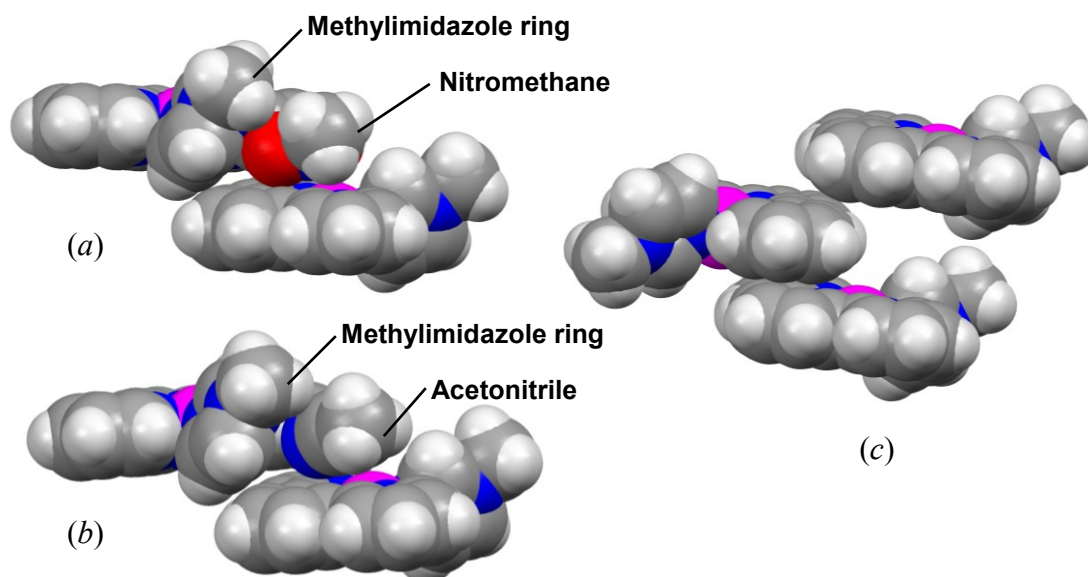


Figure 5.4: Spacefill models of (a) $\text{PtL1-MIm}(\text{CH}_3\text{NO}_2)(\text{ClO}_4)_2$ (b) $\text{PtL1-MIm}(\text{CH}_3\text{CN})(\text{ClO}_4)_2$ and (c) $\text{PtL1-MIm}(\text{ClO}_4)_2$ showing the effect of the solvent molecule on stacking.

The presence of the solvent molecule in the lattice also appears to affect how the complexes are packed. The two complexes containing the solvent molecules appear to orientate themselves in the same way with the **MIm** groups alternating by 90° whereas the complex without solvent seems to pack in a more head-to-tail arrangement, *Figure 5.5*. The packing in this latter crystal appears to be in two directions.

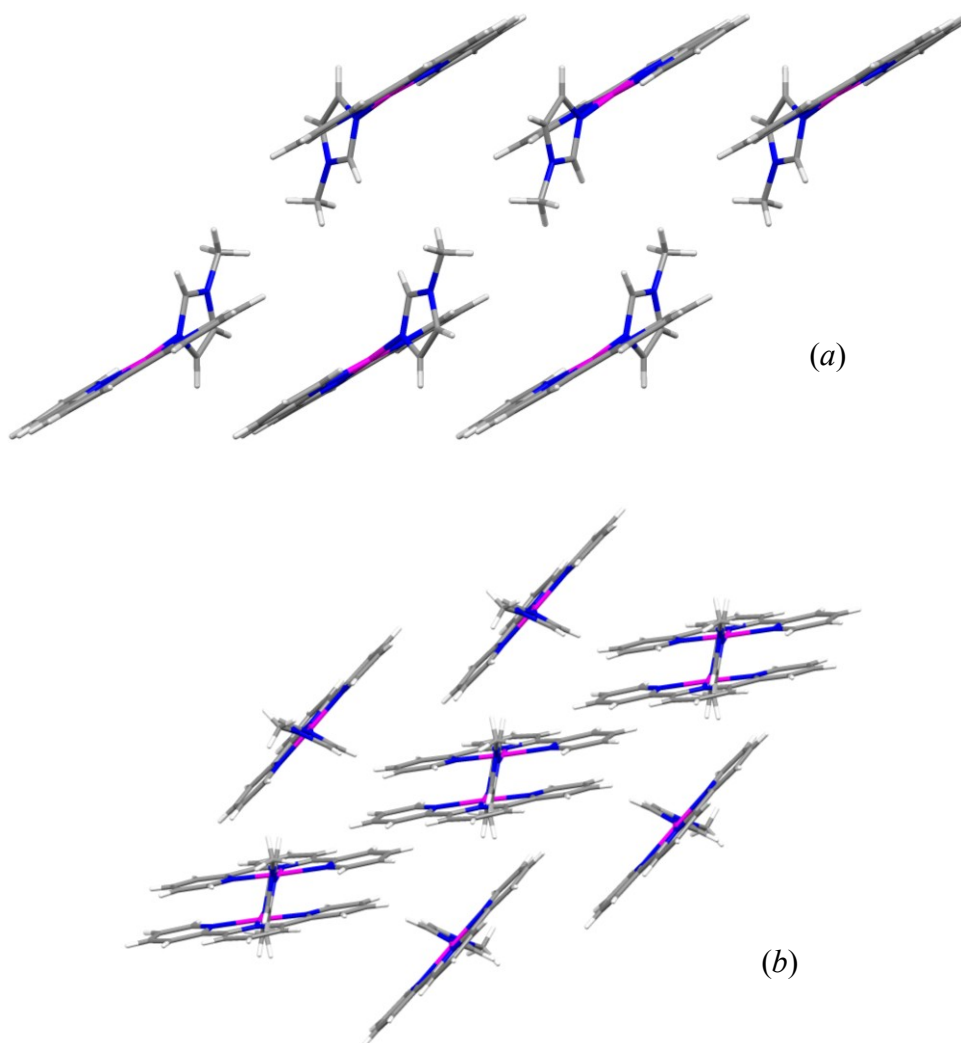


Figure 5.5: Capped-stick diagrams of (a) $\text{PtL1-MIm}(\text{CH}_3\text{NO}_2)(\text{ClO}_4)_2$ viewed down the b -axis and (b) $\text{PtL1-MIm}(\text{ClO}_4)_2$ to show packing arrangement.

5.2 X-ray Structures of PtL1-DIm, PtL1-Pyz and PtL3-Pyz

The X-ray structures of **PtL1-DIm**, **PtL1-Pyz** and **PtL3-Pyz** were obtained from clear yellow crystals of dimensions 0.40 x 0.10 x 0.07 mm, 0.60 x 0.40 x 0.20 mm and 0.60 x 0.20 x 0.07 mm respectively at 296 K. The X-ray structures of these complexes along with their crystals and diffraction patterns are shown in *Figure 5.6*. The diffraction patterns show how strong the diffraction from the crystal is and indicate whether the crystal is single or split.

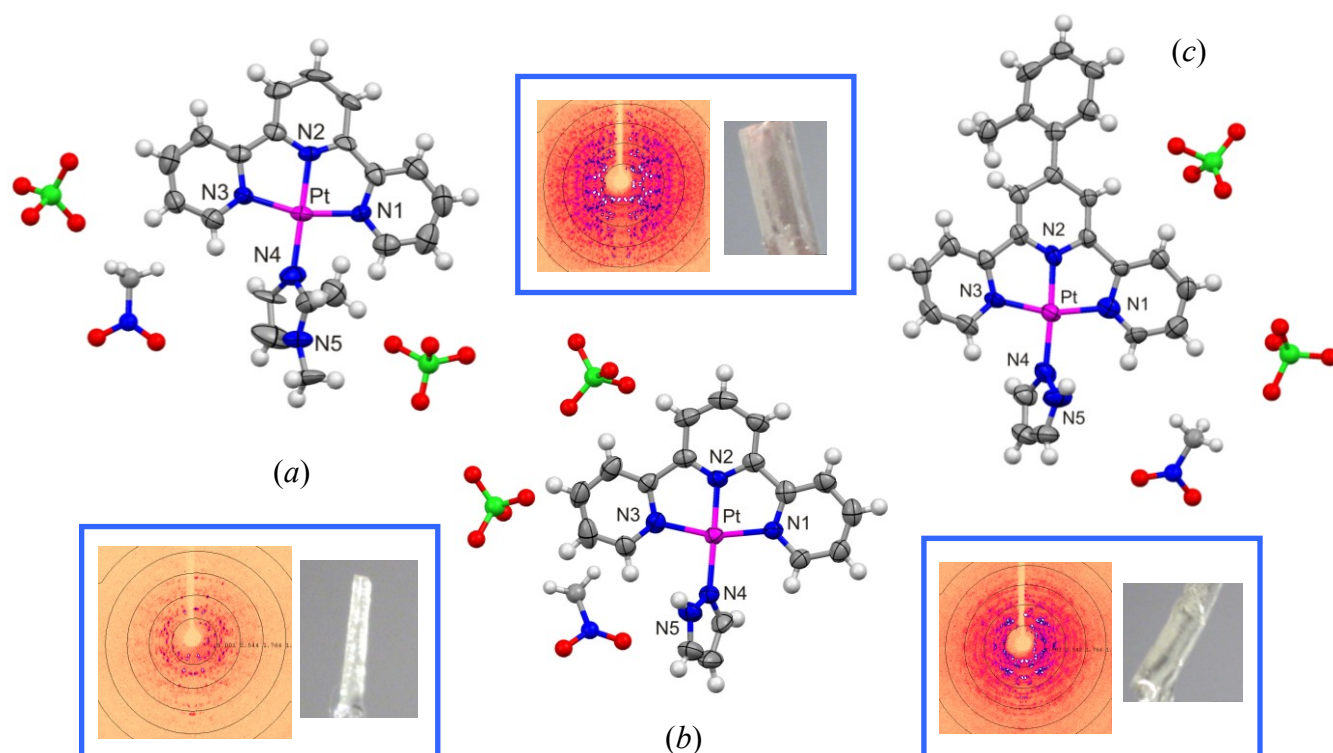


Figure 5.6: Diffraction pattern, crystal and partially labelled thermal ellipsoid plot showing 50% probability surfaces for (a) **PtL1-DIm**, (b) **PtL1-Pyz** and (c) **PtL3-Pyz**.

All three complexes have two perchlorate counterions and a nitromethane molecule in the lattice. **PtL1-DIm** and **PtL1-Pyz** crystallized in the monoclinic spacegroup $P2_1/c$ while **PtL3-Pyz** crystallized in the monoclinic spacegroup $P2_1/n$. The asymmetric unit for all three complexes contains one complete molecule with $Z = 4$

The bond lengths and bond angles obtained from the crystal structures as well as those from DFT calculations are given in *Table 5.2*.

Table 5.2: Comparison of the bond lengths and angles for **PtL1-DIm**, **PtL1-Pyz** and **PtL3-Pyz** obtained from X-ray and calculated structures.

	PtL1-DIm		PtL1-Pyz		PtL3-Pyz	
	X-ray	DFT	X-ray	DFT	X-ray	DFT
Bond distances/ Å						
Pt-N4	2.058(13)	2.075	2.011(6)	2.075	2.017(11)	2.082
Pt-N1	2.011(11)	2.066	2.017(6)	2.067	2.002(10)	2.067
Pt-N3	2.041(10)	2.066	2.025(6)	2.068	2.007(10)	2.067
Pt-N2	1.993(10)	1.973	1.924(6)	1.968	1.927(10)	1.967
Bond angles/°						
N1-Pt-N3	162.9(4)	161.0	162.2(2)	161.2	162.7(4)	161.0
N2-Pt-N4	176.5(5)	179.2	178.5(2)	179.8	175.5(4)	180.0
N1-Pt-N2	81.0(4)	80.5	81.5(3)	80.6	81.1(3)	80.5
N2-Pt-N3	81.9(4)	80.5	80.7(3)	80.6	81.8(4)	80.5
P-Dihedral[#]	—	—	—	—	40.6(13)	42.0
Dihedral*	67.0(16)	89.6	63.7(7)	88.7	76.7(13)	89.8

[#] This refers to the dihedral angle between the least-squares Pt(II) terpy plane and the plane of the phenyl-CH₃ moiety.

* This is the dihedral angle between the least-squares Pt(II) terpy plane and the plane of theazole ring.

The RMS fits of the X-ray and calculated structures of **PtL1-DIm**, **PtL1-Pyz** and **PtL3-Pyz** are shown in *Figure 5.7*. The RMS fits for **PtL1-DIm** and **PtL1-Pyz** support the fact that the structures are in relatively close agreement with RMSD values of 0.280 and 0.212 respectively.

The RMS fit for **PtL3-Pyz** does not show close agreement with a RMSD value of 0.937. This value is not a true representation of the structural differences for **PtL3-Pyz** as the geometry optimization put the structure in a different orientation to that of the X-ray structure. This made the two complexes non-superimposable and hence the RMSD value was accordingly large.

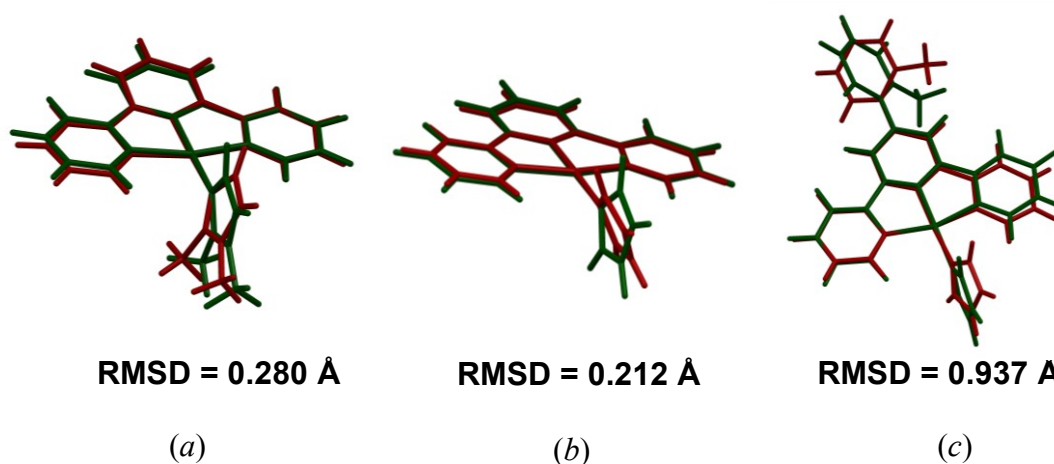


Figure 5.7: RMS fits between X-ray and the optimised DFT structures of (a) **PtL1-DIm** (b) **PtL1-Pyz** and (c) **PtL3-Pyz**. The red structure is the X-ray structure and the green structure is the DFT structure.

The DFT values for all the complexes show the azole group to be almost perpendicular to the terpy ligand, in the solid state this angle is $67.0(16)^\circ$ for **PtL1-DIm**, which differs by 25% from the calculated value. For **PtL1-Pyz** this dihedral angle is $63.7(7)^\circ$ while for **PtL3-Pyz** the angle is considerably larger with a value of $76.7(13)^\circ$ with only a 15% difference between calculated and experimental data. These differences between gas phase calculations and solid state experimental data are due to the presence of nitromethane and anions in the lattice. These in conjunction with the steric effects of the azole ligands are responsible for the differences between the structures.

The following spacefill diagrams, with and without the nitromethane solvent molecule present, *Figure 5.8*, gives a good indication of how the molecules stack in the solid state.

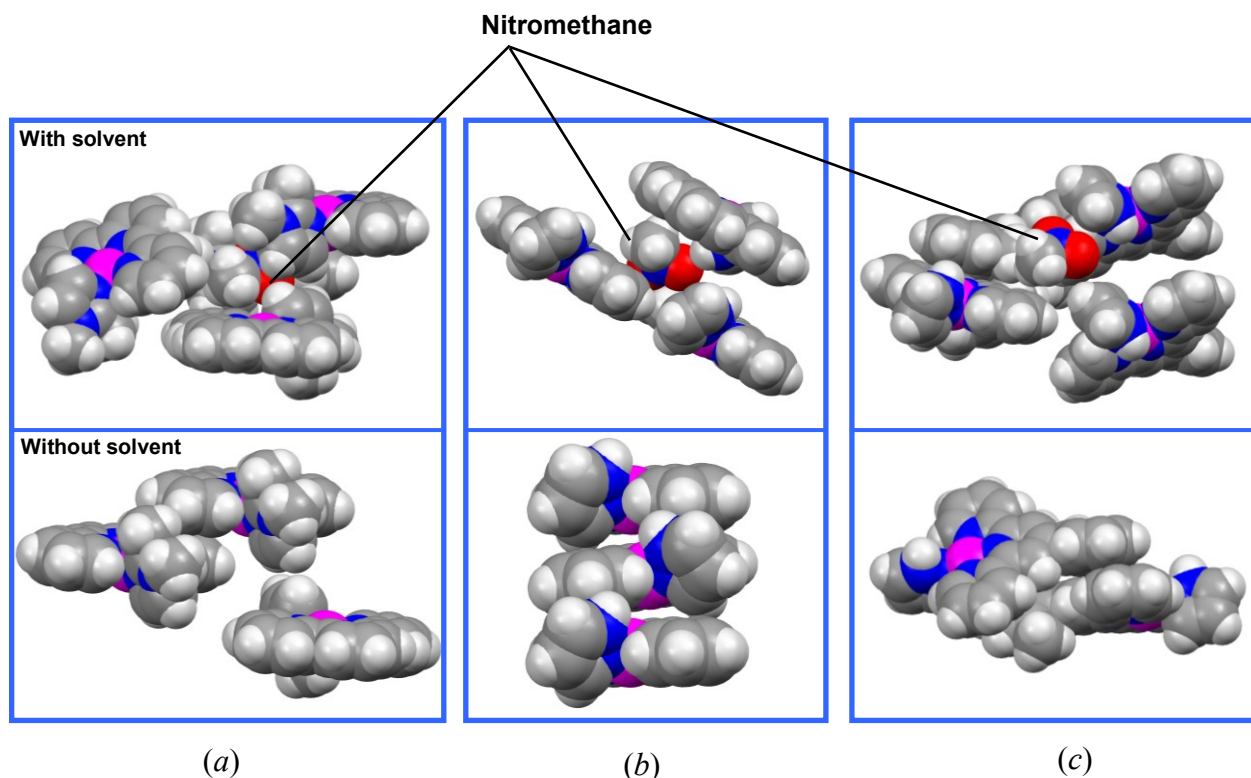


Figure 5.8: Spacefill models with and without the solvent molecules for (a) **PtL1-DIm**, (b) **PtL1-Pyz** and (c) **PtL3-Pyz**.

As can be seen from the spacefill diagrams for **PtL1-DIm**, the solvent molecule plays a small role in how the molecules pack. It is rather the bulky methyl groups in the first and second positions of the azole ring that actually dictates how close the molecules can sit to one another and in turn the size of the dihedral angle between the azole ring and the terpy backbone. For **PtL1-Pyz**, there is far less steric hindrance as there are no substituents on the azole ring. This allows the molecules to pack much closer together and hence the dihedral angle is smaller than that for **PtL1-DIm**. For **PtL3-Pyz**, although it has the less bulky Pyz nucleophile attached, it does have added steric bulk from the phenyl-CH₃ moiety on terpy ligand which does not sit in plane with the Pt(II) terpy backbone but rather at an angle of 40.6(13)^o which greatly affects how close the molecules can approach one another in the lattice. This causes the dihedral angle for **PtL3-Pyz** to be much greater than that for **PtL1-Pyz**. Due to these different steric properties, these three complexes all pack differently in space. Although **PtL3-MIm** does have the added steric bulk of an extra methyl group, it packs very similarly to **PtL1-Pyz**. Figure 5.9 shows how these molecules actually arrange themselves in space as a result of these steric and solvent effects.

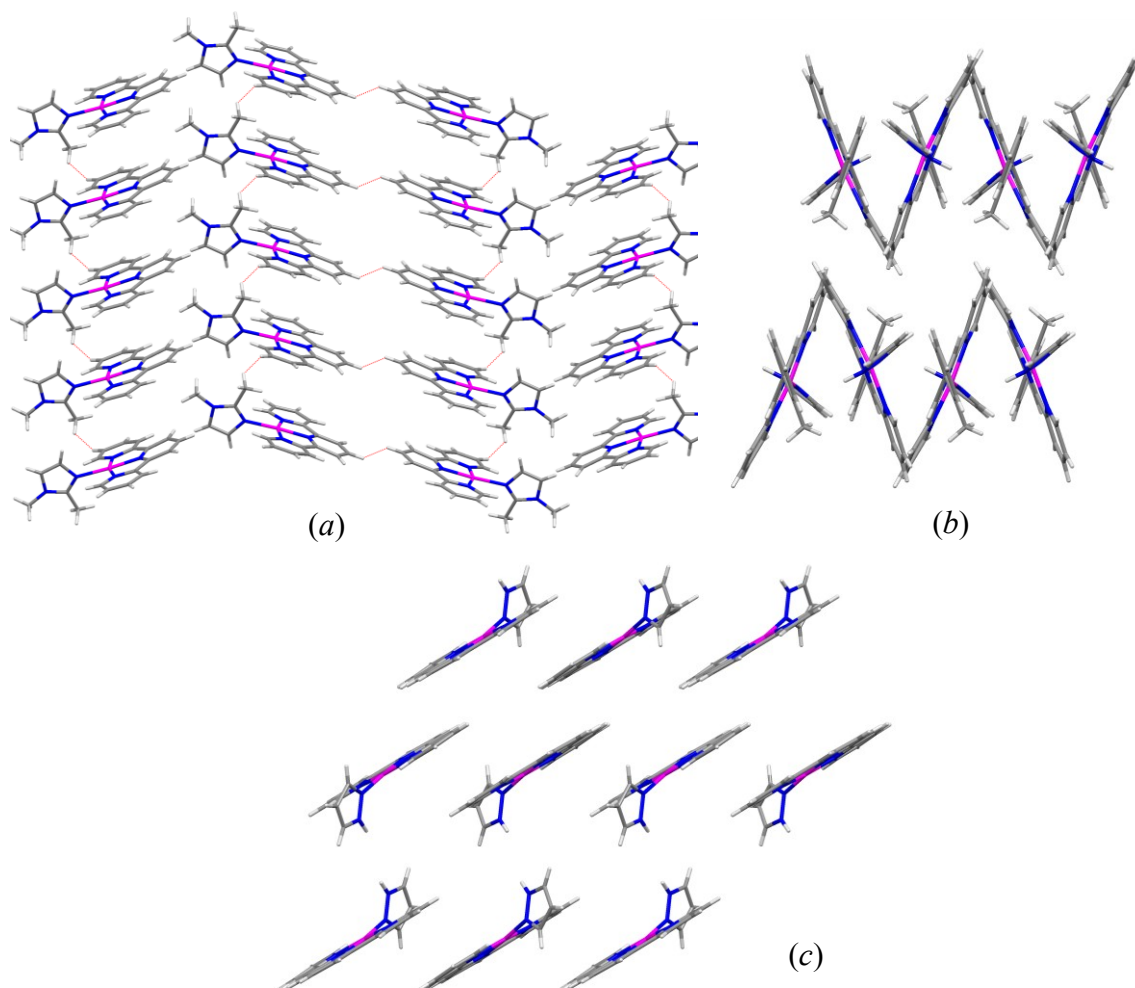


Figure 5.9: Capped stick models to show packing of (a) **PtL1-DIm**, (b) **PtL3-Pyz** viewed along the *a*-axis and (c) **PtL1-Pyz** viewed along *b*-axis.

There is no hydrogen bonding between any of the complexes. There are, however, short contacts directly between **PtL1-DIm** and **PtL1-Pyz** molecules (Figure 5.10) while **PtL3-Pyz** does not form any direct short contacts.

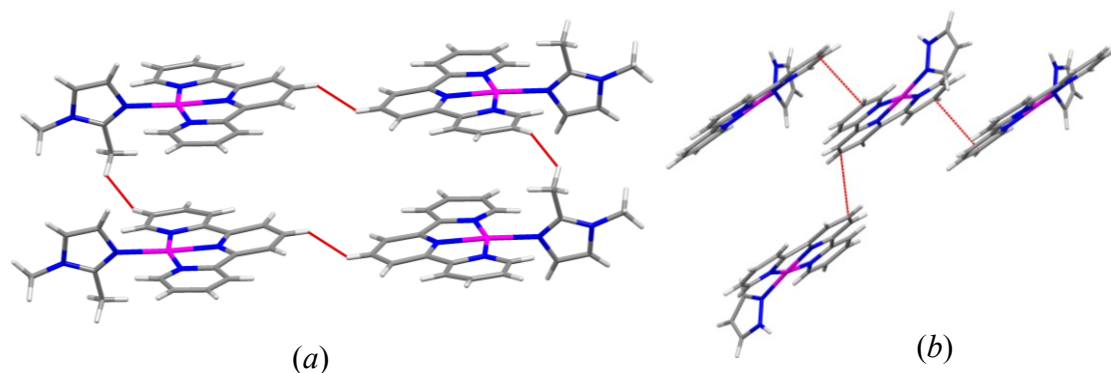


Figure 5.10: Capped stick models showing short contacts between (a) **PtL1-DIm** and (b) **PtL1-Pyz** molecules.

The interplanar distance between **PtL1-DIm** molecules is 3.438 Å which like **PtL1-MIm**'s interplanar distance of 3.589 Å suggests that any interactions between rings of adjacent molecules are very weak. For **PtL1-pyz** this interplanar distance above rings is about 3.301 Å. This would imply that there is some form of interaction between the adjacent ring systems. This interaction is often referred to as a π - π interaction, but it is actually an example of a dipole-dipole interaction rather than an attraction between overlapping π -orbitals. The slipped orientation that the molecules exhibit is ideal for these types of interactions as it is the most stable configuration as shown in *Figure 5.11*.

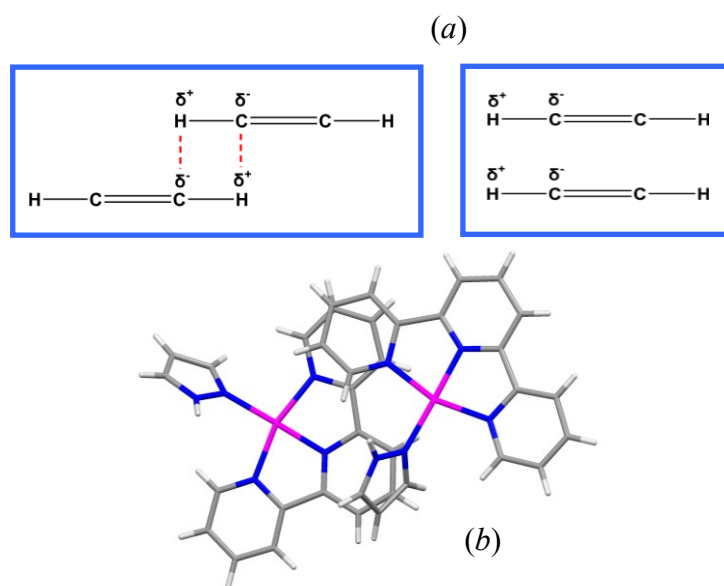


Figure 5.11: (a) Diagram showing the more stable slipped ring conformation for dipole-dipole interactions compared to the less favoured direct overlap. (b) Top view of ring overlap between two **PtL1-Pyz** molecules showing the slipped conformation.

Although from a top view of **PtL3-Pyz** it appears as if two ring systems overlap, there are no interactions between these systems as they are not actually parallel to one another, which is a requirement for interactions between π -systems, *Figure 5.12*.

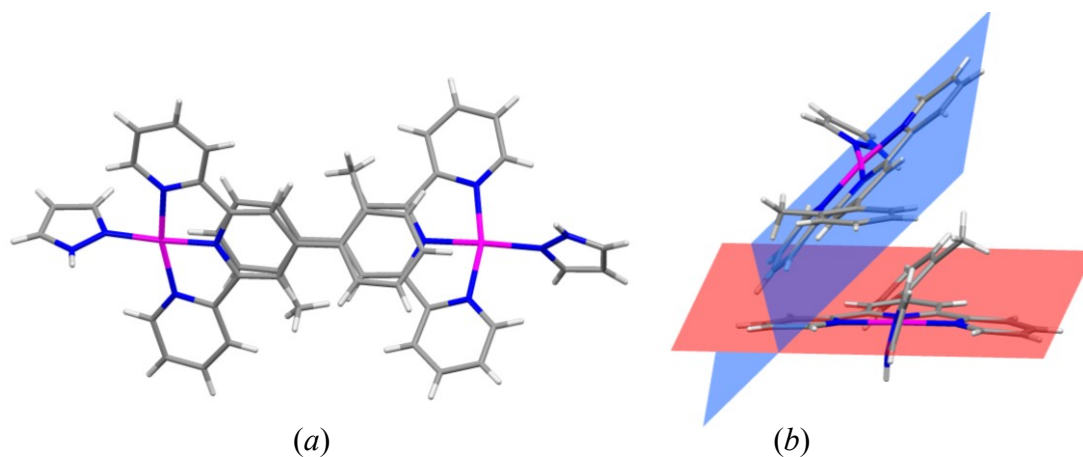


Figure 5.12: (a) Top view of two **PtL3-Pyz** molecules and (b) diagram showing the orientation of the Pt(II) terpy planes.

The **PtL1-Pyz** crystal grown in this study was bonded to **PtL1** only through the N2 atom. It is; however, possible for **Pyz** to bind through both its nitrogens, N1 and N2, and form a bridged complex as Bailey *et al.*⁶ have shown by growing a crystal of two Pt-terpy molecules bridged by a **Pyz** molecule, Figure 5.13.⁶

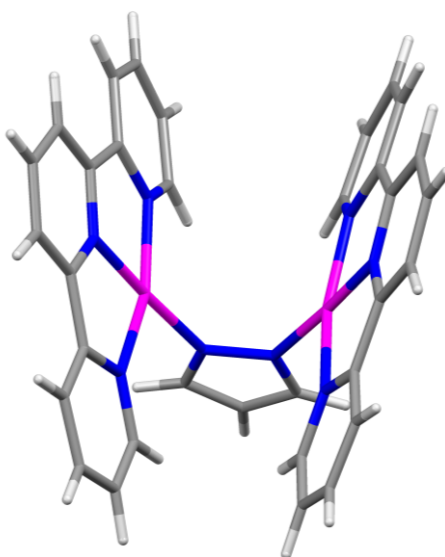
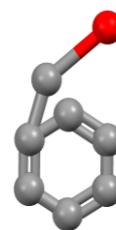


Figure 5.13: X-ray crystal structure of two Pt(II) terpys bridged by **Pyz**.

In conclusion, these crystal structures have shown how the nucleophiles bind in the solid state which gives an indication of their interactions in solution. The effects of solvents and bulky substituents have also been observed. They have also allowed for comparison of DFT structures calculated in the gas phase with experimental solid state structures.

5.4 References

69. Cambridge Crystallographic Data Centre, CSDS, 2007 release, 12 Union Rd, Cambridge CB21EZ, UK.
70. International Union of Crystallography, CheckCIF, [Online] URL: <http://www.iucr.org/>.
71. Shriver and Atkins, *Inorganic Chemistry*, 3rd Edition, Oxford University Press, pg 352.
72. A. W. Roszak, O. Clement and E. Buncel, *Acta Cryst.*, 1996, **C52**, 1654.
73. J. Muller, E. Freisinger, P. Lax, D. A. Megger and F. Polonius, *Inorg. Chim. Acta*, **360**, 2007, 255.
74. J. A. Bailey, H. B. Gray, *Acta Cryst.*, 1992, **C48**, 1420.



Results & Discussion

6.1 Results

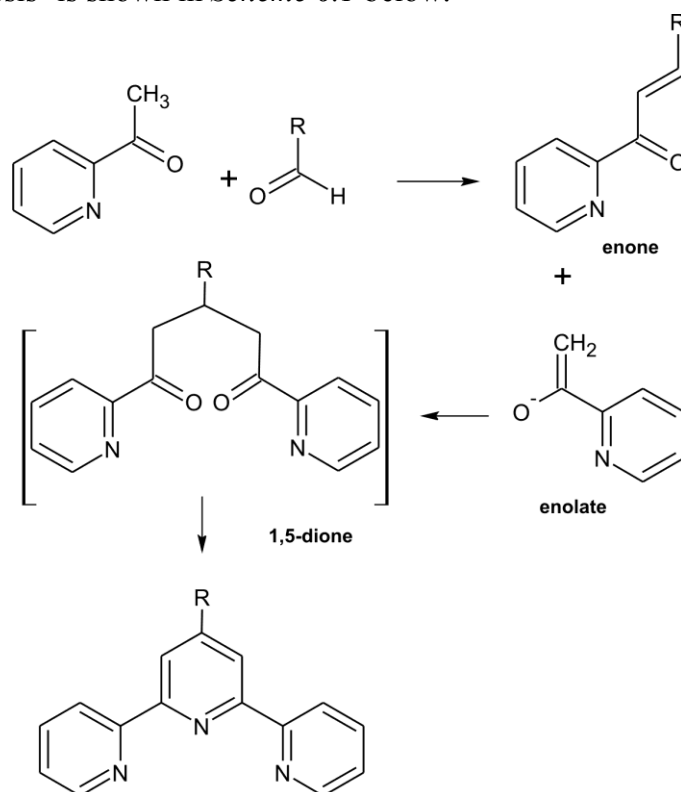
6.1.1 Ligand Synthesis

Cargill Thompson¹ has reported many methods to synthesise terpy-derived ligands; two of these general methods are: coupling methodologies and an approach involving ring assembly. The coupling approach to synthesise terpy ligands involves a copper mediated Ullman coupling of bromopyridines or oxidative coupling of pyridines by the action of iodine.² The second method for the synthesis of terpy-derived ligands involves the assembly of the central pyridine during the course of the final step of the synthesis.^{3,4}

The ligands 4'-(2'''-CH₃-Phenyl)-2,2':6',2''terpyridine (**L3**), 4'-(2'''-CF₃-Phenyl)-2,2':6',2''terpyridine (**L4**), 4'-(2'''-CF₃-Phenyl)-6-phenyl-bipyridine (**L5**) and 4'-(2'''-CH₃-Phenyl)-6-2''-pyrazinyl-2,2'bipyridine (**L6**) were prepared by the Kröhnke method of synthesis⁵. The Kröhnke method⁵ was chosen due to its flexibility in introducing new heterocycles and substituted heterocycles into the terpy ligand as well as the ability of introducing substituents in the 4'-position. An added advantage is that the reaction produces yields on a reasonable scale.

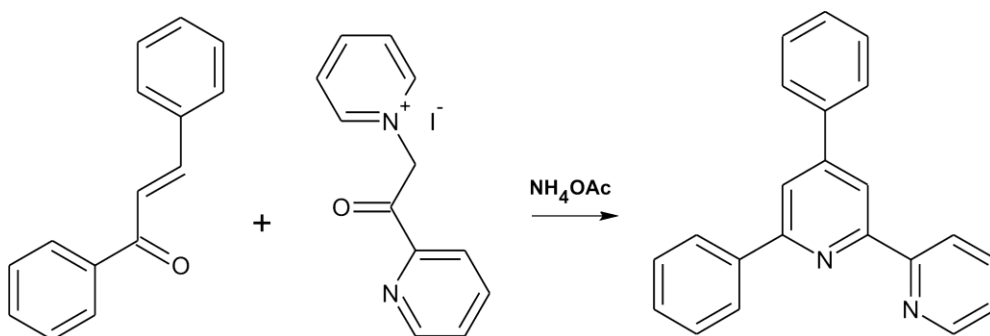
The Kröhnke synthesis⁵ falls into the second category of terpy synthesis i.e. assembly of the central pyridine during the course of the final step. This synthetic method involves the reaction of an enone with an enolate to form a pentane-1,5-dione intermediate which undergoes ring closure by the action of an ammonia source, in this case ammonium acetate. The enone is formed by the Aldol condensation of

2-acetylpyridine with an aldehyde in basic medium to give an α,β -unsaturated ketone. The choice of aldehyde determines the substituent in the 4'-position terpy. The Kröhnke synthesis⁵ is shown in *Scheme 6.1* below.



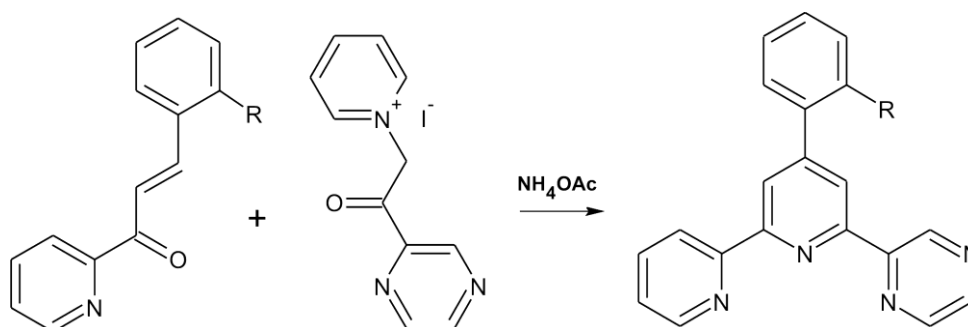
Scheme 6.1: Reaction scheme showing the general Kröhnke synthesis.⁵

If an asymmetric product is required (such as with **L5** and **L6**), the new heterocycle (i.e a heterocycle other than pyridine) can be introduced via either the enone or the enolate. Both **L5** and **L6** were synthesised by variations on the following method to synthesise 6-phenyl-2,2'-bipyridine; the desired product can be made by the reaction of 1,3-diphenyl-prop-2-en-1-one with *N*-{1-(2'-pyridyl)-1-oxo-2-ethyl}pyridinium iodide, *Scheme 6.2*.



Scheme 6.2: Method to synthesise 6-phenyl-2,2'-bipyridine.⁵

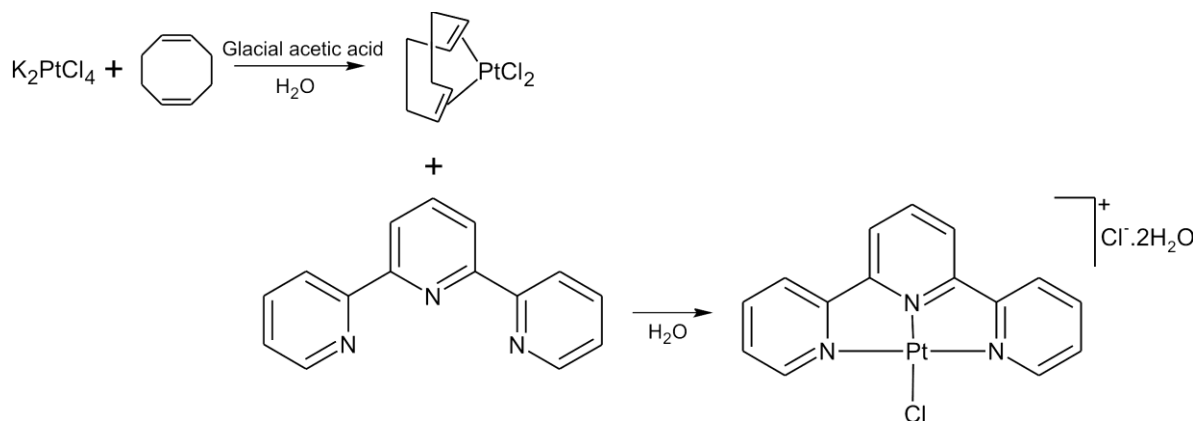
In order to assemble the desired 6-(2''-pyrazinyl)-bipyridine ligand (**L6**) the kröhnke method was extended to allow for the incorporation of the pyrazine. The pyrazine functionality was introduced via the enolate with synthesis of *N*-{1-(2'-pyrazinyl)-1-oxo-2-ethyl}pyridinium iodide. This was then reacted with the desired enone, *Scheme 6.3*.



Scheme 6.3: Synthetic route to pyrazinyl-bipyridine derivatives.⁵

6.1.2 Complex Synthesis

The complex, **PtL1** was prepared using the method of Annibale *et al.*⁹ in which [Pt(COD)Cl₂] was reacted with terpy in water. The COD ligand has a good *trans*-labilising effect which allows for easy replacement of the chloride by terpy, *Scheme 6.4*. The complex was isolated as a red dehydrate salt, [Pt(terpy)Cl]Cl·2H₂O, in good yield (85%) and characterised by elemental analysis, MS and IR.



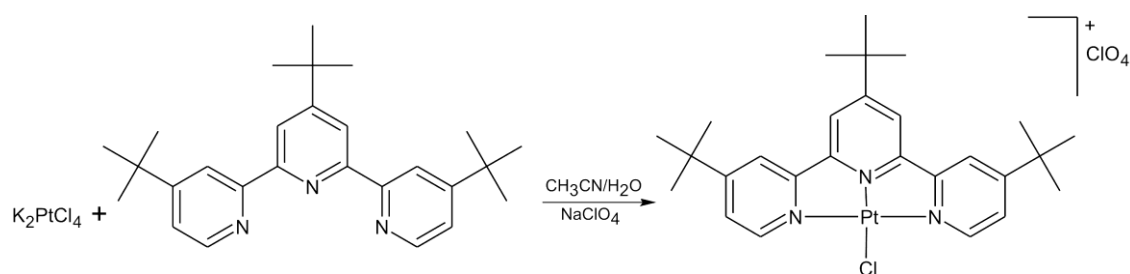
Scheme 6.4: Synthesis of **PtL1** via a Pt(COD)Cl₂ intermediate.

The elemental analysis of **PtL1** indicated the presence of the two waters of crystallization with a strong, broad peak at 3301 cm⁻¹ in the IR spectrum serving to

confirm the presence of water in the sample. A molecular ion peak was found at 463.03 on the mass spectrum which correlates to a cation molecular formula of $C_{15}H_{11}N_3ClPt$.

PtL2 was prepared by the method of Che *et al.*⁷ in which K_2PtCl_4 and tBu_3terpy was refluxed in CH_3CN/H_2O for a period of 24 hours, *Scheme 6.5*. The title complex was isolated as bright yellow crystals in a yield of 55% and fully characterised.

Metal complexes containing the ligand, tBu_3terpy have high solubility in organic solvents, due to the presence of the hydrophobic tBu groups.⁷ Thus, $[Pt({}^tBu_3terpy)Cl]^+$ is soluble in acetonitrile, whereas $[Pt(terpy)Cl]^+$ has low solubility in dichloromethane and acetonitrile. The bulky tBu substituents also minimize intermolecular interactions in solution and solid states.⁷

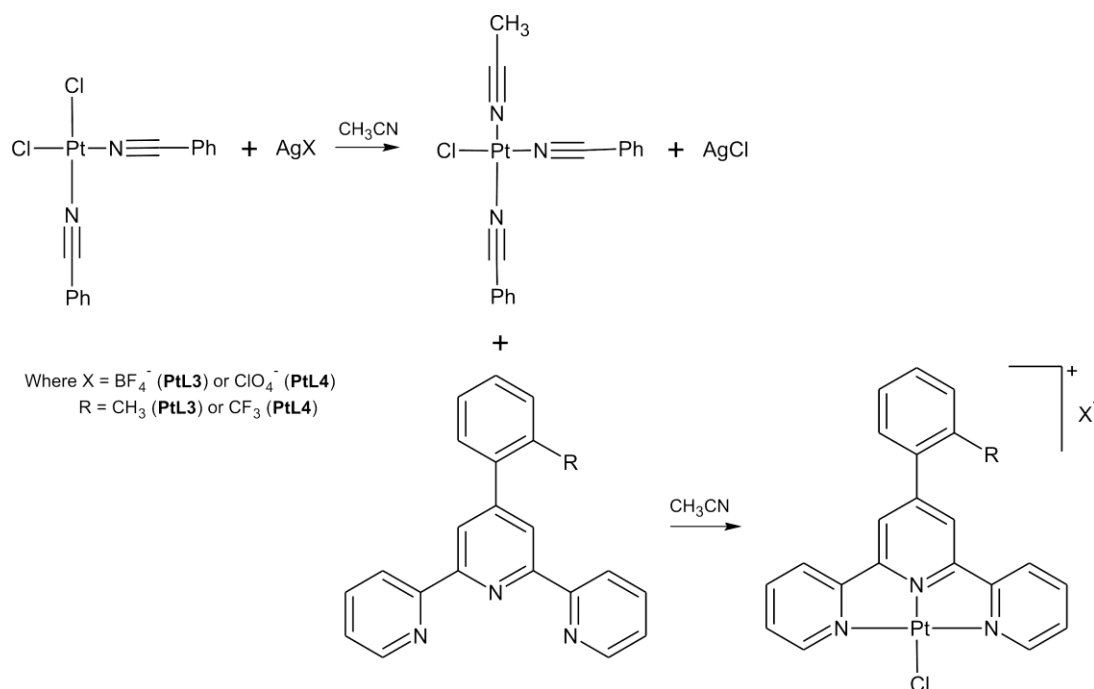


Scheme 6.5: Reaction scheme illustrating the synthesis of **PtL2**.

This complex has a ^{195}Pt NMR shift at -2731.7 ppm in acetonitrile. As expected the tBu_3 groups are found far upfield in the 1H NMR spectrum ($DMSO-d_6$ solvent) and are resolved into two peaks integrating to 9 and 18 for the middle tBu group and the two outer symmetric tBu groups respectively. The rest of the phenyl peaks are found between 7.70 and 8.65 ppm. A molecular ion peak was found at 631.22 on the mass spectrum which corresponds to a cation molecular formula of $C_{27}H_{35}N_3ClPt$.

Both **PtL3** and **PtL4** were synthesised using similar methods by Field *et al.*^{8,9} whereby $[Pt(C_6H_5CN)_2Cl_2]$ was treated with an equimolar amount of AgX (where $X = BF_4^-$ or $CF_3SO_3^-$) in refluxing CH_3CN . This leads to the formation of a species which can be described as $[Pt(C_6H_5CN)_{3-n}(CH_3CN)_nCl]X$ ($n = 1, 2$ or 3). This species is reacted with one equivalent of the appropriate ligand and refluxed to afford a bright yellow powder of **PtL3** in good yield (75%) or an orange powder of **PtL4** in a 70%

yield. *Scheme 6.6* illustrates this method of synthesis. Both complexes were characterised by elemental analysis, MS, NMR and IR.



Scheme 6.6 Method used to synthesise **PtL3** and **PtL4**.

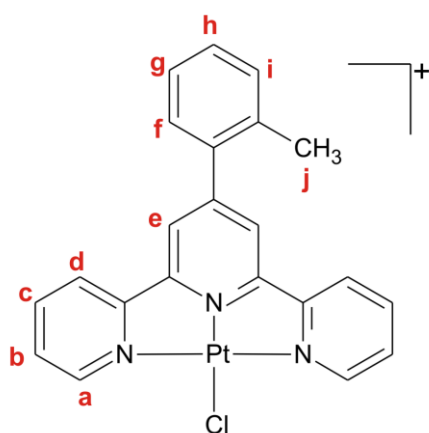


Figure 6.1: Labeled structure of **PtL3**

used for ^1H NMR.

For **PtL3**, the BF_4^- counterion was identified in the IR spectrum as having a very strong, broad peak at 1051 cm^{-1} . **PtL3** has a ^{195}Pt NMR shift at -2721.8 ppm in DMSO-d_6 . The assignment of the NMR spectrum was difficult due to the vast number of multiplets between 7.5 and 8.7 ppm. A number of 2D NMR experiments had to be employed in the assignment of the

spectra. The methyl group (**j**) was found as a singlet at 2.47 ppm with the phenyl group (**f, g, h, i**) shift being found integrating to 4 at 7.50 ppm. From a ^{15}N - ^1H HMBC experiment, the shift at 7.80 ppm was shown to correlate to **b** and its corresponding symmetric proton. From COSY experiments it was determined that the shift at 8.40 ppm was related to **c** and its symmetrically equivalent proton while the shift at 8.66, which integrated to 4 protons, was due to **a, d** and their related protons. The remaining singlet at 8.71 ppm correlated to **e** and its symmetrically equivalent proton. A

molecular ion peak was found at 553.08 on the mass spectrum which corresponds to a cation molecular formula of $C_{22}H_{17}N_3ClPt$.

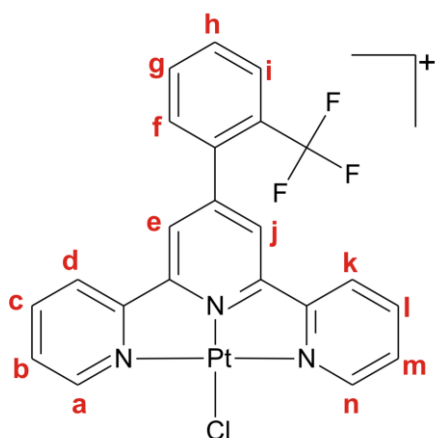
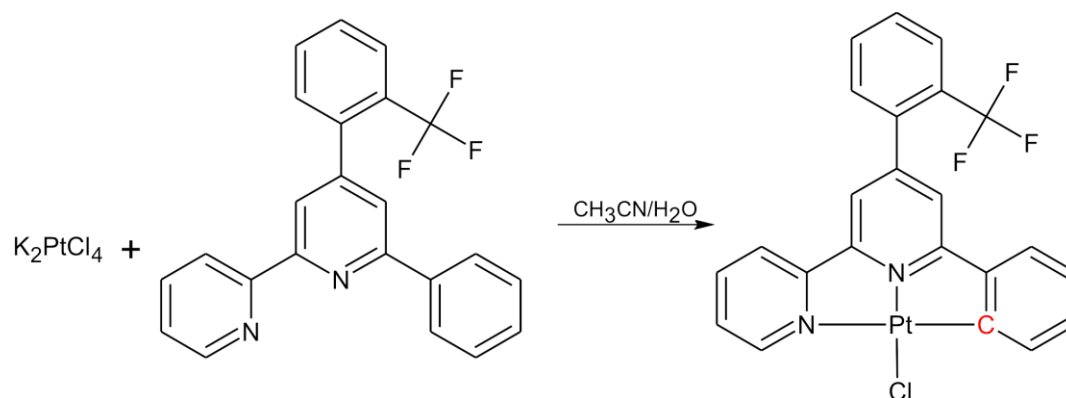


Figure 6.2: Labelled structure of **PtL4** used for 1H NMR.

For **PtL4**, the $CF_3SO_3^-$ counterion was identified on the IR spectrum by strong peaks at 1029, 1263 and 1316 cm^{-1} . **PtL4** has a ^{195}Pt NMR shift very similar to **PtL3** situated at -2724.1 ppm in DMSO- d_6 solvent. Again many 2D experiments had to be used in the assignment of the 1H NMR spectrum for this complex, namely: ^{15}N - 1H HMBC, NOESY and COSY / SELCOSY experiments. The singlet at 8.78 ppm could be readily

identified as **e** and **j**. A NOESY experiment was then used to identify the shift at 7.70 ppm as the proton at **f**. The shift at 8.65 ppm could be assigned to **d** and **k** as it was coupled to **e** and **j** according to the NOESY experiment. A COSY experiment showed that the peak at 8.48 ppm was **c** and **l** as there was coupling to **d** and **k**. The peaks **g**, **h**, **b**, **m** were found overlapping as a large multiplet at 7.85-7.97 ppm with the peaks at 8.06 and 8.85 ppm corresponding to **i** and **a** respectively. A molecular ion peak was found at 607.05 on the mass spectrum which corresponds to a cation molecular formula of $C_{22}H_{14}N_3F_3ClPt$.

The synthesis of **PtL5** follows that described by Cheung *et al.*¹⁰ An equimolar mixture of $K_2[PtCl_4]$ and 4'-(2'''- CF_3 -Phenyl)-6-phenyl-bipyridine (**L5**) in 50% aqueous acetonitrile was refluxed to afford an orange product of **PtL5** in good yield (91%). Scheme 6.7 below illustrates this method of synthesizing **PtL5**. The product was fully characterised.



Scheme 6.7: Reaction scheme illustrating the synthesis of **PtL5**.

The sample was too dilute to obtain a ^{195}Pt spectrum. The ^1H NMR spectrum in DMSO d_6 has been previously fully assigned and the spectrum obtained in this study compared favourably. A molecular ion peak was found at 628.0343 on the mass spectrum which corresponds to a cation molecular formula of $\text{C}_{23}\text{H}_{14}\text{N}_2\text{F}_3\text{NaClPt}$. The sodium that is present just indicates that Na^+ has charged the species rather than H^+ in ES^+ .

The complex, **PtL6** was synthesised using methods described by Field *et al.*¹¹, whereby $[\text{Pt}(\text{PhCN})_2\text{Cl}_2]$ was refluxed overnight in acetonitrile in the presence of one equivalent of AgCF_3SO_3 . The addition of an equimolar amount of **L6** afforded the red product. This approach was successful although yields were noticeably reduced (45%). A more favourable method would probably be one using $[\text{Pt}(1,5\text{-COD})\text{-I}_2]$ as a starting material as employed by Lowe and Vilaivan.¹²

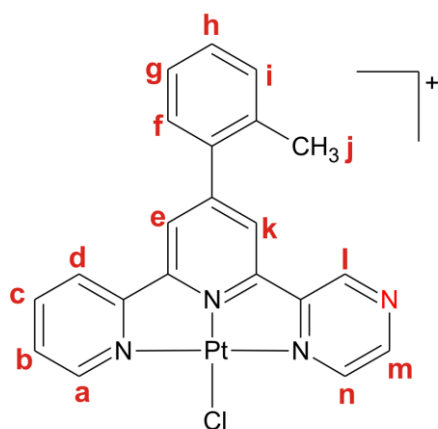


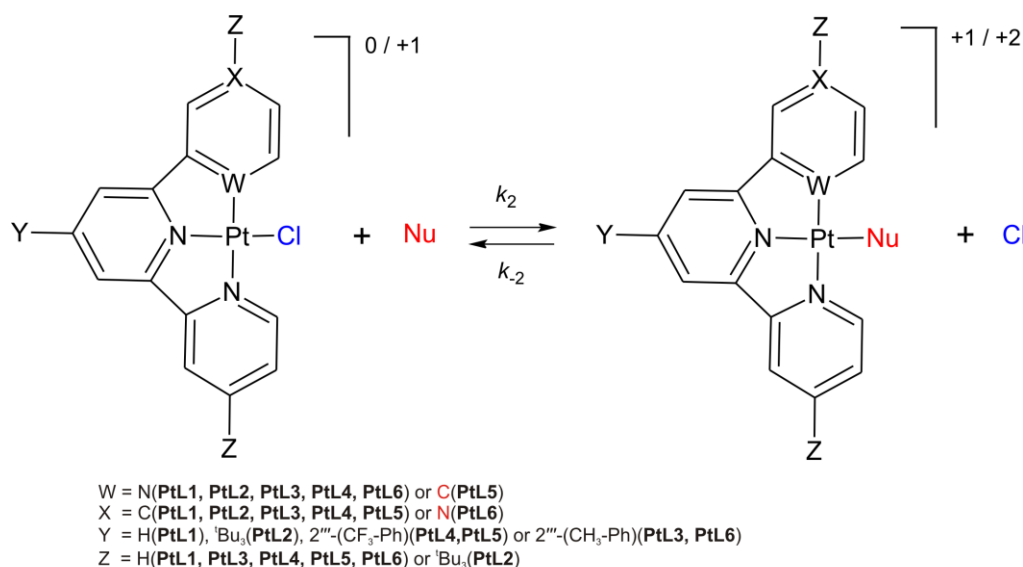
Figure 6.3: Labelled structure of **PtL6** used for ^1H NMR.

For **PtL6**, the CF_3SO_3^- counterion was identified on the IR spectrum by strong peaks at 1030, 1142 and 1261 cm^{-1} . **PtL6** has a ^{195}Pt NMR shift of -2724.1 ppm in DMSO- d_6 . The methyl group (**j**) was found at 2.45 ppm in the ^1H NMR spectrum (DMSO- d_6) with the phenyl protons (**f**, **g**, **h**, **i**) present as a multiplet between 7.49-7.55 ppm. The protons **l**, **n** and **m** are the most downfield at 9.91, 9.16 and 8.93 ppm respectively. Using NOESY and COSY

experiments the shifts at 7.96, 8.54, 8.75, 8.81, 8.86 and 8.89 ppm were assigned to the protons **b**, **c**, **d**, **e**, **k** and **a** respectively. A molecular ion peak was found at 554.07 on the mass spectrum which corresponds to a cation molecular formula of $C_{21}H_{16}N_4ClPt$.

6.1.3 Kinetic Measurements

Substitution of the coordinated chloride from Pt(II) terpy and analogous complexes by five different nucleophiles (Nu), namely: imidazole (**Im**), 1-methylimidazole (**MIm**), 1,2-dimethylimidazole (**DIm**), pyrazole (**Pyz**) and 1,2,4-triazole (**Trz**) was investigated (Scheme 6.8) under *pseudo* first-order conditions as a function of concentration and temperature. Conventional UV/Visible spectrophotometry was initially used to follow the course of the reaction in order to ascertain the time-scale for complete ligand substitution. Substitutions occurring in less than sixteen minutes were followed using stopped-flow spectrophotometry whilst those requiring longer times were followed using conventional UV/Visible techniques.



Scheme 6.8: Substitution of labile chloride ligand from Pt(II) terpy and analogous complexes by a series of azole ligands..

A typical prerun was completed by mixing solutions of **PtL3** (2.43×10^{-5} M) and **Im** (2.43×10^{-4} M) at an ionic strength of 0.1 M (90 mM LiCF₃SO₃ and 10 mM NaCl*) in a cuvette and a spectrum of absorbance vs wavelength was recorded over time by the

* The 10 mM NaCl was added to prevent solvolysis.

UV/Visible spectrophotometer (Figure 6.4). The spectra of other complexes and nucleophiles give similar results.

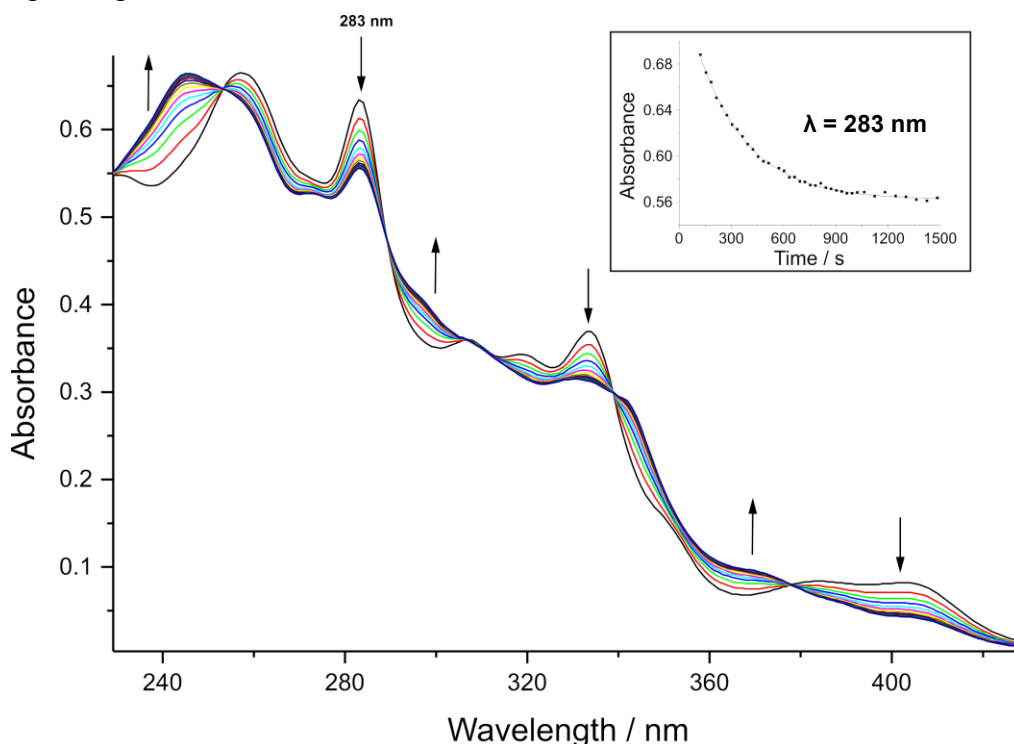


Figure 6.4: Absorbance spectrum of **PtL3** (2.43×10^{-5} M) and **Im** (2.43×10^{-4} M) at an ionic strength of 0.1 M (90 mM LiCF_3SO_3 and 10 mM NaCl) at 25 °C with the corresponding kinetic trace inset.

The observed *pseudo* first-order rate constants, k_{obs} , were calculated from the kinetic traces using the online non-linear least-squares fit of exponential data to Equation 6.1:

$$A_t = A_0 + A_\infty - A_\infty \exp(-k_{\text{obs}} t) \quad \dots 6.1$$

where A_0 , A_t and A_∞ represent the absorbance of the reaction mixture initially, at time t and at the end of the reaction respectively. This plot is shown as an insert in Figure 6.1 based on 283 wavelength.

The *pseudo* first-order rate constants were plotted against the concentration of the nucleophiles according to Equation 6.2. The values represent an average of two from the UV/visible spectrophotometer or five to eight independent runs from the stopped-flow spectrophotometer. Straight lines with zero intercepts were obtained for the substitution reactions of **PtL2** with **Im**, **MIm** and **DIm** and for **PtL5** with all

nucleophiles. Straight lines with appreciable intercepts were obtained for the remainder of the complexes with the nucleophiles, indicating that reverse reactions were present.

$$k_{obs} = k_2[\text{Nu}] + k_{-} \quad \dots 6.2$$

The second-order rate constant, k_2 , for the forward reaction of each metal complex with a particular nucleophile was obtained from the slope and the rate constant for the reverse reaction, k_{-} , was calculated from the y-intercept of a linear regression from these plots. A typical plot is shown in *Figure 6.5(a)* for the substitution reaction of **PtL3** with **Im**. The data for k_2 and k_{-} are tabulated in *Table 6.1*.

The temperature dependence of the rate constants were studied in a similar manner over the range 15 to 35 or 40 °C using all the nucleophile concentrations for the reversible reactions and only the 30x nucleophile concentration for the irreversible reactions. The activation parameters, ΔH^\ddagger and ΔS^\ddagger were calculated from the rate constants at the different temperatures using the Eyring equation (*Equation 3.58*). Examples of plots obtained are shown in *Figure 6.5(b)* and *(c)* with the corresponding data in *Table 6.1*. Further tables with reaction rates and activation parameters at 15, 20, 30 and 35 °C can be found in **Appendix C**.

$$\ln\left(\frac{k_2}{T}\right) = \frac{\Delta H^\ddagger}{R} \cdot \frac{1}{T} + \left[\ln\left(\frac{k_b}{h}\right) + \frac{\Delta S^\ddagger}{R} \right] \quad \dots 3.58$$

Where $\ln \frac{k_b}{h} = 23.8$.

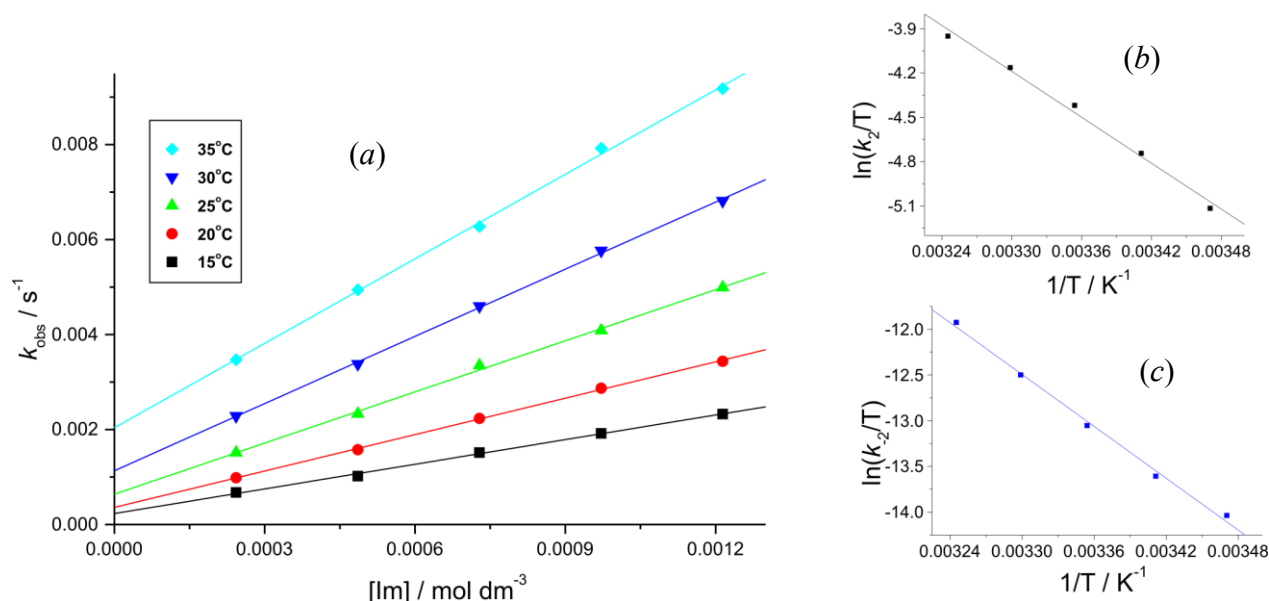
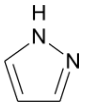
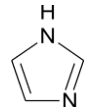
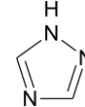
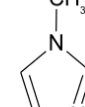
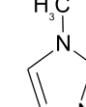
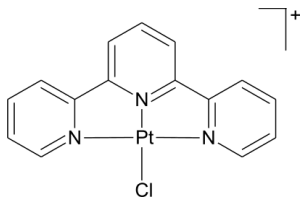
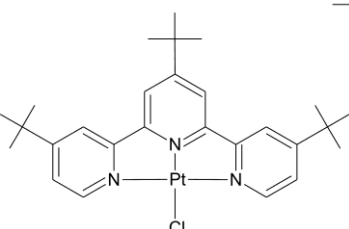


Figure 6.5: (a) Plot to determine rate constants from the slopes and y-intercepts for **PtL3** and **Im** at varying temperatures. Eyring plot to determine ΔH^\ddagger and ΔS^\ddagger for the (b) forward reaction and (c) reverse reaction.

Table 6.1: Experimentally measured reaction rates with associated errors and activation parameters for the substitution reactions of Pt(II) terpy and analogous complexes with Nu at 25 °C.

Complexes	Kinetic / Thermodynamic Parameter	Pyz 	Im 	Trz 	MIm 	DIm 
PtL1 	k_2 (M ⁻¹ s ⁻¹)	2.25 ± 0.11	3.89 ± 0.05	1.04 ± 0.07	3.84 ± 0.04	1.62 ± 0.04
	ΔH (kJ mol ⁻¹)	42 ± 1	41 ± 0.3	40 ± 2	42 ± 0.4	46 ± 1
	ΔS (J K ⁻¹ mol ⁻¹)	-96 ± 5	-96 ± 1	-107 ± 6	-91 ± 1	-88 ± 3
	k_{-2} (M ⁻¹ s ⁻¹)	6.91x10 ⁻⁴ ± 6.5x10 ⁻⁵	1.44x10 ⁻³ ± 5x10 ⁻⁵	1.60x10 ⁻⁴ ± 4.0x10 ⁻⁵	1.31x10 ⁻³ ± 2x10 ⁻⁵	1.19x10 ⁻⁴ ± 2.0x10 ⁻⁵
	ΔH (kJ mol ⁻¹)	40 ± 1	77 ± 2	50 ± 5	77 ± 2	84 ± 2
	ΔS (J K ⁻¹ mol ⁻¹)	-169 ± 5	-46 ± 5	-153 ± 18	-41 ± 6	-40 ± 8
PtL2 	k_2 (M ⁻¹ s ⁻¹)	0.648 ± 0.033	1.42 ± 0.01	0.846 ± 0.034	1.61 ± 0.02	0.624 ± 0.001
	ΔH (kJ mol ⁻¹)	45 ± 3	47 ± 0.7	57 ± 3.0	45 ± 0.5	47 ± 0.4
	ΔS (J K ⁻¹ mol ⁻¹)	-98 ± 9	-84 ± 2	-56 ± 10	-91 ± 2	-90 ± 1
	k_{-2} (M ⁻¹ s ⁻¹)	7.45x10 ⁻⁴ ± 9.1 x10 ⁻⁵		3.64x10 ⁻⁴ ± 9.2 x10 ⁻⁵		
	ΔH (kJ mol ⁻¹)	63 ± 5	*	70 ± 10	*	*
	ΔS (J K ⁻¹ mol ⁻¹)	-94 ± 15		-79 ± 35		

* No reverse reactions were observed

Table 6.1 continued...

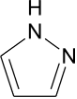
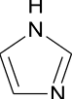
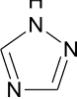
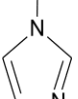
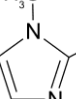
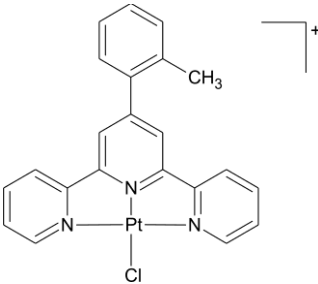
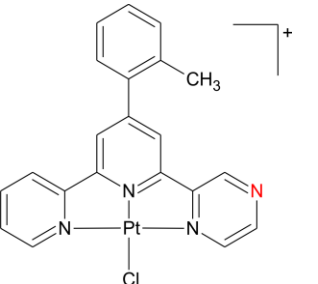
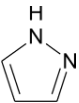
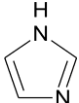
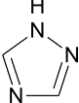
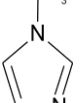
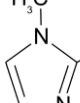
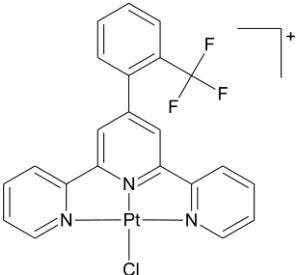
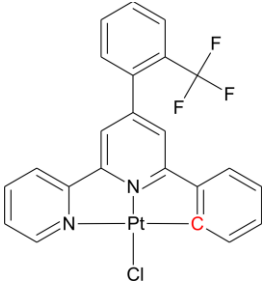
Complexes	Kinetic / Thermodynamic Parameter	Pyz 	Im 	Trz 	MIm 	DIm 
PtL3 	k_2 ($\text{M}^{-1}\text{s}^{-1}$)	2.39 ± 0.13	3.59 ± 0.09	0.851 ± 0.043	3.26 ± 0.10	1.04 ± 0.03
	ΔH (kJ mol^{-1})	45 ± 3	43 ± 2	40 ± 2	48 ± 1	50 ± 2
	ΔS ($\text{J K}^{-1} \text{mol}^{-1}$)	-86 ± 11	-91 ± 7	-110 ± 6	-75 ± 5	-77 ± 8
	k_2 ($\text{M}^{-1}\text{s}^{-1}$)	$1.02 \times 10^{-3} \pm 1.0 \times 10^{-4}$	$6.39 \times 10^{-4} \pm 7.0 \times 10^{-5}$	$9.73 \times 10^{-5} \pm 3.50 \times 10^{-5}$	$8.01 \times 10^{-4} \pm 7.9 \times 10^{-5}$	$1.04 \times 10^{-4} \pm 2.2 \times 10^{-5}$
	ΔH (kJ mol^{-1})	85 ± 5	79 ± 3	67 ± 4	78 ± 4	85 ± 6
	ΔS ($\text{J K}^{-1} \text{mol}^{-1}$)	-18 ± 18	-43 ± 11	-98 ± 12	-42 ± 12	-39 ± 18
PtL6 	k_2 ($\text{M}^{-1}\text{s}^{-1}$)	6.09 ± 0.48	11.1 ± 0.4	1.70 ± 0.10	12.9 ± 0.8	3.15 ± 0.11
	ΔH (kJ mol^{-1})	30 ± 1	48 ± 1	45 ± 3	45 ± 2	41 ± 1
	ΔS ($\text{J K}^{-1} \text{mol}^{-1}$)	-128 ± 3	-64 ± 5	-92 ± 9	-74 ± 6	-97 ± 3
	k_2 ($\text{M}^{-1}\text{s}^{-1}$)	$1.19 \times 10^{-3} \pm 1.9 \times 10^{-4}$	$2.53 \times 10^{-3} \pm 1.4 \times 10^{-4}$	$3.91 \times 10^{-4} \pm 3.7 \times 10^{-5}$	$3.60 \times 10^{-3} \pm 3.1 \times 10^{-4}$	$3.49 \times 10^{-4} \pm 4.2 \times 10^{-5}$
	ΔH (kJ mol^{-1})	72 ± 8	76 ± 5	46 ± 4	78 ± 3	91 ± 4
	ΔS ($\text{J K}^{-1} \text{mol}^{-1}$)	-61 ± 28	-39 ± 15	-154 ± 12	-30 ± 11	-7 ± 13

Table 6.1 continued...

Complexes	Kinetic / Thermodynamic Parameter	Pyz 	Im 	Trz 	MIm 	DIm 
PtL4 	k_2 ($\text{M}^{-1}\text{s}^{-1}$)	2.71 ± 0.16	4.97 ± 0.11	6.20 ± 0.29	1.44 ± 0.03	1.80 ± 0.07
	ΔH (kJ mol^{-1})	51 ± 4	41 ± 1	47 ± 2	52 ± 2	43 ± 1
	ΔS ($\text{J K}^{-1} \text{mol}^{-1}$)	-66 ± 12	-95 ± 4	-72 ± 7	-68 ± 7	-97 ± 4
	k_{-2} ($\text{M}^{-1}\text{s}^{-1}$)	$1.01 \times 10^{-3} \pm 1.3 \times 10^{-4}$	$1.32 \times 10^{-3} \pm 9 \times 10^{-5}$	$1.43 \times 10^{-3} \pm 2.3 \times 10^{-4}$	$1.46 \times 10^{-4} \pm 2.1 \times 10^{-5}$	$2.26 \times 10^{-4} \pm 5.2 \times 10^{-5}$
	ΔH (kJ mol^{-1})	37 ± 2	79 ± 2	82 ± 3	52 ± 2	80 ± 2
	ΔS ($\text{J K}^{-1} \text{mol}^{-1}$)	-180 ± 7	-35 ± 7	-24 ± 10	-146 ± 6	-23 ± 7
PtL5 	k_2 ($\text{M}^{-1}\text{s}^{-1}$)	0.236 ± 0.006	0.248 ± 0.002	0.257 ± 0.002	0.262 ± 0.004	0.161 ± 0.003
	ΔH (kJ mol^{-1})	55 ± 3	47 ± 0.3	47 ± 1	50 ± 2	47 ± 2
	ΔS ($\text{J K}^{-1} \text{mol}^{-1}$)	-74 ± 9	-100 ± 1	-100 ± 5	-88 ± 6	-105 ± 8
	k_{-2} ($\text{M}^{-1}\text{s}^{-1}$)					
	ΔH (kJ mol^{-1})	*	*	*	*	*
	ΔS ($\text{J K}^{-1} \text{mol}^{-1}$)					

* No reverse reactions were observed

DFT (Density Functional Theory) calculated data for the unsubstituted complexes was also obtained in addition to the experimental kinetic results. These calculations give bond lengths and angles as well as NBO (Natural Bond Orbital) charges on atoms. This data is shown in *Table 6.2*. It also gives information on the energies of the frontier orbitals of the complexes with the energy gap between the HOMO (Highest Occupied Molecular Orbital) and LUMO (Lowest Unoccupied Molecular Orbital) ($\Delta E = E_{\text{HOMO}} - E_{\text{LUMO}}$), as shown in *Table 6.3*. This data is important in understanding the electronic properties and reactivity of the complexes

The accuracy of a DFT calculation depends on the size of the basis set and the density functional used. The basis set is the set of atomic functions that describes the number and type of atomic orbitals considered in the calculation for a particular atom or molecule. Essentially it is the region in space that each electron is restricted to.^{13,14} The fewer the number of restrictions on the position of each electron, the more accurate the prediction of the molecular orbitals. However, the computational time taken increases greatly with fewer restrictions imposed on the electrons. The density functional used for all Spartan '08 for Windows¹⁵ calculations was the B3LYP¹⁶ density functional method and the LACVP+** (Los Alamos core valence potentials)¹⁷ basis set was also used. Computational modelling of the nucleophiles in a methanol solvent was done using the Gaussian 03¹⁸ and the density functional used was PBE1PBE¹⁷ with the basis set 6-311G. Further information on these density functionals can be found in the Experimental section (*Section 4.5.7*).

Table 6.2: Computational analysis of Pt(II) terpy analogues

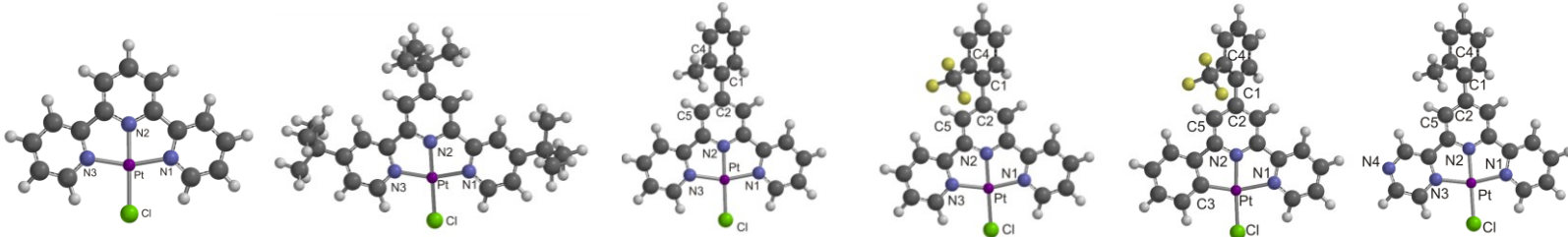
	PtL1	PtL2	PtL3	PtL4	PtL5	PtL6
						
Bond Lengths / Å						
Pt-Cl	2.347	2.352	2.350	2.349	2.359	2.348
Pt-N1	2.052	2.050	2.053	2.056	2.186	2.051
Pt-N2	1.966	1.963	1.964	1.965	1.979	1.966
Pt-N3/C3	2.052	2.050	2.053	2.054	1.996	2.049
Bond Angle / °						
N1-Pt-N3/C	161.56	161.08	161.27	161.16	160.43	161.21
N1-Pt-N2	80.78	80.49	80.64	80.54	78.26	80.59
N2-Pt-N3/C3	80.78	80.59	80.62	80.63	82.18	80.62
C4-C1-C2-C5	—	—	49.87	52.74	60.26	49.15
NBO Charges						
Pt	1.226	1.220	1.222	1.224	1.156	1.228
N1	-0.598	-0.605	-0.599	-0.598	-0.591	-0.601
N2	-0.565	-0.569	-0.572	-0.568	-0.565	-0.574
N3/C3	-0.598	-0.606	-0.599	-0.599	-0.371	-0.575
Cl	-0.637	-0.651	-0.645	-0.643	-0.681	-0.639

Table 6.3 shows the energies of the frontier orbitals of the complexes with the energy gap between the HOMO and LUMO.

Table 6.3: Summary of the HOMO and LUMO values for the Pt(II) terpy analogues from geometry optimisation studies.

	PtL1	PtL2	PtL3	PtL4	PtL5	PtL6
HOMO/eV	-9.45	-8.96	-9.14	-9.23	-5.59	-9.33
LUMO/eV	-6.16	-5.57	-5.92	-5.97	-2.52	-6.25
ΔE /eV	3.29	3.39	3.22	3.26	3.07	3.08

Structural elucidation via X-ray diffraction was undertaken to determine the manner in which the azole nucleophiles bind to the metal centre in the platinum(II) terpyridyl systems and to allow for comparison with gas phase structures obtained from computational modelling. All X-ray crystallographic results may be found in Chapter 5, as well as a discussion on these results.

6.2 Discussion

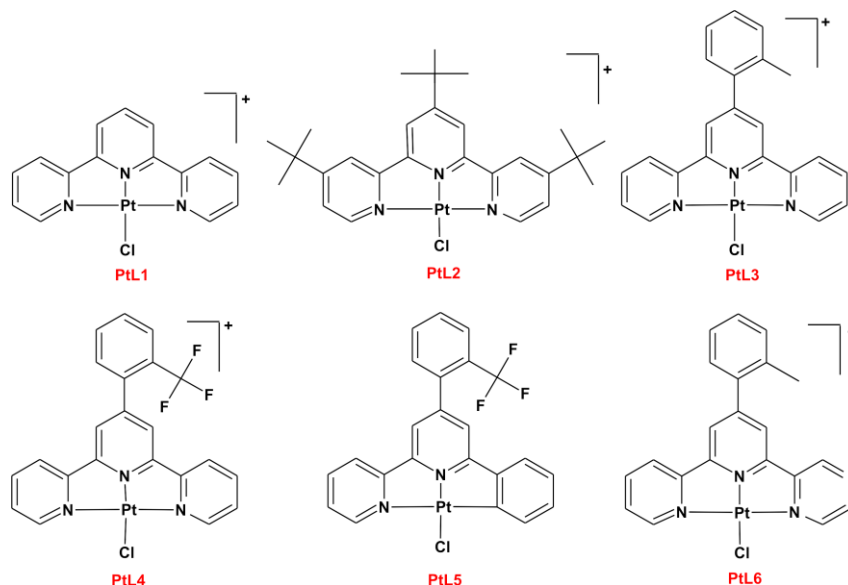
There are two aspects to this study: the first focuses on the manner in which the steric and electronic factors of the metal complexes affect their reactivity and the second aspect focuses on the reactivity trend between the nucleophiles utilised.

6.2.1 Reactivity of Metal Complexes

The six complexes used in this investigation were chosen for their structural similarity. Terpy was chosen as the framework since previous studies by van Eldik *et al.*^{19,20} have shown that by adding π -acceptor pyridine rings to the chelating ligand, the reactivity of the metal centre is increased due to increased π -backdonation and increased electronic communication between the π -accepting ligands.

Starting with terpy as the framework (Scheme 6.9, **PtL1**), variation was achieved through slight modification of the framework by either substituting electron-donating

or –withdrawing groups in ancillary positions (*Scheme 6.9*, **PtL2** – **PtL4**) or by modification of the attached ligand *cis* to the metal centre (*Scheme 6.9*, **PtL5** and **PtL6**).



Scheme 6.9: Structures of complexes utilised in this study.

The general reactivity trend for the investigated complexes with **Im** is shown in *Figure 6.6*. It can be seen from this figure that the reactivity of the metal centre for the forward reaction varies as shown (i.e. **PtL5** < **PtL2** < **PtL3** < **PtL1** < **PtL4** < **PtL6**) with **PtL6** being the most reactive of the investigated complexes.

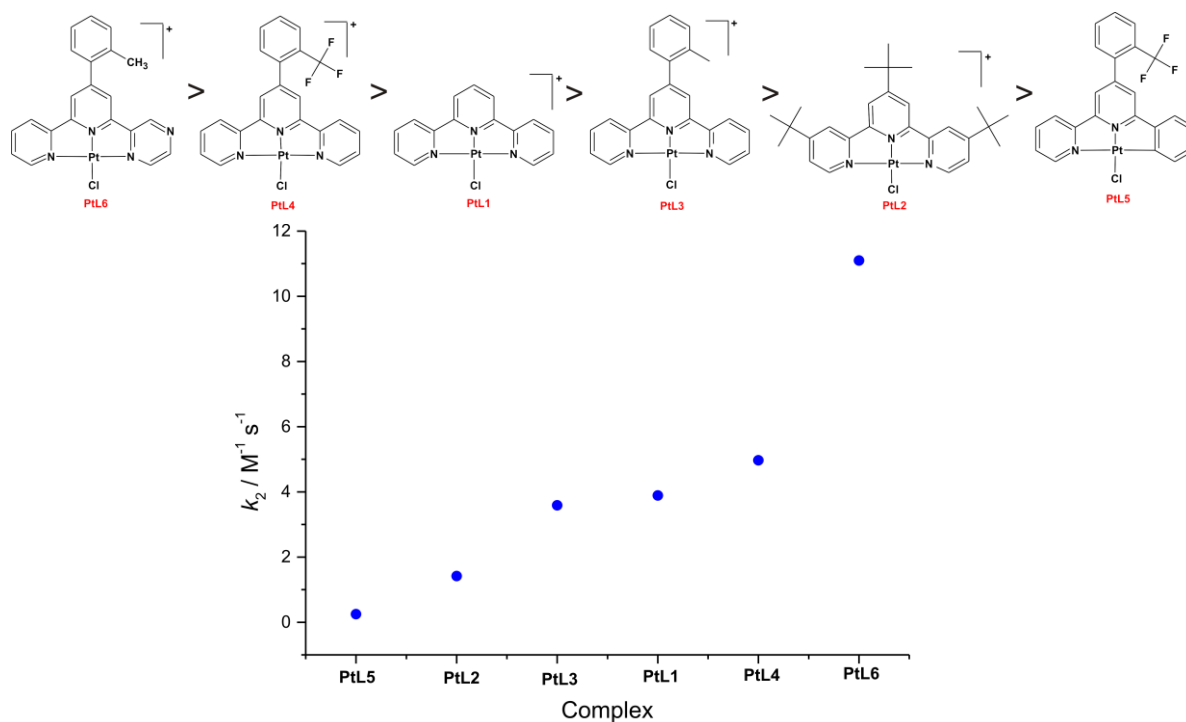


Figure 6.6: Graph showing a comparison of the variation of the rate of chloride substitution for the different Pt(II) terpyridine analogues with **Im**.

Given that slight modifications to the terpy framework can influence the electrophilicity of the metal centre,¹⁹⁻²³ we shall now examine the expression of this behaviour in this study.

From *Table 6.2*, it can be observed that the structures of these complexes are similar in terms of planarity, bond lengths and angles. The coordination geometry of the Pt(II) centre in all the complexes is slightly distorted square planar with an angle of about 161° which deviates from linearity. The 4'-phenyl group is not co-planar with the central terpy ligand. This group can be out of plane by as much as 60.3° for **PtL5** or as little as 49.2° for **PtL6** respectively. Due to this out-of-plane orientation, there are no π interactions between the 4'-phenyl ring and the chelate and any extension of π -backbonding i.e. electronic communication is not possible. In addition, the proximity of the phenyl ring to the metal centre also eliminates any possible steric hindrance for the entering nucleophile. Thus, the difference in the rate of substitution of all the complexes is suggested to be purely electronic in nature.

In comparing the reactivity of **PtL1** and **PtL2**, we find that by simply adding electron-donating *tert*-butyl groups in the ancillary positions of the three pyridine rings in **PtL2** decreases the reactivity of this complex with **Im** by a factor of 3 when compared with **PtL1**.

This work correlates well with what has been observed previously by Jaganyi *et al.*²¹ in their study on the substitution kinetics of $[\text{Pt}(\text{terpy})\text{Cl}]^+$ and $[\text{Pt}(\text{}^t\text{Bu}_3\text{terpy})\text{Cl}]^+$ with the nucleophiles: TU, DMTU, TMTU, iodide and thiocyanate. Their studies showed that the extent of π -backbonding can be controlled by the introduction of an electron-donating group at the 4,4' and 4'' positions of the terpy backbone. They found that the chloride substitution by TU was slower by a factor of 3 for $[\text{Pt}(\text{}^t\text{Bu}_3\text{terpy})\text{Cl}]^+$ compared with $[\text{Pt}(\text{terpy})\text{Cl}]^+$. The authors explained that the introduction of the strong σ -donating groups on the terpy backbone in $[\text{Pt}(\text{}^t\text{Bu}_3\text{terpy})\text{Cl}]^+$ results in a decrease in reactivity by decreasing the positive charge on the metal centre and increases the HOMO-LUMO energy gap which leads to a less reactive metal centre.²¹ Introduction of an electron-withdrawing group, on the other hand, leads to an increased positive charge on the metal centre leading to increased reactivity. As explained by Jaganyi *et al.*²¹ this is due to the electron-donating groups reducing the

π -backbonding ability of the terpy ligand and thus causing the platinum centre to be less electrophilic and hence less reactive towards the nucleophiles.

On analysing complexes **PtL3** and **PtL4**, it is evident that these differ only by a CH_3 and CF_3 group respectively. However, it is evident that **PtL4** is more reactive than **PtL1** by a factor of 1.3 while **PtL3** is a factor of 1.1 less reactive than **PtL1** for the substitution reaction with **Im**. As discussed above, if the phenyl moiety in the 4' position was in-plane with the rest of the terpy ligand then this would enhance the π -backdonation effect; however, this ring is not flat (from X-ray diffraction data of **PtL3** and the SbF_6 salt of **PtL4**, the dihedral angle between phenyl ring and the rest of the terpy backbone is as much as 69.9° and 62.1° respectively)⁹. As such the phenyl rings functions as a σ -donating group, the effectiveness of which is controlled by the *ortho* substituent.

Jaganyi *et al.*^{22,23} have previously investigated similar complexes, viz. the substitution kinetics of the complexes $[\text{Pt}\{4'-(2'''\text{-CH}_3\text{-Ph})\text{-terpy}\}\text{Cl}]^+$ (**CH₃PhPtCl**), $[\text{Pt}\{4'\text{-Ph}\text{-terpy}\}\text{Cl}]^+$ (**PhPtCl**), $[\text{Pt}(\text{terpy})\text{Cl}]^+$ (**PtCl**), $[\text{Pt}\{4'-(o\text{-Cl-Ph})\text{-terpy}\}\text{Cl}]^+$ (**ClPhPtCl**) and $[\text{Pt}\{4'-(o\text{-CF}_3\text{-Ph})\text{-terpy}\}\text{Cl}]^+$ (**CF₃PhPtCl**) with the nucleophiles TU, DMTU and TMTU. The reactivity trend with TU was found to be **CF₃PhPtCl** > **ClPhPtCl** > **PtCl** > **PhPtCl** > **CH₃PhPtCl**.²² Jaganyi *et al.*²² reported that the reactivity of **PtCl** is higher than **PhPtCl** by a factor of 1.3 and can be accounted for by steric hindrance and σ -donicity of the phenyl substituent on the terpy backbone. They also reported that the addition of substituents in the *ortho* position of this phenyl group influences the extent of π -backbonding in the terpy ring which controls the electrophilicity of the metal centre and hence the reactivity of the complex.

They reported that electron-withdrawing groups such as CF_3 and chloro groups in this *ortho* position increased the rate of the chloride substitution while electron donating groups such as CH_3 groups decreased the reaction rate.²² The electron-withdrawing groups reduce the σ -donation effect of the phenyl-moeity which in turn increases the π -acceptor ability of the terpy ligand with electron-donating groups having the opposite effect.

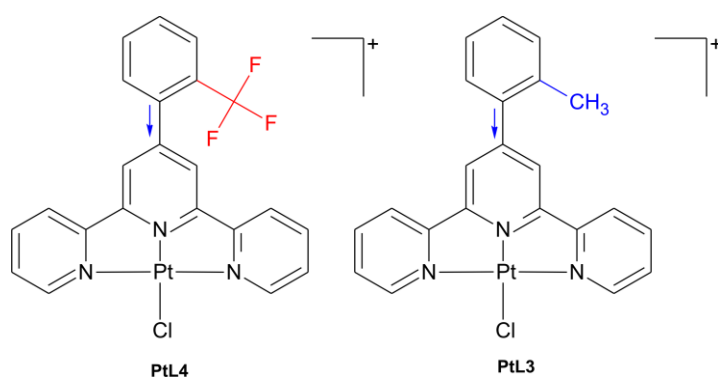


Figure 6.7: The electron withdrawing effect of the CF₃ group of **PtL4** increases the overall π -backdonation effect onto the terpy ligand while the CH₃ group of **PtL3** decreases this effect.

Results of this study compares favorably with these findings as we do indeed find that **PtL4** reacts faster than **PtL3**. The σ -donating strength of the phenyl moiety in the 4' position is controlled by the substituents present on the ring. In the case of **PtL3**, in which there is a methyl group (electron-donating) in the *ortho*

position of the phenyl ring, the overall σ -donating capacity of the 4' group is slightly enhanced, consequently lessening π -backbonding through the terpy fragment. In the case of **PtL4**, which has a trifluoromethyl (electron-withdrawing) group in the *ortho* position of the phenyl ring, the σ -donating capacity of the phenyl group is reduced which increases the terpy π -backbonding effect. The overall effect of these electron-donating and -withdrawing groups is, however, minor. This is due to their relative distance to the metal centre and results in only small differences in reactivity between these complexes. *Figure 6.7* shows the different electron donating and withdrawing effects of **PtL4** and **PtL3**.

The next complex is **PtL5** which has a Pt–C bond located *cis* to the leaving group. The *cis* effect is usually a difficult effect to analyse due to the fact that Pt(II) complexes react at different rates depending on the σ -donor, π -acceptor and steric properties of the *cis* ligand.²⁴

This study shows that **PtL5** is much less reactive than any of the complexes even though it only differs structurally from its analogue **PtL4** by the presence of a carbon atom *cis* to the leaving group. This lowers the reactivity of the complex by 20-fold compared to **PtL4** with **Im**.

Jaganyi *et al.*²³ have previously studied the *cis* effect when they analysed the substitution reactions of $[\text{Pt}(4'-(2'''-\text{CF}_3-\text{Ph})\text{-terpy})]^+$ and $[\text{Pt}(4'-(2'''-\text{CF}_3-\text{Ph})\text{-6-Ph-2,2'-bipy})]$ with TU, DMTU and TMTU. They noted that there was a 16 fold decrease in reactivity for the chloro substitution by TU in $[\text{Pt}(4'-(2'''-\text{CF}_3-\text{Ph})\text{-6-Ph-2,2'-bipy})]$ when compared to its analogue $[\text{Pt}(4'-(2'''-\text{CF}_3-\text{Ph})\text{-terpy})]^+$. The authors reported that this was due to the accumulation of electron density on the metal centre through the σ -donation effect of the bipyridyl group.²³ This not only hinders the approach of the nucleophiles but also prevents stabilization of the transition state.

In addition, studies by van Eldik *et al.*²⁵ have attempted to further rationalise the *cis* effect by studying the reaction kinetics of the complexes $[\text{Pt}(\text{6-phenyl-2,2'-bipyridine})\text{Cl}]$ (**PtNNC**), $[\text{Pt-1,3-di(2-pyridyl)benzene})\text{Cl}]$ (**PtNCN**) and $[\text{Pt(terpy)}\text{Cl}]$ (**PtNNN**) with TU, DMTU and TMTU. This enabled them to analyse the *cis* and *trans* effects and the influence of the strong σ -donor carbon on the electron withdrawing π -acceptor ligand backbone. The data showed that for the substitution reaction by TU, the **PtNCN** complex reacted 30x faster than **PtNNN** and 455x faster than the **PtNNC** complex.²⁵ The σ -*cis* effect is, therefore, larger than the corresponding σ -*trans* effect. They explained these results by stating that the σ -donor effect of the carbon weakens the π -acceptor effect significantly as the electron donating properties of the σ -donor counteracts the electron withdrawing affect of the π -acceptors. This effect is clearly illustrated when the Pt–C bond is *cis* to the leaving group. Van Eldik *et al.*²⁵ reported that the magnitude of this *cis* effect depends on three factors:

- σ -donor strength: with increasing σ -donor strength leads to a decrease in reactivity
- π -acceptor ability: an increase in the π -acceptor ability of the *cis* ligand will lead to increased reactivity.
- Steric bulk: Increasing steric bulk of the *cis* ligand will slow a reaction due to increased steric hindrance in the transition state.

When the Pt–C bond is *trans* to the leaving group, the π -acceptor effect from the pyridyl/phenyl rings is small but still significant. The reactivity of this complex is thus

the highest due to the highly destabilized ground state (labilisation of Pt-Cl by *trans* influence).²⁵

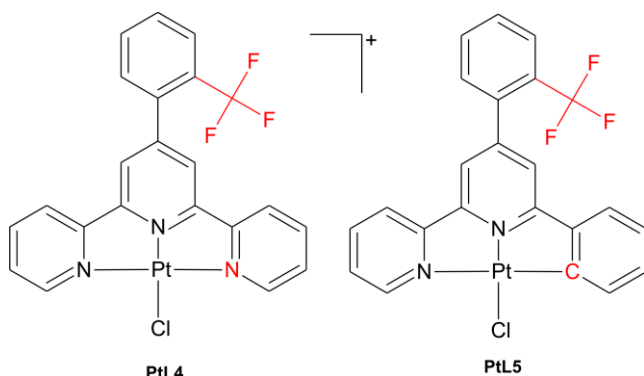


Figure 6.8: The σ -donation ability of the carbon *cis* to the leaving group in **PtL5** reduces the overall π -backdonation effect onto the terpy ligand.

Thus, the decrease in reactivity of **PtL5** relative to **PtL4** can be explained as being due to the accumulation of electron density at the metal centre due to the σ -donation ability of the phenyl ring in the *cis* position in comparison to the pyridine ring in **PtL4**. This σ -donation reduces the π -backdonation effect of the ligand making the Pt(II) centre more electronegative or

less electrophilic with the net effect of repelling the incoming nucleophile and decreasing the rate of substitution. This effect is illustrated in Figure 6.8.

Similarly, this effect can be used to explain the reactivity of **PtL6**. To the best of our knowledge, there have been no previous reports of the substitution kinetics of **PtL6**. Complex **PtL6** reacts much faster than any other complex in this study. **PtL6** differs from its analogue **PtL3** only by the presence of a pyrazinyl ring *cis* to the leaving group, yet it reacts faster than **PtL3** with **Im** by a factor of 3. The pyrazinyl ring is a good π -acceptor and thus enhances the π -backdonation effect.

This falls under Van Eldik's²⁵ second point (as presented earlier) on the factors affecting the magnitude of this *cis* effect which states that an increase in the π -acceptor ability of the *cis* ligand will lead to increased reactivity. As this pyrazinyl ligand is pulling more electron density away from the metal, the π -back donation effect is enhanced and the Pt(II) centre becomes more electron deficient which has a large effect on its reactivity. This shows that adding a strong π -acceptor to the complex increases the reactivity more than by adding an electron-withdrawing group to the chelate as **PtL6** reacts faster than **PtL4** by a factor of 2 with the same nucleophile.

As mentioned earlier, the reactivity of the complexes in this study follows the trend **PtL6** > **PtL4** > **PtL1** > **PtL3** > **PtL2** > **PtL5**. In order to further explore the reasons for this reactivity trend, computational analyses of the investigated complexes were carried at DFT level, the results of which are presented in *Tables 6.2* and *6.3*.

Looking at *Table 6.1*, the rate of substitution involving **PtL5** with all the nucleophiles investigated are very similar in value. One notes from *Table 6.2* that this complex has the least positive NBO charge on the Pt(II) centre (1.156) of all the complexes due to the σ -donation of the bipyridyl ring reducing the π -backdonation effect of the terpy chelate. The kinetic results show that the less electrophilic metal centre in **PtL5** is less selective and cannot distinguish between the nucleophiles despite these having different pK_a values. This observation is against the norm whereby in general the more electrophilic the metal centre, the less selective the complex.^{19,20} A possible explanation for this is that the rate determining step in the substitution process involves to a large extent a weakening of the Pt–Cl bond. The DFT data in *Table 6.2* shows the Pt–Cl bond for **PtL5** to be 2.359 Å which is longer when compared to other complexes.

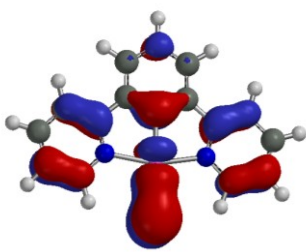
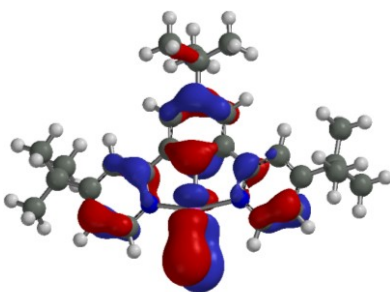
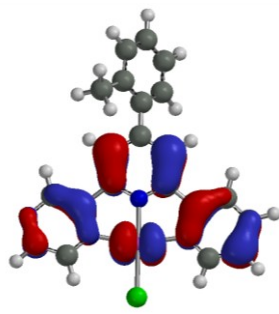
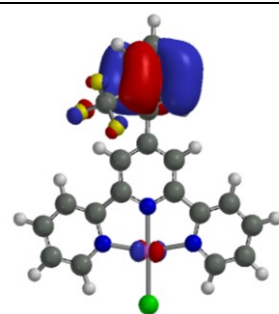
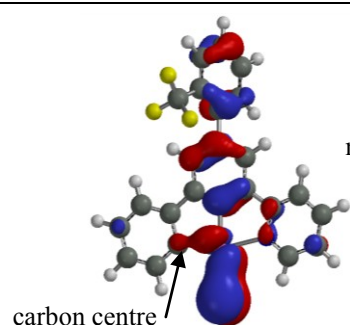
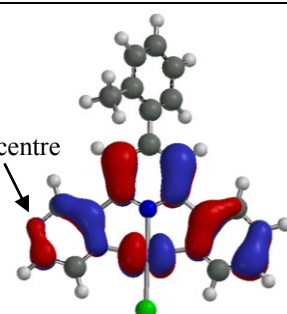
The differences in the electrophilicity of the metal centres can be seen by examining the NBO charges of the Pt(II) centre given in *Table 6.2*. From the reactivity series, **PtL5** reacts the slowest and it has an NBO charge of 1.156 at the platinum centre while **PtL6** reacts the fastest of the complexes and has a Pt(II) NBO charge of 1.228 which is the most positive Pt(II) NBO value of the complexes. The reasons for this higher NBO value have been discussed above. The more positive the charge on the metal centre, the more electrophilic the complex is and the faster it reacts.

As discussed by van Eldik *et al.*,²⁰ the more the electron density of the HOMO that is centered above and below the metal centre, the less electrophilic the complex, whereas when there is more electron density located on the ligand than the metal centre, this indicates a more electrophilic complex. *Table 6.4* shows the DFT calculated HOMOs of the complexes used in this study. The complex **PtL1** has a fair amount of electron density distributed on the terpy ring due to the π -backdonation effect. On **PtL2** the electron density is pushed closer to the metal centre by the electron-donating ^tBu groups causing this complex to be less reactive than **PtL1**. On

comparing the HOMO of **PtL3** and **PtL4**, **PtL3** has no electron density on the 4'-phenyl moiety due to the electron-donating methyl group enhancing the σ -donation effect of the phenyl group which causes there to be more electron density on the metal centre. Conversely, in **PtL4** most of the electron density is on the 4'-phenyl moiety due to the electron withdrawing effect of the trifluoromethyl group which reduces the σ -donation effect of the phenyl group causing less electron density to be positioned over the metal centre. The HOMO of **PtL5** has more electron-density over the metal centre than **PtL4**, again confirming the σ -donation effect of the bipyridyl ring in **PtL5**. The effect of the pyrazinyl ring is not clearly evident from the DFT data as the HOMO of **PtL3** does not differ from that of **PtL6**, although experimentally they react very differently.

The energy gap of the frontier orbitals as shown in *Table 6.3*, has been used in previous papers to explain the reactivity series of complexes.^{21,22} This is also true in this study with the exception of **PtL5** which is the slowest and non-selective when undergoing a substitution reaction.

Table 6.4: DFT calculated HOMOs for the Pt(II) terpy analogues.

PtL1	PtL2	PtL3
		
PtL4	PtL5	PtL6
		

In summation, the general reactivity and selectivity trend for the complexes is: **PtL6** > **PtL4** > **PtL1** > **PtL3** > **PtL2** > **PtL5**. This trend is supported by the NBO charges which are; 1.228, 1.224, 1.226, 1.222, 1.220, 1.156 respectively.

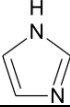
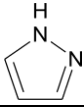
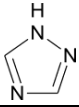
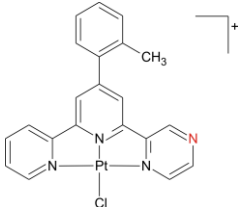
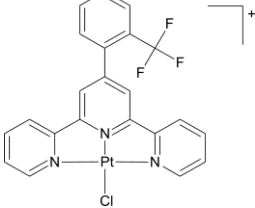
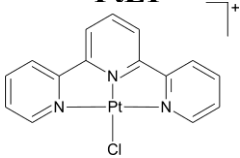
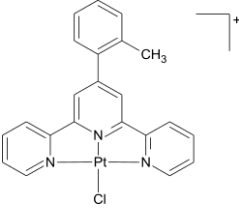
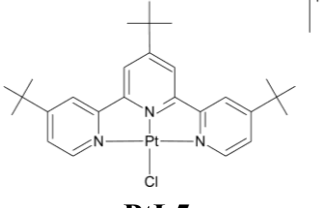
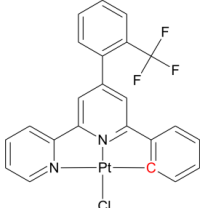
6.2.2 Reactivity of Nucleophiles

The second aspect of this study focuses on the reactivity of the nucleophiles and the factors affecting this. To meaningfully compare the reactivities of the nucleophiles, it is useful to divide them into groups of structural similarities which allow for fair evaluation of the data. Hence, **Im**, **Pyz** and **Trz** can all be compared as nucleophiles without any substituents. Substituents would add another dimension to the reactivity through steric or inductive effects. These nucleophiles differ only in number and position of nitrogen atoms in the ring. The second group for comparison is **Im**, **MIm** and **DIm** as they all contain nitrogen atoms in the same position on the ring and differ only in the number of methyl substituents.

Table 6.5 focuses on the second order rate constants, k_2 , for the substitution reaction of the chloride ligand for the azole ligands (forward reaction) at 25 °C for the first group of nucleophiles; **Im**, **Pyz** and **Trz**. The reverse reaction, k_{-2} must not be ignored. As discussed in *Chapter 2*, an associative mechanism can proceed by one of two pathways: direct substitution or an associative solvolysis pathway whereby there is the formation of the reactive intermediate, L_3MS (the solvated complex where M = metal centre, L = ligand and S = solvent).^{26,27}

In order to block the solvolysis pathway the substitution reaction was done in the presence of 10 mM NaCl. Therefore, the reverse reaction was observed, an indication of the chloride attacking the substituted complex. There is no specific reactivity trend for this reverse reaction, although *Table 6.1* shows that the reverse reactions involving **Trz** and **DIm** are slower than for the other nucleophiles, indicating the presence of a more stable product.

Table 6.5: Second order rate constants, k_2 , at 25 °C for the substitution reactions involving **Im**, **Pyz** and **Trz**.

	Im: 	Pyz: 	Trz: 
PtL6 	11.1 ± 0.4	6.09 ± 0.48	1.70 ± 0.10
PtL4 	4.97 ± 0.11	2.71 ± 0.16	1.44 ± 0.03
PtL1 	3.89 ± 0.05	2.25 ± 0.11	1.04 ± 0.07
PtL3 	3.59 ± 0.09	2.39 ± 0.13	0.851 ± 0.043
PtL2 	1.42 ± 0.006	0.648 ± 0.033	0.846 ± 0.034
PtL5 	0.248 ± 0.002	0.236 ± 0.006	0.262 ± 0.004

From examining the data in *Table 6.5* it can be seen that there is a general reactivity trend where **Im** > **Pyz** > **Trz**. It appears that this reactivity trend is related to the basicity of the nucleophile. The pK_a values for **Im**, **Pyz** and **Trz** are reported as 7.00, 2.52 and 2.19 respectively.²⁸⁻³² The difference in pK_a values can be explained by mesomeric shifts such as those shown in *Figure 6.9*. These shifts increase the electron density on the nitrogen atom and facilitate reactions with electrophilic reagents. This mesomeric effect dominates when the nitrogen atoms are in the 1 and 3 positions such as with **Im** whereas the inductive effect dominates when they are in the 1 and 2 positions as with **Pyz**.²⁸ The dominance of the mesomeric effect can be seen by the difference in pK_a values of **Im** compared to that of **Pyz**. The acidity of the ring system increases as the number of nitrogen atoms increases which is the reason for the low pK_a value of **Trz**.²⁸

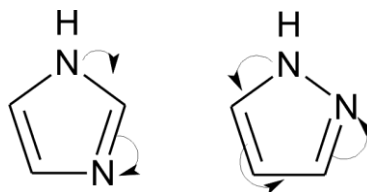


Figure 6.9: Mesomeric shifts for **Im** and **Pyz**.²⁸

Although these reactions were all done in methanol, the basicity can still be considered as methanol can behave in a similar manner to water and abstract a proton from the nucleophile.

Pitteri *et al.*^{33,34} have studied the nucleophilicity of a range of different nitrogen donor heterocycles and pyridines towards $[\text{Pt}(\text{terpy})\text{Cl}]^+$ in methanol. They concluded that the reactivity of the entering group depends linearly on the basicity of the nucleophile. The authors explained the results by saying that their data supports a reaction profile involving a transition state where the Pt—N bond is significantly weaker than the fully formed Pt—Cl bond, thus leading to a situation where the reactivity of the entering group depends linearly on the basicity of the nucleophile.^{33,34}

The findings of this study are in agreement with those determined by Pitteri *et al.*^{33,34} in that there is definitely an increase in reactivity with increasing basicity of the nucleophile. Pitteri *et al.*^{33,34} did not study reactions involving **Trz**, which is a very

interesting nucleophile in that it has different tautomeric forms and binding sites which affect its reactivity.

Bugaric *et al.*^{35,36} studied the substitution reactions of the replacement of H₂O and Cl⁻ ligands in the complexes of [Pt(dien)OH₂]²⁺, [Pt(dien)Cl]⁺, [Pd(dien)OH₂]²⁺, [Pd(dien)Cl]⁺, [Pd(bpma)OH₂]²⁺ and [Pd(bpma)Cl]⁺ respectively with **Trz** and **Pyz** in water. They, however, found that the rate of the reaction followed the trend **Trz** > **Pyz** which is contrary to the results found in this study.^{35,36} They also explained their results in terms of basicity quoting values of 2.24 for **Pyz** and 2.30 for **Trz**. According to numerous books and articles²⁸⁻³² **Trz** is less basic than **Pyz** (2.19 and 2.52 respectively) and therefore should be less reactive. This difference in trend is possibly due to the difference in the metal complex, [Pt(dien)Cl]⁺ which displays no π -acceptor properties, and the solvent (water instead of methanol) used.

The nucleophiles, **Im**, **Pyz** and **Trz** all exhibit a tautomeric equilibrium as shown by Figure 6.10. In this figure it is shown that two tautomeric forms exist for **Im** and **Pyz** and these tautomeric forms essentially show no structural differences.

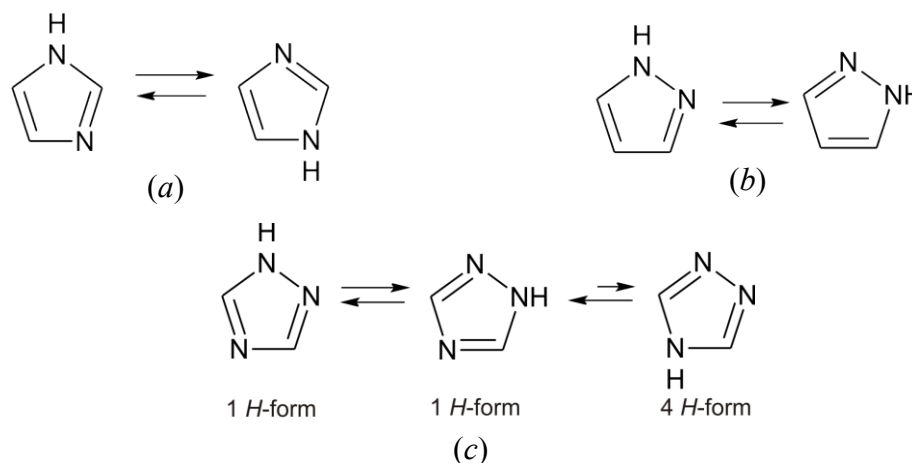


Figure 6.10: Tautomeric equilibria of (a) **Im**, (b) **Pyz** and (c) **Trz**.²⁸

Three tautomers exist for **Trz** (Figure 6.10(c)), namely two 1 *H*-forms and one 4 *H*-form.^{28,29} Most experimental and theoretical calculations; however, show the 1 *H*-form as the predominant or only tautomer. Microwave spectra show that only the 1 *H*-forms exist in the gas phase and ¹H-NMR also shows that the 1 *H*-form is the more dominant form in solution.^{28,29} Katritzky *et al.*²⁸ believe that by changing solvents, temperatures and energy input of different analytical methods that this will

lead to variations in the preferred tautomer. As the bulk of evidence is in favour of the 1 *H*-form, it is believed that this is the predominant form in this study.

The following tables show the NBO charges for the atoms in the different nucleophiles. *Table 6.6* shows the Spartan '08¹⁵ calculated NBO values with no solvent present and *Table 6.7* shows the Gaussian '03¹⁸ calculated values with and without methanol present as a solvent. Solvent effects on the NBO charges were determined by placing the molecule of interest in a solvent continuum.³⁷ The advantage of this is that no solvent molecules are included explicitly in the calculations. Rather, the molecule is placed in a field with the same dielectric constant as the solvent. By not including explicit solvent molecules in the calculation, the computational time is reduced.

Table 6.6: DFT-calculated (Spartan '08¹⁵) NBO charges for the azole nucleophiles without solvent present. Also shown are electron-density plots for these nucleophiles. Red represents the more electron-rich region whilst blue indicates the electron-deficient region.

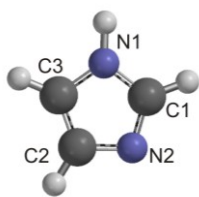
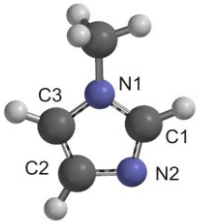
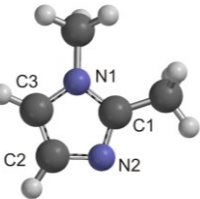
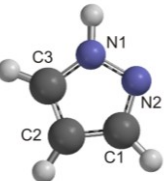
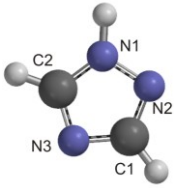
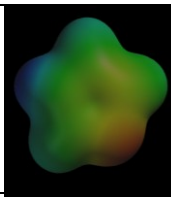
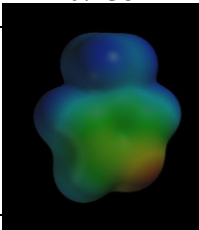
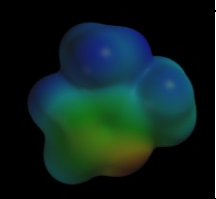
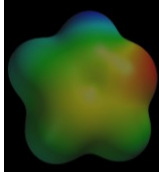
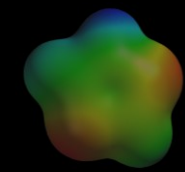
	Im	MIm	DIm	Pyz	Trz
					
N1	-0.574	-0.400	-0.398	-0.363	-0.389
N2	-0.498	-0.479	-0.501	-0.293	-0.307
N3	—	—	—	—	-0.514
C1	0.170	0.0247	0.384	-0.0655	0.138
C2	-0.103	-0.747	-0.0971	-0.361	0.175
C3	-0.114	0.135	-0.108	-0.0680	—
					

Table 6.7: DFT-calculated NBO charges for the nucleophiles with and without solvent present using the computational software Gaussian '03¹⁸.

	Solvent:	N1	N2	N3
Im	None	-0.649	-0.341	—
	MeOH	-0.359	-0.407	—
MIm	None	-0.356	-0.33	—
	MeOH	-0.351	-0.410	—
DIM	None	-0.378	-0.355	—
	MeOH	-0.395	-0.422	—
Pyz	None	-0.34	-0.227	—
	MeOH	-0.256	-0.286	—
Trz	None	-0.499	-0.129	-0.346
	MeOH	-0.244	-0.257	-0.412

These tables show that there is a reasonable difference in the Gaussian '03 and Spartan '08 values since the two software programmes are different. As the values given from DFT calculations are all relative rather than absolute, it is only important to note that both software programmes arrive at the same trend. Differences also exist between the values with and without the methanol solvent present especially in the case of **Im** and **Trz**. In general, the methanol appears to make the protonated nitrogen atoms less nucleophilic and the deprotonated nitrogen atoms more nucleophilic and therefore the preferred sites for electrophilic attack.

This DFT data shows that the **Im** bonding does take place through the nitrogen atom in the 3' position of the ring whereas binding for **Pyz** takes place through the nitrogen atom in the 2' position. The 3' nitrogen atom of **Im** is much more electronegative with an NBO charge of -0.407 (from Gaussian data in MeOH) than the 2' nitrogen of **Pyz** which has an NBO charge of -0.286 (from Gaussian data in MeOH). These results support the observed kinetic data.

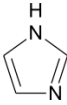
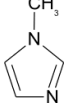
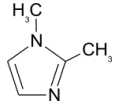
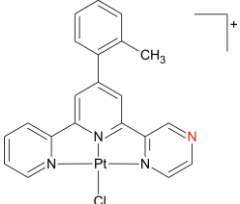
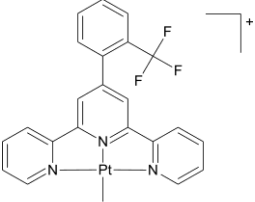
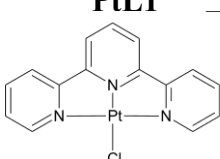
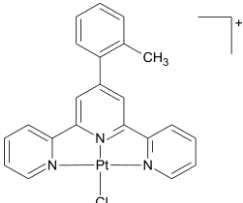
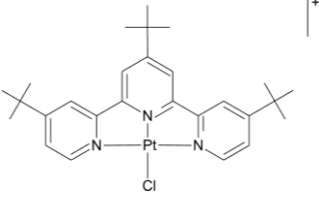
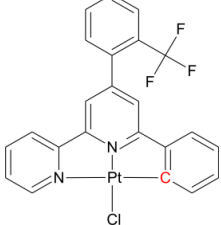
The X-ray structures of **PtL1-Pyz** and **PtL3-Pyz** shown in *Chapter 5* prove experimentally that **Pyz** does in fact bond to complexes through the nitrogen atom in the 2' position. Unfortunately, no crystal structures of **Im** were obtained, however,

from literature,^{38,39} it is known that this nucleophile does bind through its 3' nitrogen atom.

Trz has the potential to bond through its nitrogen either in the 2' or 4' position on the ring. From the data the nitrogen atom in the 4' position of the ring is more electronegative than that in the 2' position which suggests that the 4' nitrogen is the preferred position for binding to electrophilic centres. As the 4' nitrogen is more electronegative than the 3' nitrogen of **Im** and the 2' nitrogen of **Pyz**, according to the computational data, it would be expected that **Trz** would react the fastest of the three nucleophiles, yet it does not. This can be explained in terms of the aromaticity of the nucleophile. NBO charges are a measure of π -electron delocalization and the degree of aromaticity of the atom in the system.⁴⁰ The aromaticity increases when the nitrogen atoms are either not in the vicinal position to each other or if there are more nitrogen atoms in the ring system. This decreases the polarisability of the azole nucleophile, accounting for the reactivity of **Trz**.

Table 6.8 shows the rate constants of the chloride substitution reaction with **Im**, **MIm** and **DIm**. The complexes have been ordered from the fastest reacting complex down to the slowest.

Table 6.8: Rate constants for the forward reaction at 25 °C for the substitution reactions involving **Im**, **MIm** and **DIm**.

	Im: 	MIm: 	DIm: 
PtL6 	11.1 ± 0.4	12.9 ± 0.8	3.15 ± 0.11
PtL4 	4.97 ± 0.11	6.20 ± 0.29	1.80 ± 0.07
PtL1 	3.89 ± 0.05	3.84 ± 0.04	1.62 ± 0.04
PtL3 	3.59 ± 0.09	3.26 ± 0.10	1.04 ± 0.03
PtL2 	1.42 ± 0.01	1.61 ± 0.02	0.624 ± 0.001
PtL5 	0.248 ± 0.002	0.257 ± 0.002	0.161 ± 0.003

From examining *Table 6.8* it can be seen that there is a general reactivity trend where **MIm** > **Im** > **DIm**. The pK_a s for **Im**, **MIm**, and **DIm** are 7.00, 7.30 and 7.85²⁸ respectively. Hence, it appears that the reactivity of **MIm** and **Im** are linked to basicity whilst clearly the reactivity of **DIm** does not follow this trend.

It has been discovered that an *N*-methyl group is base-strengthening in **Im**.²⁸ This is due to the electron-donation effect of the methyl group into the ring system. This explains why **MIm** has a higher pK_a than **Im** and in general reacts slightly faster than **Im**.

Although the nucleophile, **DIm**, has the highest basicity with a pK_a of 7.85,²⁸ it is notably less reactive than **Im** and **MIm** and hence does not follow the trend based on basicity. For reactions with the complex **PtL1**, **DIm** is about 2.4x slower than **Im** and **MIm**. This divergence from the trend can be explained considering the added steric bulk of the methyl group in the 2' position which should slow the **DIm**'s approach to the complex. Thus, the steric effect is obviously more dominant than the added inductive effect of the extra methyl group.

When one looks at the general trend of this set of nucleophiles with those shown in *Table 6.5*, the reactivity follows a similar trend with the exception of **DIm** due to steric hindrance. It is also observed that the reactivity with **PtL5** are of the same magnitude and are not very different, emphasizing the lack of selectivity of the complex.

6.2.3 Activation Parameters

The ΔH^\ddagger values for all the reactions of the complexes with the nucleophiles are large and positive while ΔS^\ddagger values are large and negative, both of which are indicative of an associative mechanism of substitution which is typical for platinum square planar complexes.^{24,26,41,42}

For the nucleophile, **Im**, the reactivity trend has been established as **PtL6** > **PtL4** > **PtL1** > **PtL3** > **PtL2** > **PtL5** with ΔH^\ddagger values of 48, 41, 41, 43, 47 and 47 kJ mol⁻¹ respectively for the forward reaction. In general, slightly increased values of

ΔH^\ddagger correlate to lower rates of substitution. The ΔH^\ddagger values for the reverse reactions are in some case approximately 1.5 to 2x greater than the value for the forward reaction indicating that it is more difficult for the reverse substitution reaction to occur.

When looking at the ΔS^\ddagger value for **Trz** and in some cases for **Pyz**, particularly for the reverse reaction, it can be observed that this value is much more negative than for the other nucleophiles. For example in the reverse reaction with **PtL1** the ΔS^\ddagger values for **Im**, **MIm** and **DIm** are -46.3, -41.0 and -40.2 J K⁻¹ mol⁻¹ respectively whereas the values for **Pyz** and **Trz** are -169 and -153 J K⁻¹ mol⁻¹ respectively. A less negative ΔS^\ddagger value is indicative of a transition state whereby the degree of bonding to the incoming group is more substantial than the bonding to the leaving group while when ΔS^\ddagger is more negative the transition state becomes more organised. Thus, the magnitude of the ΔS^\ddagger value gives an indication to what is happening in the transition state, although it must be remembered that this value has a large error associated with it due to extrapolation of data.

6.2.4 Conclusion

In conclusion, the general reactivity and selectivity trend for the complexes is: **PtL6**>**PtL4**>**PtL1**>**PtL3**>**PtL2**>**PtL5**. The difference in the rate of substitution of all the complexes is purely electronic in nature. Changing the substituents on the terpy moiety or changing the moiety itself affects the π -backdonation ability of the chelate and hence the electrophilicity of the metal centre. This trend is supported by the NBO charges on the Pt(II) centre which are: 1.228, 1.224, 1.226, 1.222, 1.220, 1.156 respectively. The kinetic results show that the less electrophilic metal centre in **PtL5** is less selective than the other complexes and cannot distinguish between the nucleophiles despite these having different pK_a values.

For the nucleophiles, there is a general reactivity trend where **Im**>**Pyz**>**Trz**. It appears that this reactivity trend is related to the basicity of the nucleophile with the pK_a values for **Im**, **Pyz** and **Trz** being 7.00, 2.52 and 2.19 respectively.³⁶⁻⁴⁰

For the remaining nucleophiles, there is a general reactivity trend where **MIm**>**Im**>**DIm** with pK_a s of **Im**, **MIm**, and **DIm** being 7.00, 7.30 and 7.85³⁶ respectively. The reactivity of **MIm** and **Im** is linked to basicity. However, the reactivity of **DIm** does not follow this trend. This can be explained to be due to the added steric bulk of the methyl group in the 2' position slowing the nucleophile's approach to the complex.

The activation parameters indicate an associative mechanism of activation.

6.3 References

1. A. M. W. Cargill Thompson, *Coord. Chem. Rev.*, 1997, **160**, 1.
2. F. H. Burstall, *J. Chem. Soc.*, 1938, 1662.
3. K. T. Potts, M. J. Cipullo, P. Ralliand and G. Theodoridis, *J. Org. Chem.*, 1982, **47**, 3027.
4. J. C. Jeffrey, J. P. Maher, C. A. Otter, P. Thornton and M. D. Ward, *Dalton Trans.*, 1995, 819.
5. F. Kröhnke, *Synthesis*, 1976, 1.
6. G. Annibale, M. Brandolisio and B. Pitteri, *Polyhedron*, 1995, **14**, 451.
7. S.-W. Lai, Michael C. W. Chan, K.-K. Cheung, and C.-M. Che, *Inorg. Chem.*, 1999, **38**, 4262.
8. J. S. Field, R. J. Haines, D. R. McMillin and G. C. Summerton, *Dalton Trans.*, 2002, 1369.
9. Summerton, G. C. PhD Thesis, *Solid State Structures and Photophysical Properties of Polypyridyl Complexes of Platinum(II)*, University of Natal, Pietermaritzburg, South Africa, 1997, pgs 51,53,71-77, 94-107,150-156.
10. T-C Cheung, K-K Cheung, S-M Peng and C-M Che, *Dalton Trans.*, 1996, 1645.
11. J. A. Gertenbach, PhD Thesis, *Synthesis and Emission Studies of Polypyridyl Complexes of Platinum (II)*, University of Natal, Pietermaritzburg, South Africa, 2002, pgs 220-230, 260-262.
12. G. Lowe and T. Vilaivan, *J. Chem. Soc., Perkin Trans*, 1996, **1**, 1499.
13. F. Jensen, *Introduction to Computational Chemistry*, John Wiley and Sons, New York, 1999.
14. D. Young, *Computational Chemistry: A Practical Guide for Applying Techniques to Real World Problems*, Wiley-Interscience, New York, 2001.
15. *Spartan '08*, Wavefunction, Inc., 18401 Von Karman Avenue, Suite 370, Irvine, CA, 92612, USA; Q-Chem, Inc., The Design Center, Suite 690, 5001 Baum Blvd., Pittsburgh, PA, 15213, USA, 2008, <http://www.wavefun.com/>
16. A. D. Becke, *J. Chem. Phys.*, 1993, **98**, 5648.
17. P. J. Hay and W. R. Wadt, *J. Chem. Phys.*, 1985, **82**, 299

18. Gaussian 03, Revision A.1, M. J. Frisch, G. W. Trucks, H. B. Schlegel, G. E. Scuseria, M. A. Robb, J. R. Cheeseman, J. A. Montgomery, Jr., T. Vreven, K. N. Kudin, J. C. Burant, J. M. Millam, S. S. Iyengar, J. Tomasi, V. Barone, B. Mennucci, M. Cossi, G. Scalmani, N. Rega, G. A. Petersson, H. Nakatsuji, M. Hada, M. Ehara, K. Toyota, R. Fukuda, J. Hasegawa, M. Ishida, T. Nakajima, Y. Honda, O. Kitao, H. Nakai, M. Klene, X. Li, J. E. Knox, H. P. Hratchian, J. B. Cross, C. Adamo, J. Jaramillo, R. Gomperts, R. E. Stratmann, O. Yazyev, A. J. Austin, R. Cammi, C. Pomelli, J. W. Ochterski, P. Y. Ayala, K. Morokuma, G. A. Voth, P. Salvador, J. J. Dannenberg, V. G. Zakrzewski, S. Dapprich, A. D. Daniels, M. C. Strain, O. Farkas, D. K. Malick, A. D. Rabuck, K. Raghavachari, J. B. Foresman, J. V. Ortiz, Q. Cui, A. G. Baboul, S. Clifford, J. Cioslowski, B. B. Stefanov, G. Liu, A. Liashenko, P. Piskorz, I. Komaromi, R. L. Martin, D. J. Fox, T. Keith, M. A. Al-Laham, C. Y. Peng, A. Nanayakkara, M. Challacombe, P. M. W. Gill, B. Johnson, W. Chen, M. W. Wong, C. Gonzalez, and J. A. Pople, Gaussian, Inc., Pittsburgh PA, 2003.
19. D. Jaganyi, A. Hofmann, and R. van Eldik, *Angew. Chem. Int. Ed.*, 2001, **40**, 1680.
20. A. Hofmann, D. Jaganyi, O. Q. Munro, G. Liehr, and R. van Eldik, *Inorg Chem*, 2003, **42**, 1688.
21. D. Reddy and D. Jaganyi, *Dalton Trans.*, 2008, 6724.
22. D. Jaganyi, K-L. De Boer, J. A. Gertenbach and J. Perils, *International Journal of Chemical Kinetics*, 2008, 808-818.
23. D. Jaganyi, D. Reddy, J. A. Gertenbach, A. Hofmann and R. van Eldik, *Dalton Trans.*, 2004, 299-304.
24. J. D. Atwood, *Inorganic and Organometallic Reaction Mechanisms*, Wiley-VCH, New York, 1997, 2nd ed., 51.
25. A. Hofmann, L. Dahlenburg and R. van Eldik, *Inorg. Chem.*, 2003, **42**, 6528.
26. M. L. Tobe and J. Burgess, *Inorganic Reaction Mechanisms*, Addison Wesley Longman Limited, New York, 1999
27. M. L. Tobe, *Inorganic Reaction Mechanisms Studies in Modern Chemistry*, Nelson, London, 1972.
28. R. Katritzky and C. W. Rees, *Comprehensive Heterocyclic Chemistry*, Vol 5, Pergamon Press, Oxford, 1984, 35-50, 169-225, 374-386, 734-747.

29. T. Eicher and S. Hauptmann, *The Chemistry of Heterocycles*, Wiley-VCH Verlag GmbH & Co. KGaA, 2003, Germany, 165-174, 179-184, 208-212.
30. T. Tynkkynen, M. Tiainen, P. Soininen and R. Laatikainen, *Anal. Chim. Acta*, 2009, **648**, 105.
31. S. Luo, X. Mi, P. G. Wang and J-P. Cheng, *Tetrahedron Letters*, 2004, **45**, 5171.
32. J-L. Brisset and V. Ilimbi, *Can. J. Chem*, 1980, 1250.
33. B. Pitteri and M. Bortoluzzi, *Polyhedron*, 2006, **25**, 2698-2704.
34. B. Pitteri, G. Marangoni, F. V. Visentini, L. Cattalini and T. Bobbo, *Polyhedron*, 1998, **17**, 475-482.
35. J. Rosic, B. Petrovic, M. Djuran and Z. D. Bugarcic, *Chemical Monthly*, 2007, **138**, 1.
36. Z. D. Bugarcic, S. T. Nandibewoor, M. S. A. Hamza, F. Heinemann and R. van Eldik, *Dalton Trans.*, 2006, 2984.
37. A. Hinchliffe, *Modelling Molecular Structures*, 2nd edition (2000), John Wiley and Sons.
38. Y. Nishida, K. Kino and S. Kida, *Dalton Trans*, 1987, 1157.
39. N. Masciocchi, G. A. Ardizzoi, G. LaMonica, A. Maspero, S. Galli and A. Sironi, *Inorg Chem*, 2001, **40**, 6983.
40. V. E. Matulis, Y. S. Halauko, O. A. Ivaehkevich and P. N. Gaponik., *J. Mol. Struct.*, 2009, **909**, 19.
41. R. B. Jordan, *Reaction Mechanisms of Inorganic and Organometallic Systems*, Oxford University Press Inc., 1991, pgs 29-74.
42. R. G. Wilkins, *Kinetics and Mechanism of Reactions Transition Metal Complexes*, VCH, Weinheim, 2nd edition, 1991, pgs 199-201, 221, 232-242.



Conclusions, Current and Future Work

7.1 Conclusions

The study of substitution kinetics of $[\text{Pt}(\text{terpy})\text{Cl}]\text{Cl}\cdot 2\text{H}_2\text{O}$ (**PtL1**), $[\text{Pt}(\text{tBu}_3\text{terpy})\text{Cl}]\text{ClO}_4$ (**PtL2**), $[\text{Pt}\{4'-(2'''-\text{CH}_3-\text{Ph})\text{terpy}\}\text{Cl}]\text{BF}_4$ (**PtL3**), $[\text{Pt}\{4'-(2'''-\text{CF}_3-\text{Ph})\text{terpy}\}\text{Cl}]\text{CF}_3\text{SO}_4$ (**PtL4**), $[\text{Pt}\{4'-(2'''-\text{CF}_3-\text{Ph})-6-\text{Ph-bipy}\}\text{Cl}]$ (**PtL5**) and $[\text{Pt}\{4'-(2'''-\text{CH}_3-\text{Ph})-6-\text{pyrazin-2-yl-2',2'-bipy}\}\text{Cl}]\text{CF}_3\text{SO}_3$ (**PtL6**) with azoles (Imidazole (**Im**), 1-methylimidazole (**MIm**), 1,2-dimethylimidazole (**DIm**), pyrazole (**Pyz**) and 1,2,4-triazole(**Trz**)) was chosen for this study, not only to help in the design of future platinum-based drugs, but also from a bioinorganic viewpoint in order to gain further understanding of other important reactions occurring in the body.^{1,2}

The kinetic study showed the general reactivity and selectivity trend for the forward reaction, k_2 , for the complexes to be; **PtL6** > **PtL4** > **PtL1** > **PtL3** > **PtL2** > **PtL5**. There is no specific reactivity trend for the reverse reaction, k_{-2} , although the reverse reactions involving **Trz** and **DIm** are slower than for the other nucleophiles indicating the presence of a more stable product.

The experimental kinetics results were further supported by density functional theory (DFT) calculations of the chloride complexes. These calculations were done in order to gain a greater understanding of how the electronic properties of the complex influence their reactivity. The DFT data showed that the structures of these complexes are similar in terms of planarity, bond lengths and angles and that the difference in the rate of substitution of all the complexes for the forward reaction is mostly electronic in nature.

The results show that changing the π -acceptor properties of the chelate through structural modifications of the ligand can control the electrophilicity of the metal centre. The more electrophilic a metal centre leads to an increase in reactivity. For an electron-donating group on the *ortho* substituent on the phenyl ring at the 4'-position

on the terpy backbone (CH_3 , **PtL3**) the reactivity of the metal centre is decreased whilst electron-withdrawing groups in this position (CF_3 , **PtL4**) lead to a moderate increase in reactivity. Electron-donating groups attached directly to the terpy moiety ($^t\text{Bu}_3$, **PtL2**) also decrease the rate of substitution. A strong σ -donor *cis* to the leaving group (**PtL5**) greatly decreases the reactivity of a complex. The addition of a good π -acceptor group to the terpy chelate (**PtL6**) significantly enhances the reactivity.

Thus, changing the substituents on the terpy moiety or changing the moiety itself effects the π -backdonation ability of the chelate and hence the electrophilicity and reactivity of the metal centre. This trend is supported by the NBO charges on the Pt(II) centre which are; 1.228, 1.224, 1.226, 1.222, 1.220, 1.156 for **PtL6**, **PtL4**, **PtL1**, **PtL3**, **PtL2**, **PtL5** respectively.

The nucleophiles were compared in groups according to structural similarities. For the first set of nucleophiles there is a general reactivity trend where **Im** > **Pyz** > **Trz**. This reactivity trend is related to the basicity of the nucleophile with the $\text{p}K_{\text{a}}$ values for **Im**, **Pyz** and **Trz** being 7.00, 2.52 and 2.19 respectively.³ This trend is not linear as **Trz** is a very interesting nucleophile that has different properties affecting its reactivity when compared to **Im** and **Pyz**. Three tautomers exist for **Trz**, namely two 1 *H*-forms and one 4 *H*-form.³ The 1 *H*-form is believed to be the predominant or only tautomer.³ **Trz** also has the potential to bond through its nitrogen atom either in the 2' or 4' position on the ring. From the NBO charges on the azole ring of **Trz**, the 4' nitrogen is the preferred position for binding to electrophilic centres. As aromaticity increases when the nitrogen atoms are either not in the vicinal position to each other or if more nitrogen atoms in the ring system, the polarisability of the azole decreases which accounts for the reactivity of **Trz**.

For the remaining nucleophiles, there is a general reactivity trend where **MIm** > **Im** > **DIm** with $\text{p}K_{\text{a}}$'s of **Im**, **MIm**, and **DIm** being 7.00, 7.30 and 7.85 respectively³. The reactivity of **MIm** and **Im** is related to basicity. However, the reactivity of **DIm** does not follow this trend. **DIm** has the added steric bulk of the methyl group in the 2' position, slowing the nucleophile's approach to the complex.

The results indicate an associative mechanism of substitution with large and positive ΔH^\ddagger values and ΔS^\ddagger values that are large and negative.

In addition, the following complexes were elucidated from single crystals grown by slow diffusion of diethyl ether into nitromethane containing the product; [Pt(terpy)Pyz](ClO₄)₂CH₃NO₂ (**PtL1-Pyz**), [Pt(terpy)MIm](ClO₄)₂CH₃NO₂ (**PtL1-MIm**), [Pt(terpy)DIm](ClO₄)₂CH₃NO₂ (**PtL1-DIm**) and [Pt{4'-(2'''-CH₃-Ph)terpy}Pyz](ClO₄)₂CH₃NO₂ (**PtL3-Pyz**). **PtL1-Pyz**, **PtL1-MIm** and **PtL1-DIm** all crystallized in the monoclinic spacegroup P2₁/c while **PtL3-Pyz** crystallized in the monoclinic spacegroup P2₁/n. The asymmetric unit for all the complexes contains one complete molecule with Z = 4. **Pyz** binds to the complexes through its nitrogen atom in the 2' position of theazole ring while **MIm** and **DIm** bind through the nitrogen atom in the 3' position of the ring. These crystal structures have shown how the nucleophiles bind in the solid state which gives an indication of their interactions in solution.

Considering that most platinum-based anticancer agents exhibit their cytotoxicity by binding to DNA through the metal centre, the reactivity of the Pt(II) ion is of vital importance.⁴ These results show that for future drug design, adding or changing groups on the terpy fragment affects the π -backdonation ability of the chelate and hence the reactivity time of the drugs can be manipulated depending on its function.

The proposed aims have mostly been covered in the study; model compounds which mimic metal ion interaction with proteins were synthesised, the reaction kinetics and mechanism of these square-planar complexes with azoles was determined and the effect of structural modifications on the chelates and nucleophiles was investigated. However, in order to achieve the final aim of effectively using the conclusions of this study to aid in future anticancer drug design, the reactions need to be done under physiological conditions with pH control.

7.2 Current Work

7.2.1 Other Reactions Attempted During this Study

This study can also be further extended to include new analogues of the Pt(II) terpy system. Indeed, work on the following complexes has already began as an extension of the current study: $[\text{Pt}(\text{bzimpy})\text{Cl}]\text{PF}_6$ (**Ptbzimpy**) and $[\text{Pt}(\text{Me}_2\text{bzimpy})\text{Cl}]\text{Cl} \cdot 2.5\text{H}_2\text{O}$ (**PtMe₂bzimpy**) where $\text{bzimpy} = 2,6\text{-bis}(\text{benzimidazo-2-yl})\text{pyridine}$, (Figure 7.1).

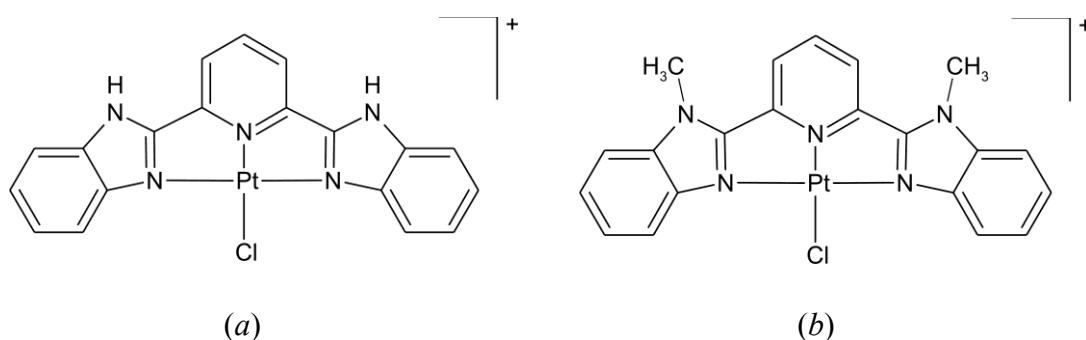


Figure 7.1: Diagrams of (a) **Ptbzimpy** and (b) **PtMe₂bzimpy**.

To our knowledge a full study of the substitution kinetics of these complexes has not yet been reported. However, Nair *et al.*⁵ have studied the emission and absorbance spectroscopy of **Ptbzimpy** on binding to hemoglobin. The crystal structure of hemoglobin shows two potential binding sites: two sulfur containing amino acids, Met32 and Cys104. They carried out an absorption titration of **Ptbzimpy** with L-cysteine and L-methionine and found that it binds more strongly to L-cysteine. Connick *et al.*⁶ have carried out emission studies on **Pt(Me₂bzimpy)**.

The complex, **Ptbzimpy**, was selected for this study due to its similarity to the terpy system and in order to investigate the effect of π -backdonation in this system. Nair *et al.*⁵ have reported that **Ptbzimpy** is an effective biosensor and mimics the behaviour of the organic fluorophore, 8-anilino-1-naphthalenesulfonic acid (ANS) which is used as a probe to study the conformational changes of proteins. There are a number of reports on the interaction of Pt(II) complexes with DNA in comparison with the few reports published on the binding of Pt(II) complexes to proteins.⁷⁻⁹ As

the complex has already shown potential from a bioinorganic viewpoint, it would be of great interest to study its substitution kinetics, especially with proteins.

An area of concern with using the **Ptbzimpy** complex is the presence of the reactive N–H protons which could result in undesirable side reactions with the nucleophiles, potentially affecting the substitution kinetics. Thus, the methylated form, **PtMe₂bzimpy**, was chosen so the proton effect would be absent and any reactivity behaviour can be explained simply by the chelate.

This study can be further expanded to include ligands such as 1,3-bis(benzothiazol-2-yl)-benzene coordinated to platinum(II), as shown in *Figure 7.2* as well as platinum complexes of Et₂bzimpy and Bu₂bzimpy.

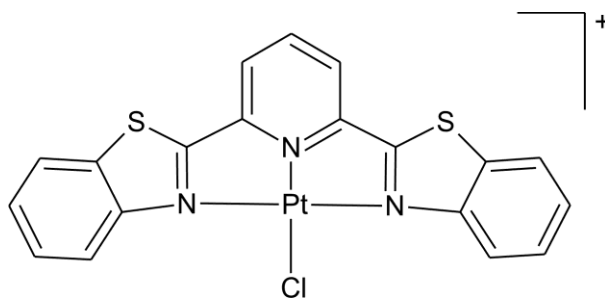


Figure 7.2: Diagram of [Pt(1,3-bis(benzothiazol-2-yl)-benzene)Cl]⁺.

Ptbzimpy and **PtMe₂bzimpy** were difficult to work with due to poor solubility. The ionic strength solution used was a methanolic solution of 0.1 M NaCl. A preliminary kinetic study involving **PtMe₂bzimpy** with the standard nucleophiles: **TU** and **DMTU** have been investigated. *Figure 7.3* shows the absorbance spectrum of **PtMe₂bzimpy** with **TU** with the corresponding kinetics trace inset. From this figure, it is clearly shown that two reactions are occurring. We tentatively propose that the first reaction is the very fast substitution of the chloride by **TU** and the second very slow reaction is the precipitation of this substituted complex.

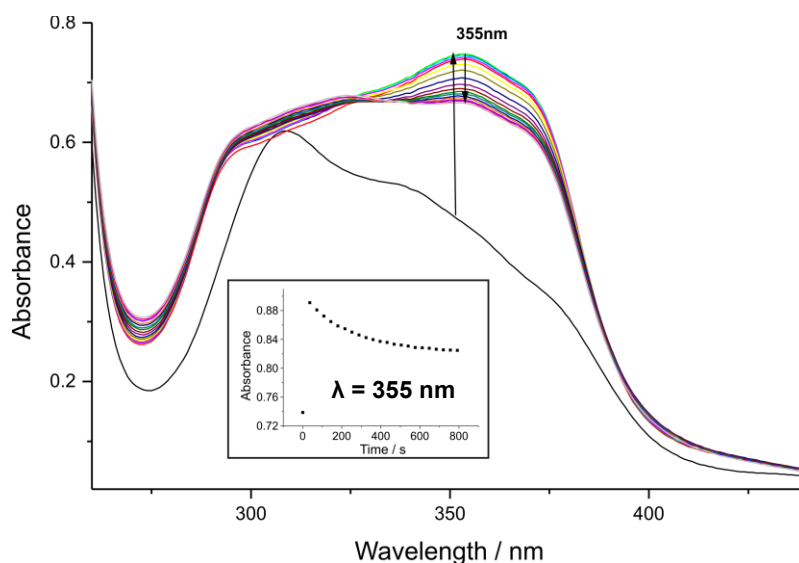


Figure 7.3: Absorbance spectrum of **PtMe₂bzimpy** (2.35x10⁻⁵ M) and **TU** (2.35x10⁻⁴ M) at an ionic strength of 0.1 M (NaCl) at 25 °C with the corresponding kinetic trace inset.

As the first reaction, the substitution of the labile chloride by the incoming nucleophile, was very fast, it had to be studied on the stopped-flow spectrophotometer. Straight lines with zero intercepts were obtained for the substitution reactions of **PtMe₂bzimpy** with **TU**; however, appreciable intercepts were obtained for the substitution reaction with **DMTU** as represented *Equation 6.2*.

$$k_{obs} = k_2[\text{Nu}] + k_- \quad \dots 6.2$$

Figure 7.4(a) shows the kinetic plot for the substitution reaction of **PtMe₂bzimpy** with **TU** at 25 °C where the rate constant for the forward reaction, k_2 , can be determined from the slope. *Figure 7.4(b)* shows the corresponding Eyring plot.

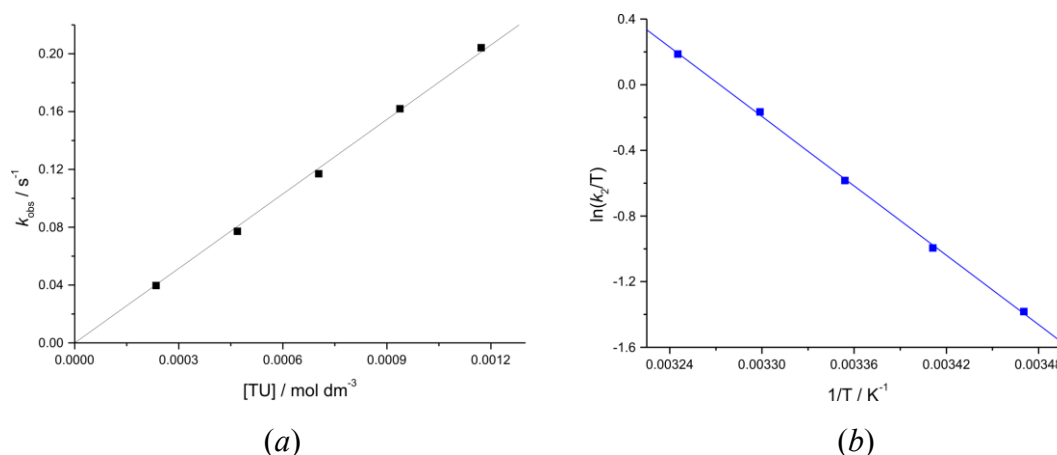
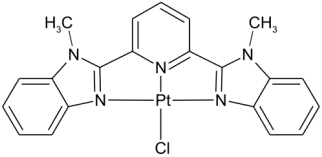


Figure 7.4: (a) Plot to determine rate constant from the slope for **PtMe₂bzimpy** and **TU** at 25 °C. (b) Eyring plot to determine ΔH^\ddagger and ΔS^\ddagger for the forward reaction.

The results of the kinetic study can be found in Table 7.1.

Table 7.1: Experimentally measured rate constants with associated errors and activation parameters for the substitution reactions of **PtMe₂bzimpy** with **TU** and **DMTU** at 25 °C.

	TU	DMTU
PtMe₂bzimpy		
		
k_2 ($\text{M}^{-1}\text{s}^{-1}$)	171 ± 2	46.5 ± 0.7
ΔH (kJ mol^{-1})	59 ± 1	56 ± 0.6
ΔS ($\text{J K}^{-1} \text{mol}^{-1}$)	-6 ± 3	-24 ± 2
k_2 ($\text{M}^{-1}\text{s}^{-1}$)		$7.67 \times 10^{-3} \pm 5.2 \times 10^{-4}$
ΔH (kJ mol^{-1})	*	87 ± 4
ΔS ($\text{J K}^{-1} \text{mol}^{-1}$)		6 ± 15

These results support the findings of other studies whereby **TU** was found to be the better nucleophile with **DMTU** being weaker due to the steric effect.¹⁰⁻¹² **PtMe₂bzimpy** reacts significantly slower with **TU** and **DMTU** than **PtL1** as Jaganyi *et al.*¹² reported **PtL1** reacting at a rate of $1494 \pm 10 \text{ M}^{-1} \text{ s}^{-1}$ with **TU**. Due to

the added conjugation, it was expected that the π -backdonation effect would be greater for **PtMe₂bzimpy** making the metal centre more electrophilic and hence more reactive, however this is obviously not the case and other factors need to be taken into consideration.

Thus for future work on these bzimpy complexes:

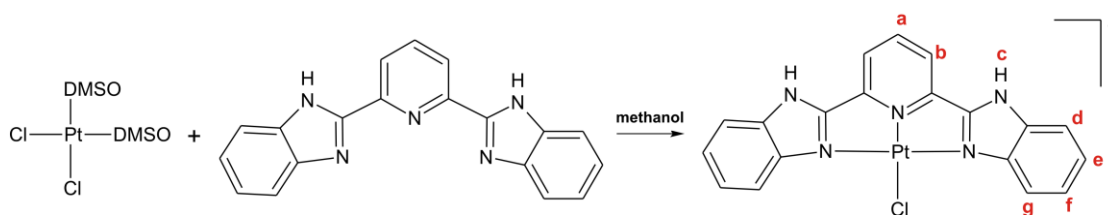
- Further work to determine a viable solvent system or pH to enable the substitution kinetics of the complexes has to be done.
- Synthesis of the aqua species needs to be undertaken.
- A full DFT study needs to be completed in order to gain an understanding of the ground state complexes.

7.2.2 Experiments Conducted

General methods

Organic solvents used in the syntheses were from Aldrich and used as received except for acetone which was dried over CaH₂. The synthesis of Pt(DMSO)₂Cl₂ complex was reported by Price *et al.*¹³ 2,6 bis(benzimidazo-2-yl)pyridine] (**bzimpy**) and NH₄PF₆ was purchased from Aldrich and used as received. NaH was also purchased from Aldrich and was stored and used under an inert atmosphere at room temperature whereas MeI (Aldrich) was stored at 0 °C. K₂PtCl₄ was purchased from Strem and used as supplied. **PtMe₂bzimpy** was synthesised using a method reported by Connick *et al.*⁶ The nucleophiles **TU** and **DMTU** were purchased from Aldrich and used as supplied.

Synthesis of [Pt(**bzimpy**)Cl]PF₆ (**Ptbzimpy**)



Scheme 7.1: Synthesis of **Ptbzimpy**.

To a refluxing suspension of $\text{Pt}(\text{DMSO})_2\text{Cl}_2$ (324 mg, 0.77 mmol) in methanol, 2,6 bis(benzimidazo-2-yl)pyridine] (**bzimpy**) (241 mg, 0.77 mmol) was added. The solution was refluxed for 2 hours and an orange precipitate formed. The orange precipitate was filtered and washed with diethyl ether. The precipitate was partially dissolved in DMSO and a saturated aqueous solution of NH_4PF_6 was added to dissolve the complex completely. The orange complex was precipitated out with water, filtered and dried. The orange precipitate turns red on drying. *Scheme 7.1* shows the reaction scheme for the synthesis of **Ptbzimpy**.

Yield: 0.272 mg, (60 %)

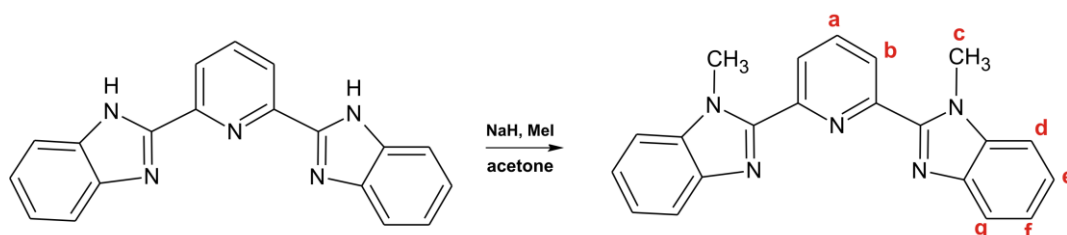
m/z: 542.0586 (M^+) $\text{C}_{19} \text{H}_{14} \text{N}_5 \text{Cl Pt}$

^{195}Pt NMR: (DMSO- d_6) -2559.9 ppm

^1H NMR: (DMSO- d_6)

Shift: (ppm)	Multiplicity:	Integration:	Coupling: (Hz)	Assignment:
3.5-5	s			c
7.09	t	2	7.914	e,f
7.23	t	2	7.474	e,f
7.38	d	2	7.914	b
7.61	d	2	7.914	d,g
7.68	d	2	7.914	d,g
8.01	t	1	7.914	a

Synthesis of **Me₂bzimpy**



Scheme 7.2: Synthesis of **Me₂bzimpy**.

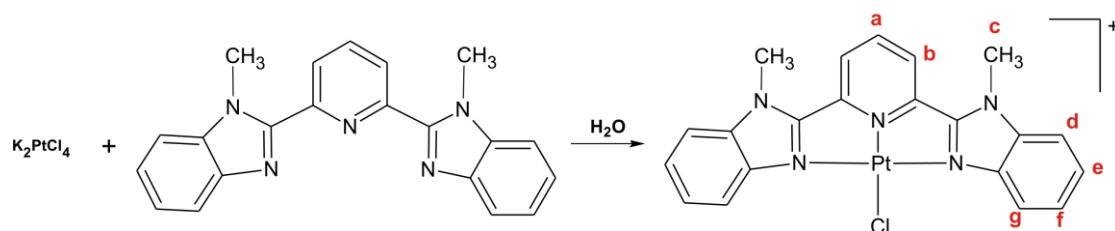
Dissolved 2,6-bis(benzimidazo-2-yl)pyridine] (**bzimpy**) (150 mg, 0.48 mmol) in dry acetone and the solution went yellow. Added NaH (23 mg, 0.96 mmols) to the solution under an inert atmosphere and the solution turned orange after 30 min of stirring. MeI (0.09 ml, 1.4 mmol) was added and the solution was left stirring for another 2 hours over which time it turned yellow in colour. The methylated product 2,6-bis(1-methyl-benzimidazo-2-yl)pyridine] (**Me₂bzimpy**), was precipitated by the addition of water. The white product was filtered and left to air dry. *Scheme 7.2* shows the reaction scheme for the synthesis of **Me₂bzimpy**.

Yield: 148 mg, (91 %)

¹H NMR: (acetone)

Shift: (ppm)	Multiplicity:	Integration:	Coupling: (Hz)	Assignment:
4.37	s	6		c
7.29-7.38	m	4		e.f
7.61	d	2	8.06	d,g
7.75	d	2	7.556	d,g
8.19	t	1	7.556	a
8.46	d	2	8.06	b

Synthesis of [Pt(Me₂bzimpy)Cl]Cl.2.5H₂O (PtMe₂bzimpy)



Scheme 7.3: Synthesis of **PtMe₂bzimpy**.

2,6-bis(1-methyl-benzimidazo-2-yl)pyridine] (**Me₂bzimpy**) (142 mg, 0.42 mmol) was added to a solution of K₂PtCl₄ (144 mg, 0.35 mmol) in distilled water (20 ml). The solution was refluxed for 3 days. Over this time the solution became darker red in

colour. The mixture was centrifuged as the precipitate was too fine to filter off. The filtrate was separated and reduced to dryness. The reaction scheme for the synthesis of **PtMe₂bzimpy** is shown in *Scheme 7.3*.

Yield: 156 mg, (57 %)

m/z: 569.0820 (M⁺) C₂₁ H₁₇ N₅ Cl Pt

¹⁹⁵Pt NMR: (DMSO-d₆) -2605.3 ppm

¹H NMR: (DMSO-d₆)

Shift: (ppm)	Multiplicity:	Integration:	Coupling: (Hz)	Assignment:
3.92	s	6	—	c
7.11	d	2	7.682	d
7.24	t	2	7.17	e,f
7.34	t	2	7.682	e,f
7.61	d	2	7.682	g
8.42	d	2	7.682	b
8.53	t	1	7.682	a

Supporting documentation relating to the analysis of the complexes is attached as **Appendix E**. These include ¹H NMR and ¹⁹⁵Pt NMR spectra as well as mass spectra for both complexes.

Preparation of Complex and Nucleophile Solutions for Kinetic Analysis

The 0.1 M ionic strength solution used in the preparation of the complex and neutral nucleophile solutions were made up by dissolving the required amount of NaCl in HPLC grade methanol.

The metal complex solution was prepared by dissolving the required amount of metal complex in 100 ml of the ionic strength solution (the methanolic NaCl solution). The nucleophile solutions of 50 times the concentration of the metal complex solution for

TU and DMTU was prepared by dissolving a known amount of a select nucleophile in 100 ml of the ionic strength solution. Subsequent dilutions of the 50 times nucleophile solution affords solutions of concentrations 10, 20, 30 and 40 times the concentration of the metal complex in addition to the 50 times solution.

Instrumentation and Measurements

The instrumentation and measurements for these complexes was the same as that described in *Section 4.5*.

7.3 Future work

The results obtained in this current study showed that the basicity of the nucleophiles plays an important role in terms of their reactivity with metal complexes. This, coupled with the acidity of the metal complexes themselves particularly in aqueous solution, should prove to be of significant interest and thus studies in which the pH environment of both the metal complex and the nucleophile is carefully controlled would prove useful.

It has already been shown how this study can be extended by increasing the variety of complexes, the study can also be extended by expanding the number and types of nucleophiles used.

7.3.1 Extension of Nucleophile Study

This study can be further extended to include a large number and variety of nucleophiles, as shown in *Figure 7.5*.

There are a number of nitrogen donor azole nucleophiles that have not been explored in this research but an investigation into their substitution kinetics could either serve to support the theories put forward in this study or indicate different trends. This could potentially be an interesting path to follow as it could give further clarity to the behaviour of **Trz**. Commercially available nitrogen donor azoles include

benzimidazole, 1-methylpyrazole, 3,5-dimethylimidazole, 1,2,3-triazole, tetrazole and many substituted derivatives of these compounds.

There are also many 6 membered nitrogen-donor rings (azines) that can act as nucleophiles. These compounds include: pyridine, pyrimidine, pyrazine, pyridazine and other substituted analogues. The azines have lower pK_a values than the azoles used in this study, e.g pyrazine ($pK_a = 0.37$)¹⁴ and pyrimidine ($pK_a = 1.10$)¹⁴ and therefore they are expected to react even slower than the azoles. Using the azines as nucleophiles, could again serve to support or detract from the theories put forward in this current study.

The study could also be further extended to include other hetero atoms compounds such as those containing sulfur and possibly oxygen atoms in order to determine the effect that changing the hetero atom has on the substitution kinetics. Sulfur-donor heterocycles such as the thiazoles have a wide range of applications due to their antibacterial¹⁵, anti-inflammatory^{16,17}, antitubercular¹⁸, anti-HIV¹⁹, antidegenerative²⁰ and biological properties²¹⁻²⁴. Thiazole-based chemisensors have been shown to be successful in biological systems²¹⁻²⁴. Thiazole has a pK_a of 2.55²⁵, therefore if the basicity of the nucleophile plays a role in the reaction rate, it is predicted to react slower than **Im** and faster than **Pyz**. Oxygen-donor heterocycles include oxazole and isoxazole with pK_a 's of 0.8 and 1.30 respectively²⁵, which indicates that substitution reactions with these nucleophiles could be relatively slow.

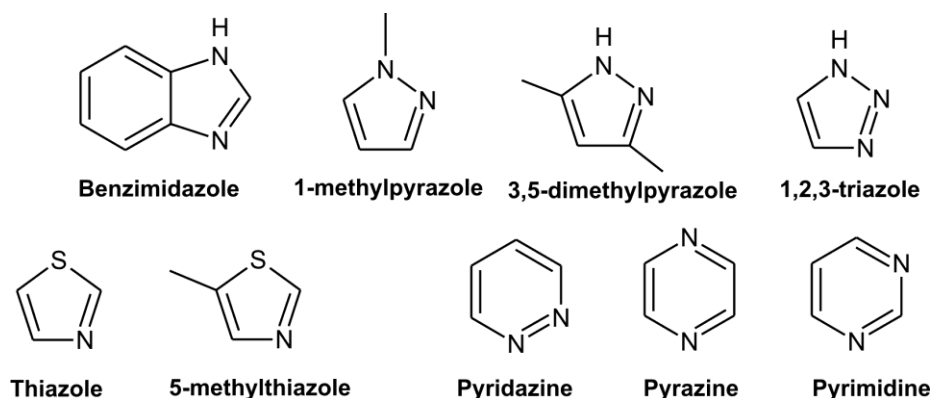


Figure 7.5: Commercially available nitrogen- and sulfur-donor nucleophiles.

The list of nucleophiles could also be further extended to include biological nucleophiles such as the amino acids: cysteine and histidine. Cysteine is very

important in biological systems as it has antioxidant properties which are expressed in the tripeptide glutathione.² Cysteine is also plays a significant role in forming disulfide bonds in proteins. It is involved in the crosslinking of proteins, such as in insulin, which increases the rigidity of these proteins. Many metal cofactors in enzymes are bound to the thiol group of cysteine such as iron in cytochrome P450, copper in the blue copper proteins and alcohol dehydrogenase.² Histidine is a common coordinating ligand in metalloproteins, such as hemeproteins, and is a part of the catalytic sites in certain enzymes.² Thus, as cysteine and histidine have wide applications in biological systems, it would be of great interest to study these amino acids and to understand the manner in which they bind.

Absorption titrations can also be carried out using the different DNA base pairs to determine binding constants of the complexes to DNA.

7.4 References:

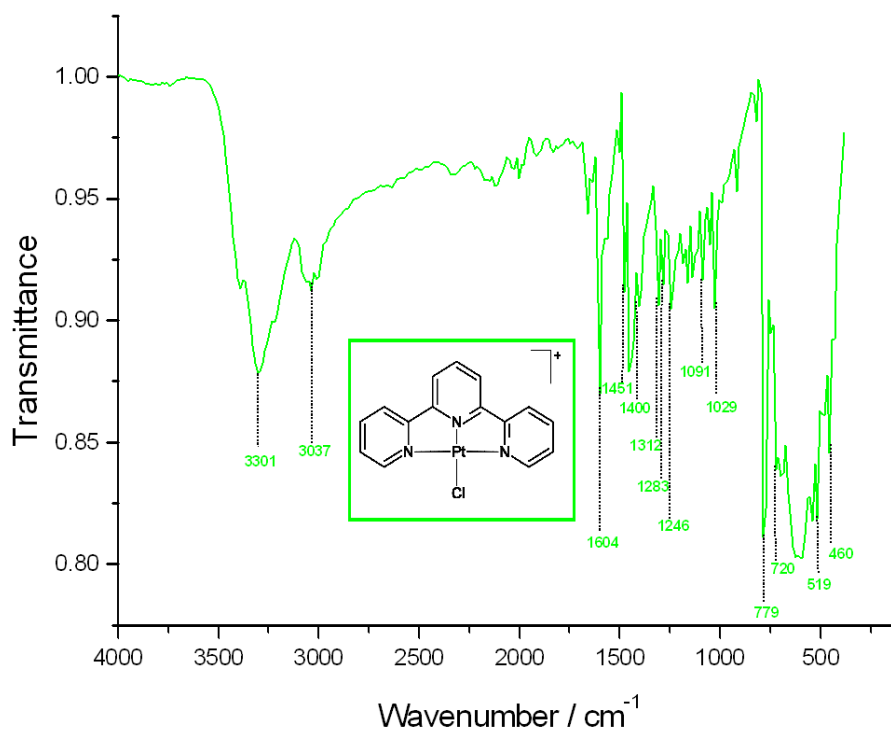
75. J. Rosic, B. Petrovic, M. Djuran and Z. D. Bugarcic, *Chemical Monthly*, 2007, **138**, 1.
76. W. Kaim and B. Schwederski, *Bioinorganic Chemistry: Inorganic Elements in the Chemistry of Life*, 1st edition, John Wiley & Sons, New York, 1994, pgs 16-35, 106-123.
77. R. Katritzky and C. W. Rees, *Comprehensive Heterocyclic Chemistry*, Vol 5, Pergamon Press, Oxford, 1984, 35-50, 169-225, 374-386, 734-747.
78. S. D. Cummings, *Coord. Chem. Rev.*, 2009, **253**, 449.
79. V. G. Vaidyanathan and B. U. Nair, *Eur. J. Inorg. Chem*, 2005, 3756.
80. L. J. Grove, J. M. Rennekamp, H. Jude and W. B. Connick, *J. Am. Chem. Soc.*, 2004, **126**, 1594.
81. B. P. Esposito and R. Najjar, *Coord. Chem. Rev.*, 2002, **232**, 137.
82. M. D. Hall and T. W. Hambley, *Coord. Chem. Rev.*, 2002, **232**, 49.
83. L. T. Lemiesz, H. Kozlowski and B. K. Kepler, *J. Inorg. Biochem.*, 1999, **77**, 144.
84. D. Reddy and D. Jaganyi, *Dalton Trans.*, 2008, 6724.
85. D. Jaganyi, K-L. De Boer, J. A. Gertenbach and J. Perils, *International Journal of Chemical Kinetics*, 2008, 808-818.
86. D. Jaganyi, D. Reddy, J. A. Gertenbach, A. Hofmann and R. van Eldik, *Dalton Trans.*, 2004, 299-304.
87. J. H. Price, A. N Williamson, R. F. Schramm and B. B. Wayland, *Inorg Chem*, 1972, **11**, 1280.
88. Z. D Bugarcic, S. T. Nandibewoor, M. S. A. Hamza, F. Heinemann and R. van Eldik, *Dalton Trans.*, 2006, 2984.
89. N. Agarwal, S. Kumar, A. K. Srivastava, and K. P. C. Sarkar, *Ind. J. Het. Chem.*, 1997, **6**, 291.
90. J. D. Hadjipavlou-Litina and A. Geronikaki, *Arz. Forsch./Drug Res.*, 1996, **46**, 805.
91. L. D. Hadjipavlou, A. Geronikaki, E. Sotiropoulou, *Res. Commun. Chem. Pathol.*, 1993, **79**, 355.
92. M. Tsuruoka and I. Seikutsugaka, *Med. Biol.*, 1974, **10**, 296.

93. G. Maass, U. Immendoerfer, B. Koenig, U. Leser, B. Mueller, R. Goody, B. Pfatt, *Antimicrob. Agents Chemother.*, 1993, **37**, 2612.
94. M. P. Anna, G. Athina, M. Remi, C. Venera, G. Barbara and D. Irini, *Bioorg. Med. Chem.*, 2003, **11**, 2983.
95. J. Michel Grivy, F. Tellez, S. Bernes, H. Noth, R. Contreras and N. Bahba-Behrens, *Inorg. Chim. Acta*, 2002, 339, 532.
96. A. Benalte-Garcia, F. J. Garcia-Barros, F. J. Higes-Rolando and F. Luma-Giles, *Polyhedron*, 1999, 18, 2907.
97. M. J. M. Campbell, *Coord. Chem. Rev.*, 1975, **15**, 279.
98. S. Padhye and G. B. Kauffman, *Coord. Chem. Rev.*, 1985, **63**, 127.
99. B. Pitteri and M. Bortoluzzi, *Polyhedron*, 2006, **25**, 2698-2704.

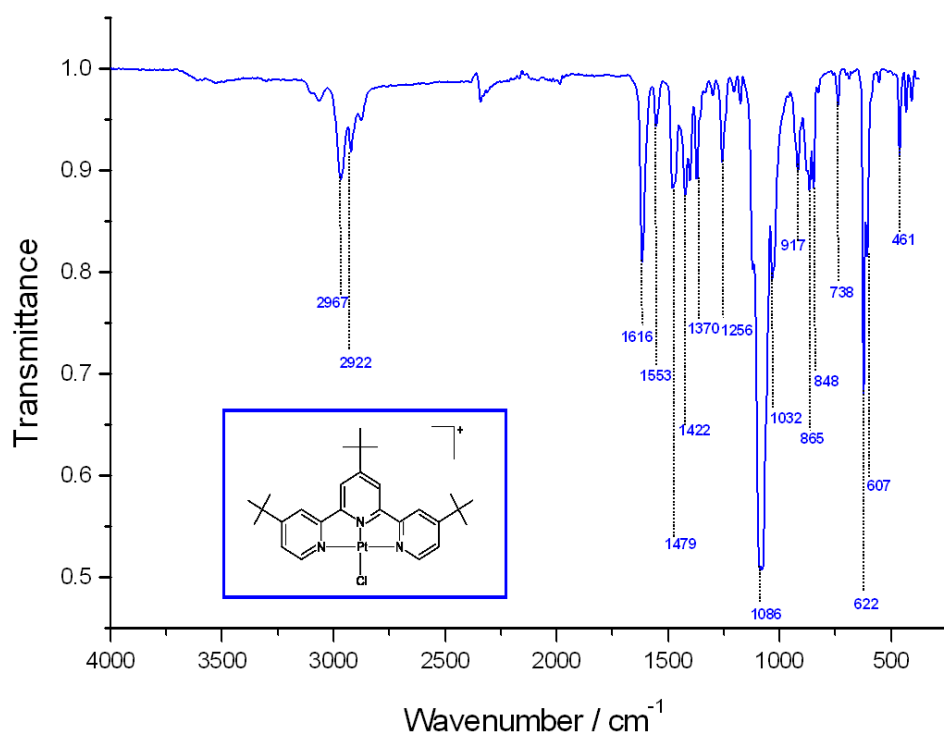
APPENDIX A

A.1 Infrared Spectra

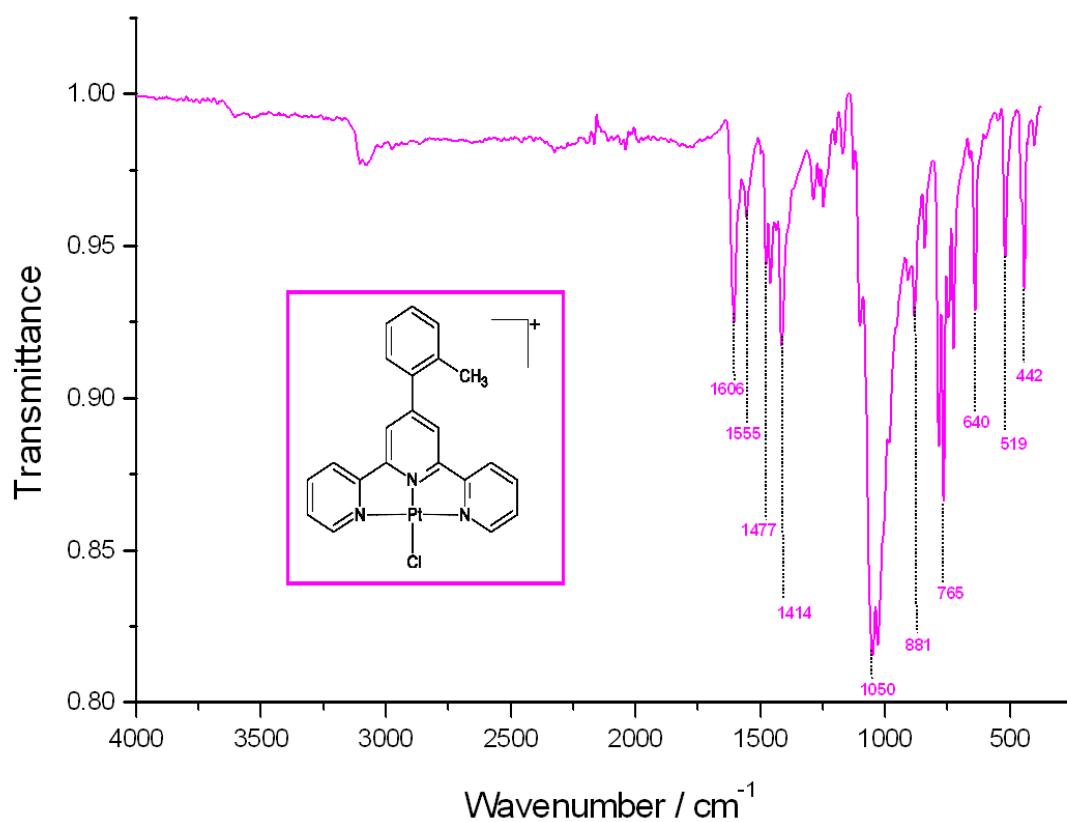
A.1.1 Infrared Spectrum of PtL1



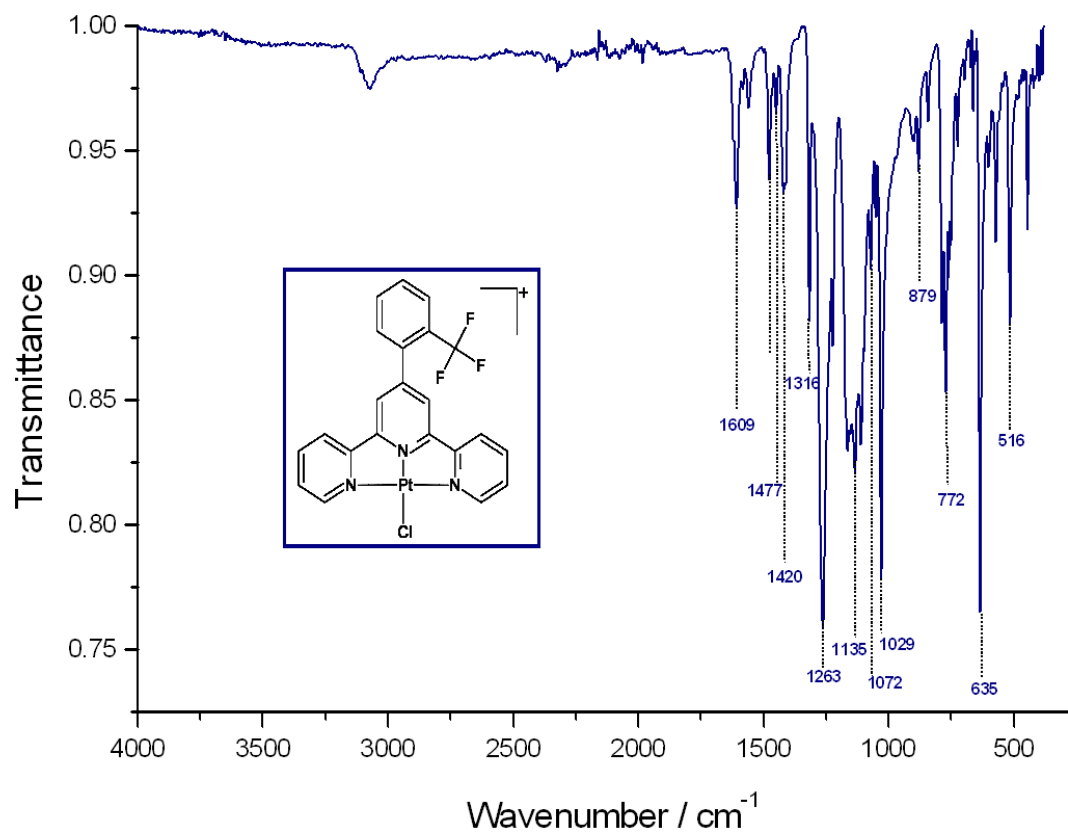
A.1.2 Infrared Spectrum of PtL2

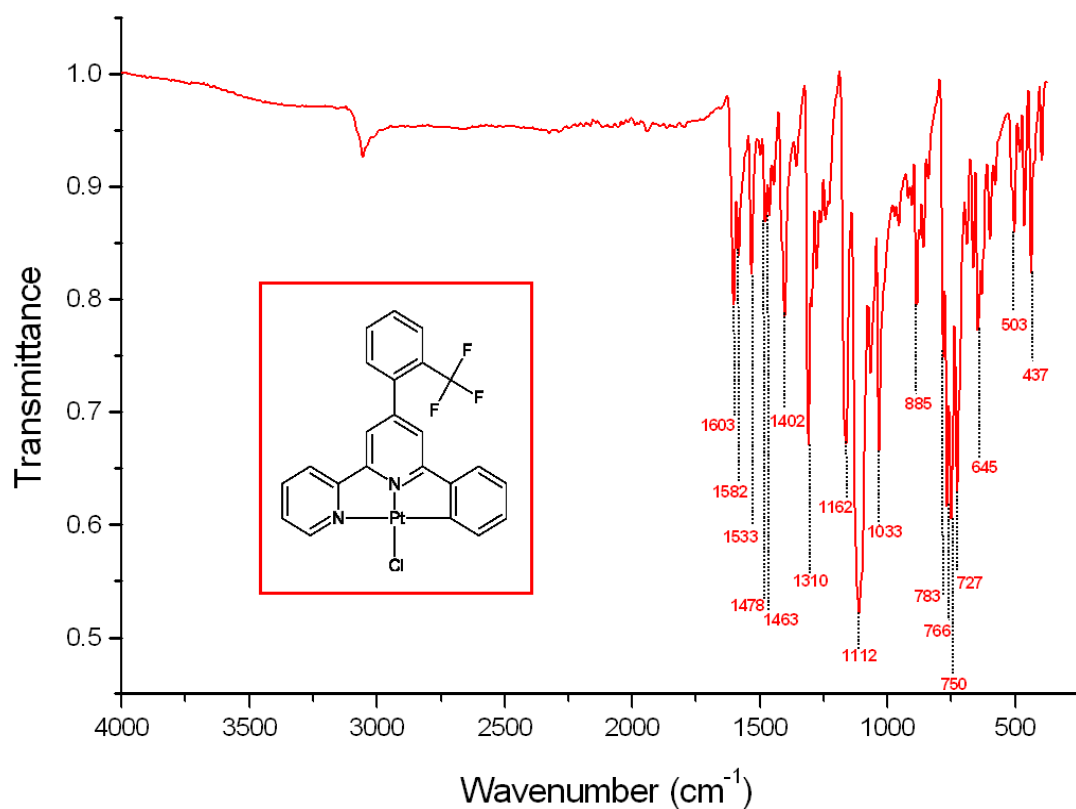
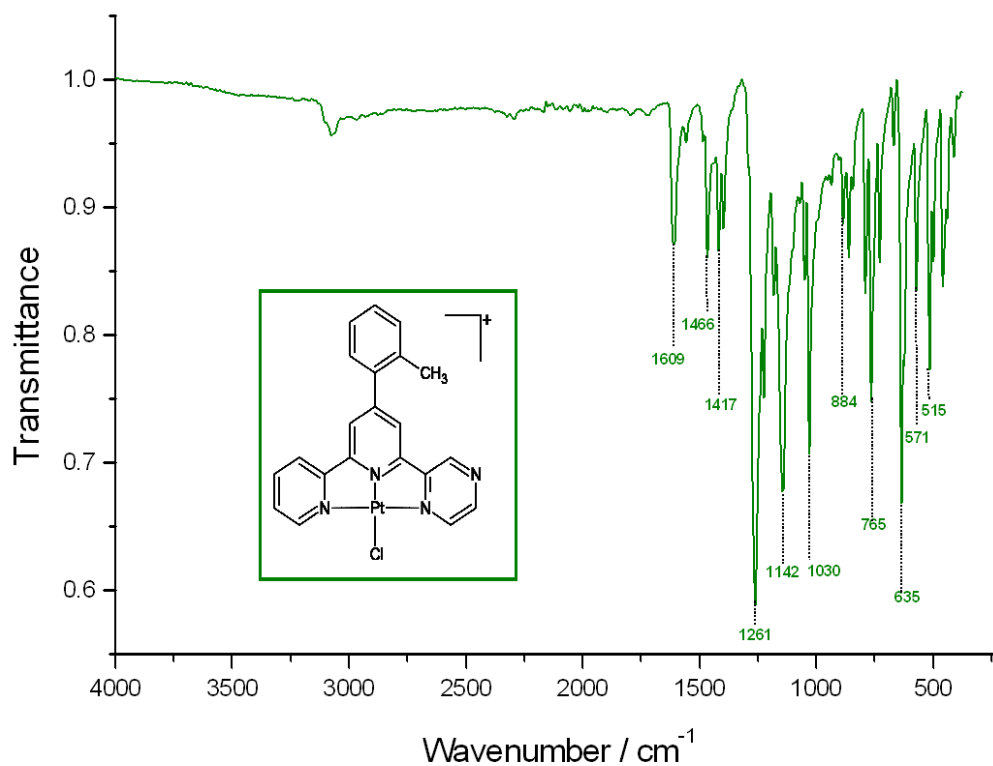


A.1.3 Infrared Spectrum of PtL3



A.1.4 Infrared Spectrum of PtL4



A.1.5 Infrared Spectrum of PtL5**A.1.6 Infrared Spectrum of PtL6**

A.2 Mass Spectra

A.2.1 Mass Spectrum of PtL1

Single Mass Analysis

Tolerance = 50.0 PPM / DBE: min = -1.5, max = 50.0

Element prediction: Off

Number of isotope peaks used for i-FIT = 3

Monoisotopic Mass, Even Electron Ions

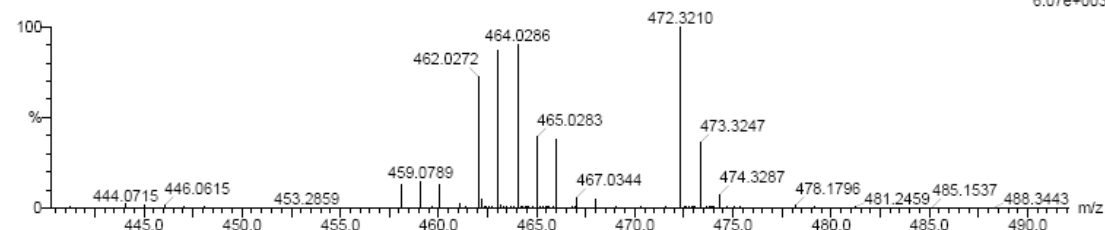
18 formula(e) evaluated with 1 results within limits (all results (up to 1000) for each mass)

Elements Used:

C: 10-20 H: 10-15 N: 0-5 Cl: 0-1 Pt: 0-1

Kate Gillham
Ptterpy 12 (0.188)

TOF MS ES+
6.07e+003



Minimum: -1.5
Maximum: 50.0

Mass	Calc. Mass	mDa	PPM	DBE	i-FIT	i-FIT (Norm)	Formula
463.0290	463.0289	0.1	0.2	12.5	160.5	0.0	C15 H11 N3 Cl Pt

Theoretical values:

463.8044 gmol⁻¹

C₁₅H₁₁N₃ClPt

Lock mass: Terfenadine = 472

A.2.2 Mass Spectrum of PtL2

Single Mass Analysis

Tolerance = 5.0 PPM / DBE: min = -1.5, max = 50.0

Element prediction: Off

Number of isotope peaks used for i-FIT = 3

Monoisotopic Mass, Even Electron Ions

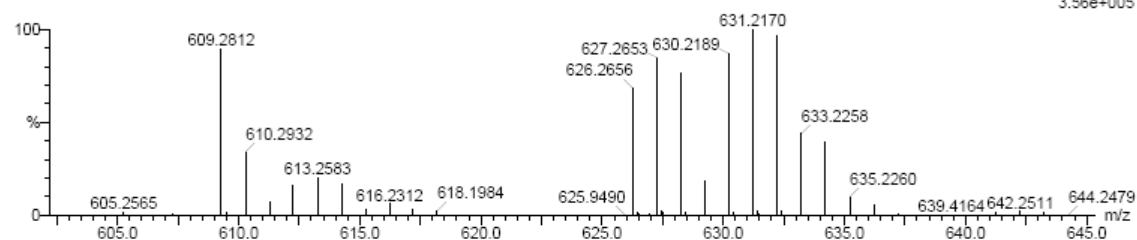
11 formula(e) evaluated with 1 results within limits (all results (up to 1000) for each mass)

Elements Used:

C: 25-30 H: 30-40 N: 0-5 Cl: 1-1 Pt: 0-1

Kate Gillham
Pt(t)Bu3terpy 9 (0.153) Cm (1:11)

TOF MS ES+
3.56e+005



Minimum: -1.5
Maximum: 50.0

Mass	Calc. Mass	mDa	PPM	DBE	i-FIT	i-FIT (Norm)	Formula
631.2170	631.2167	0.3	0.5	12.5	300.2	0.0	C27 H35 N3 Cl Pt

Theoretical values:

632.1234 gmol⁻¹

C₂₇H₃₅ClN₃Pt

Lock mass: reserpine = 609

A.2.3 Mass Spectrum of PtL3

Single Mass Analysis

Tolerance = 5.0 PPM / DBE: min = -1.5, max = 50.0

Element prediction: Off

Number of isotope peaks used for i-FIT = 3

Monoisotopic Mass, Even Electron Ions

9 formula(e) evaluated with 1 results within limits (all results (up to 1000) for each mass)

Elements Used:

C: 20-25 H: 15-20 N: 0-5 Cl: 1-1 Pt: 0-1

Theoretical values:

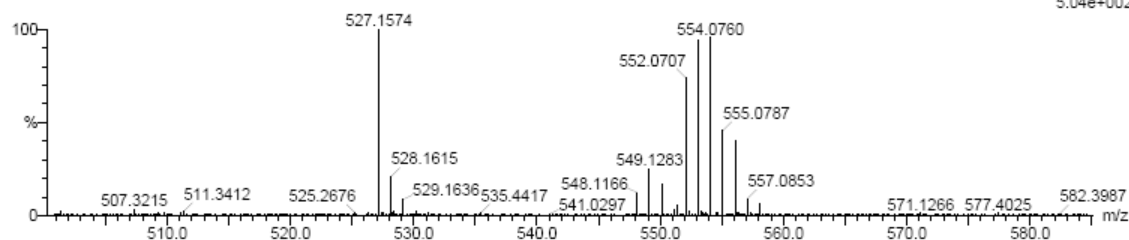
553.9269 gmol^{-1}

$\text{C}_{22}\text{H}_{17}\text{Cl N}_3\text{Pt}$

Lock mass: raffinose = 527

Kate Gillham
PterpyCH3 22 (0.358)

TOF MS ES+
5.04e+002



Minimum:				-1.5					
Maximum:				50.0					
Mass	Calc. Mass	mDa	PPM	DBE	i-FIT	i-FIT (Norm)	Formula		
553.0756	553.0759	-0.3	-0.5	16.5	84.0	0.0	C22	H17	N3 Cl Pt

A.2.4 Mass Spectrum of PtL4

Single Mass Analysis

Tolerance = 5.0 PPM / DBE: min = -1.5, max = 50.0

Element prediction: Off

Number of isotope peaks used for i-FIT = 3

Monoisotopic Mass, Odd and Even Electron Ions

49 formula(e) evaluated with 1 results within limits (all results (up to 1000) for each mass)

Elements Used:

C: 20-25 H: 10-15 N: 0-5 F: 0-5 Cl: 1-1 Pt: 0-1

Theoretical values:

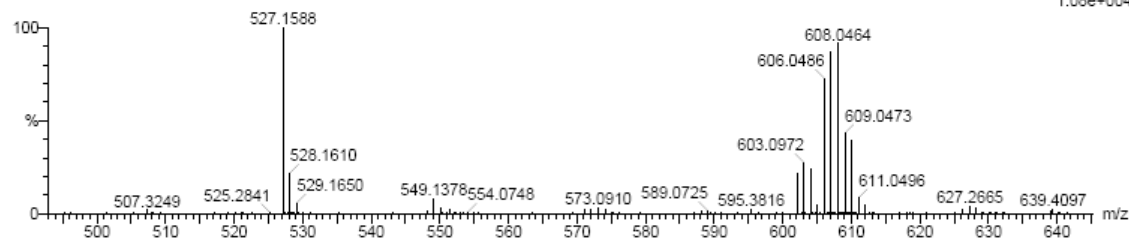
607.8983 gmol^{-1}

$\text{C}_{22}\text{H}_{14}\text{ClF}_3\text{N}_3\text{Pt}$

Lock mass: raffinose = 527

Kate Gillham
PterpyCF3 7 (0.102) Cm (1:7)

TOF MS ES+
1.08e+004



Minimum:				-1.5					
Maximum:				50.0					
Mass	Calc. Mass	mDa	PPM	DBE	i-FIT	i-FIT (Norm)	Formula		
607.0481	607.0476	0.5	0.8	16.5	281.2	0.0	C22	H14	N3 F3 Cl Pt

A.2.5 Mass Spectrum of PtL5

Single Mass Analysis

Tolerance = 5.0 PPM / DBE: min = -1.5, max = 50.0

Element prediction: Off

Number of isotope peaks used for i-FIT = 3

Monoisotopic Mass, Even Electron Ions

102 formula(e) evaluated with 1 results within limits (all results (up to 1000) for each mass)

Elements Used:

C: 20-24 H: 10-15 N: 0-5 F: 0-5 Na: 0-1 Cl: 1-1 Pt: 0-1

Theoretical values:

605.9029 gmol^{-1}

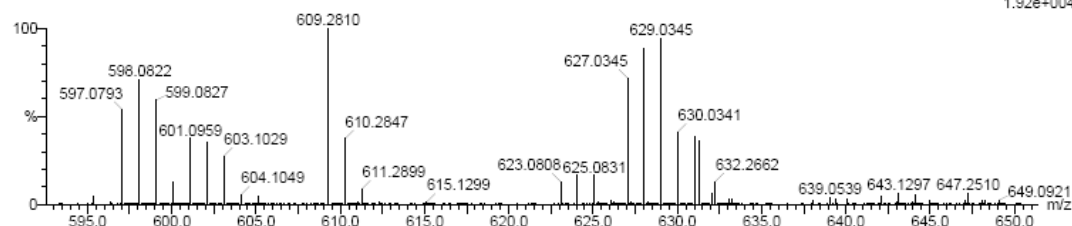
$\text{C}_{23}\text{H}_{14}\text{ClF}_3\text{N}_2\text{Pt}$

Lock mass: reserpine = 609

Kate Gillham

PtbipyCF3 50 (0.837) Cm (1:59)

TOF MS ES+
1.92e+004



Minimum: -1.5
Maximum: 5.0 5.0 50.0

Mass	Calc. Mass	mDa	PPM	DBE	i-FIT	i-FIT (Norm)	Formula
628.0343	628.0343	0.0	0.0	16.5	418.9	0.0	$\text{C}_{23}\text{H}_{14}\text{N}_2\text{F}_3\text{NaClPt}$

A.2.6 Mass Spectrum of PtL6

Single Mass Analysis

Tolerance = 5.0 PPM / DBE: min = -1.5, max = 50.0

Element prediction: Off

Number of isotope peaks used for i-FIT = 3

Monoisotopic Mass, Even Electron Ions

9 formula(e) evaluated with 1 results within limits (all results (up to 1000) for each mass)

Elements Used:

C: 20-24 H: 15-20 N: 0-5 Cl: 1-1 Pt: 0-1

Theoretical values:

554.9150 gmol^{-1}

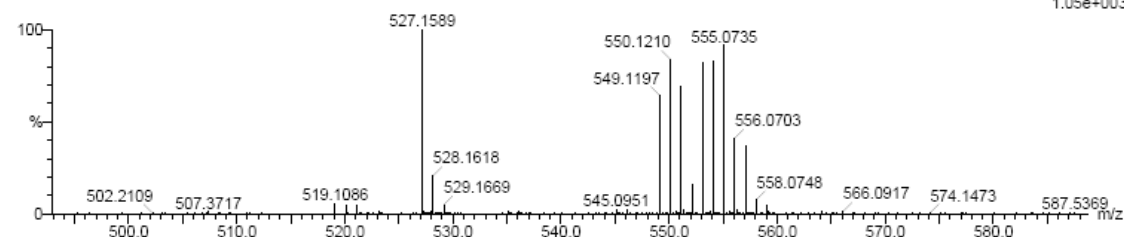
$\text{C}_{21}\text{H}_{16}\text{ClN}_4\text{Pt}$

Lock mass: raffinose = 527

Kate Gillham

PtL7CH3 10 (0.154)

TOF MS ES+
1.05e+003



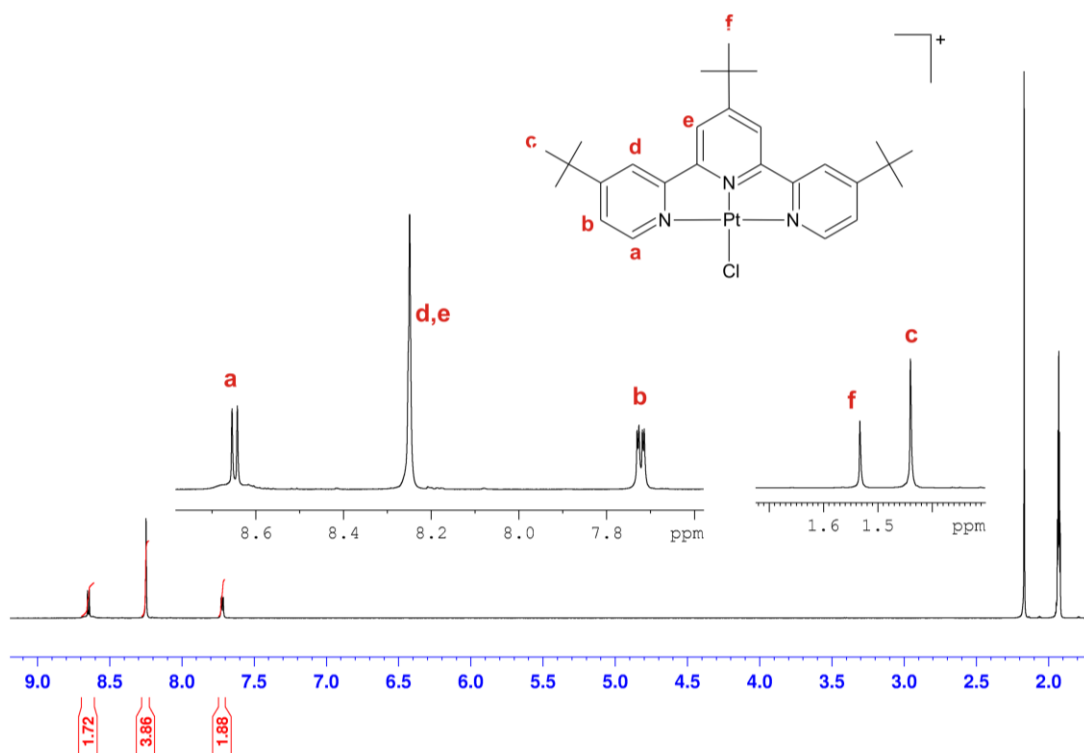
Minimum: -1.5
Maximum: 5.0 5.0 50.0

Mass	Calc. Mass	mDa	PPM	DBE	i-FIT	i-FIT (Norm)	Formula
554.0710	554.0711	-0.1	-0.2	16.5	103.0	0.0	$\text{C}_{21}\text{H}_{16}\text{N}_4\text{ClPt}$

A.3 NMR Spectra

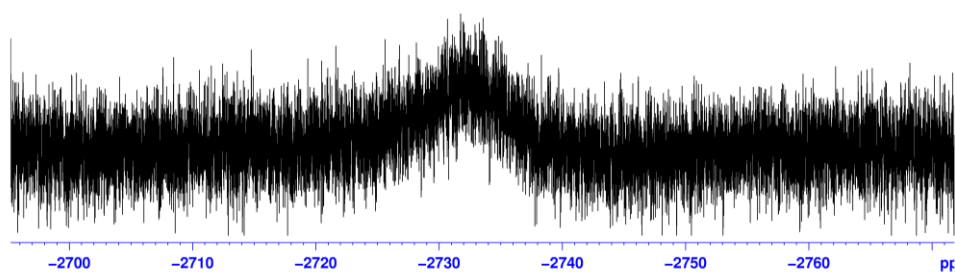
A.3.1 ^1H NMR Spectrum of PtL2

(DMSO- d_6)



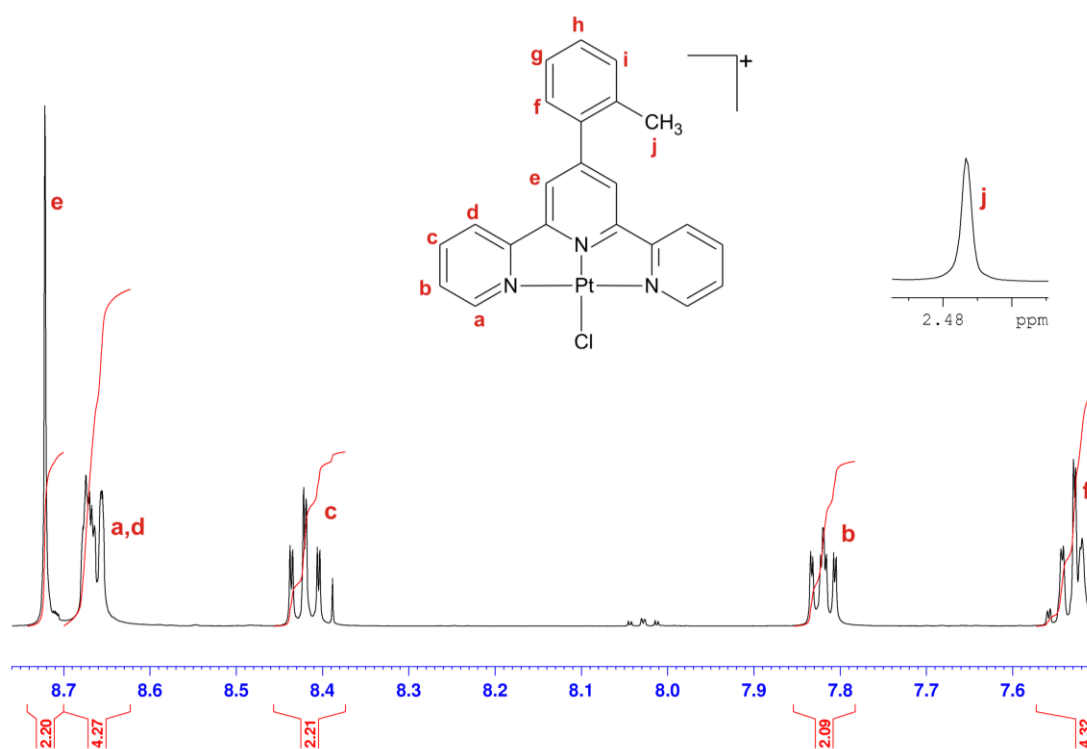
A.3.2 ^{195}Pt NMR Spectrum of PtL2

(CD_3CN)



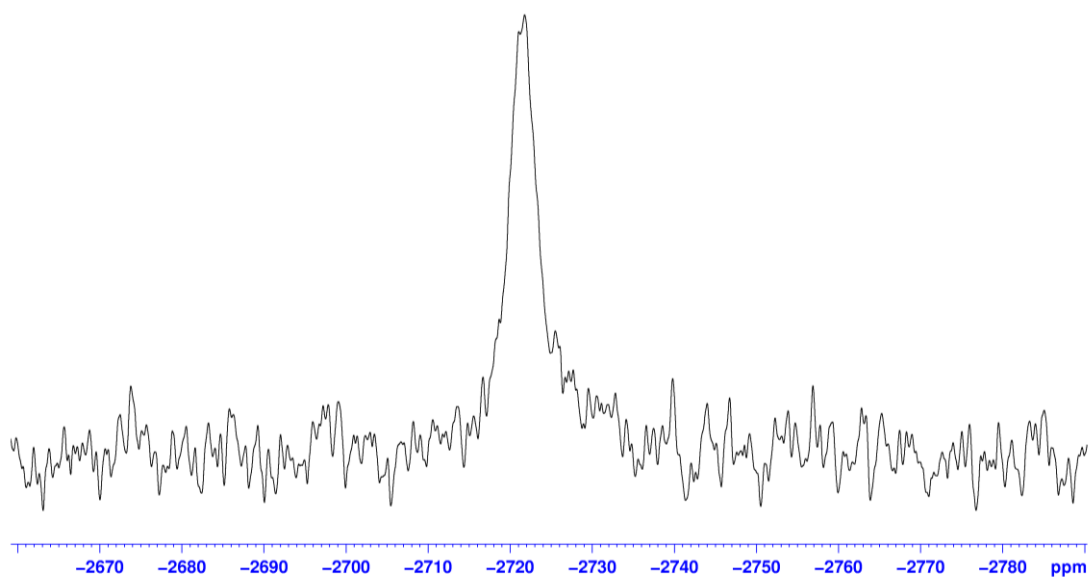
A.3.3 ^1H NMR Spectrum of PtL3

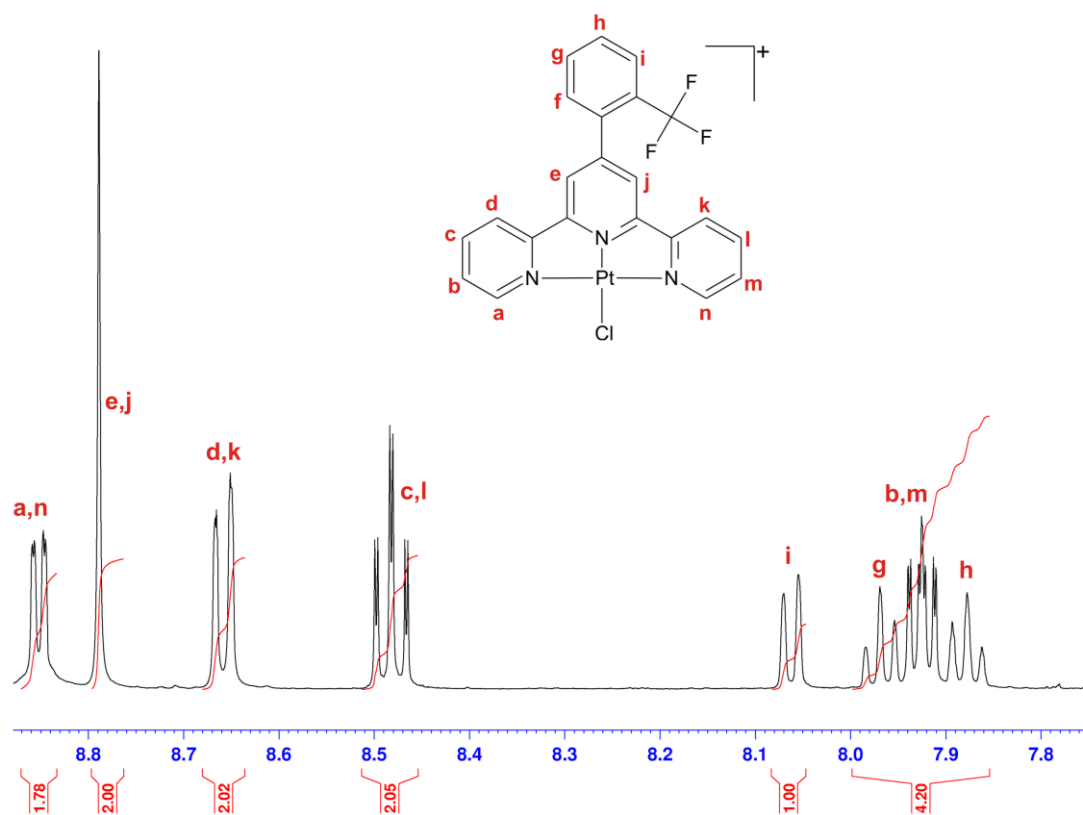
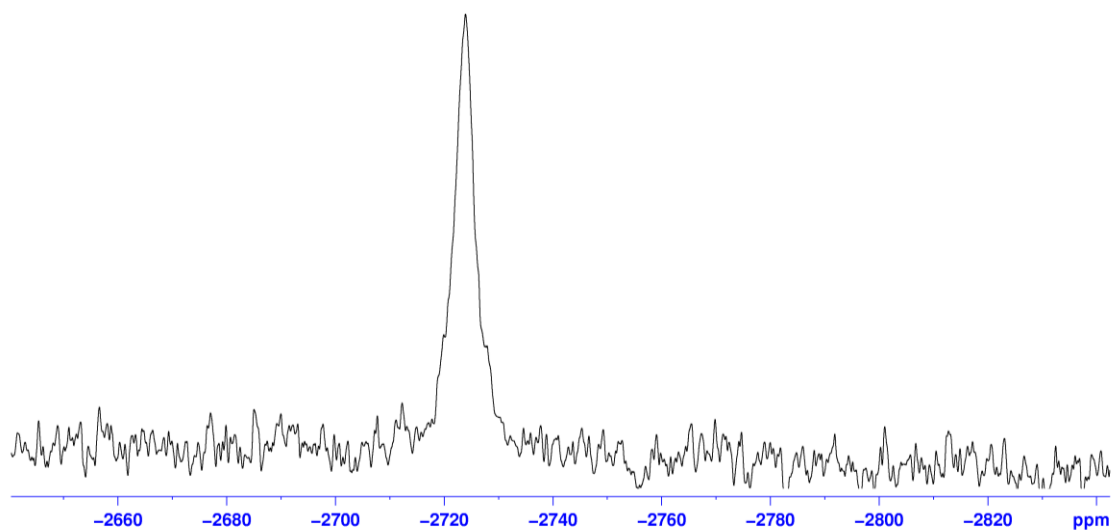
(DMSO-d₆)



A.3.4 ^{195}Pt NMR Spectrum of PtL3

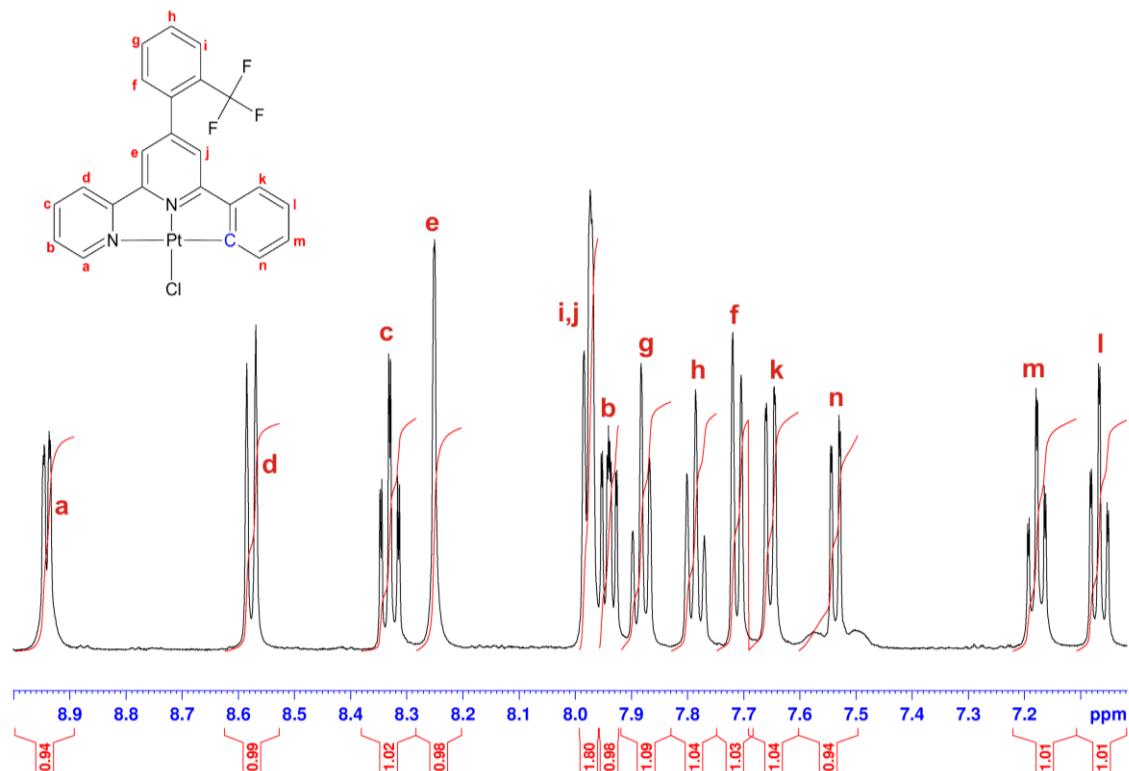
(DMSO-d₆)



A.3.5 ^1H NMR Spectrum of PtL4(DMSO-d₆)**A.3.6 ^{195}Pt NMR Spectrum of PtL4**(DMSO-d₆)

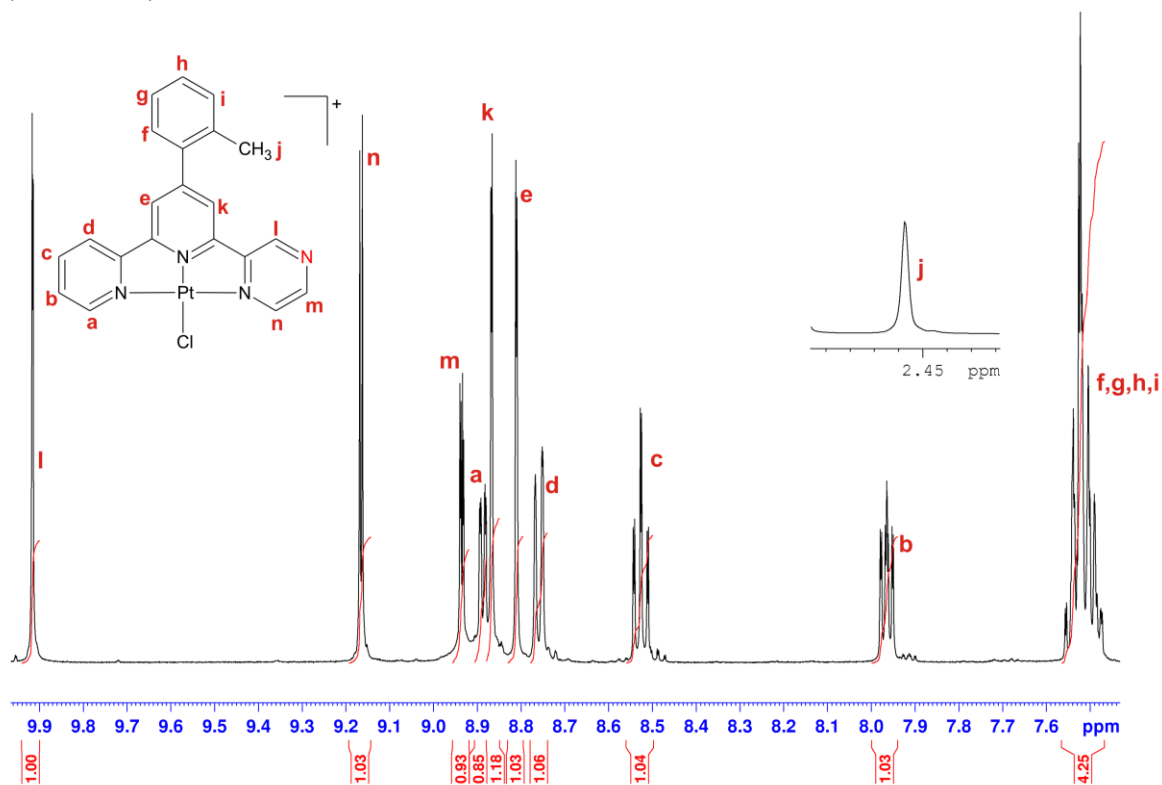
A.3.7 ^1H NMR Spectrum of PtL5

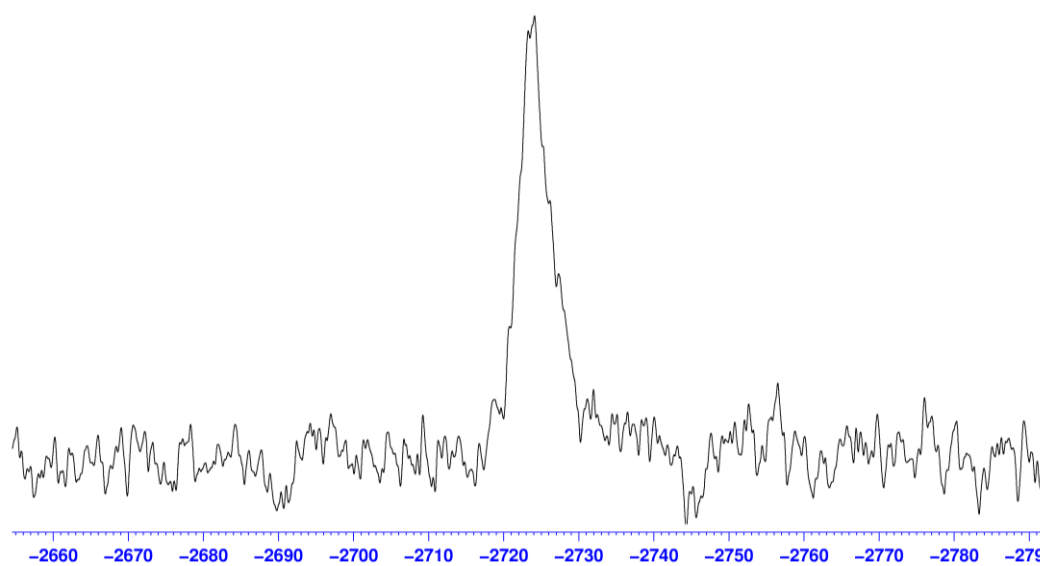
(DMSO-d₆)



A.3.8 ^1H NMR Spectrum of PtL6

(DMSO-d₆)



A.3.9 ^{195}Pt NMR Spectrum of PtL6(DMSO-d₆)

APPENDIX B

B.1 IUCR CIF Check Report for PtL1-MIm

IUCR checkCIF/PLATON report (basic structural check)

Datablock: PtL1-MIm

Bond precision:	C-C = 0.0123 Å	Wavelength=0.71073
Cell:	a=16.389(5) b=11.582(6) c=14.538(4)	
	alpha=90 beta=110.147(5) gamma=90	
Temperature:	296 K	
	Calculated	Reported
Volume	2590.7(17)	2590.7(16)
Space group	P 21/c	P21/c
Hall group	-P 2ybc	-P 2ybc
Moiety formula	C19 H17 N5 Pt, C H3 N O2, 2(Cl O4)	C19 H17 N5 Pt, C H3 N O2, 2(Cl O4)
Sum formula	C20 H20 Cl2 N6 O10 Pt	C20 H20 Cl2 N6 O10 Pt
Mr	770.40	770.41
Dx, g cm ⁻³	1.975	1.975
Z	4	4
Mu (mm ⁻¹)	5.688	5.688
F000	1496.0	1496.0
F000'	1491.23	
h, k, lmax	20, 14, 17	20, 14, 17
Nref	5113	5102
Tmin, Tmax	0.046, 0.033	0.132, 0.132
Tmin'	0.024	
Correction method=	MULTI-SCAN	
Data completeness=	0.998	Theta(max)= 26.060
R(reflections)=	0.0452(3881)	wR2(reflections)= 0.1178(5102)
S =	0.980	Npar= 354

The following ALERTS were generated. Each ALERT has the format

test-name_ALERT_alert-type_alert-level.

Click on the hyperlinks for more details of the test.

●Alert level C

[PLAT342 ALERT 3 C](#) Low Bond Precision on C-C Bonds (x 1000) Ang ..
12

[PLAT244 ALERT 4 C](#) Low 'Solvent' Ueq as Compared to Neighbors of
N1S

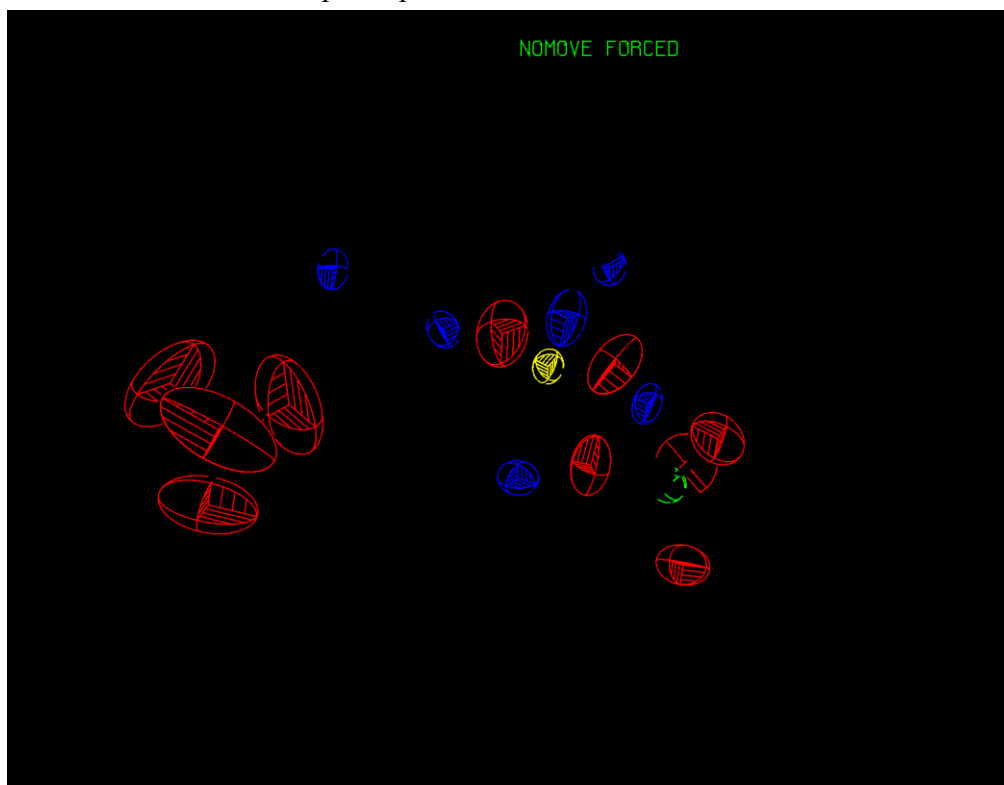
[PLAT790 ALERT 4 C](#) Centre of Gravity not Within Unit Cell: Resd. #
2 C H3 N O2

●Alert level G

[PLAT720 ALERT 4 G](#) Number of Unusual/Non-Standard Labels
3

PLATON version of 13/08/2009; check.def file version of 12/08/2009

Datablock PtL1-MIm - ellipsoid plot



B.2 IUCR CIF Check Report for PtL1-DIm

IUCR checkCIF/PLATON report (basic structural check)

Datablock: PtL1-DIm

Bond precision:	C-C = 0.0222 Å	Wavelength=0.71073
Cell:	a=7.718(5) b=20.820(5) c=16.791(5)	
	alpha=90 beta=94.536(5) gamma=90	
Temperature:	296 K	
	Calculated	Reported
Volume	2690(2)	2690(2)
Space group	P 21/c	P21/c
Hall group	-P 2ybc	-P 2ybc
Moiety formula	C20 H19 N5 Pt, C H3 N O2, 2(Cl O4)	C20 H19 N5 Pt, C H3 N O2, 2(Cl O4)
Sum formula	C21 H22 Cl2 N6 O10 Pt	C21 H22 Cl2 N6 O10 Pt
Mr	784.43	784.44
Dx, g cm ⁻³	1.937	1.937
Z	4	4
Mu (mm ⁻¹)	5.480	5.481
F000	1528.0	1528.0
F000'	1523.23	
h,k,lmax	9,25,20	9,25,20
Nref	5368	5336
Tmin,Tmax	0.523,0.681	0.218,0.700
Tmin'	0.111	
Correction method=	MULTI-SCAN	
Data completeness=	0.994	Theta(max)= 26.130
R(reflections)=	0.0859(3468)	wR2(reflections)= 0.2242(5336)
S =	1.021	Npar= 364

The following ALERTS were generated. Each ALERT has the format

test-name_ALERT_alert-type_alert-level.

Click on the hyperlinks for more details of the test.

Alert level B

[PLAT241 ALERT 2 B](#) Check High Ueq as Compared to Neighbors for C18
[PLAT342 ALERT 3 B](#) Low Bond Precision on C-C Bonds (x 1000) Ang .. 22

Alert level C

[PLAT213 ALERT 2 C](#) Atom C8 has ADP max/min Ratio 3.50 oblat
[PLAT213 ALERT 2 C](#) Atom C17 has ADP max/min Ratio 3.90 prola
[PLAT230 ALERT 2 C](#) Hirshfeld Test Diff for C17 -- C18 .. 6.73 su
[PLAT241 ALERT 2 C](#) Check High Ueq as Compared to Neighbors for C8
[PLAT242 ALERT 2 C](#) Check Low Ueq as Compared to Neighbors for N5

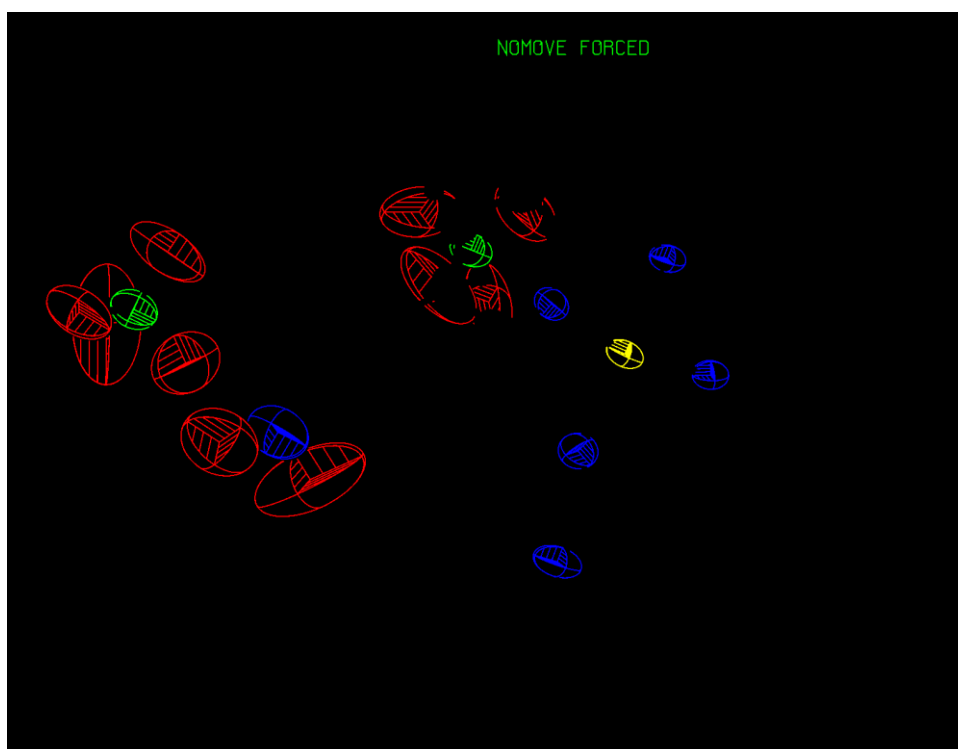
[PLAT242 ALERT 2 C](#) Check Low Ueq as Compared to Neighbors for C17
[PLAT153 ALERT 1 C](#) The su's on the Cell Axes are Equal (x 100000) 500 Ang.
[PLAT234 ALERT 4 C](#) Large Hirshfeld Difference N1 -- C1 .. 0.19 Ang.
[PLAT234 ALERT 4 C](#) Large Hirshfeld Difference N5 -- C18 .. 0.20 Ang.
[PLAT234 ALERT 4 C](#) Large Hirshfeld Difference C13 -- C14 .. 0.18 Ang.
[PLAT244 ALERT 4 C](#) Low 'Solvent' Ueq as Compared to Neighbors of N1S
[PLAT244 ALERT 4 C](#) Low 'Solvent' Ueq as Compared to Neighbors of C11
[PLAT244 ALERT 4 C](#) Low 'Solvent' Ueq as Compared to Neighbors of C12

● Alert level G

[PLAT072 ALERT 2 G](#) SHELXL First Parameter in WGHT Unusually Large.. 0.14
[PLAT860 ALERT 3 G](#) Note: Number of Least-Squares Restraints 6
[PLAT720 ALERT 4 G](#) Number of Unusual/Non-Standard Labels 3

PLATON version of 13/08/2009; check.def file version of 12/08/2009

Datablock PtL1-DIm - ellipsoid plot



B.3 IUCR CIF Check Report for PtL1-Pyz

IUCR checkCIF/PLATON report (basic structural check)

Datablock: PtL1-Pyz

Bond precision:	C-C = 0.0134 Å	Wavelength=0.71073
Cell:	a=16.351(5) b=11.534(6) c=14.075(4)	
	alpha=90 beta=111.311(5) gamma=90	
Temperature:	296 K	
	Calculated	Reported
Volume	2472.9(17)	2472.9(16)
Space group	P 21/c	P21/c
Hall group	-P 2ybc	-P 2ybc
Moiety formula	C18 H15 N5 Pt, C H3 N O2, 2(C1 O4)	C18 H15 N5 Pt, C H3 N O2, 2(C1 O4)
Sum formula	C19 H18 Cl2 N6 O10 Pt	C19 H18 Cl2 N6 O10 Pt
Mr	756.37	756.38
Dx, g cm ⁻³	2.032	2.032
Z	4	4
Mu (mm ⁻¹)	5.957	5.957
F000	1464.0	1464.0
F000'	1459.23	
h, k, lmax	20, 14, 17	20, 14, 17
Nref	4885	4879
Tmin, Tmax	0.072, 0.304	0.124, 0.382
Tmin'	0.022	
Correction method=	MULTI-SCAN	
Data completeness=	0.999	Theta(max)= 26.040
R(reflections)=	0.0475(3850)	wR2(reflections)= 0.1296(4879)
S =	1.008	Npar= 344

The following ALERTS were generated. Each ALERT has the format
[test-name](#) [ALERT](#) [alert-type](#) [alert-level](#).
Click on the hyperlinks for more details of the test.

● Alert level C

[PLAT241 ALERT 2 C](#) Check High Ueq as Compared to Neighbors for C16

[PLAT342 ALERT 3 C](#) Low Bond Precision on C-C Bonds (x 1000) Ang .. 13

[PLAT234 ALERT 4 C](#) Large Hirshfeld Difference N3 -- C10 .. 0.15 Ang.

[PLAT234 ALERT 4 C](#) Large Hirshfeld Difference C2 -- C3 .. 0.18 Ang.

[PLAT234 ALERT 4 C](#) Large Hirshfeld Difference C15' -- C16 .. 0.21 Ang.

[PLAT244 ALERT 4 C](#) Low 'Solvent' Ueq as Compared to Neighbors of N1S'

[PLAT790 ALERT 4 C](#) Centre of Gravity not Within Unit Cell: Resd. # 4

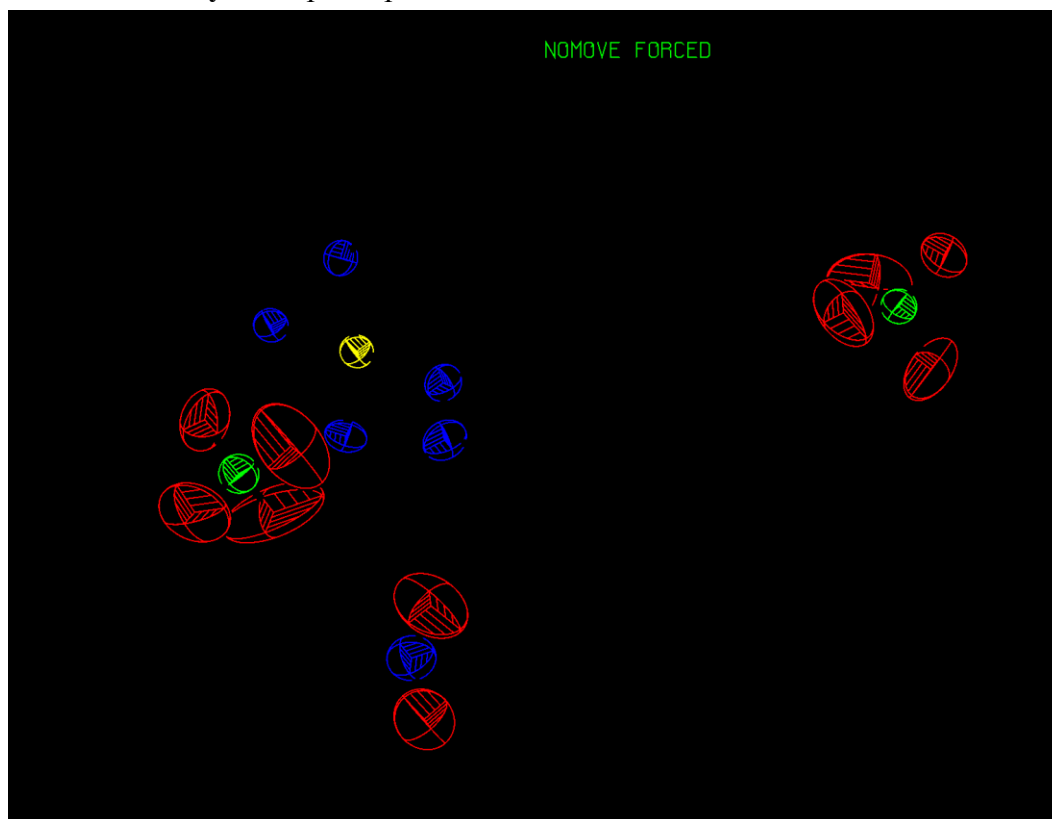
C1 O4

● Alert level G

PLAT720 ALERT 4 G Number of Unusual/Non-Standard Labels
9

PLATON version of 13/08/2009; check.def file version of 12/08/2009

Datablock PtL1-Pyz - ellipsoid plot



B.4 IUCR CIF Check Report for PtL3-Pyz

IUCR checkCIF/PLATON report (basic structural check)

Datablock: PtL3-Pyz

Bond precision:	C-C = 0.0180 Å	Wavelength=0.71073
Cell:	a=19.749(5) b=7.453(4) c=21.273(6)	
	alpha=90 beta=110.843(5) gamma=90	
Temperature:	296 K	
	Calculated	Reported
Volume	2926.3(19)	2926(2)
Space group	P 21/n	P21/n
Hall group	-P 2yn	-P 2yn
Moiety formula	C25 H21 N5 Pt, C H3 N O2, 2(Cl O4)	C25 H21 N5 Pt, C H3 N O2, 2(Cl O4)
Sum formula	C26 H24 Cl2 N6 O10 Pt	C26 H24 Cl2 N6 O10 Pt
Mr	846.49	846.50
Dx, g cm ⁻³	1.921	1.921
Z	4	4
Mu (mm ⁻¹)	5.046	5.046
F000	1656.0	1656.0
F000'	1651.25	
h, k, lmax	24, 9, 26	24, 9, 26
Nref	5859	5790
Tmin, Tmax	0.310, 0.702	0.152, 0.719
Tmin'	0.047	
Correction method=	MULTI-SCAN	
Data completeness=	0.988	Theta(max)= 26.170
R(reflections)=	0.0736(4059)	wR2(reflections)= 0.2081(5790)
S =	1.011	Npar= 412

The following ALERTS were generated. Each ALERT has the format

test-name_ALERT_alert-type_alert-level.

Click on the hyperlinks for more details of the test.

● Alert level C

[PLAT342 ALERT 3 C](#) Low Bond Precision on C-C Bonds (x 1000) Ang ..
18

[PLAT234 ALERT 4 C](#) Large Hirshfeld Difference Cl8 -- Cl9 ..
0.15 Ang.

[PLAT234 ALERT 4 C](#) Large Hirshfeld Difference Cl9 -- C20 ..
0.19 Ang.

[PLAT243 ALERT 4 C](#) High 'Solvent' Ueq as Compared to Neighbors of
Cl1

[PLAT243 ALERT 4 C](#) High 'Solvent' Ueq as Compared to Neighbors of
Cl2

[PLAT244 ALERT 4 C](#) Low 'Solvent' Ueq as Compared to Neighbors of
N1S

[PLAT790 ALERT 4 C](#) Centre of Gravity not Within Unit Cell: Resd. #
2C H3 N O2

[PLAT790 ALERT 4 C](#) Centre of Gravity not Within Unit Cell: Resd. #
4 Cl O4

● **Alert level G**

[PLAT072 ALERT 2 G](#) SHELXL First Parameter in WGHT Unusually Large..
0.14

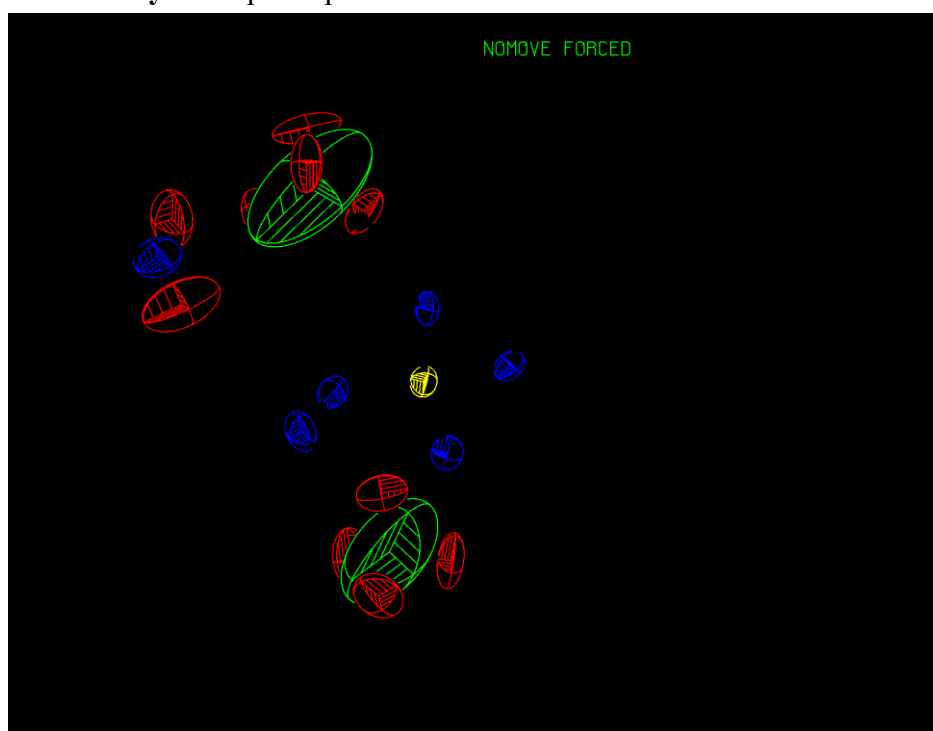
[PLAT860 ALERT 3 G](#) Note: Number of Least-Squares Restraints
1

[PLAT128 ALERT 4 G](#) Non-standard setting of Space-group P21/c
P21/n

[PLAT720 ALERT 4 G](#) Number of Unusual/Non-Standard Labels
3

PLATON version of 13/08/2009; check.def file version of 12/08/2009

Datablock PtL3-Pyz - ellipsoid plot



APPENDIX C

C.1 Kinetic and Thermodynamic Data for PtL1

C.1.1 Pyrazole

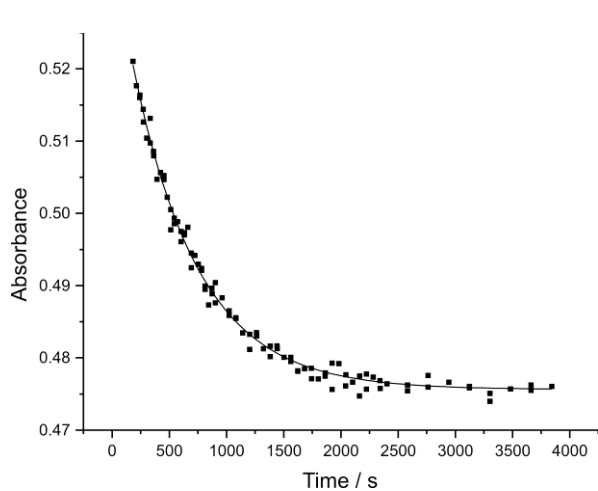
Wavelength: 281 nm

Reaction Rates:

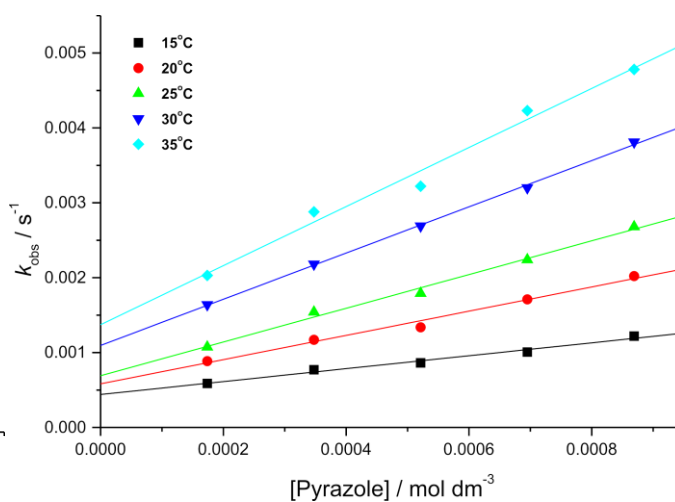
	k_2 (s ⁻¹)	Error	k_{-2} (s ⁻¹)	Error	K
15 °C	0.863	0.065	4.40x10 ⁻⁴	3.7x10 ⁻⁵	1.96x10 ³
20 °C	1.62	0.11	5.82x10 ⁻⁴	6.1x10 ⁻⁵	2.78x10 ³
25 °C	2.25	0.11	6.91x10 ⁻⁴	6.5x10 ⁻⁵	3.26x10 ³
30 °C	3.09	0.06	1.10x10 ⁻³	3x10 ⁻⁵	2.81x10 ³
35 °C	3.95	0.29	1.40x10 ⁻³	1.7x10 ⁻⁴	2.82x10 ³

Eyring Plot:

	Slope:	y-intercept:	ΔH (kJ mol ⁻¹)	ΔS (J K ⁻¹ mol ⁻¹)
k_2	-5104	12.22	42	-96
Error:	200	0.67	2	6
k_{-2}	-4871	3.51	41	-169
Error:	184	0.62	2	5



(a)



(b)

Figure C.1: (a) Kinetic Trace (281 nm) of **PtL1** (1.74×10^{-5} M) and **Pyz** (5.22×10^{-4} M) at an ionic strength of 0.1 M (90 mM LiCF_3SO_3 and 10 mM NaCl) at 25 °C. (b) Plot to determine rate constants from the slopes and y-intercepts for **PtL1** and **Pyz** at varying temperatures.

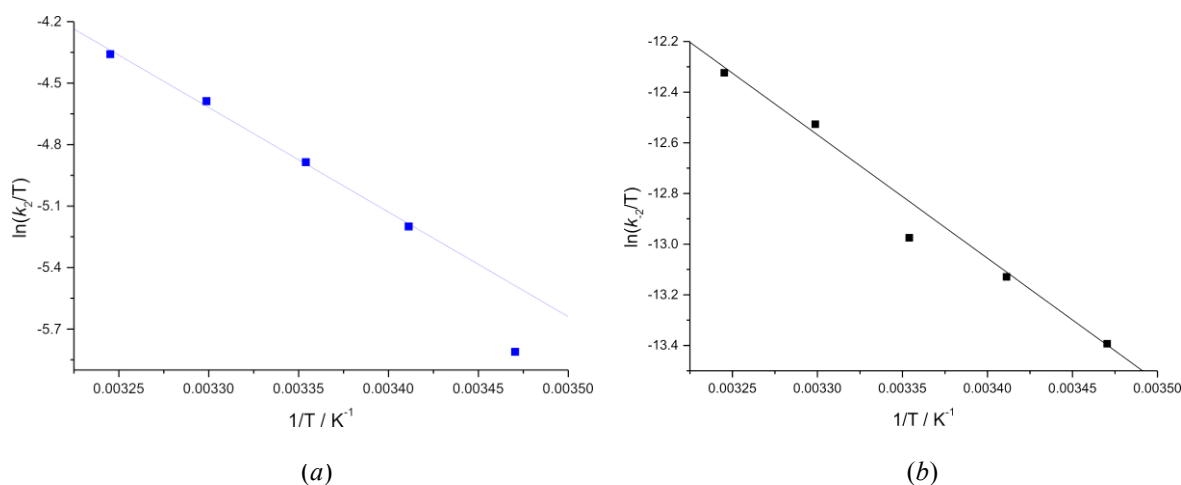


Figure C.2: Eyring plot for **PtL1** and **Pyz** to determine ΔH^\ddagger and ΔS^\ddagger for the (a) forward reaction and (b) reverse reaction.

C.1.2 Imidazole

Wavelength: 281 nm

Reaction Rates:

	k_2 (s ⁻¹)	Error	k_{-2} (s ⁻¹)	Error	K
20 °C	2.90	0.03	4.66x10 ⁻⁴	1.9 x10 ⁻⁵	1.53 x10 ⁵
25 °C	3.894	0.05	8.31x10 ⁻⁴	2.9 x10 ⁻⁵	1.37 x10 ⁵
30 °C	5.27	0.09	1.44x10 ⁻³	4.9 x10 ⁻⁴	1.08 x10 ⁵
35 °C	6.95	0.20	2.39x10 ⁻³	1.1x10 ⁻⁴	6.21 x10 ⁴
40 °C	9.03	0.24	3.70x10 ⁻³	1.4x10 ⁻⁴	6.45 x10 ⁴

Eyring Plot:

	Slope:	y-intercept:	ΔH (kJ mol ⁻¹)	ΔS (J K ⁻¹ mol ⁻¹)
K_2	-4934	12.22	41	-96
Error:	40	0.13	0.3	1
k_{-2}	-9250	18.23	77	-46
Error:	191	0.63	2	5

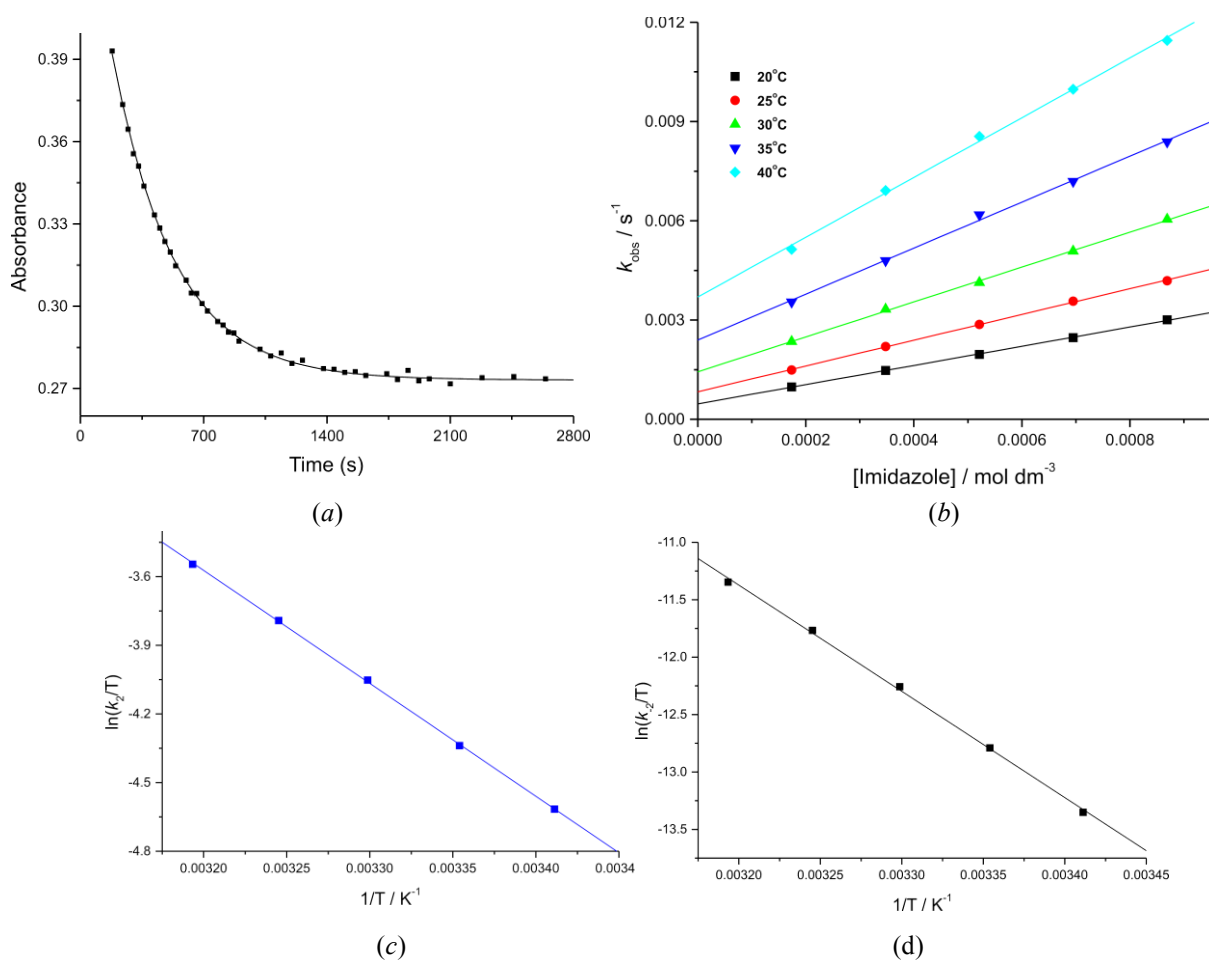


Figure C.3: (a) Kinetic Trace (281 nm) of **PtL1** (1.74×10^{-5} M) and **Im** (5.22×10^{-4} M) at an ionic strength of 0.1 M (90 mM LiCF_3SO_3 and 10 mM NaCl) at 25 °C. (b) Plot to determine rate constants from the slopes and y-intercepts for **PtL1** and **Im** at varying temperatures. Eyring plot to determine ΔH^\ddagger and ΔS^\ddagger for the (c) forward reaction and (d) reverse reaction.

C.1.3 1,2,4-Triazole

Wavelength: 345 nm

Reaction Rates:

	$k_2 (\text{s}^{-1})$	Error	$k_2 (\text{s}^{-1})$	Error	K
15 °C	0.619	0.027	7.39×10^{-5}	1.57×10^{-5}	8.38×10^3
20 °C	0.805	0.068	8.59×10^{-5}	3.91×10^{-5}	9.37×10^3
25 °C	1.04	0.07	1.60×10^{-4}	4.0×10^{-5}	6.50×10^3
30 °C	1.42	0.03	1.98×10^{-4}	1.9×10^{-5}	7.17×10^3
35 °C	2.03	0.09	2.83×10^{-4}	5.2×10^{-5}	7.16×10^3

Eyring Plot:

	Slope:	y-intercept:	ΔH (kJ mol ⁻¹)	ΔS (J K ⁻¹ mol ⁻¹)
K_2	-4914	10.88	41	-107
Error:	204	0.68	2	6
k_2	-5952	5.41	49	-153
Error:	651	2.19	5	18

C.1.4 1-Methylimidazole**Wavelength:** 282 nmReaction Rates:

	k_2 (s ⁻¹)	Error	k_2 (s ⁻¹)	Error	K
15 °C	2.05	0.04	4.47x10 ⁻⁴	2.5x10 ⁻⁵	4.59x10 ³
20 °C	2.86	0.03	7.25x10 ⁻⁴	1.4x10 ⁻⁵	3.95x10 ³
25 °C	3.84	0.04	1.31x10 ⁻³	2x10 ⁻⁵	2.93x10 ³
30 °C	5.21	0.02	2.22x10 ⁻³	1x10 ⁻⁵	2.35x10 ³
35 °C	7.02	0.13	3.81x10 ⁻³	7x10 ⁻⁵	1.84x10 ³

Eyring Plot:

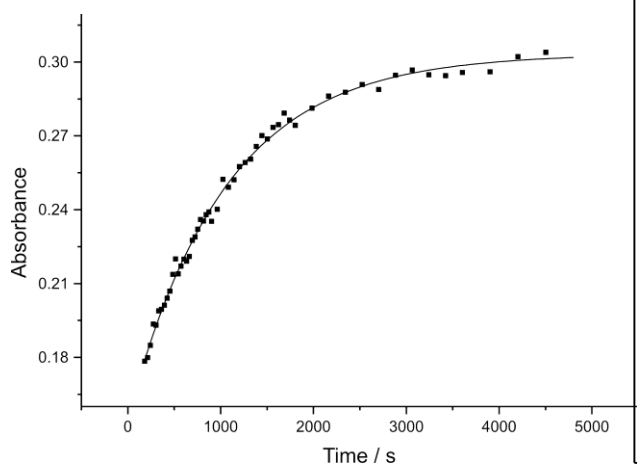
	Slope:	y-intercept:	ΔH (kJ mol ⁻¹)	ΔS (J K ⁻¹ mol ⁻¹)
K_2	-5139	12.89	43	-91
Error:	45	0.15	0.4	1
k_2	-9301	18.86	77	-41
Error:	204	0.68	2	6

C.1.5. 1,2-Dimethylimidazole**Wavelength:** 343 nmReaction Rates:

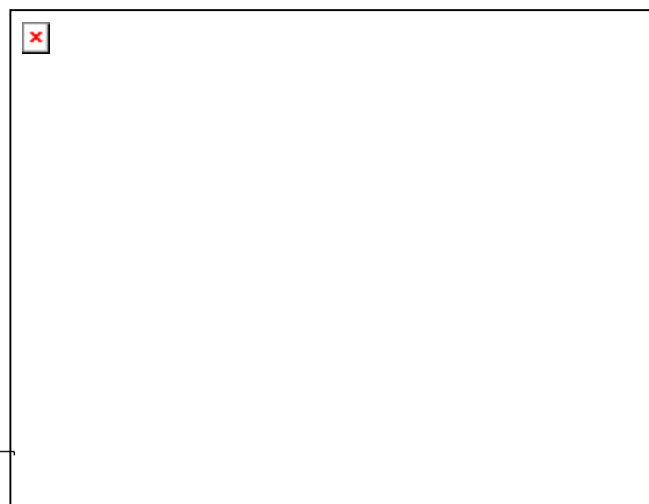
	k_2 (s ⁻¹)	Error	k_2 (s ⁻¹)	Error	K
15 °C	0.819	0.015	3.37x10 ⁻⁵	8.5x10 ⁻⁶	2.43x10 ⁴
20 °C	1.17	0.01	6.05x10 ⁻⁵	3.9x10 ⁻⁶	1.93x10 ⁴
25 °C	1.62	0.04	1.19x10 ⁻⁴	2.0x10 ⁻⁵	1.37x10 ⁴
30 °C	2.26	0.01	2.12x10 ⁻⁴	7x10 ⁻⁶	1.07x10 ⁴
35 °C	3.04	0.04	3.65x10 ⁻⁴	2.1x10 ⁻⁵	8.32x10 ³

Eyring Plot:

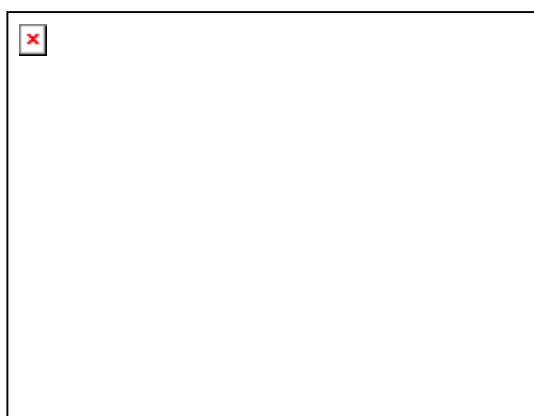
	Slope:	y-intercept:	ΔH (kJ mol ⁻¹)	ΔS (J K ⁻¹ mol ⁻¹)
k_2	-5494	13.22	46	-88
Error:	94	0.32	1	3
k_{-2}	-10051	18.97	84	-40
Error:	288	0.97	2	8



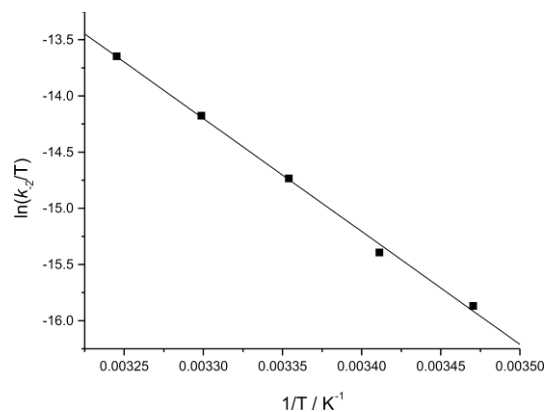
(a)



(b)



(c)



(d)

Figure C.4: (a) Kinetic Trace (343 nm) of **PtL1** (1.74×10^{-5} M) and **DIIm** (5.22×10^{-4} M) at an ionic strength of 0.1 M (90 mM LiCF₃SO₃ and 10 mM NaCl) at 25 °C. (b) Plot to determine rate constants from the slopes and y-intercepts for **PtL1** and **DIIm** at varying temperatures. Eyring plot to determine ΔH^\ddagger and ΔS^\ddagger for the (c) forward reaction and (d) reverse reaction.

C.2 Kinetic and Thermodynamic Data for PtL2

C.2.1 Pyrazole

Wavelength: 320 nm

Reaction Rates:

	k_2 (s ⁻¹)	Error	k_{-2} (s ⁻¹)	Error	K
15 °C	0.299	0.015	3.51×10^{-4}	4.2×10^{-5}	8.52×10^2
20 °C	0.462	0.019	4.56×10^{-4}	5.2×10^{-5}	1.01×10^3
25 °C	0.648	0.033	7.45×10^{-4}	9.1×10^{-5}	8.70×10^2
30 °C	0.825	0.037	1.30×10^{-3}	1.0×10^{-4}	6.35×10^2
35 °C	1.11	0.03	1.90×10^{-3}	9×10^{-5}	5.86×10^2

Eyring Plot:

	Slope:	y-intercept:	ΔH (kJ mol ⁻¹)	ΔS (J K ⁻¹ mol ⁻¹)
K_2	-5413	11.97	45	-98
Error:	305	1.02	3	8
k_{-2}	-7550	12.49	63	-94
Error:	547	1.835	5	15

C.2.2 Imidazole

Wavelength: 320 nm

Reaction Rates:

	k_2 (s ⁻¹)	Error	k_{-2} (s ⁻¹)	Error	K
15 °C	0.695	0.002			
20 °C	1.00	0.004			
25 °C	1.42	0.01	*	*	*
30 °C	1.98	0.03			
35 °C	2.65	0.03			

Eyring Plot:

	Slope:	y-intercept:	ΔH (kJ mol ⁻¹)	ΔS (J K ⁻¹ mol ⁻¹)
K_2	-5671	13.66	47	-84
Error:	81	0.27	1	2
k_{-2}	*	*	*	*
Error:				

C.2.3 1,2,4-Triazole

Wavelength: 341 nm

Reaction Rates:

	k_2 (s ⁻¹)	Error	k_{-2} (s ⁻¹)	Error	K
15 °C	0.345	0.020	9.00x10 ⁻⁵	5.51x10 ⁻⁵	3.83x10 ³
20 °C	0.508	0.014	1.33x10 ⁻⁴	3.7x10 ⁻⁵	3.82x10 ³
25 °C	0.846	0.034	3.64x10 ⁻⁴	9.2x10 ⁻⁵	2.33x10 ³
30 °C	1.26	0.03	4.17x10 ⁻⁴	2.20x10 ⁻⁴	3.01x10 ³
35 °C	1.63	0.02	5.99x10 ⁻⁴	1.06x10 ⁻⁴	2.73x10 ³

Eyring Plot:

	Slope:	y-intercept:	ΔH (kJ mol ⁻¹)	ΔS (J K ⁻¹ mol ⁻¹)
K_2	-6842	17.03	57	-56
Error:	362	1.22	3	10
k_2	-8420	14.29	70	-79
Error:	1239	4.16	10	35

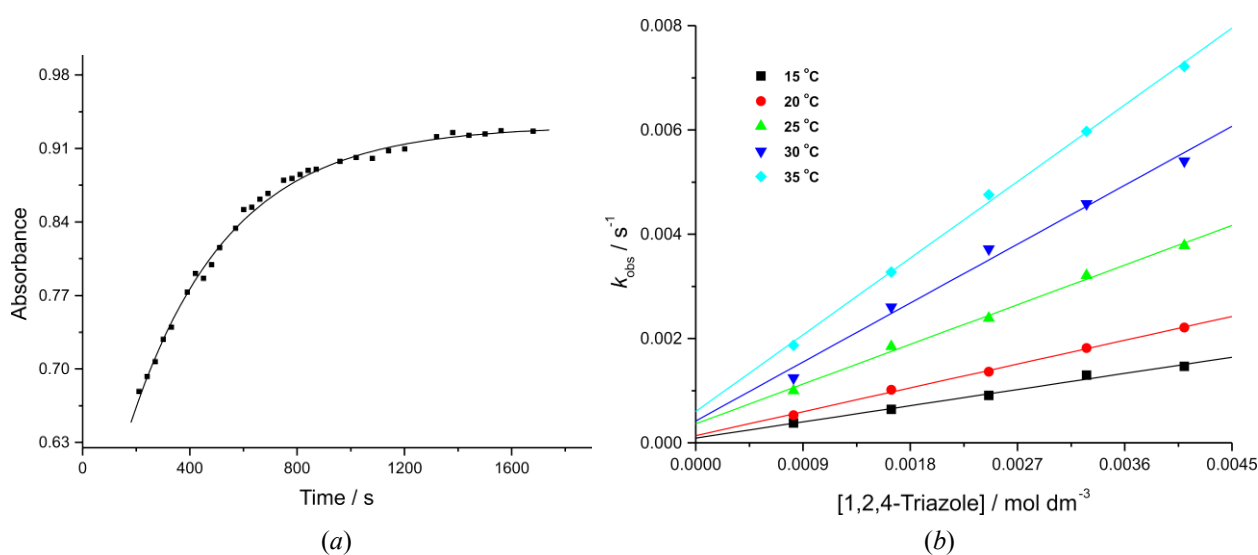


Figure C.5: (a) Kinetic Trace (341 nm) of **PtL2** (8.20×10^{-5} M) and **Trz** (2.46×10^{-4} M) at an ionic strength of 0.1 M (90 mM NaClO₄ and 10 mM NaCl) at 25 °C. (b) Plot to determine rate constants from the slopes and y-intercepts for **PtL2** and **Trz** at varying temperatures.

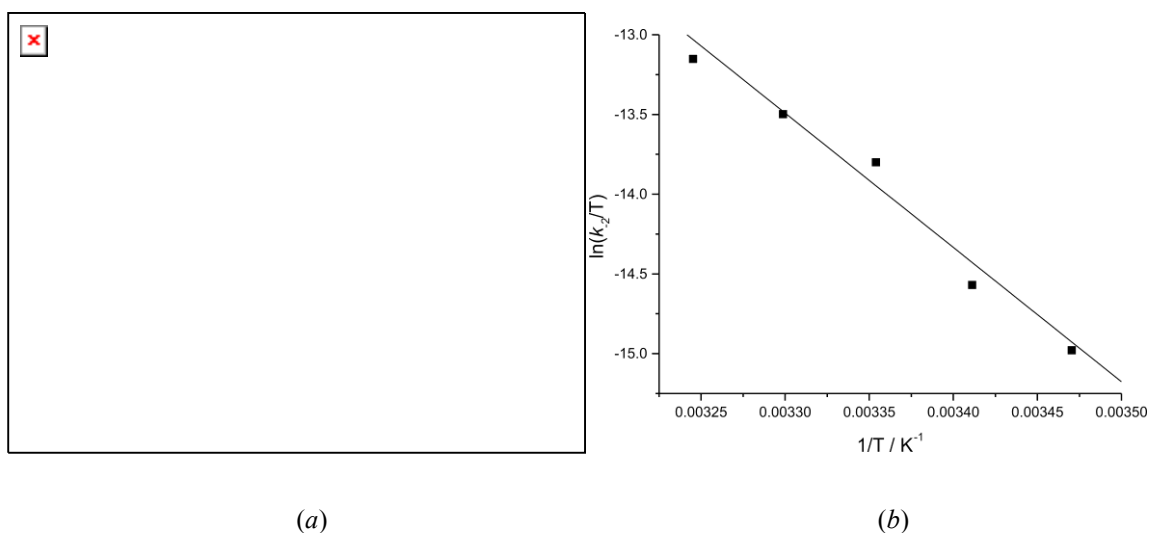


Figure C.6: Eyring plot for **PtL2** and **Trz** to determine ΔH^\ddagger and ΔS^\ddagger for the (a) forward reaction and (b) reverse reaction.

C.2.4 1-Methylimidazole

Wavelength: 339 nm

Reaction Rates:

	k_2 (s ⁻¹)	Error	k_{-2} (s ⁻¹)	Error	K
15°C	0.819	0.005			
20°C	1.16	0.01			
25°C	1.61	0.02	*	*	*
30°C	2.18	0.03			
35°C	2.94	0.04			

Eyring Plot:

	Slope:	y-intercept:	ΔH (kJ mol ⁻¹)	ΔS (J K ⁻¹ mol ⁻¹)
k_2	-5393	12.86	45	-91
Error:	56	0.19	0.5	2
k_{-2}	*	*	*	*
Error:	*	*	*	*

* No reverse reaction observed

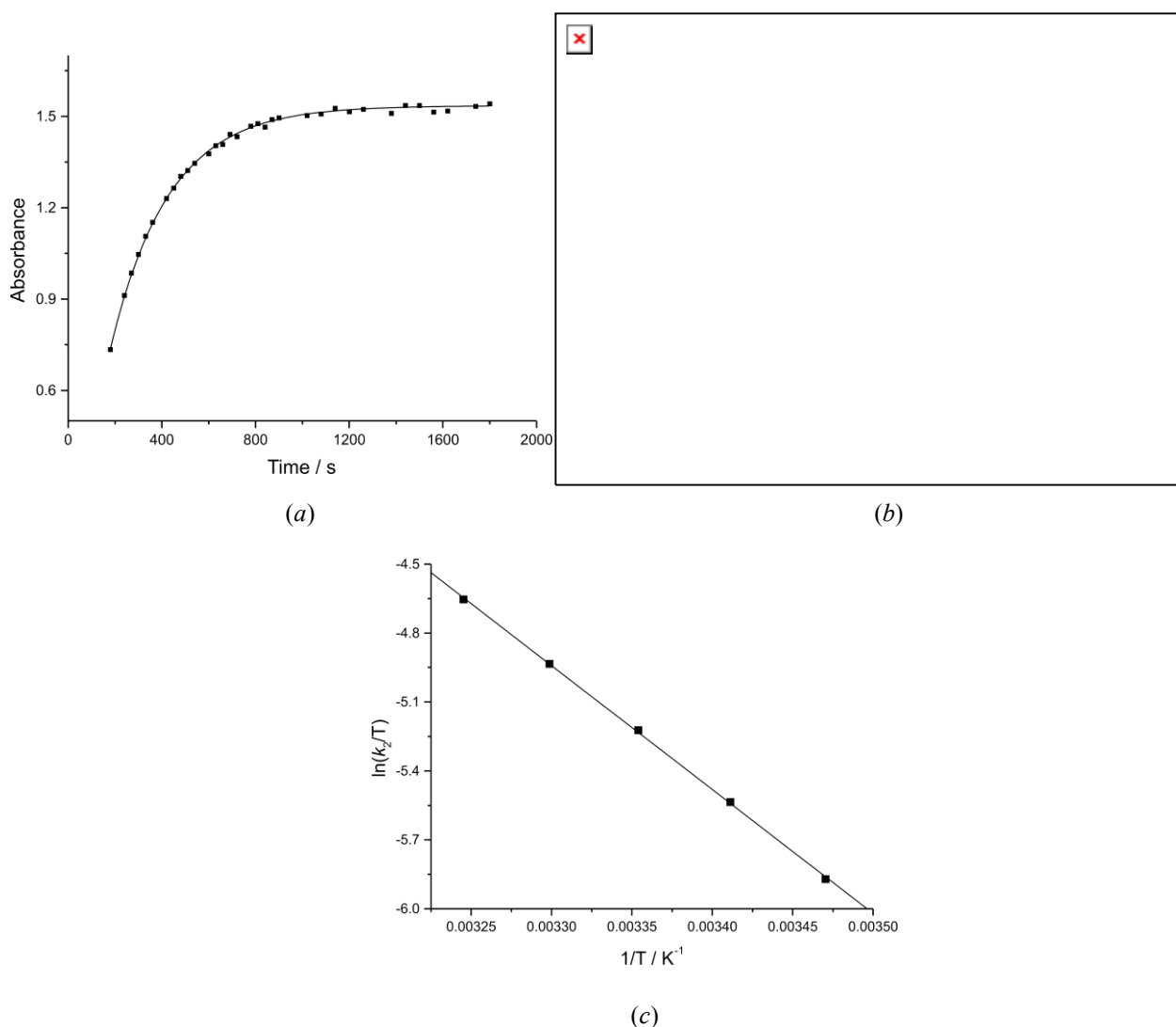


Figure C.7: (a) Kinetic Trace (339 nm) of **PtL2** (8.20×10^{-5} M) and **MIm** (2.46×10^{-4} M) at an ionic strength of 0.1 M (90 mM NaClO_4 and 10 mM NaCl) at 25 °C. (b) Plot to determine rate constants from the slopes and y-intercepts for **PtL2** and **MIm** at varying temperatures. (c) Eyring plot to determine ΔH^\ddagger and ΔS^\ddagger for the forward reaction.

C.2.5 1,2-Dimethylimidazole

Wavelength: 340 nm

Reaction Rates:

	k_2 (s^{-1})	Error	k_2 (s^{-1})	Error	K
15°C	0.306				
20°C	0.439				
25°C	0.624	0.001	*	*	*
30°C	0.854				
35°C	1.19				

Eyring Plot:

	Slope:	y-intercept:	ΔH (kJ mol ⁻¹)	ΔS (J K ⁻¹ mol ⁻¹)
k_2	-5700	12.94	47	-90.31
Error:	45	0.15	0.4	1
k_{-2}	*	*	*	*
Error:				

C.3 Kinetic and Thermodynamic Data for PtL3

C.3.1 Pyrazole

Wavelength: 283 nm

Reaction Rates:

	k_2 (s ⁻¹)	Error	k_{-2} (s ⁻¹)	Error	K
15 °C					
20 °C	1.61	0.07	5.90x10 ⁻⁴	5.8x10 ⁻⁵	2.72x10 ³
25 °C	2.39	0.13	1.02x10 ⁻³	1.0x10 ⁻⁴	2.34x10 ³
30 °C	3.28	0.06	1.70x10 ⁻³	5x10 ⁻⁵	1.93x10 ³
35 °C	4.16	0.16	3.46x10 ⁻³	1.3x10 ⁻⁴	1.20x10 ³

Eyring Plot:

	Slope:	y-intercept:	ΔH (kJ mol ⁻¹)	ΔS (J K ⁻¹ mol ⁻¹)
k_2	-5451	13.42	45	-86
Error:	392	1.30	3	11
k_{-2}	-10195	21.62	85	-18
Error:	650	2.16	5	18

C.3.2 Imidazole

Wavelength: 283 nm

Reaction Rates:

	k_2 (s ⁻¹)	Error	k_{-2} (s ⁻¹)	Error	K
15 °C	1.73	0.05	2.31x10 ⁻⁴	3.7x10 ⁻⁵	7.49x10 ³
20 °C	2.55	0.04	3.61x10 ⁻⁴	2.9x10 ⁻⁵	7.07x10 ³
25 °C	3.59	0.09	6.39x10 ⁻⁴	7.0x10 ⁻⁵	5.62x10 ³
30 °C	4.72	0.06	1.13x10 ⁻³	5x10 ⁻⁵	4.17x10 ³
35 °C	5.93	0.12	2.04x10 ⁻³	1.0x10 ⁻⁴	2.91x10 ³

Eyring Plot:

	Slope:	y-intercept:	ΔH (kJ mol ⁻¹)	ΔS (J K ⁻¹ mol ⁻¹)
k_2	-5177	12.90	43	-91
Error:	277	0.93	2	8
k_{-2}	-9450	18.69	79	-42
Error:	19	1.28	3	11

C.3.3 1,2,4-Triazole

Wavelength: 283 nm

Reaction Rates:

	k_2 (s ⁻¹)	Error	k_{-2} (s ⁻¹)	Error	K
15 °C	0.505	0.024	1.40x10 ⁻⁵	1.91x10 ⁻⁵	3.61x10 ⁴
20 °C	0.663	0.021	5.44x10 ⁻⁵	1.69x10 ⁻⁵	1.22x10 ⁴
25 °C	0.851	0.043	9.73x10 ⁻⁵	3.50x10 ⁻⁵	8.75x10 ³
30 °C	1.20	0.07	1.41x10 ⁻⁴	5.2x10 ⁻⁵	8.50x10 ³
35 °C	1.61	0.06	2.41x10 ⁻⁴	5.1x10 ⁻⁵	6.67x10 ³

Eyring Plot:

	Slope:	y-intercept:	ΔH (kJ mol ⁻¹)	ΔS (J K ⁻¹ mol ⁻¹)
k_2	-4863	10.50	40	-111
Error:	203	0.68	2	6
k_{-2}	-8046	12.02	67	-98
Error:	418	1.39	3	12

C.3.4 1-Methylimidazole

Wavelength: 283 nm

Reaction Rates:

	k_2 (s ⁻¹)	Error	k_{-2} (s ⁻¹)	Error	K
15 °C	1.51	0.08	2.97x10 ⁻⁴	6.2x10 ⁻⁵	5.10x10 ³
20 °C	2.20	0.03	4.52x10 ⁻⁴	2.2x10 ⁻⁵	4.88x10 ³
25 °C	3.26	0.10	8.01x10 ⁻⁴	7.9x10 ⁻⁵	4.07x10 ³
30 °C	4.26	0.10	1.52x10 ⁻³	8x10 ⁻⁵	2.80x10 ³
35 °C	6.01	0.12	2.49x10 ⁻³	9x10 ⁻⁵	2.41x10 ³

Eyring Plot:

	Slope:	y-intercept:	ΔH (kJ mol ⁻¹)	ΔS (J K ⁻¹ mol ⁻¹)
k_2	-5774	14.81	48	-75
Error:	173	0.58	1	5
k_{-2}	-9405	18.78	78	-42
Error:	429	1.44	4	12

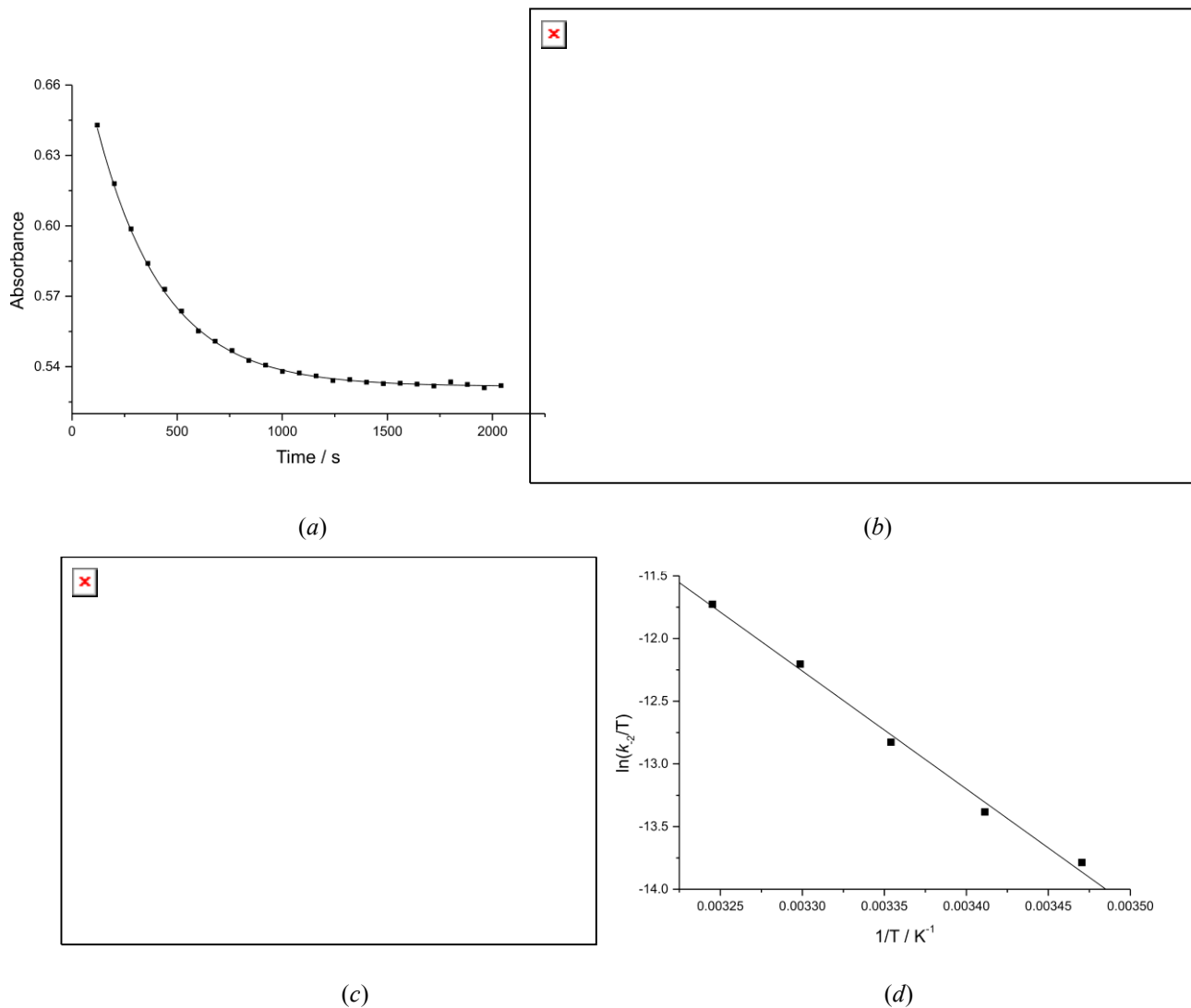


Figure C.8: (a) Kinetic Trace (283 nm) of **PtL3** (2.43×10^{-5} M) and **MIm** (7.28×10^{-4} M) at an ionic strength of 0.1 M (90 mM LiCF₃SO₃ and 10 mM NaCl) at 25 °C. (b) Plot to determine rate constants from the slopes and y-intercepts for **PtL3** and **MIm** at varying temperatures. Eyring plot to determine ΔH^\ddagger and ΔS^\ddagger for the (c) forward reaction and (d) reverse reaction.

C.3.5 1,2-Dimethylimidazole

Wavelength: 283 nm

Reaction Rates:

	k_2 (s ⁻¹)	Error	k_{-2} (s ⁻¹)	Error	K
15 °C	0.452	0.041	2.39x10 ⁻⁵	3.28x10 ⁻⁵	1.89x10 ⁴
20 °C	0.609	0.029	5.28x10 ⁻⁵	2.34x10 ⁻⁵	1.15x10 ⁴
25 °C	1.04	0.03	1.04x10 ⁻⁴	2.2x10 ⁻⁵	1.00x10 ⁴
30 °C	1.40	0.03	2.05x10 ⁻⁴	2.7x10 ⁻⁵	6.83x10 ³
35 °C	1.87	0.01	2.75x10 ⁻⁴	1.1x10 ⁻⁵	6.80x10 ³
40 °C	2.61	0.02	4.62x10 ⁻⁴	2.0x10 ⁻⁵	5.64x10 ³

Eyring Plot:

	Slope:	y-intercept:	ΔH (kJ mol ⁻¹)	ΔS (J K ⁻¹ mol ⁻¹)
k_2	-6058	14.57	50	-77
Error:	289	0.96	2	8
k_{-2}	-10180	19.17	85	-39
Error:	656	2.17	5	18

C.4 Kinetic and Thermodynamic Data for PtL4

C.4.1 Pyrazole

Wavelength: 285 nm

Reaction Rates:

	k_2 (s ⁻¹)	Error	k_{-2} (s ⁻¹)	Error	K
15 °C	1.35	0.08	5.57x10 ⁻⁴	6.1x10 ⁻⁵	2.41x10 ³
20 °C	2.15	0.05	7.67x10 ⁻⁴	4.2x10 ⁻⁵	2.80x10 ³
25 °C	2.71	0.16	1.01x10 ⁻³	1.3x10 ⁻⁴	2.69x10 ³
30 °C	4.53	0.19	1.34x10 ⁻³	1.5x10 ⁻⁴	3.38x10 ³
35 °C	5.63	0.33	1.58x10 ⁻³	2.6x10 ⁻⁴	3.56x10 ³

Eyring Plot:

	Slope:	y-intercept:	ΔH (kJ mol ⁻¹)	ΔS (J K ⁻¹ mol ⁻¹)
k_2	-6109	15.86	51	-66
Error:	442	1.48	4	12
k_{-2}	-4402	2.15	37	-180
Error:	233	0.78	2	7

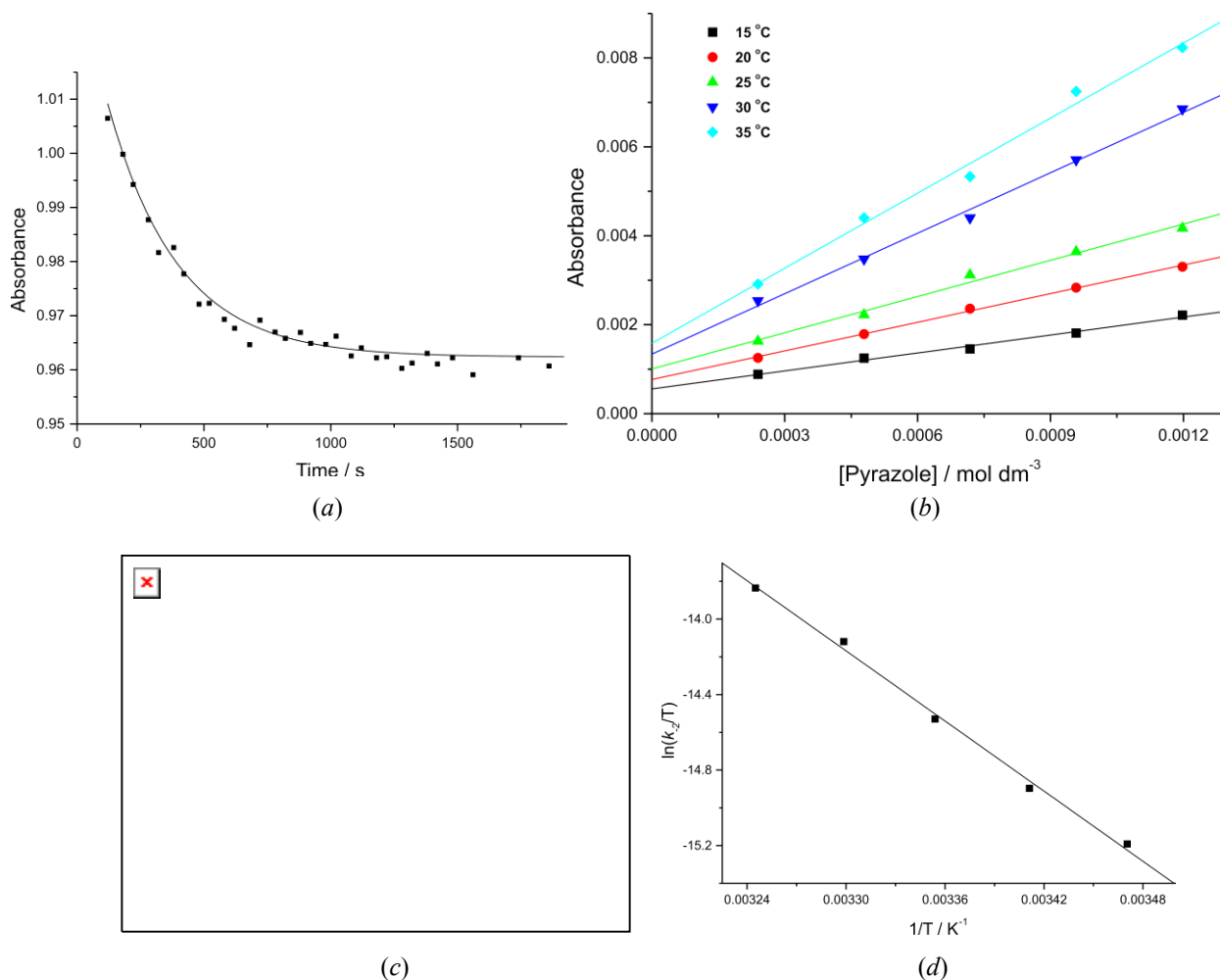


Figure C.9: (a) Kinetic Trace (285 nm) of **PtL4** (2.39×10^{-5} M) and **Pyz** (7.17×10^{-4} M) at an ionic strength of 0.1 M (90 mM LiCF₃SO₃ and 10 mM NaCl) at 25 °C. (b) Plot to determine rate constants from the slopes and y-intercepts for **PtL4** and **Pyz** at varying temperatures. Eyring plot to determine ΔH^\ddagger and ΔS^\ddagger for the (c) forward reaction and (d) reverse reaction.

C.4.2 Imidazole

Wavelength: 285 nm

Reaction Rates:

	k_2 (s ⁻¹)	Error	k_{-2} (s ⁻¹)	Error	K
15°C	2.71	0.06	3.97×10^{-4}	4.8×10^{-5}	6.84×10^3
20°C	3.82	0.07	6.85×10^{-4}	5.2×10^{-5}	5.58×10^3
25°C	4.97	0.11	1.32×10^{-3}	9×10^{-5}	3.77×10^3
30°C	6.86	0.08	2.18×10^{-3}	7×10^{-5}	3.15×10^3
35°C	8.74	0.44	3.54×10^{-3}	3.5×10^{-4}	2.47×10^3

Eyring Plot:

	Slope:	y-intercept:	ΔH (kJ mol ⁻¹)	ΔS (J K ⁻¹ mol ⁻¹)
k_2	-4901	12.36	41	-95
Error:	128	0.43	1	4
k_{-2}	-9540	19.61	7	-35
Error:	241	0.81	2	7

C.4.3 1,2,4-Triazole

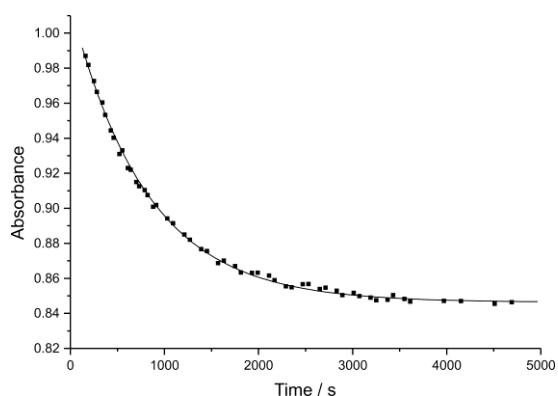
Wavelength: 285 nm

Reaction Rates:

	k_2 (s ⁻¹)	Error	k_{-2} (s ⁻¹)	Error	K
15 °C	0.657	0.029	7.28×10^{-5}	2.31×10^{-5}	9.03×10^3
20 °C	0.983	0.047	9.95×10^{-5}	3.73×10^{-5}	9.88×10^3
25 °C	1.44	0.027	1.46×10^{-4}	2.1×10^{-5}	9.88×10^3
30 °C	2.17	0.07	2.24×10^{-4}	5.5×10^{-5}	9.70×10^3
35 °C	2.80	0.01	3.02×10^{-4}	1.1×10^{-5}	9.26×10^3

Eyring Plot:

	Slope:	y-intercept:	ΔH (kJ mol ⁻¹)	ΔS (J K ⁻¹ mol ⁻¹)
k_2	-6262	15.66	52	-68
Error:	236	0.79	2	7
k_{-2}	-6195	6.28	52	-146
Error:	220	0.77	2	6



(a)



(b)

Figure C.10: (a) Kinetic Trace (285 nm) of **PtL4** (2.39×10^{-5} M) and **Trz** (7.17×10^{-4} M) at an ionic strength of 0.1 M (90 mM LiCF₃SO₃ and 10 mM NaCl) at 25 °C. (b) Plot to determine rate constants from the slopes and y-intercepts for **PtL4** and **Trz** at varying temperatures.

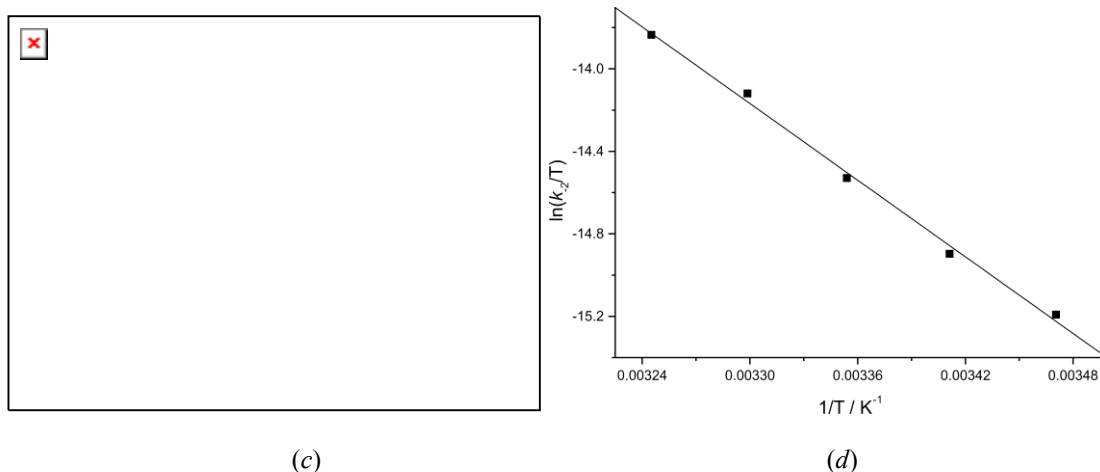


Figure C.11: Eyring plot for **PtL4** and **Trz** to determine ΔH^\ddagger and ΔS^\ddagger for the (a) forward reaction and (b) reverse reaction.

C.4.4 1-Methylimidazole

Wavelength: 285 nm

Reaction Rates:

	k_2 (s ⁻¹)	Error	k_{-2} (s ⁻¹)	Error	K
15 °C	2.85	0.12	4.19x10 ⁻⁴	9.4x10 ⁻⁵	6.80x10 ³
20 °C	4.46	0.27	7.74x10 ⁻⁴	2.17x10 ⁻⁴	5.76x10 ³
25 °C	6.20	0.29	1.43x10 ⁻⁴	2.29x10 ⁻⁴	4.33x10 ³
30 °C	8.09	0.25	2.67x10 ⁻³	2.0x10 ⁻⁴	3.03x10 ³
35 °C	11.4	0.7	3.96x10 ⁻³	5.8x10 ⁻⁴	2.88x10 ³

Eyring Plot:

	Slope:	y-intercept:	ΔH (kJ mol ⁻¹)	ΔS (J K ⁻¹ mol ⁻¹)
k_2	-5684	15.16	47	-72
Error:	262	0.88	2	7
k_{-2}	-9886	20.89	82	-24
Error:	363	1.22	3	10

C.4.5 1,2-Dimethylimidazole

Wavelength: 285 nm

Reaction Rates:

	k_2 (s ⁻¹)	Error	k_{-2} (s ⁻¹)	Error	K
15 °C	0.780	0.063	7.28×10^{-5}	4.97×10^{-5}	1.07×10^4
20 °C	1.30	0.053	1.29×10^{-4}	4.2×10^{-5}	1.01×10^4
25 °C	1.80	0.07	2.26×10^{-4}	5.2×10^{-5}	7.96×10^3
30 °C	2.45	0.09	4.08×10^{-4}	7.0×10^{-5}	6.00×10^3
35 °C	3.19	0.09	7.12×10^{-4}	6.8×10^{-5}	4.48×10^3

Eyring Plot:

	Slope:	y-intercept:	ΔH (kJ mol ⁻¹)	ΔS (J K ⁻¹ mol ⁻¹)
k_2	-5153	12.16	43	-97
Error:	141	0.47	1	4
k_{-2}	-9671	18.39	80	-23
Error:	257	0.86	2	7

C.5 Kinetic and Thermodynamic Data for PtL5

C.5.1 Pyrazole

Wavelength: 328 nm

Reaction Rates:

	k_2 (s ⁻¹)	Error	k_{-2} (s ⁻¹)	Error	K
15°C	0.118				
20°C	0.193				
25°C	0.236	0.006	*	*	*
30°C	0.396				
35°C	0.566				

Eyring Plot:

	Slope:	y-intercept:	ΔH (kJ mol ⁻¹)	ΔS (J K ⁻¹ mol ⁻¹)
k_2	-6554	14.97	55	-73
Error:	305	1.023	3	9
k_{-2}	*	*	*	*
Error:				

C.5.2 Imidazole

Wavelength: 328 nm

Reaction Rates:

	k_2 (s ⁻¹)	Error	k_{-2} (s ⁻¹)	Error	K
15°C	0.126				
20°C	0.179				
25°C	0.248	0.002	*	*	*
30°C	0.349				
35°C	0.481				

Eyring Plot:

	Slope:	y-intercept:	ΔH (kJ mol ⁻¹)	ΔS (J K ⁻¹ mol ⁻¹)
k_2	-5639	11.83	47	-100
Error:	40	0.13	0.3	1
k_{-2}	*	*	*	*
Error:				

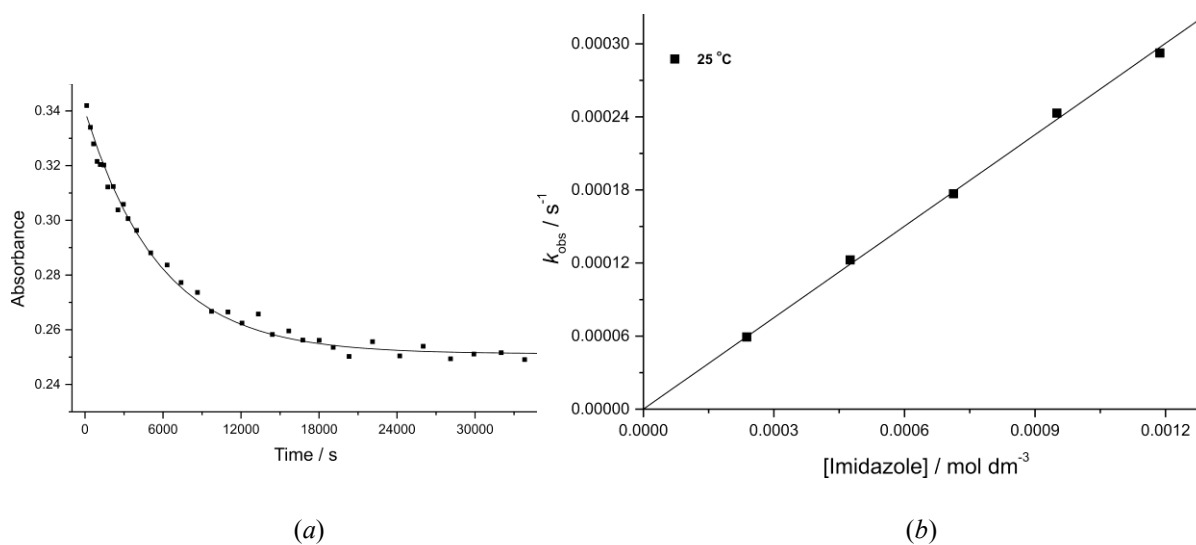


Figure C.12: (a) Kinetic Trace (328 nm) of **PtL5** (3.38×10^{-5} M) and **Im** (1.01×10^{-3} M) at an ionic strength of 0.1 M (90 mM NaClO₄ and 10 mM NaCl) at 25 °C. (b) Plot to determine rate constants from the slopes and y-intercepts for **PtL5** and **Im** at varying temperatures



Figure C.13: Eyring plot for **PtL5** and **Im** to determine ΔH^\ddagger and ΔS^\ddagger for the forward reaction.

C.5.3 1,2,4-Triazole

Wavelength: 328 nm

Reaction Rates:

	k_2 (s ⁻¹)	Error	k_{-2} (s ⁻¹)	Error	K
15 °C	0.135				
20 °C	0.194				
25 °C	0.262	0.004	*	*	*
30 °C	0.402				
35 °C	0.556				

Eyring Plot:

	Slope:	y-intercept:	ΔH (kJ mol ⁻¹)	ΔS (J K ⁻¹ mol ⁻¹)
k_2	-6023	13.22	50	-88
Error:	201	0.68	2	6
k_{-2}	*	*	*	*
Error:				

C.5.4 1-Methylimidazole

Wavelength: 329 nm

Reaction Rates:

	k_2 (s ⁻¹)	Error	k_{-2} (s ⁻¹)	Error	K
15°C	0.123				
20°C	0.180				
25°C	0.257	0.002	*	*	*
30°C	0.354				
35°C	0.463				

Eyring Plot:

	Slope:	y-intercept:	ΔH (kJ mol ⁻¹)	ΔS (J K ⁻¹ mol ⁻¹)
k_2	-5616	11.75	47	-100
Error:	166	0.56	1	5
k_{-2}	*	*	*	*
Error:				

C.5.5 1,2-Dimethylimidazole

Wavelength: 328 nm

Reaction Rates:

	k_2 (s ⁻¹)	Error	k_{-2} (s ⁻¹)	Error	K
15 °C	0.073				
20 °C	0.108				
25 °C	0.161	0.003	*	*	*
30 °C	0.201				
35 °C	0.280				

Eyring Plot:

	Slope:	y-intercept:	ΔH (kJ mol ⁻¹)	ΔS (J K ⁻¹ mol ⁻¹)
K_2	-5592	11.16	47	-105
Error:	286	0.96	2	8
k_{-2}	*	*	*	*
Error:				

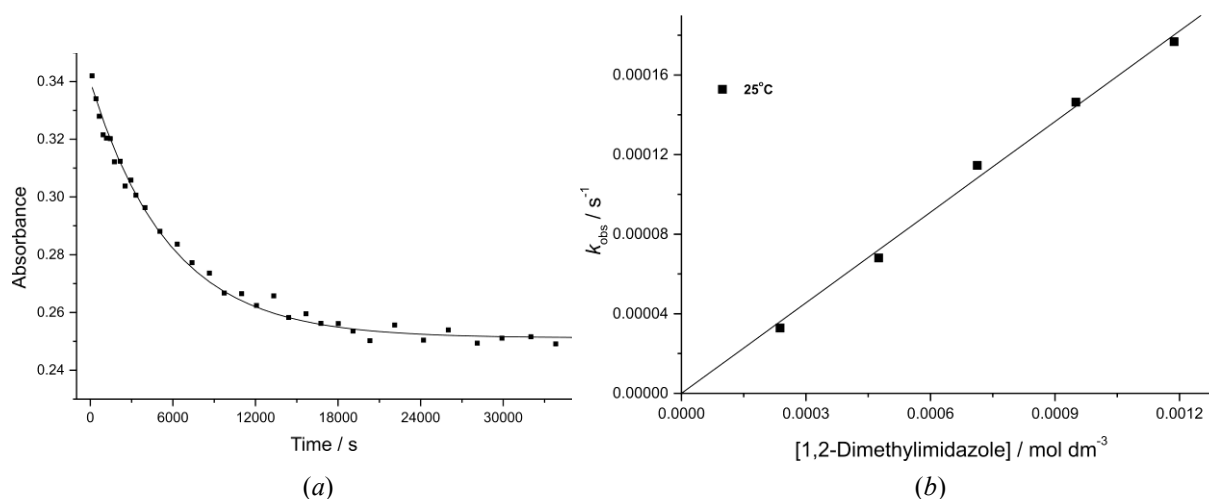


Figure C.14: (a) Kinetic Trace (328 nm) of **PtL5** (3.38×10^{-5} M) and **DIm** (1.01×10^{-3} M) at an ionic strength of 0.1 M (90 mM NaClO₄ and 10 mM NaCl) at 25 °C. (b) Plot to determine rate constants from the slopes and y-intercepts for **PtL5** and **DIm** at varying temperatures



Figure C.15: Eyring plot for **PtL5** and **DIm** to determine ΔH^\ddagger and ΔS^\ddagger for the forward reaction.

C.6 Kinetic and Thermodynamic Data for PtL6

C.6.1 Pyrazole

Wavelength: 286 nm

Reaction Rates:

	k_2 (s ⁻¹)	Error	k_{-2} (s ⁻¹)	Error	K
15 °C	3.80	0.24	4.21x10 ⁻⁴	9.7x10 ⁻⁵	9.03x10 ³
20 °C	4.70	0.28	8.92x10 ⁻⁴	1.09x10 ⁻⁴	5.27x10 ³
25 °C	6.09	0.48	1.20x10 ⁻³	1.9x10 ⁻⁴	5.11x10 ³
30 °C	7.44	0.75	2.08x10 ⁻³	3.0x10 ⁻⁴	3.58x10 ³
35 °C					

Eyring Plot:

	Slope:	y-intercept:	ΔH (kJ mol ⁻¹)	ΔS (J K ⁻¹ mol ⁻¹)
K_2	-3655	8.36	30	-128
Error:	89	0.30	1	3
k_{-2}	-8597	16.47	71	-61
Error:	1005	3.40	8	28

C.6.2 Imidazole

Wavelength: 286 nm

Reaction Rates:

	k_2 (s ⁻¹)	Error	k_{-2} (s ⁻¹)	Error	K
15 °C	5.35	0.32	1.01x10 ⁻³	1.3x10 ⁻⁴	5.30x10 ³
20 °C	8.18	0.53	1.48x10 ⁻³	2.1x10 ⁻⁴	5.53x10 ³
25 °C	11.1	0.4	2.53x10 ⁻³	1.4x10 ⁻⁴	4.39x10 ³
30 °C	15.8	1.1	4.58x10 ⁻³	4.4x10 ⁻⁴	3.45x10 ³
35 °C	21.3	1.3	8.23x10 ⁻³	4.9x10 ⁻⁴	2.59x10 ³

Eyring Plot:

	Slope:	y-intercept:	ΔH (kJ mol ⁻¹)	ΔS (J K ⁻¹ mol ⁻¹)
K_2	-5790	16.14	48	-64
Error:	163	0.55	1	5
k_2	-9143	19.07	76	-39
Error:	537	1.80	4	15

C.6.3 1,2,4-Triazole

Wavelength: 286 nm

Reaction Rates:

	k_2 (s ⁻¹)	Error	k_2 (s ⁻¹)	Error	K
15 °C	0.847	0.032	2.17x10 ⁻⁴	1.3x10 ⁻⁵	3.91x10 ³
20 °C	1.32	0.04	3.08x10 ⁻⁴	1.4x10 ⁻⁵	4.28x10 ³
25 °C	1.70	0.10	3.91x10 ⁻⁴	3.7x10 ⁻⁵	4.35x10 ³
30 °C	2.47	0.15	5.40x10 ⁻⁴	6.0x10 ⁻⁵	4.58x10 ³
35 °C	3.03	0.21	8.58x10 ⁻⁴	8.1x10 ⁻⁵	3.53x10 ³

Eyring Plot:

	Slope:	y-intercept:	ΔH (kJ mol ⁻¹)	ΔS (J K ⁻¹ mol ⁻¹)
k_2	-5353	12.80	45	-91
Error:	337	1.13	3	9
k_2	-5576	5.22	46	-154
Error:	426	1.43	4	12

C.6.4 1-Methylimidazole

Wavelength: 286 nm

Reaction Rates:

	k_2 (s ⁻¹)	Error	k_2 (s ⁻¹)	Error	K
15 °C	6.27	0.51	1.27x10 ⁻³	2.0x10 ⁻⁴	4.94x10 ³
20 °C	8.61	0.45	2.33x10 ⁻³	1.8x10 ⁻⁴	3.69x10 ³
25 °C	12.9	0.8	3.60x10 ⁻³	3.1x10 ⁻⁴	3.57x10 ³
30 °C	16.7	1.0	6.34x10 ⁻³	3.9x10 ⁻⁴	2.64x10 ³
35 °C	22.2	0.6	1.19x10 ⁻²	2.3x10 ⁻⁴	1.87x10 ³

Eyring Plot:

	Slope:	y-intercept:	ΔH (kJ mol ⁻¹)	ΔS (J K ⁻¹ mol ⁻¹)
k_2	-5380	14.85	45	-74
Error:	199	0.67	2	6
k_{-2}	-9391	20.25	78	-30
Error:	1387	1.30	3	11

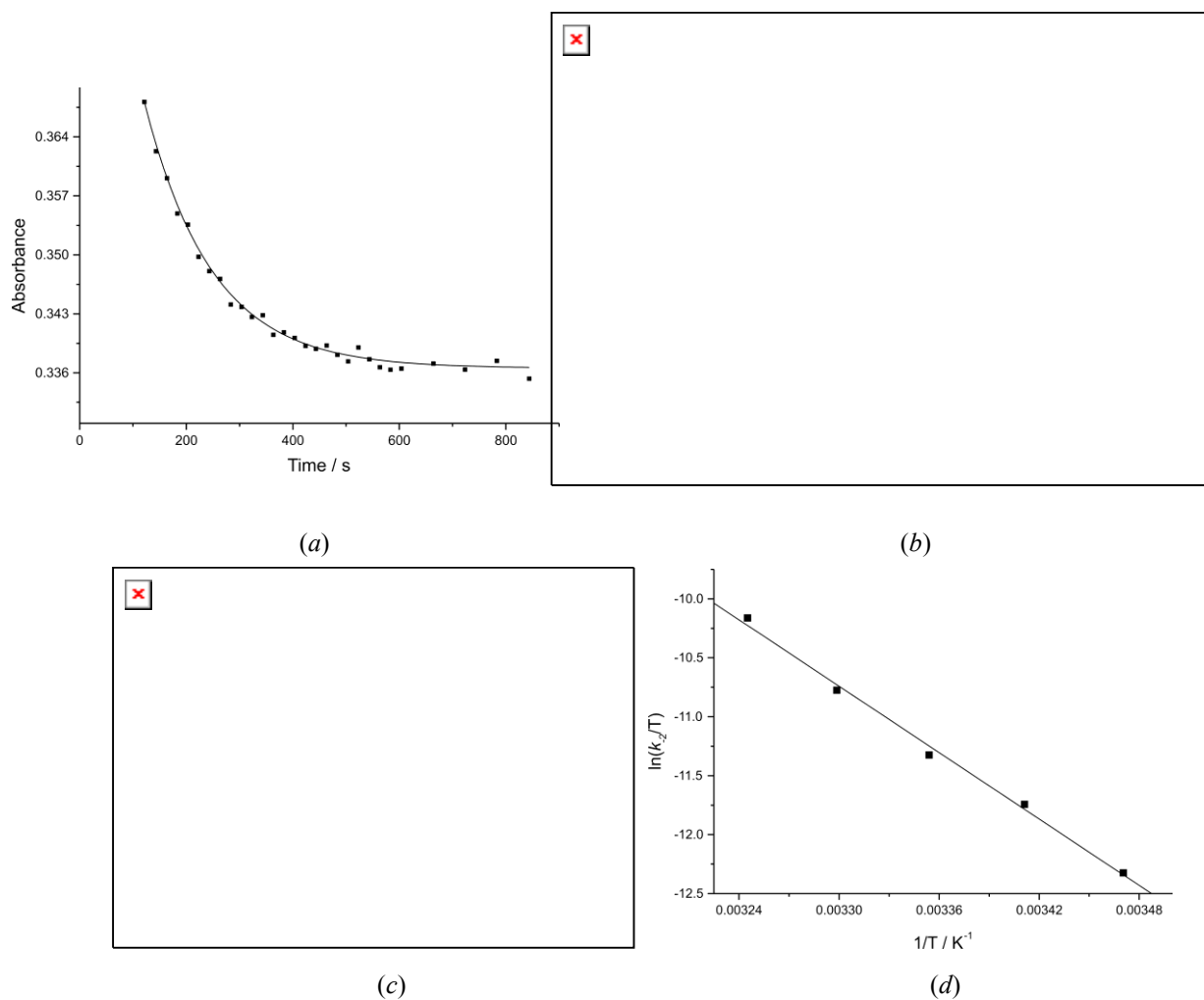


Figure C.16: (a) Kinetic Trace (286 nm) of **PtL6** (1.19×10^{-5} M) and **MIm** (3.57×10^{-4} M) at an ionic strength of 0.1 M (90 mM LiCF_3SO_3 and 10 mM NaCl) at 25 °C. (b) Plot to determine rate constants from the slopes and y-intercepts for **PtL6** and **MIm** at varying temperatures. Eyring plot to determine ΔH^\ddagger and ΔS^\ddagger for the (c) forward reaction and (d) reverse reaction.

C.6.5 1,2-Dimethylimidazole

Wavelength: 286 nm

Reaction Rates:

	k_2 (s ⁻¹)	Error	k_{-2} (s ⁻¹)	Error	K
15 °C	1.68	0.03	8.47×10^{-5}	1.28×10^{-5}	1.98×10^4
20 °C	2.33	0.04	1.62×10^{-4}	1.7×10^{-5}	1.44×10^4
25 °C	3.15	0.11	3.49×10^{-4}	4.2×10^{-5}	9.02×10^3
30 °C	4.06	0.10	6.36×10^{-4}	3.8×10^{-5}	6.38×10^3
35 °C	5.62	0.15	1.01×10^{-3}	6×10^{-5}	5.56×10^3

Eyring Plot:

	Slope:	y-intercept:	ΔH (kJ mol ⁻¹)	ΔS (J K ⁻¹ mol ⁻¹)
k_2	-4980	12.14	41	-97
Error:	118	0.40	1	3
k_{-2}	-10945	22.97	91	-7
Error:	448	1.51	4	13

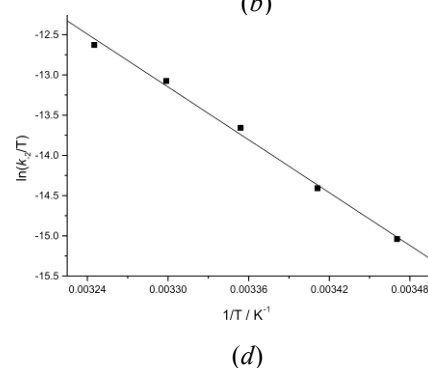
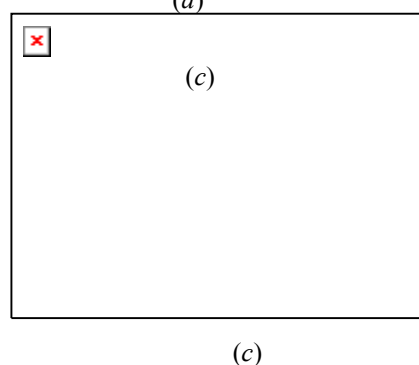
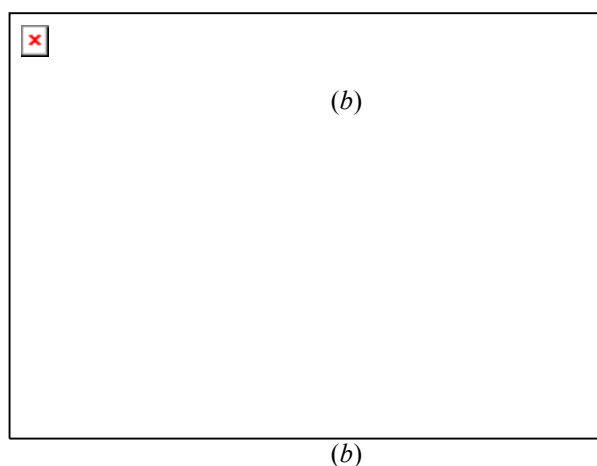
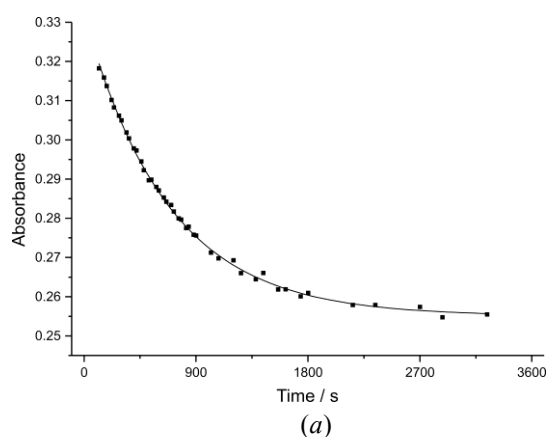
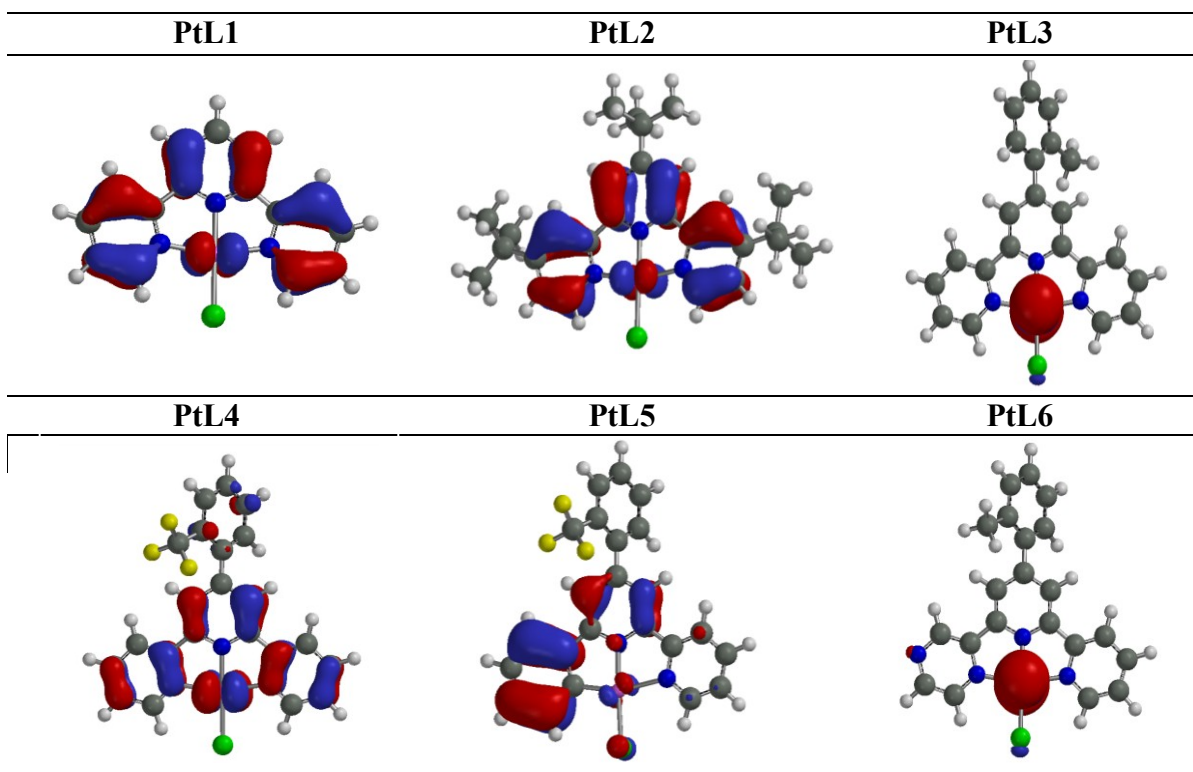


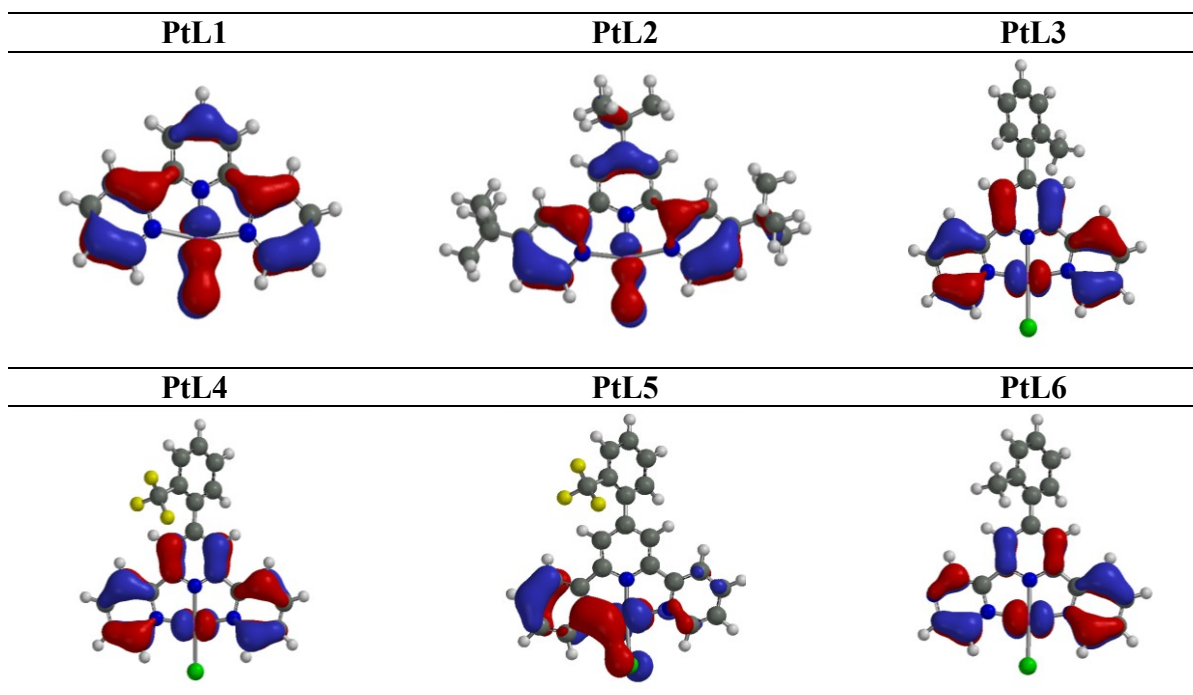
Figure C.17: (a) Kinetic Trace (286 nm) of **PtL6** (1.19×10^{-5} M) and **DIm** (3.57×10^{-4} M) at an ionic strength of 0.1 M (90 mM LiCF₃SO₃ and 10 mM NaCl) at 25 °C. (b) Plot to determine rate constants from the slopes and y-intercepts for **PtL6** and **DIm** at varying temperatures. Eyring plot to determine ΔH^\ddagger and ΔS^\ddagger for the (c) forward reaction and (d) reverse reaction.

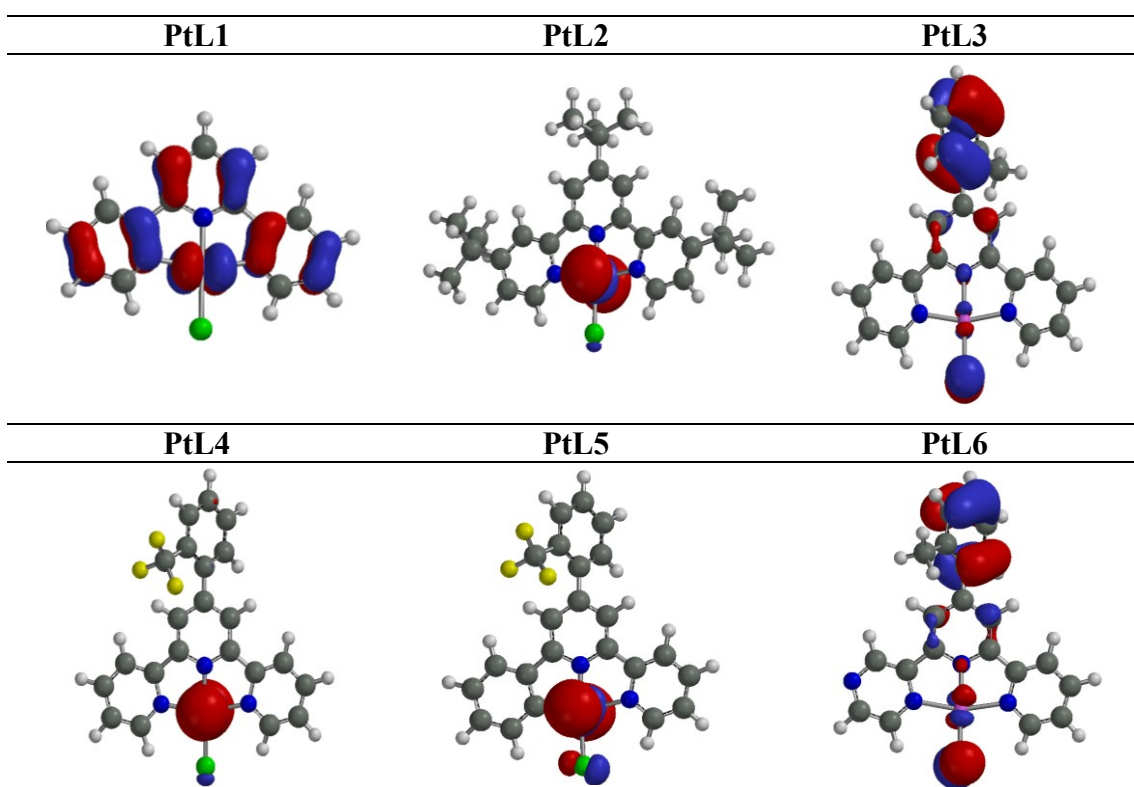
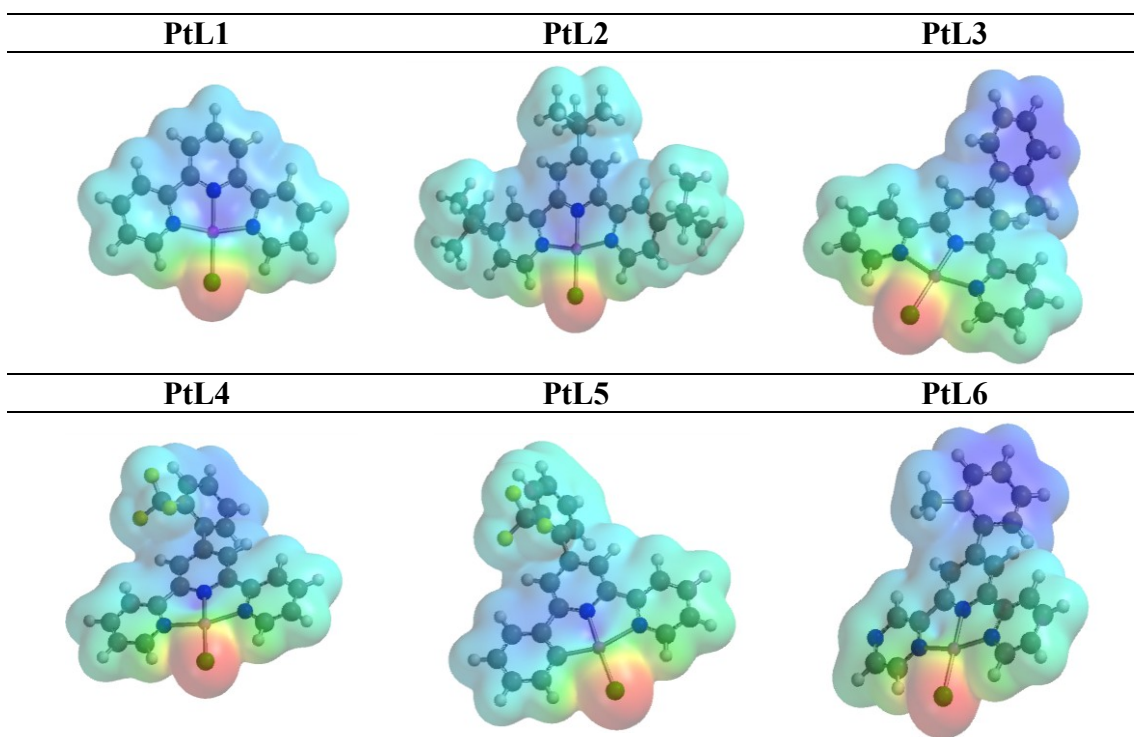
APPENDIX D

D.1 LUMO Plots



D.2 HOMO-1 Plots

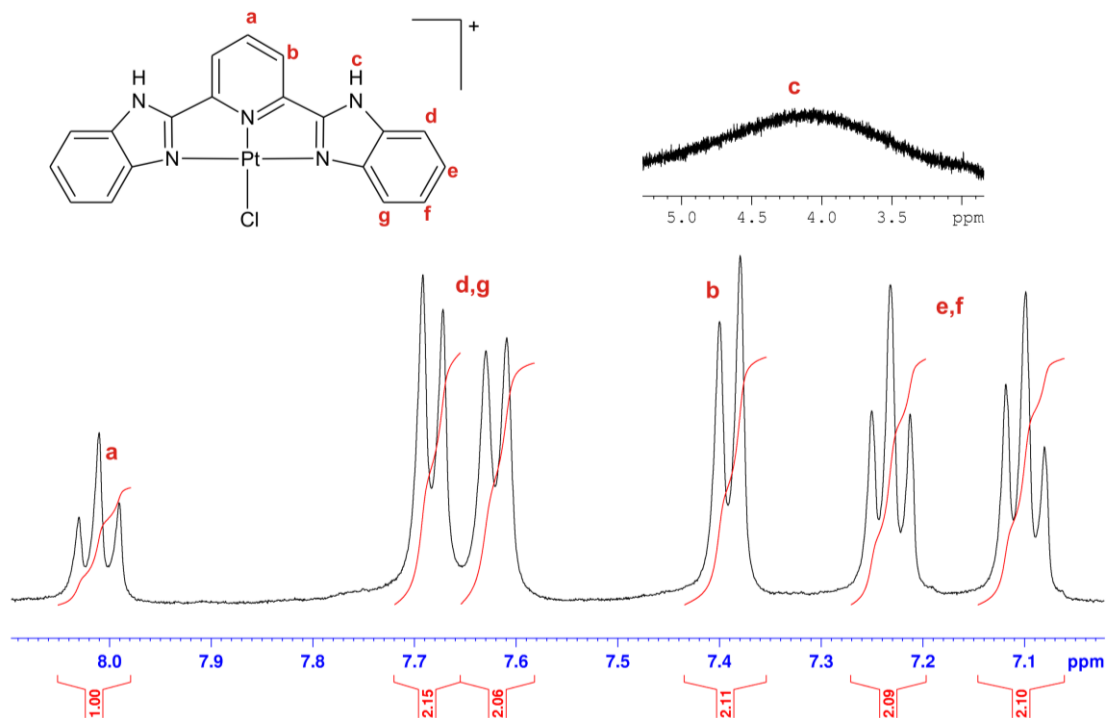


D.3 LUMO+1 Plots**D.4 Density Plots**

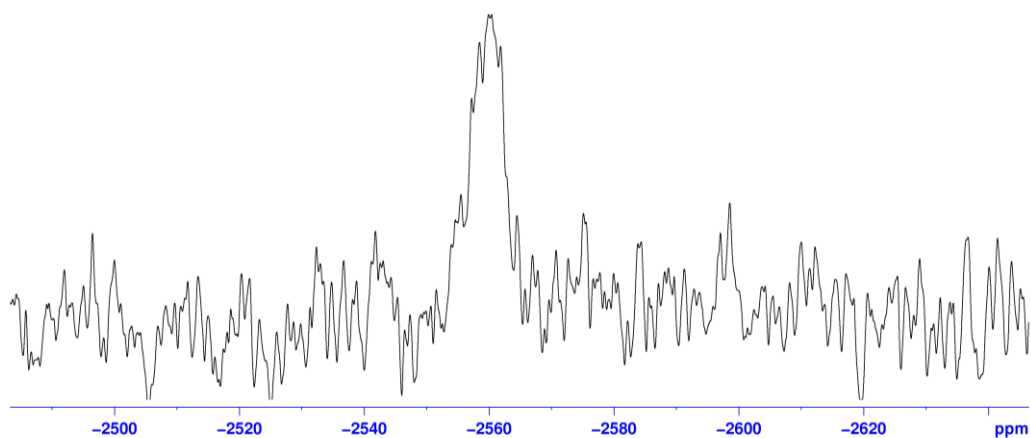
APPENDIX E

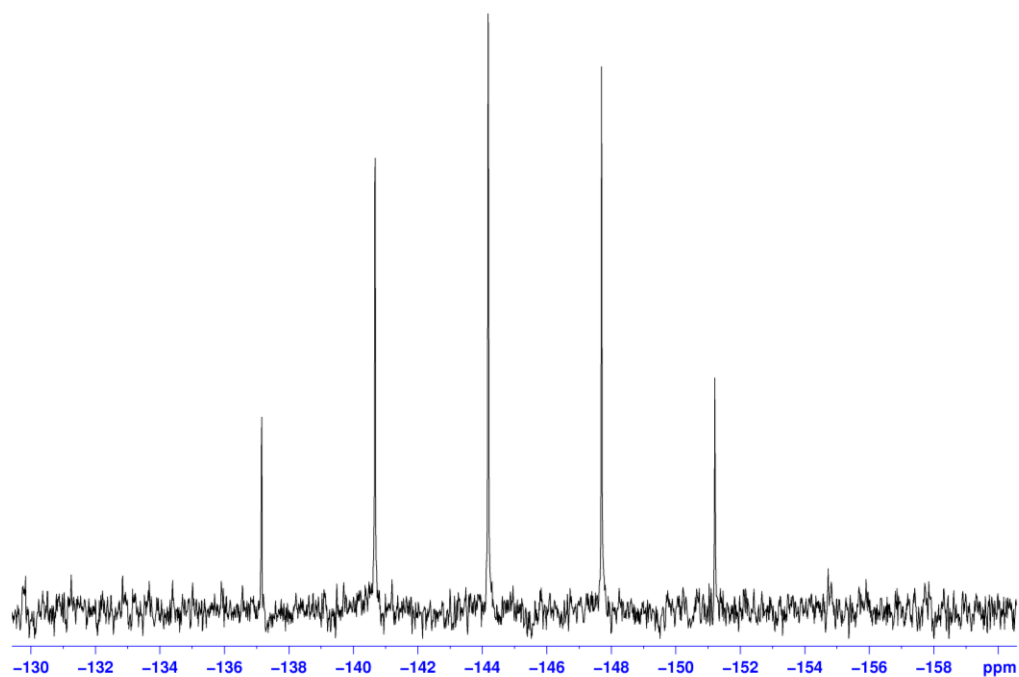
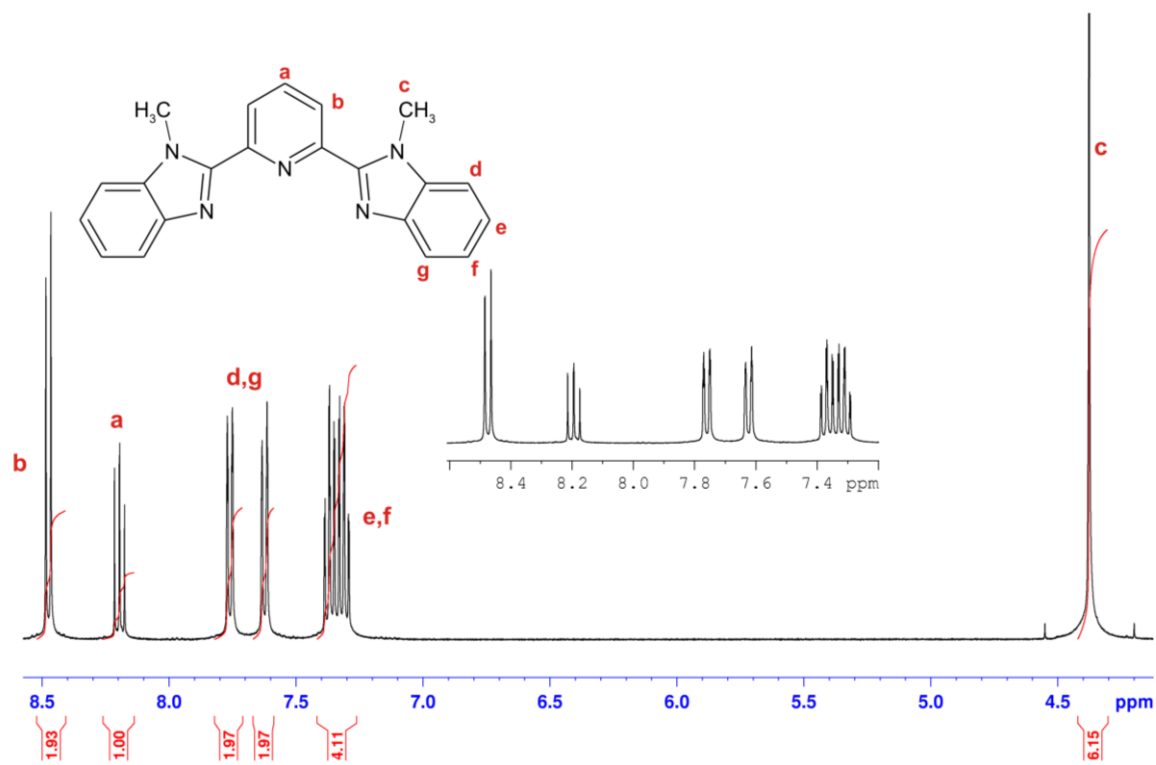
E.1 NMR Spectra

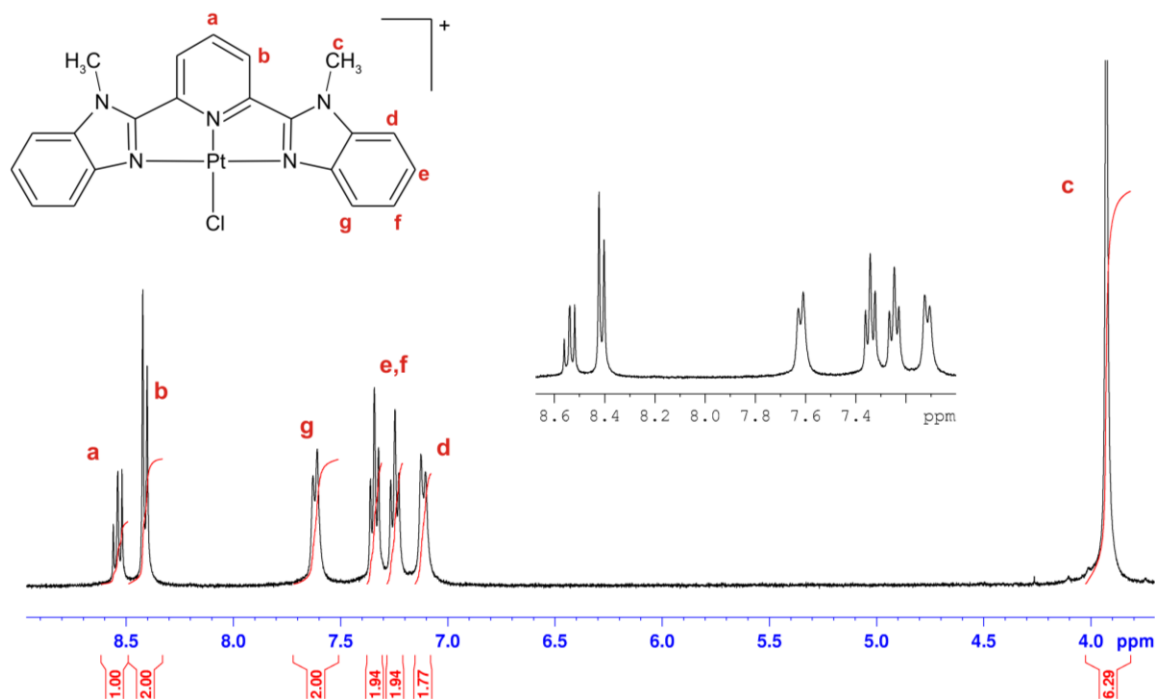
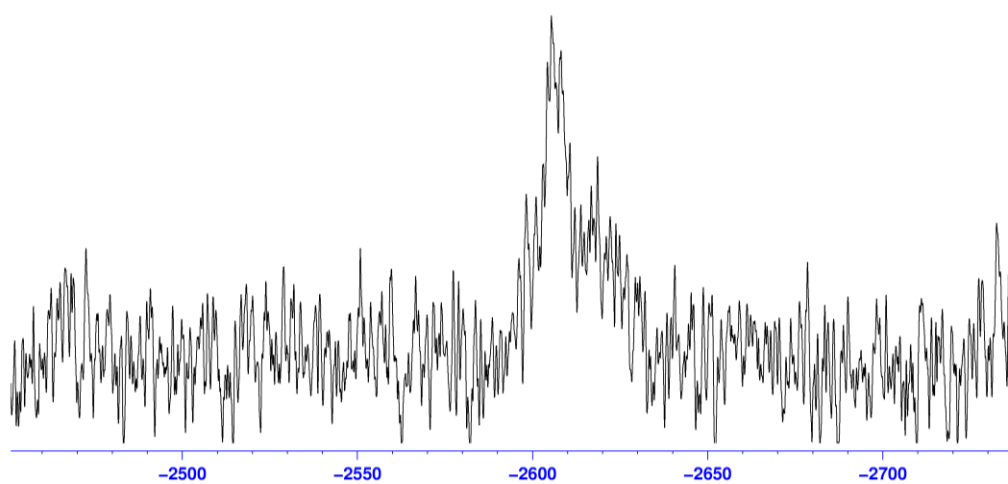
E.1.1 ^1H NMR Spectrum of Ptbzimpy



E.1.2 ^{195}Pt NMR spectrum of Ptbzimpy



E.1.3 ^{31}P NMR spectrum of Ptbzimpy**E.1.4 ^1H NMR spectrum of Me_2bzimpy** 

E.1.5 ^1H NMR spectrum of $\text{PtMe}_2\text{bzimpy}$ **E.1.6 ^{195}Pt NMR spectrum of $\text{PtMe}_2\text{bzimpy}$** 

E.2 Mass Spectra

E.1.2 Mass spectrum of Ptbzimpy

Single Mass Analysis

Tolerance = 10.0 PPM / DBE: min = -1.5, max = 50.0

Element prediction: Off

Number of isotope peaks used for i-FIT = 3

Monoisotopic Mass, Odd and Even Electron Ions

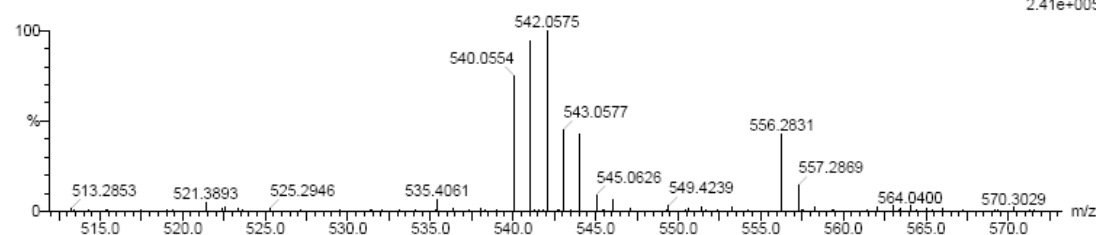
26 formula(e) evaluated with 1 results within limits (all results (up to 1000) for each mass)

Elements Used:

C: 0-50 H: 0-50 N: 0-5 Cl: 1-1 Pt: 1-1

Kate Gillham
ptbzimpy 14 (0.221) Cm (1:59)

TOF MS ES+
2.41e+005



Minimum:

Maximum:

Mass	Calc. Mass	mDa	PPM	DBE	i-FIT	i-FIT (Norm)	Formula
542.0575	542.0586	-1.1	-2.0	16.0	512.9	0.0	C19 H14 N5 Cl Pt

E.2.2 Mass spectrum of PtMe₂bzimpy

Single Mass Analysis

Tolerance = 5.0 PPM / DBE: min = -1.5, max = 50.0

Element prediction: Off

Number of isotope peaks used for i-FIT = 3

Monoisotopic Mass, Even Electron Ions

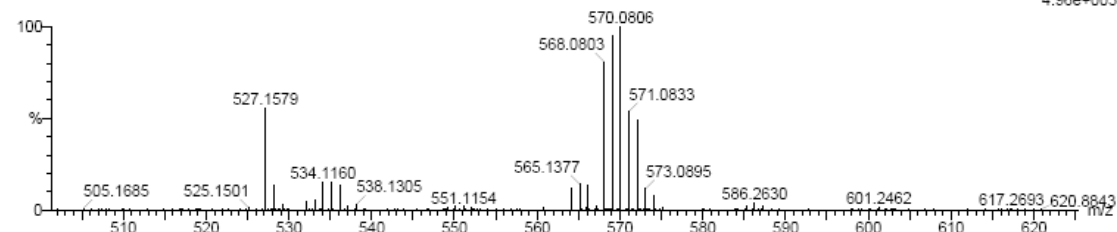
26 formula(e) evaluated with 1 results within limits (all results (up to 1000) for each mass)

Elements Used:

C: 0-25 H: 0-20 N: 0-10 Cl: 1-1 Pt: 0-1

Kate Gillham
Ptmbzimpy 7 (0.103)

TOF MS ES+
4.96e+003



Minimum:

Maximum:

Mass	Calc. Mass	mDa	PPM	DBE	i-FIT	i-FIT (Norm)	Formula
569.0818	569.0820	-0.2	-0.4	16.5	125.3	0.0	C21 H17 N5 Cl Pt

APPENDIX F:

F.1 X-ray Tables for PtL1-MIm

Table F.1.1: Bond lengths of **PtL1-MIm**

Bond:	Length (Å):	Bond:	Length (Å):
C(1)-N(1)	1.353(10)	C(16)-N(5)	1.307(8)
C(1)-C(2)	1.382(11)	C(16)-N(4)	1.356(8)
C(1S)-N(1S)	1.434(13)	C(17)-C(18)	1.359(11)
C(2)-C(3)	1.366(13)	C(17)-N(5)	1.363(10)
C(3)-C(4)	1.372(13)	C(18)-N(4)	1.357(9)
C(4)-C(5)	1.356(10)	C(19)-N(5)	1.452(8)
C(5)-N(1)	1.365(9)	N(1)-Pt	2.025(6)
C(5)-C(6)	1.485(13)	N(1S)-O(1S)	1.168(9)
C(6)-C(7)	1.345(11)	N(1S)-O(2S)	1.192(11)
C(6)-N(2)	1.372(9)	N(2)-Pt	1.925(5)
C(7)-C(8)	1.367(13)	N(3)-Pt	2.021(6)
C(8)-C(9)	1.374(11)	N(4)-Pt	2.013(6)
C(9)-C(10)	1.400(10)	O(1)-Cl(1)	1.234(16)
C(10)-N(2)	1.330(9)	O(2)-Cl(1)	1.327(11)
C(10)-C(11)	1.489(10)	O(3)-Cl(1)	1.343(12)
C(11)-C(12)	1.369(11)	O(4)-Cl(1)	1.359(14)
C(11)-N(3)	1.372(9)	O(5)-Cl(2)	1.413(7)
C(12)-C(13)	1.351(12)	O(6)-Cl(2)	1.450(8)
C(13)-C(14)	1.366(12)	O(7)-Cl(2)	1.415(8)
C(14)-C(15)	1.368(11)	O(8)-Cl(2)	1.393(7)
C(15)-N(3)	1.349(9)		

Table F.1.2: Bond angles of **PtL1-MIm**

Bond:	Angle (deg):	Bond:	Angle (deg):
N(1)-C(1)-C(2)	119.5(8)	O(2S)-N(1S)-C(1S)	117.9(9)
C(3)-C(2)-C(1)	122.0(9)	C(10)-N(2)-C(6)	122.9(6)
C(2)-C(3)-C(4)	117.0(8)	C(10)-N(2)-Pt	119.1(5)
C(5)-C(4)-C(3)	121.5(8)	C(6)-N(2)-Pt	117.9(5)
C(4)-C(5)-N(1)	120.8(8)	C(15)-N(3)-C(11)	117.9(7)
C(4)-C(5)-C(6)	124.4(7)	C(15)-N(3)-Pt	128.5(5)

Bond:	Angle (deg):	Bond:	Angle (deg):
N(1)-C(5)-C(6)	114.8(6)	C(11)-N(3)-Pt	113.6(5)
C(7)-C(6)-N(2)	118.1(8)	C(16)-N(4)-C(18)	106.5(6)
C(7)-C(6)-C(5)	129.6(7)	C(16)-N(4)-Pt	126.5(4)
N(2)-C(6)-C(5)	112.3(6)	C(18)-N(4)-Pt	127.0(5)
C(6)-C(7)-C(8)	120.4(8)	C(16)-N(5)-C(17)	109.4(6)
C(7)-C(8)-C(9)	121.9(8)	C(16)-N(5)-C(19)	125.4(7)
C(8)-C(9)-C(10)	116.8(8)	C(17)-N(5)-C(19)	125.1(7)
N(2)-C(10)-C(9)	119.9(7)	O(1)-Cl(1)-O(2)	118.1(12)
N(2)-C(10)-C(11)	112.8(6)	O(1)-Cl(1)-O(3)	108.6(15)
C(9)-C(10)-C(11)	127.3(7)	O(2)-Cl(1)-O(3)	112.9(11)
C(12)-C(11)-N(3)	121.0(7)	O(1)-Cl(1)-O(4)	106.3(19)
C(12)-C(11)-C(10)	125.3(7)	O(2)-Cl(1)-O(4)	103.3(9)
N(3)-C(11)-C(10)	113.7(6)	O(3)-Cl(1)-O(4)	106.7(10)
C(13)-C(12)-C(11)	119.7(8)	O(8)-Cl(2)-O(5)	112.5(6)
C(12)-C(13)-C(14)	120.4(8)	O(8)-Cl(2)-O(7)	113.6(5)
C(13)-C(14)-C(15)	118.7(8)	O(5)-Cl(2)-O(7)	112.7(5)
N(3)-C(15)-C(14)	122.3(8)	O(8)-Cl(2)-O(6)	104.8(5)
N(5)-C(16)-N(4)	109.3(6)	O(5)-Cl(2)-O(6)	105.8(5)
C(18)-C(17)-N(5)	106.0(7)	O(7)-Cl(2)-O(6)	106.6(6)
N(4)-C(18)-C(17)	108.8(7)	N(2)-Pt-N(4)	178.5(2)
C(1)-N(1)-C(5)	119.3(6)	N(2)-Pt-N(3)	80.7(3)
C(1)-N(1)-Pt	127.3(5)	N(4)-Pt-N(3)	100.6(2)
C(5)-N(1)-Pt	113.4(5)	N(2)-Pt-N(1)	81.5(3)
O(1S)-N(1S)-O(2S)	123.1(10)	N(4)-Pt-N(1)	97.2(2)
O(1S)-N(1S)-C(1S)	118.9(10)	N(3)-Pt-N(1)	162.2(2)

Table F.1.3: Atomic coordinates ($\times 10^4$) and equivalent isotropic displacement parameters ($\text{\AA}^2 \times 10^3$) for **PtL1-MIm**. $U(\text{eq})$ is defined as one third of the trace of the orthogonalized U^{ij} tensor.

	x	y	z	U(eq)
C(1)	6697(5)	4867(7)	10042(6)	59(2)
C(1S)	9475(7)	921(12)	10904(9)	118(4)
C(2)	6293(6)	5379(8)	10631(6)	69(2)
C(3)	5873(5)	4746(9)	11124(6)	71(3)
C(4)	5882(5)	3568(9)	11025(6)	63(2)

	x	y	z	U(eq)
C(5)	6272(4)	3058(7)	10446(5)	45(2)
C(6)	6301(4)	1792(8)	10298(5)	48(2)
C(7)	5995(5)	928(9)	10705(6)	60(2)
C(8)	6121(5)	-197(8)	10502(6)	61(2)
C(9)	6548(5)	-487(7)	9871(5)	59(2)
C(10)	6871(4)	424(6)	9465(5)	44(2)
C(11)	7363(4)	341(6)	8776(5)	45(2)
C(12)	7570(5)	-665(7)	8412(6)	62(2)
C(13)	8024(6)	-627(7)	7794(7)	69(2)
C(14)	8241(5)	410(8)	7494(6)	67(2)
C(15)	8030(4)	1402(7)	7870(6)	53(2)
C(16)	8566(4)	4276(6)	8775(5)	43(2)
C(17)	7844(6)	5684(7)	7859(6)	61(2)
C(18)	7266(5)	4945(6)	8026(5)	48(2)
C(19)	9464(5)	5765(8)	8392(7)	80(3)
N(1)	6682(4)	3704(6)	9951(4)	45(1)
N(1S)	8913(5)	1653(8)	11213(6)	72(2)
N(2)	6734(4)	1509(5)	9674(4)	43(1)
N(3)	7591(4)	1392(5)	8502(4)	44(1)
N(4)	7711(4)	4065(5)	8597(4)	40(1)
N(5)	8647(4)	5235(5)	8340(4)	47(1)
O(1)	9410(20)	7727(17)	10390(30)	380(20)
O(1S)	8411(5)	1229(7)	11517(5)	102(2)
O(2)	8371(10)	7867(13)	11015(11)	203(7)
O(2S)	8951(5)	2668(7)	11098(8)	114(3)
O(3)	8708(12)	6230(12)	10429(10)	252(8)
O(4)	9562(13)	7038(14)	11756(10)	261(10)
O(5)	4957(4)	1229(6)	7854(5)	92(2)
O(6)	4009(6)	2158(7)	6530(6)	104(3)
O(7)	3906(7)	2504(6)	8042(7)	96(3)
O(8)	5069(5)	3205(8)	7608(7)	109(3)
Cl(1)	8990(2)	7258(2)	10844(2)	67(1)
Cl(2)	4510(1)	2285(2)	7563(1)	47(1)
Pt	7210(1)	2747(1)	9132(1)	36(1)

Table F.1.4: Anisotropic displacement parameters ($\text{\AA}^2 \times 10^3$) for **PtL1-MIm**. The anisotropic displacement factor exponent takes the form: $-2\pi^2 [h^2 a^{*2} U^{11} + \dots + 2 h k a^* b^* U^{12}]$

	U^{11}	U^{22}	U^{33}	U^{23}	U^{13}	U^{12}
C(1)	69(5)	40(5)	72(5)	-12(4)	30(4)	-7(4)
C(1S)	88(8)	126(12)	134(10)	-5(9)	32(8)	26(8)
C(2)	73(6)	56(6)	76(6)	-22(5)	25(5)	5(5)
C(3)	64(6)	82(7)	72(5)	-20(5)	28(5)	3(5)
C(4)	49(5)	87(8)	59(5)	-6(4)	25(4)	-11(4)
C(5)	30(4)	52(5)	54(4)	3(3)	16(3)	-3(3)
C(6)	32(4)	66(5)	45(4)	6(4)	11(3)	-9(4)
C(7)	43(4)	76(7)	55(4)	9(4)	12(4)	-16(4)
C(8)	50(5)	70(6)	57(5)	14(4)	10(4)	-19(4)
C(9)	59(5)	44(5)	61(5)	4(4)	5(4)	-20(4)
C(10)	34(4)	40(4)	47(4)	2(3)	2(3)	-10(3)
C(11)	35(4)	41(4)	54(4)	4(3)	8(3)	0(3)
C(12)	65(5)	35(4)	79(6)	-9(4)	18(5)	-3(4)
C(13)	66(6)	40(5)	107(7)	-23(5)	37(5)	-5(4)
C(14)	60(5)	63(6)	88(6)	-21(5)	38(5)	-6(4)
C(15)	36(4)	51(5)	74(5)	-11(4)	24(4)	-10(3)
C(16)	44(4)	35(4)	48(4)	4(3)	12(3)	-3(3)
C(17)	81(6)	35(4)	67(5)	5(4)	27(5)	1(4)
C(18)	44(4)	44(4)	51(4)	5(3)	12(3)	9(3)
C(19)	71(6)	68(6)	107(7)	6(5)	38(5)	-32(5)
N(1)	35(3)	50(4)	50(3)	-4(3)	13(3)	6(3)
N(1S)	51(5)	68(6)	82(5)	12(4)	5(4)	-17(4)
N(2)	32(3)	39(4)	57(3)	2(3)	13(3)	-11(2)
N(3)	31(3)	36(3)	65(4)	1(3)	17(3)	-1(2)
N(4)	43(3)	30(3)	46(3)	-1(2)	14(3)	1(3)
N(5)	48(4)	37(3)	58(3)	-6(3)	21(3)	-14(3)
O(1)	440(40)	270(20)	640(50)	160(20)	430(40)	20(20)
O(1S)	83(5)	123(7)	107(5)	26(5)	41(4)	-20(5)
O(2)	140(11)	250(16)	216(15)	-20(11)	57(10)	98(11)
O(2S)	60(5)	95(7)	164(9)	15(6)	11(5)	-6(4)
O(3)	390(20)	153(12)	218(13)	-97(11)	112(14)	-87(13)
O(4)	330(20)	270(18)	130(10)	-18(11)	16(12)	168(17)
O(5)	82(5)	66(4)	123(6)	16(4)	30(4)	30(4)
O(6)	98(6)	116(7)	84(5)	6(4)	13(4)	6(4)
O(7)	125(7)	74(5)	125(7)	1(4)	88(6)	16(4)

	U^{11}	U^{22}	U^{33}	U^{23}	U^{13}	U^{12}
O(8)	95(6)	76(5)	167(7)	-16(5)	57(5)	-38(5)
Cl(1)	81(2)	58(1)	68(1)	0(1)	37(1)	7(1)
Cl(2)	48(1)	37(1)	63(1)	4(1)	26(1)	4(1)
Pt	30(1)	33(1)	44(1)	0(1)	11(1)	-4(1)

Table F.1.5: Hydrogen coordinates ($\times 10^4$) and isotropic displacement parameters ($\text{\AA}^2 \times 10^3$) for **PtL1-MIm**.

	x	y	z	U(eq)
H(1)	6976	5318	9712	71
H(1S1)	9664	286	11351	176
H(1S2)	9972	1356	10896	176
H(1S3)	9167	633	10258	176
H(2)	6308	6179	10693	82
H(3)	5594	5097	11509	86
H(4)	5614	3110	11363	76
H(7)	5695	1096	11128	72
H(8)	5911	-782	10798	73
H(9)	6620	-1253	9721	70
H(12)	7398	-1371	8590	74
H(13)	8190	-1310	7572	83
H(14)	8527	440	7042	80
H(15)	8195	2107	7684	63
H(16)	9022	3812	9149	52
H(17)	7717	6360	7491	73
H(18)	6665	5028	7788	57
H(19A)	9931	5231	8681	121
H(19B)	9556	6450	8786	121
H(19C)	9446	5962	7744	121

Table F.1.6: Torsion angles

Bond:	Angle (deg):	Bond:	Angle (deg):
N(1)-C(1)-C(2)-C(3)	0.3(14)	C(14)-C(15)-N(3)-C(11)	0.8(11)
C(1)-C(2)-C(3)-C(4)	1.2(14)	C(14)-C(15)-N(3)-Pt	-179.5(6)
C(2)-C(3)-C(4)-C(5)	1.5(13)	C(12)-C(11)-N(3)-C(15)	-0.5(10)
C(3)-C(4)-C(5)-N(1)	1.0(12)	C(10)-C(11)-N(3)-C(15)	-179.3(6)
C(3)-C(4)-C(5)-C(6)	179.5(7)	C(12)-C(11)-N(3)-Pt	1.0(7)
C(4)-C(5)-C(6)-C(7)	2.5(12)	C(10)-C(11)-N(3)-Pt	0.1(7)
N(1)-C(5)-C(6)-C(7)	177.0(7)	N(5)-C(16)-N(4)-C(18)	0.0(8)
C(4)-C(5)-C(6)-N(2)	179.8(7)	N(5)-C(16)-N(4)-Pt	177.2(5)
N(1)-C(5)-C(6)-N(2)	0.6(8)	C(17)-C(18)-N(4)-C(16)	177.6(7)
N(2)-C(6)-C(7)-C(8)	0.4(11)	C(17)-C(18)-N(4)-Pt	0.0(9)
C(5)-C(6)-C(7)-C(8)	177.1(7)	N(4)-C(16)-N(5)-C(17)	-148(9)
C(6)-C(7)-C(8)-C(9)	0.9(12)	N(4)-C(16)-N(5)-C(19)	29(9)
C(7)-C(8)-C(9)-C(10)	1.7(11)	C(18)-C(17)-N(5)-C(16)	2.5(5)
C(8)-C(9)-C(10)-N(2)	1.9(10)	C(18)-C(17)-N(5)-C(19)	-177.0(5)
C(8)-C(9)-C(10)-C(11)	179.2(7)	C(10)-N(2)-Pt-N(4)	0.0(5)
N(2)-C(10)-C(11)-C(12)	177.8(7)	C(6)-N(2)-Pt-N(4)	-91(9)
C(9)-C(10)-C(11)-C(12)	1.1(12)	C(10)-N(2)-Pt-N(3)	119.0(6)
N(2)-C(10)-C(11)-N(3)	0.9(9)	C(6)-N(2)-Pt-N(3)	114.9(5)
C(9)-C(10)-C(11)-N(3)	179.8(6)	C(10)-N(2)-Pt-N(1)	-61.7(6)
N(3)-C(11)-C(12)-C(13)	1.7(12)	C(6)-N(2)-Pt-N(1)	-1.8(4)
C(10)-C(11)-C(12)-C(13)	179.7(7)	C(16)-N(4)-Pt-N(2)	177.4(5)
C(11)-C(12)-C(13)-C(14)	3.2(14)	C(18)-N(4)-Pt-N(2)	-179.9(7)
C(12)-C(13)-C(14)-C(15)	3.4(14)	C(16)-N(4)-Pt-N(3)	-0.2(10)
C(13)-C(14)-C(15)-N(3)	2.2(13)	C(18)-N(4)-Pt-N(3)	179.9(6)
N(5)-C(17)-C(18)-N(4)	0.0(8)	C(16)-N(4)-Pt-N(1)	-0.4(5)
C(2)-C(1)-N(1)-C(5)	0.3(11)	C(18)-N(4)-Pt-N(1)	0.6(7)
C(2)-C(1)-N(1)-Pt	179.4(6)	C(15)-N(3)-Pt-N(2)	-179.7(5)
C(4)-C(5)-N(1)-C(1)	0.0(11)	C(11)-N(3)-Pt-N(2)	178.3(7)
C(6)-C(5)-N(1)-C(1)	179.6(6)	C(15)-N(3)-Pt-N(4)	-2.0(10)
C(4)-C(5)-N(1)-Pt	179.8(6)	C(11)-N(3)-Pt-N(4)	177.4(5)
C(6)-C(5)-N(1)-Pt	0.6(7)	C(15)-N(3)-Pt-N(1)	-179.9(7)
C(9)-C(10)-N(2)-C(6)	1.5(10)	C(11)-N(3)-Pt-N(1)	-0.2(10)
C(11)-C(10)-N(2)-C(6)	179.5(6)	C(1)-N(1)-Pt-N(2)	179.9(6)
C(9)-C(10)-N(2)-Pt	178.4(5)	C(5)-N(1)-Pt-N(2)	-0.4(5)
C(11)-C(10)-N(2)-Pt	2.5(8)	C(1)-N(1)-Pt-N(4)	0.6(7)
C(7)-C(6)-N(2)-C(10)	0.7(10)	C(5)-N(1)-Pt-N(4)	-179.7(5)

Bond:	Angle (deg):	Bond:	Angle (deg):
C(5)-C(6)-N(2)-C(10)	177.2(6)	C(1)-N(1)-Pt-N(3)	178.3(7)
C(7)-C(6)-N(2)-Pt	177.7(5)	C(5)-N(1)-Pt-N(3)	-2.0(10)
C(5)-C(6)-N(2)-Pt	0.3(7)		

Symmetry transformations used to generate equivalent atoms.

F.2 X-ray Tables for PtL1-DIm

Table F.2.1: Bond lengths of PtL1-DIm.

Bond:	Length (Å):	Bond:	Length (Å):
Pt-N(2)	1.993(10)	C(10)-C(9)	1.388(19)
Pt-N(1)	2.011(11)	C(10)-C(11)	1.458(19)
Pt-N(3')	2.041(10)	C(11)-N(3')	1.378(16)
Pt-N(4)	2.058(13)	N(5)-C(16)	1.299(19)
Cl(1)-O(4)	1.324(18)	N(5)-C(18)	1.43(2)
Cl(1)-O(1)	1.339(17)	N(3')-C(15)	1.310(18)
Cl(1)-O(2)	1.37(2)	C(18)-C(17)	1.33(3)
Cl(1)-O(3)	1.37(2)	N(1S)-O(1S)	1.12(4)
Cl(2)-O(5)	1.28(2)	N(1S)-O(2S)	1.15(3)
Cl(2)-O(7)	1.32(2)	N(1S)-C(1S)	1.44(4)
Cl(2)-O(8)	1.408(17)	C(9)-C(8)	1.39(2)
Cl(2)-O(6)	1.43(2)	C(6)-C(7)	1.405(18)
C(12)-C(13)	1.35(2)	C(6)-C(5)	1.439(19)
C(12)-C(11)	1.38(2)	C(13)-C(14)	1.39(2)
N(4)-C(16)	1.266(19)	C(8)-C(7)	1.38(2)
N(4)-C(17)	1.421(18)	C(4)-C(5)	1.37(2)
N(1)-C(1)	1.336(19)	C(4)-C(3)	1.38(3)
N(1)-C(5)	1.389(17)	C(1)-C(2)	1.38(2)
N(2)-C(6)	1.290(16)	C(14)-C(15)	1.39(2)
N(2)-C(10)	1.354(16)	C(3)-C(2)	1.35(3)
C(19)-N(5)	1.415(18)	C(20)-C(16)	1.48(2)

Table F.2.2: Bond angles of **Ptl1-DIm**.

Bond:	Angle (deg):	Bond:	Angle (deg):
N(2)-Pt-N(1)	81.0(4)	N(3')-C(11)-C(10)	115.6(12)
N(2)-Pt-N(3')	81.9(4)	C(12)-C(11)-C(10)	124.2(13)
N(1)-Pt-N(3')	162.9(4)	C(16)-N(5)-C(19)	133.8(16)
N(2)-Pt-N(4)	176.5(5)	C(16)-N(5)-C(18)	105.1(14)
N(1)-Pt-N(4)	98.5(5)	C(19)-N(5)-C(18)	121.1(16)
N(3')-Pt-N(4)	98.5(5)	C(15)-N(3')-C(11)	120.2(12)
O(4)-Cl(1)-O(1)	110.2(17)	C(15)-N(3')-Pt	127.6(10)
O(4)-Cl(1)-O(2)	116.1(12)	C(11)-N(3')-Pt	112.1(9)
O(1)-Cl(1)-O(2)	114.6(12)	C(17)-C(18)-N(5)	107.1(16)
O(4)-Cl(1)-O(3)	102(2)	O(1S)-N(1S)-O(2S)	117(4)
O(1)-Cl(1)-O(3)	103.8(17)	O(1S)-N(1S)-C(1S)	125(4)
O(2)-Cl(1)-O(3)	108.7(13)	O(2S)-N(1S)-C(1S)	118(4)
O(5)-Cl(2)-O(7)	116(2)	C(10)-C(9)-C(8)	118.0(14)
O(5)-Cl(2)-O(8)	111.9(12)	N(2)-C(6)-C(7)	115.5(13)
O(7)-Cl(2)-O(8)	107.0(13)	N(2)-C(6)-C(5)	116.6(12)
O(5)-Cl(2)-O(6)	104.7(16)	C(7)-C(6)-C(5)	127.8(13)
O(7)-Cl(2)-O(6)	101.8(17)	C(12)-C(13)-C(14)	119.0(15)
O(8)-Cl(2)-O(6)	115.4(13)	C(7)-C(8)-C(9)	121.7(13)
C(13)-C(12)-C(11)	119.8(16)	C(18)-C(17)-N(4)	106.4(15)
C(16)-N(4)-C(17)	107.1(14)	C(5)-C(4)-C(3)	120.1(17)
C(16)-N(4)-Pt	130.5(11)	N(1)-C(1)-C(2)	120.4(17)
C(17)-N(4)-Pt	122.1(10)	C(13)-C(14)-C(15)	120.0(14)
C(1)-N(1)-C(5)	119.5(13)	C(8)-C(7)-C(6)	119.0(13)
C(1)-N(1)-Pt	128.5(11)	C(4)-C(5)-N(1)	120.0(14)
C(5)-N(1)-Pt	112.0(9)	C(4)-C(5)-C(6)	125.2(14)
C(6)-N(2)-C(10)	129.8(12)	N(1)-C(5)-C(6)	114.7(12)
C(6)-N(2)-Pt	115.4(8)	C(2)-C(3)-C(4)	118.5(17)
C(10)-N(2)-Pt	114.3(9)	N(3')-C(15)-C(14)	120.6(15)
N(2)-C(10)-C(9)	115.8(12)	C(3)-C(2)-C(1)	121.3(18)
N(2)-C(10)-C(11)	115.9(12)	N(4)-C(16)-N(5)	114.2(15)
C(9)-C(10)-C(11)	128.3(13)	N(4)-C(16)-C(20)	125.1(16)
N(3')-C(11)-C(12)	120.3(13)	N(5)-C(16)-C(20)	120.7(15)

Table F.2.3: Atomic coordinates ($\times 10^4$) and equivalent isotropic displacement parameters ($\text{\AA}^2 \times 10^3$) for **PtL1-DIm**. $U(\text{eq})$ is defined as one third of the trace of the orthogonalized U^{ij} tensor.

	x	y	z	U(eq)
Pt	5093(1)	2127(1)	3794(1)	50(1)
Cl(1)	4854(5)	1871(2)	6327(2)	64(1)
Cl(2)	9186(6)	-213(2)	8635(3)	70(1)
C(12)	9075(19)	3092(8)	5153(9)	63(4)
N(4)	5396(19)	1167(6)	3547(7)	72(4)
N(1)	2684(15)	2247(5)	3266(7)	51(3)
N(2)	4720(14)	3041(5)	4089(6)	40(2)
C(19)	5730(30)	-244(8)	2387(13)	107(7)
C(10)	6038(17)	3301(6)	4563(7)	48(3)
C(11)	7572(18)	2898(6)	4718(8)	51(3)
N(5)	5575(17)	258(6)	2945(8)	70(4)
O(4)	3600(40)	1473(9)	6063(19)	280(20)
O(2)	4760(20)	2483(10)	6021(11)	152(7)
O(3)	6300(40)	1575(12)	6073(16)	228(13)
N(3')	7445(13)	2286(5)	4405(6)	47(3)
C(18)	5470(30)	125(11)	3778(13)	126(10)
O(8)	10940(20)	-382(8)	8805(12)	127(6)
N(1S)	9550(40)	-142(13)	6051(19)	126(8)
C(9)	5750(20)	3915(7)	4846(9)	65(4)
C(6)	3199(18)	3269(6)	3877(9)	53(3)
C(13)	10410(20)	2677(11)	5285(10)	74(5)
C(8)	4150(20)	4201(7)	4631(12)	88(6)
C(17)	5340(20)	686(6)	4146(10)	72(5)
C(4)	430(20)	3030(8)	3065(11)	70(4)
O(1)	5090(40)	1842(11)	7125(10)	199(11)
C(1)	1700(20)	1826(9)	2833(9)	66(4)
C(1S)	9500(40)	521(13)	6281(15)	156(13)
C(14)	10250(20)	2061(8)	4974(10)	64(4)
C(7)	2848(19)	3879(6)	4185(10)	64(4)
O(7)	8260(30)	-598(18)	9060(17)	278(19)
C(5)	2033(18)	2856(7)	3403(9)	55(3)
C(3)	-550(20)	2601(12)	2588(11)	89(6)
C(15)	8722(19)	1877(8)	4544(9)	60(4)
C(2)	80(20)	1999(11)	2504(11)	82(6)
O(6)	8480(30)	-347(10)	7837(12)	184(9)

	x	y	z	U(eq)
C(20)	5640(20)	1202(9)	2108(10)	81(5)
C(16)	5520(20)	881(8)	2889(10)	66(4)
O(5)	8940(30)	389(10)	8730(20)	251(17)
O(2S)	10540(40)	-473(16)	6393(17)	192(11)
O(1S)	8690(40)	-360(20)	5550(20)	330(30)

Table F.2.4: Anisotropic displacement parameters ($\text{\AA}^2 \times 10^3$) for **PtL1-DIm**. The anisotropic displacement factor exponent takes the form: $-2\pi^2 [h^2 a^{*2} U^{11} + \dots + 2 h k a^* b^* U^{12}]$

	U ¹¹	U ²²	U ³³	U ²³	U ¹³	U ¹²
Pt	61(1)	28(1)	60(1)	-7(1)	1(1)	3(1)
Cl(1)	69(2)	44(2)	78(3)	-12(2)	0(2)	5(2)
Cl(2)	72(3)	50(2)	87(3)	-1(2)	16(2)	-11(2)
C(12)	54(9)	58(9)	76(10)	-4(8)	-2(8)	-13(7)
N(4)	119(11)	41(7)	55(7)	4(6)	-7(7)	-11(7)
N(1)	57(7)	36(7)	57(7)	-10(5)	-9(5)	-3(5)
N(2)	55(6)	27(5)	40(5)	-2(4)	13(5)	-5(4)
C(19)	141(18)	43(10)	139(18)	-47(11)	27(14)	-11(10)
C(10)	57(8)	38(7)	51(7)	11(6)	12(6)	-4(6)
C(11)	62(8)	37(7)	56(8)	3(6)	16(6)	-6(6)
N(5)	92(10)	35(7)	85(9)	-11(6)	21(7)	-5(6)
O(4)	280(30)	83(13)	440(40)	92(19)	-260(30)	-73(16)
O(2)	200(20)	83(15)	172(15)	21(12)	26(13)	12(12)
O(3)	300(30)	150(20)	260(30)	39(18)	140(20)	110(20)
N(3')	44(6)	35(6)	60(7)	-3(5)	-1(5)	4(4)
C(18)	210(30)	57(13)	116(18)	29(11)	62(18)	25(14)
O(8)	100(11)	86(12)	198(17)	-16(11)	37(10)	11(9)
N(1S)	120(20)	100(19)	160(20)	-14(16)	20(16)	11(14)
C(9)	73(10)	35(8)	86(11)	-5(7)	9(8)	-20(7)
C(6)	57(8)	21(6)	81(10)	13(6)	1(7)	-5(5)
C(13)	54(9)	102(15)	65(10)	2(9)	-7(7)	-11(9)
C(8)	88(12)	18(7)	160(18)	-22(9)	20(12)	-1(7)
C(17)	138(15)	13(6)	69(9)	9(6)	35(9)	14(7)
C(4)	56(9)	55(10)	99(13)	14(9)	13(9)	6(7)
O(1)	390(40)	123(17)	89(12)	-16(11)	50(16)	-50(20)
C(1)	70(10)	59(10)	72(10)	-4(8)	19(8)	-3(8)
C(1S)	250(40)	80(19)	150(20)	32(16)	70(20)	40(20)
C(14)	57(9)	59(10)	76(10)	9(8)	-8(8)	6(7)

	U^{11}	U^{22}	U^{33}	U^{23}	U^{13}	U^{12}
C(7)	58(8)	28(7)	107(12)	13(7)	15(8)	14(6)
O(7)	130(17)	410(50)	300(30)	200(30)	51(19)	-20(20)
C(5)	51(8)	52(9)	61(8)	19(7)	5(6)	0(7)
C(3)	61(11)	113(17)	89(13)	15(12)	-18(9)	6(11)
C(15)	68(10)	46(8)	65(9)	3(7)	2(7)	6(7)
C(2)	60(10)	118(19)	68(11)	-8(10)	0(8)	-10(10)
O(6)	260(30)	152(19)	134(15)	13(13)	-4(16)	-53(18)
C(20)	88(12)	84(14)	72(11)	8(9)	10(9)	6(10)
C(16)	69(10)	58(10)	69(10)	-11(8)	-4(8)	1(8)
O(5)	166(19)	85(14)	480(40)	-70(20)	-150(20)	38(13)
O(2S)	220(30)	170(30)	190(20)	-10(20)	70(20)	30(20)
O(1S)	160(20)	510(70)	320(40)	-260(50)	-20(30)	10(30)

Table F.2.5: Hydrogen coordinates ($\times 10^4$) and isotropic displacement parameters ($\text{\AA}^2 \times 10^3$) for**PtL1-DIm.**

	x	y	z	U(eq)
H(12)	9166	3508	5355	76
H(19A)	4872	-191	1948	161
H(19B)	5567	-649	2642	161
H(19C)	6871	-231	2194	161
H(18)	5495	-279	4016	151
H(9)	6598	4128	5169	78
H(13)	11427	2802	5579	89
H(8)	3954	4620	4793	106
H(17)	5224	751	4687	86
H(4)	-6	3438	3158	84
H(1)	2121	1414	2753	80
H(1S1)	9081	555	6803	234
H(1S2)	8740	753	5904	234
H(1S3)	10650	699	6291	234
H(14)	11163	1772	5054	77
H(7)	1753	4063	4088	77
H(3)	-1604	2723	2329	107
H(15)	8604	1459	4352	72
H(2)	-608	1695	2220	99
H(20A)	5397	1651	2159	122
H(20B)	4815	1014	1718	122

Table F.2.6: Torsion angles

Bond:	Angle (deg):	Bond:	Angle (deg):
N(2)-Pt-N(4)-C(16)	149(7)	C(11)-C(10)-C(9)-C(8)	-178.3(14)
N(1)-Pt-N(4)-C(16)	67.0(16)	C(10)-N(2)-C(6)-C(7)	0(2)
N(3')-Pt-N(4)-C(16)	-113.2(15)	Pt-N(2)-C(6)-C(7)	171.0(10)
N(2)-Pt-N(4)-C(17)	-24(8)	C(10)-N(2)-C(6)-C(5)	-176.3(12)
N(1)-Pt-N(4)-C(17)	-106.7(13)	Pt-N(2)-C(6)-C(5)	-4.9(15)
N(3')-Pt-N(4)-C(17)	73.2(14)	C(11)-C(12)-C(13)-C(14)	0(2)
N(2)-Pt-N(1)-C(1)	178.4(13)	C(10)-C(9)-C(8)-C(7)	3(3)
N(3')-Pt-N(1)-C(1)	175.4(13)	N(5)-C(18)-C(17)-N(4)	-1(2)
N(4)-Pt-N(1)-C(1)	-5.1(13)	C(16)-N(4)-C(17)-C(18)	1(2)
N(2)-Pt-N(1)-C(5)	-2.4(10)	Pt-N(4)-C(17)-C(18)	176.4(16)
N(3')-Pt-N(1)-C(5)	-5(2)	C(5)-N(1)-C(1)-C(2)	2(2)
N(4)-Pt-N(1)-C(5)	174.1(10)	Pt-N(1)-C(1)-C(2)	-179.0(12)
N(1)-Pt-N(2)-C(6)	4.1(9)	C(12)-C(13)-C(14)-C(15)	-1(2)
N(3')-Pt-N(2)-C(6)	-176.8(10)	C(9)-C(8)-C(7)-C(6)	-6(3)
N(4)-Pt-N(2)-C(6)	-79(8)	N(2)-C(6)-C(7)-C(8)	4(2)
N(1)-Pt-N(2)-C(10)	176.8(9)	C(5)-C(6)-C(7)-C(8)	179.9(15)
N(3')-Pt-N(2)-C(10)	-4.1(8)	C(3)-C(4)-C(5)-N(1)	0(2)
N(4)-Pt-N(2)-C(10)	94(7)	C(3)-C(4)-C(5)-C(6)	176.8(16)
C(6)-N(2)-C(10)-C(9)	-2(2)	C(1)-N(1)-C(5)-C(4)	-3(2)
Pt-N(2)-C(10)-C(9)	-173.8(9)	Pt-N(1)-C(5)-C(4)	177.8(11)
C(6)-N(2)-C(10)-C(11)	176.9(12)	C(1)-N(1)-C(5)-C(6)	179.9(12)
Pt-N(2)-C(10)-C(11)	5.5(14)	Pt-N(1)-C(5)-C(6)	0.7(16)
C(13)-C(12)-C(11)-N(3')	-1(2)	N(2)-C(6)-C(5)-C(4)	-174.2(14)
C(13)-C(12)-C(11)-C(10)	178.2(14)	C(7)-C(6)-C(5)-C(4)	10(2)
N(2)-C(10)-C(11)-N(3')	-3.9(17)	N(2)-C(6)-C(5)-N(1)	2.8(19)
C(9)-C(10)-C(11)-N(3')	175.2(13)	C(7)-C(6)-C(5)-N(1)	-172.6(14)
N(2)-C(10)-C(11)-C(12)	176.6(12)	C(5)-C(4)-C(3)-C(2)	4(3)
C(9)-C(10)-C(11)-C(12)	-4(2)	C(11)-N(3')-C(15)-C(14)	-3(2)
C(12)-C(11)-N(3')-C(15)	3(2)	Pt-N(3')-C(15)-C(14)	-179.9(11)
C(10)-C(11)-N(3')-C(15)	-176.8(12)	C(13)-C(14)-C(15)-N(3')	2(2)
C(12)-C(11)-N(3')-Pt	179.9(11)	C(4)-C(3)-C(2)-C(1)	-5(3)
C(10)-C(11)-N(3')-Pt	0.4(14)	N(1)-C(1)-C(2)-C(3)	2(3)
N(2)-Pt-N(3')-C(15)	178.9(12)	C(17)-N(4)-C(16)-N(5)	-1(2)
N(1)-Pt-N(3')-C(15)	-178.1(14)	Pt-N(4)-C(16)-N(5)	-175.3(11)
N(4)-Pt-N(3')-C(15)	2.4(13)	C(17)-N(4)-C(16)-C(20)	-179.0(16)
N(2)-Pt-N(3')-C(11)	1.9(9)	Pt-N(4)-C(16)-C(20)	7(3)
N(1)-Pt-N(3')-C(11)	5(2)	C(19)-N(5)-C(16)-N(4)	-178.7(18)

Bond:	Angle (deg):	Bond:	Angle (deg):
N(4)-Pt-N(3')-C(11)	-174.6(9)	C(18)-N(5)-C(16)-N(4)	0(2)
C(16)-N(5)-C(18)-C(17)	1(2)	C(19)-N(5)-C(16)-C(20)	-1(3)
C(19)-N(5)-C(18)-C(17)	179.8(19)	C(18)-N(5)-C(16)-C(20)	178.3(17)
N(2)-C(10)-C(9)-C(8)	1(2)		

Symmetry transformations used to generate equivalent atoms:

F.3 X-ray Tables for PtL1-Pyz

Table F.3.1: Bond lengths of PtL1-Pyz.

Bond:	Length (Å):	Bond:	Length (Å):
C(1)-N(1)	1.306(10)	C(15')-C(16)	1.300(15)
C(1)-C(2)	1.352(12)	C(15')-N(5')	1.320(10)
C(1S')-N(1S')	1.456(16)	C(16)-C(19)	1.426(14)
C(2)-C(3)	1.353(14)	C(17)-N(2)	1.351(10)
C(3)-C(4)	1.364(13)	C(19)-N(4)	1.313(10)
C(4)-C(5)	1.348(11)	N(1)-Pt	2.025(6)
C(5)-N(1)	1.368(9)	N(1S')-O(2S')	1.186(13)
C(5)-C(6)	1.499(11)	N(1S')-O(1S')	1.251(14)
C(6)-N(2)	1.315(10)	N(2)-Pt	1.924(6)
C(6)-C(7)	1.383(10)	N(3)-Pt	2.017(6)
C(7)-C(8)	1.353(13)	N(4)-N(5')	1.333(8)
C(8)-C(9)	1.404(13)	N(4)-Pt	2.011(6)
C(9)-C(17)	1.352(11)	O(1)-Cl(03)	1.326(12)
C(10)-N(3)	1.363(10)	O(2)-Cl(03)	1.350(8)
C(10)-C(11)	1.369(11)	O(3)-Cl(03)	1.424(8)
C(10)-C(17)	1.490(11)	O(4)-Cl(03)	1.311(11)
C(11)-C(12)	1.377(12)	O(5)-Cl(02)	1.387(11)
C(12)-C(13)	1.367(12)	O(6)-Cl(02)	1.392(7)
C(13)-C(14)	1.373(11)	O(7)-Cl(02)	1.387(11)
C(14)-N(3)	1.335(9)	O(8)-Cl(02)	1.349(9)

Table F.3.2: Bond angles of **PtL1-Pyz**.

Bond:	Angle (deg):	Bond:	Angle (deg):
N(1)-C(1)-C(2)	122.7(8)	O(2S')-N(1S')-C(1S')	121.2(13)
C(1)-C(2)-C(3)	120.2(9)	O(1S')-N(1S')-C(1S')	113.1(11)
C(2)-C(3)-C(4)	118.4(8)	C(6)-N(2)-C(17)	122.8(6)
C(5)-C(4)-C(3)	119.3(9)	C(6)-N(2)-Pt	119.1(5)
C(4)-C(5)-N(1)	121.9(8)	C(17)-N(2)-Pt	118.0(5)
C(4)-C(5)-C(6)	124.7(7)	C(14)-N(3)-C(10)	118.6(7)
N(1)-C(5)-C(6)	113.3(6)	C(14)-N(3)-Pt	128.1(5)
N(2)-C(6)-C(7)	119.0(7)	C(10)-N(3)-Pt	113.3(5)
N(2)-C(6)-C(5)	113.3(6)	C(19)-N(4)-N(5')	106.3(7)
C(7)-C(6)-C(5)	127.7(7)	C(19)-N(4)-Pt	130.7(7)
C(8)-C(7)-C(6)	119.5(8)	N(5')-N(4)-Pt	123.0(5)
C(7)-C(8)-C(9)	120.7(8)	C(15')-N(5')-N(4)	110.7(8)
C(17)-C(9)-C(8)	117.4(8)	O(8)-Cl(02)-O(5)	111.8(9)
N(3)-C(10)-C(11)	122.3(8)	O(8)-Cl(02)-O(7)	109.3(10)
N(3)-C(10)-C(17)	114.5(7)	O(5)-Cl(02)-O(7)	105.9(10)
C(11)-C(10)-C(17)	123.2(8)	O(8)-Cl(02)-O(6)	112.7(5)
C(10)-C(11)-C(12)	117.7(8)	O(5)-Cl(02)-O(6)	109.8(8)
C(13)-C(12)-C(11)	120.6(8)	O(7)-Cl(02)-O(6)	107.1(6)
C(12)-C(13)-C(14)	119.1(8)	O(4)-Cl(03)-O(1)	101.2(13)
N(3)-C(14)-C(13)	121.7(8)	O(4)-Cl(03)-O(2)	112.3(9)
C(16)-C(15')-N(5')	109.2(9)	O(1)-Cl(03)-O(2)	112.3(10)
C(15')-C(16)-C(19)	105.4(9)	O(4)-Cl(03)-O(3)	106.8(9)
N(2)-C(17)-C(9)	120.5(7)	O(1)-Cl(03)-O(3)	109.3(9)
N(2)-C(17)-C(10)	112.6(6)	O(2)-Cl(03)-O(3)	114.0(7)
C(9)-C(17)-C(10)	126.9(8)	N(2)-Pt-N(4)	176.7(2)
N(4)-C(19)-C(16)	108.3(9)	N(2)-Pt-N(3)	81.5(3)
C(1)-N(1)-C(5)	117.4(7)	N(4)-Pt-N(3)	99.4(3)
C(1)-N(1)-Pt	129.1(6)	N(2)-Pt-N(1)	80.8(3)
C(5)-N(1)-Pt	113.4(5)	N(4)-Pt-N(1)	98.3(3)
O(2S')-N(1S')-O(1S')	125.6(13)	N(3)-Pt-N(1)	162.3(3)

Table F.3.3: Atomic coordinates ($\times 10^4$) and equivalent isotropic displacement parameters ($\text{\AA}^2 \times 10^3$) for **PtL1-Pyz**. $U(\text{eq})$ is defined as one third of the trace of the orthogonalized U^{ij} tensor.

	x	y	z	U(eq)
C(1)	6913(5)	1481(7)	2054(6)	57(2)
C(1S')	4258(8)	1554(12)	910(9)	106(4)
C(2)	6704(5)	477(9)	2407(7)	75(3)
C(3)	6958(6)	-550(8)	2139(8)	77(3)
C(4)	7444(6)	-539(7)	1530(7)	68(2)
C(5)	7637(5)	482(6)	1197(6)	47(2)
C(6)	8147(5)	615(7)	508(5)	51(2)
C(7)	8486(6)	-254(7)	82(7)	63(2)
C(8)	8910(6)	30(8)	-551(7)	71(3)
C(9)	9018(5)	1195(8)	-770(6)	59(2)
C(10)	8684(5)	3289(8)	-479(6)	50(2)
C(11)	9105(5)	3809(7)	-1047(6)	59(2)
C(12)	9087(6)	5002(8)	-1102(7)	68(2)
C(13)	8650(6)	5633(8)	-614(7)	63(2)
C(14)	8239(5)	5062(6)	-55(6)	54(2)
C(15')	5984(7)	5043(8)	1481(8)	76(3)
C(16)	6677(9)	5626(9)	2023(8)	90(4)
C(17)	8669(5)	2010(6)	-339(6)	48(2)
C(19)	7401(7)	5023(7)	1917(7)	68(2)
N(1)	7361(4)	1516(5)	1454(5)	48(1)
N(1S')	3769(7)	2639(9)	713(7)	82(2)
N(2)	8253(4)	1702(5)	295(5)	43(1)
N(3)	8261(4)	3909(5)	29(4)	46(1)
N(4)	7093(4)	4138(5)	1305(5)	50(2)
N(5')	6223(4)	4165(6)	1038(5)	64(2)
O(1)	5619(10)	3068(12)	-1110(20)	239(11)
O(1S')	3025(8)	2545(10)	766(8)	130(3)
O(2)	4854(7)	1616(13)	-2056(8)	179(5)
O(2S')	4088(9)	3512(11)	565(8)	171(5)
O(3)	6379(6)	1552(10)	-1353(7)	137(4)
O(4)	5581(9)	1540(20)	-391(9)	261(11)
O(5)	10083(10)	7085(8)	7725(16)	181(7)
O(6)	9749(7)	9006(7)	7633(7)	126(4)
O(7)	8930(9)	7758(9)	6456(8)	161(5)
O(8)	8876(11)	7686(7)	8016(11)	192(7)

	x	y	z	U(eq)
Cl(02)	9406(2)	7887(1)	7490(2)	53(1)
Cl(03)	5581(2)	1933(2)	-1266(2)	60(1)
Pt	7719(1)	2907(1)	818(1)	41(1)

Table F.3.4: Anisotropic displacement parameters ($\text{\AA}^2 \times 10^3$) for **PtL1-Pyz**. The anisotropic displacement factor exponent takes the form: $-2\pi^2 [h^2 a^{*2} U^{11} + \dots + 2 h k a^* b^* U^{12}]$.

	U¹¹	U²²	U³³	U²³	U¹³	U¹²
C(1)	53(5)	61(5)	64(5)	16(4)	28(4)	12(4)
C(1S')	88(9)	127(11)	96(8)	-13(8)	25(7)	17(8)
C(2)	48(5)	96(8)	81(6)	34(6)	23(4)	-2(5)
C(3)	73(6)	59(6)	102(7)	30(5)	36(6)	4(5)
C(4)	56(5)	48(5)	88(6)	15(4)	14(5)	4(4)
C(5)	40(4)	42(4)	51(4)	5(3)	9(3)	3(3)
C(6)	41(4)	51(4)	52(4)	-1(3)	8(3)	10(3)
C(7)	64(5)	44(4)	76(5)	-11(4)	18(4)	6(4)
C(8)	60(6)	72(6)	80(6)	-21(5)	23(5)	15(4)
C(9)	51(5)	64(5)	66(5)	-1(4)	28(4)	14(4)
C(10)	37(4)	61(4)	46(4)	3(3)	6(3)	-5(3)
C(11)	48(5)	64(5)	66(5)	9(4)	22(4)	15(4)
C(12)	57(5)	78(6)	67(5)	15(5)	21(4)	-10(4)
C(13)	66(6)	54(5)	71(5)	13(4)	28(4)	4(4)
C(14)	58(5)	45(4)	59(4)	3(3)	21(4)	3(3)
C(15')	80(7)	72(6)	93(7)	1(5)	50(6)	22(5)
C(16)	156(12)	58(6)	86(7)	-3(5)	80(8)	22(7)
C(17)	29(4)	53(5)	52(4)	0(3)	6(3)	6(3)
C(19)	102(8)	45(4)	66(5)	-13(4)	40(5)	-16(5)
N(1)	27(3)	51(4)	59(4)	7(3)	7(3)	1(2)
N(1S')	70(6)	94(7)	80(6)	5(5)	25(5)	1(5)
N(2)	30(3)	44(3)	51(3)	-3(3)	11(3)	5(2)
N(3)	46(3)	42(3)	52(3)	-2(3)	20(3)	4(3)
N(4)	51(4)	47(3)	55(4)	3(3)	23(3)	7(3)
N(5')	51(4)	67(4)	77(5)	5(3)	29(3)	17(3)
O(1)	113(11)	153(12)	390(30)	-83(13)	17(13)	45(8)
O(1S')	103(7)	116(6)	155(10)	-2(6)	29(6)	18(7)
O(2)	97(7)	279(13)	116(7)	-25(9)	-13(6)	-67(9)
O(2S')	209(12)	151(10)	123(8)	43(8)	26(8)	-55(10)
O(3)	84(6)	189(9)	137(7)	-57(7)	38(5)	19(7)

U^{11}	U^{22}	U^{33}	U^{23}	U^{13}	U^{12}	
O(4)	145(11)	540(30)	117(9)	96(15)	65(8)	-26(17)
O(5)	117(10)	111(9)	320(20)	54(9)	90(12)	43(6)
O(6)	184(9)	81(5)	156(8)	-44(5)	115(7)	-72(6)
O(7)	208(13)	145(9)	97(7)	-12(6)	16(8)	-70(8)
O(8)	380(20)	53(5)	276(15)	-24(6)	281(16)	-34(7)
Cl(02)	60(1)	43(1)	61(1)	-4(1)	30(1)	-7(1)
Cl(03)	51(1)	70(1)	54(1)	-2(1)	14(1)	-3(1)
Pt	34(1)	40(1)	45(1)	-1(1)	12(1)	3(1)

Table F.3.5: Hydrogen coordinates ($\times 10^4$) and isotropic displacement parameters ($\text{\AA}^2 \times 10^3$) for**PtL1-Pyz.**

	x	y	z	U(eq)
H(1)	6729	2176	2246	69
H(1S1)	4488	1420	382	159
H(1S2)	3874	927	920	159
H(1S3)	4733	1598	1557	159
H(2)	6385	492	2836	90
H(3)	6805	-1245	2364	92
H(4)	7641	-1231	1347	81
H(7)	8422	-1027	229	76
H(8)	9132	-553	-845	86
H(9)	9317	1398	-1194	70
H(11)	9394	3373	-1384	71
H(12)	9374	5381	-1474	81
H(13)	8631	6438	-659	76
H(14)	7938	5490	273	65
H(15')	5410	5216	1416	92
H(16)	6697	6294	2400	108
H(19)	7989	5223	2228	82
H(5')	5866	3678	633	76

Table F.3.6: Torsion angles

Bond:	Angle (deg):	Bond:	Angle (deg):
N(1)-C(1)-C(2)-C(3)	-0.3(14)	C(9)-C(17)-N(2)-Pt	-176.7(6)
C(1)-C(2)-C(3)-C(4)	1.7(14)	C(10)-C(17)-N(2)-Pt	3.4(8)
C(2)-C(3)-C(4)-C(5)	-1.6(14)	C(13)-C(14)-N(3)-C(10)	-1.8(12)
C(3)-C(4)-C(5)-N(1)	0.2(12)	C(13)-C(14)-N(3)-Pt	179.2(6)

Bond:	Angle (deg):	Bond:	Angle (deg):
C(3)-C(4)-C(5)-C(6)	-178.6(8)	C(11)-C(10)-N(3)-C(14)	1.9(11)
C(4)-C(5)-C(6)-N(2)	-179.7(7)	C(17)-C(10)-N(3)-C(14)	-179.8(7)
N(1)-C(5)-C(6)-N(2)	1.5(9)	C(11)-C(10)-N(3)-Pt	-179.0(6)
C(4)-C(5)-C(6)-C(7)	1.6(13)	C(17)-C(10)-N(3)-Pt	-0.7(8)
N(1)-C(5)-C(6)-C(7)	-177.3(7)	C(16)-C(19)-N(4)-N(5')	-0.4(9)
N(2)-C(6)-C(7)-C(8)	-0.7(12)	C(16)-C(19)-N(4)-Pt	-179.4(6)
C(5)-C(6)-C(7)-C(8)	178.0(8)	C(16)-C(15')-N(5')-N(4)	1.6(11)
C(6)-C(7)-C(8)-C(9)	0.7(14)	C(19)-N(4)-N(5')-C(15')	-0.7(9)
C(7)-C(8)-C(9)-C(17)	-1.2(14)	Pt-N(4)-N(5')-C(15')	178.5(5)
N(3)-C(10)-C(11)-C(12)	-0.5(12)	C(6)-N(2)-Pt-N(4)	-72(4)
C(17)-C(10)-C(11)-C(12)	-178.7(7)	C(17)-N(2)-Pt-N(4)	103(4)
C(10)-C(11)-C(12)-C(13)	-0.8(13)	C(6)-N(2)-Pt-N(3)	-178.3(6)
C(11)-C(12)-C(13)-C(14)	0.9(13)	C(17)-N(2)-Pt-N(3)	-3.0(5)
C(12)-C(13)-C(14)-N(3)	0.5(13)	C(6)-N(2)-Pt-N(1)	2.4(5)
N(5')-C(15')-C(16)-C(19)	-1.7(11)	C(17)-N(2)-Pt-N(1)	177.6(6)
C(8)-C(9)-C(17)-N(2)	1.6(12)	C(19)-N(4)-Pt-N(2)	-169(4)
C(8)-C(9)-C(17)-C(10)	-178.5(8)	N(5')-N(4)-Pt-N(2)	12(5)
N(3)-C(10)-C(17)-N(2)	-1.6(9)	C(19)-N(4)-Pt-N(3)	-63.7(7)
C(11)-C(10)-C(17)-N(2)	176.7(7)	N(5')-N(4)-Pt-N(3)	117.3(6)
N(3)-C(10)-C(17)-C(9)	178.4(8)	C(19)-N(4)-Pt-N(1)	116.6(7)
C(11)-C(10)-C(17)-C(9)	-3.3(13)	N(5')-N(4)-Pt-N(1)	-62.4(6)
C(15')-C(16)-C(19)-N(4)	1.3(11)	C(14)-N(3)-Pt-N(2)	-179.0(7)
C(2)-C(1)-N(1)-C(5)	-1.1(12)	C(10)-N(3)-Pt-N(2)	1.9(5)
C(2)-C(1)-N(1)-Pt	178.5(6)	C(14)-N(3)-Pt-N(4)	4.2(7)
C(4)-C(5)-N(1)-C(1)	1.2(11)	C(10)-N(3)-Pt-N(4)	-174.8(5)
C(6)-C(5)-N(1)-C(1)	-179.9(6)	C(14)-N(3)-Pt-N(1)	-176.9(7)
C(4)-C(5)-N(1)-Pt	-178.6(6)	C(10)-N(3)-Pt-N(1)	4.1(11)
C(6)-C(5)-N(1)-Pt	0.4(8)	C(1)-N(1)-Pt-N(2)	178.9(7)
C(7)-C(6)-N(2)-C(17)	1.1(11)	C(5)-N(1)-Pt-N(2)	-1.4(5)
C(5)-C(6)-N(2)-C(17)	-177.8(6)	C(1)-N(1)-Pt-N(4)	-4.3(7)
C(7)-C(6)-N(2)-Pt	176.1(6)	C(5)-N(1)-Pt-N(4)	175.4(5)
C(5)-C(6)-N(2)-Pt	-2.8(8)	C(1)-N(1)-Pt-N(3)	176.8(7)
C(9)-C(17)-N(2)-C(6)	-1.6(12)	C(5)-N(1)-Pt-N(3)	-3.5(11)
C(10)-C(17)-N(2)-C(6)	178.5(6)		

Symmetry transformations used to generate equivalent atoms:

F.4 X-ray Tables for PtL3-Pyz

Table F.4.1: Bond lengths of PtL3-Pyz.

Bond:	Length (Å):	Bond:	Length (Å):
Pt-N(2)	1.927(10)	O(2)-Cl(1)	1.45(3)
Pt-N(3)	2.002(10)	O(8)-Cl(2)	1.49(4)
Pt-N(1)	2.007(10)	C(1)-C(2)	1.417(19)
Pt-N(4)	2.017(11)	C(1)-H(1)	0.9300
N(5)-N(4)	1.322(15)	C(17)-C(18)	1.391(16)
N(5)-C(25)	1.323(19)	C(17)-H(17)	0.9300
N(5)-H(100)	0.95(2)	C(22)-C(21)	1.483(17)
N(2)-C(10)	1.348(14)	C(22)-H(22A)	0.9600
N(2)-C(6)	1.357(13)	C(22)-H(22B)	0.9600
N(1)-C(1)	1.314(14)	C(22)-H(22C)	0.9600
N(1)-C(5)	1.396(13)	C(6)-C(5)	1.499(15)
C(7)-C(6)	1.362(15)	O(1S)-N(1S)	1.227(19)
C(7)-C(8)	1.412(15)	C(14)-C(15)	1.382(19)
C(7)-H(7)	0.9300	C(14)-H(14)	0.9300
C(8)-C(9)	1.410(15)	N(1S)-O(2S)	1.16(2)
C(8)-C(16)	1.485(15)	N(1S)-C(1S)	1.39(2)
O(6)-Cl(2)	1.32(4)	C(21)-C(20)	1.385(17)
N(4)-C(23)	1.322(15)	C(23)-C(24)	1.361(17)
O(7)-Cl(2)	1.32(4)	C(23)-H(23)	0.9300
O(4)-Cl(1)	1.42(3)	O(3)-Cl(1)	1.35(4)
O(1)-Cl(1)	1.32(3)	C(18)-H(18)	0.9300
O(5)-Cl(2)	1.42(2)	C(1S)-H(1S1)	0.9600
C(16)-C(17)	1.392(16)	C(1S)-H(1S2)	0.9600
C(16)-C(21)	1.411(16)	C(1S)-H(1S3)	0.9600
C(10)-C(9)	1.382(15)	C(12)-H(12)	0.9300
C(10)-C(11)	1.469(14)	C(24)-C(25)	1.34(2)
C(9)-H(9)	0.9300	C(24)-H(24)	0.9300
C(19)-C(20)	1.37(2)	C(5)-C(4)	1.375(15)
C(19)-C(18)	1.413(19)	C(4)-C(3)	1.366(17)
C(19)-H(19)	0.9300	C(4)-H(4)	0.9300
N(3)-C(15)	1.347(14)	C(15)-H(15)	0.9300
N(3)-C(11)	1.372(14)	C(3)-C(2)	1.341(19)
C(13)-C(12)	1.369(17)	C(3)-H(3)	0.9300
C(13)-C(14)	1.381(19)	C(20)-H(20)	0.9300
C(13)-H(13)	0.9300	C(25)-H(25)	0.9300

Table F.4.2: Bond angles of **PtL3-Pyz**.

Bond:	Angle (deg):	Bond:	Angle (deg):
N(2)-Pt-N(3)	81.1(3)	C(13)-C(14)-C(15)	118.8(11)
N(2)-Pt-N(1)	81.8(4)	C(13)-C(14)-H(14)	120.6
N(3)-Pt-N(1)	162.7(4)	C(15)-C(14)-H(14)	120.6
N(2)-Pt-N(4)	175.5(4)	O(2S)-N(1S)-O(1S)	122(2)
N(3)-Pt-N(4)	97.2(4)	O(2S)-N(1S)-C(1S)	123(2)
N(1)-Pt-N(4)	100.1(4)	O(1S)-N(1S)-C(1S)	114.8(19)
N(4)-N(5)-C(25)	111.4(13)	C(20)-C(21)-C(16)	119.4(12)
N(4)-N(5)-H(100)	118(9)	C(20)-C(21)-C(22)	115.9(11)
C(25)-N(5)-H(100)	128(9)	C(16)-C(21)-C(22)	124.7(10)
C(10)-N(2)-C(6)	122.6(10)	N(4)-C(23)-C(24)	111.6(12)
C(10)-N(2)-Pt	117.8(7)	N(4)-C(23)-H(23)	124.2
C(6)-N(2)-Pt	119.2(8)	C(24)-C(23)-H(23)	124.2
C(1)-N(1)-C(5)	117.3(10)	C(17)-C(18)-C(19)	119.2(12)
C(1)-N(1)-Pt	129.8(8)	C(17)-C(18)-H(18)	120.4
C(5)-N(1)-Pt	112.9(7)	C(19)-C(18)-H(18)	120.4
C(6)-C(7)-C(8)	121.1(10)	N(1S)-C(1S)-H(1S1)	109.5
C(6)-C(7)-H(7)	119.4	N(1S)-C(1S)-H(1S2)	109.5
C(8)-C(7)-H(7)	119.4	H(1S1)-C(1S)-H(1S2)	109.5
C(9)-C(8)-C(7)	116.6(10)	N(1S)-C(1S)-H(1S3)	109.5
C(9)-C(8)-C(16)	123.8(10)	H(1S1)-C(1S)-H(1S3)	109.5
C(7)-C(8)-C(16)	119.6(9)	H(1S2)-C(1S)-H(1S3)	109.5
N(5)-N(4)-C(23)	104.3(11)	C(13)-C(12)-C(11)	119.4(12)
N(5)-N(4)-Pt	128.3(9)	C(13)-C(12)-H(12)	120.3
C(23)-N(4)-Pt	127.1(9)	C(11)-C(12)-H(12)	120.3
C(17)-C(16)-C(21)	119.1(10)	C(25)-C(24)-C(23)	104.6(12)
C(17)-C(16)-C(8)	117.9(10)	C(25)-C(24)-H(24)	127.7
C(21)-C(16)-C(8)	123.0(10)	C(23)-C(24)-H(24)	127.7
N(2)-C(10)-C(9)	119.1(10)	C(4)-C(5)-N(1)	121.3(10)
N(2)-C(10)-C(11)	112.9(9)	C(4)-C(5)-C(6)	124.0(9)
C(9)-C(10)-C(11)	128.1(10)	N(1)-C(5)-C(6)	114.7(9)
C(10)-C(9)-C(8)	120.9(10)	C(3)-C(4)-C(5)	118.7(11)
C(10)-C(9)-H(9)	119.5	C(3)-C(4)-H(4)	120.7
C(8)-C(9)-H(9)	119.5	C(5)-C(4)-H(4)	120.7
C(20)-C(19)-C(18)	119.5(11)	O(6)-Cl(2)-O(7)	120(2)
C(20)-C(19)-H(19)	120.3	O(6)-Cl(2)-O(5)	110.9(19)
C(18)-C(19)-H(19)	120.3	O(7)-Cl(2)-O(5)	118(4)

Bond:	Angle (deg):	Bond:	Angle (deg):
C(15)-N(3)-C(11)	118.5(10)	O(6)-Cl(2)-O(8)	107(4)
C(15)-N(3)-Pt	127.8(9)	O(7)-Cl(2)-O(8)	100(2)
C(11)-N(3)-Pt	113.7(7)	O(5)-Cl(2)-O(8)	94(2)
C(12)-C(13)-C(14)	120.0(12)	N(3)-C(15)-C(14)	122.2(12)
C(12)-C(13)-H(13)	120.0	N(3)-C(15)-H(15)	118.9
C(14)-C(13)-H(13)	120.0	C(14)-C(15)-H(15)	118.9
N(3)-C(11)-C(12)	121.2(10)	C(2)-C(3)-C(4)	122.0(12)
N(3)-C(11)-C(10)	114.1(9)	C(2)-C(3)-H(3)	119.0
C(12)-C(11)-C(10)	124.5(11)	C(4)-C(3)-H(3)	119.0
N(1)-C(1)-C(2)	123.6(11)	C(19)-C(20)-C(21)	121.7(12)
N(1)-C(1)-H(1)	118.2	C(19)-C(20)-H(20)	119.2
C(2)-C(1)-H(1)	118.2	C(21)-C(20)-H(20)	119.2
C(18)-C(17)-C(16)	121.1(12)	N(5)-C(25)-C(24)	108.0(14)
C(18)-C(17)-H(17)	119.5	N(5)-C(25)-H(25)	126.0
C(16)-C(17)-H(17)	119.5	C(24)-C(25)-H(25)	126.0
C(21)-C(22)-H(22A)	109.5	C(3)-C(2)-C(1)	117.1(12)
C(21)-C(22)-H(22B)	109.5	C(3)-C(2)-H(2)	121.5
H(22A)-C(22)-H(22B)	109.5	C(1)-C(2)-H(2)	121.5
C(21)-C(22)-H(22C)	109.5	O(1)-Cl(1)-O(3)	121(3)
H(22A)-C(22)-H(22C)	109.5	O(1)-Cl(1)-O(4)	111(3)
H(22B)-C(22)-H(22C)	109.5	O(3)-Cl(1)-O(4)	101.7(19)
N(2)-C(6)-C(7)	119.5(10)	O(1)-Cl(1)-O(2)	107(2)
N(2)-C(6)-C(5)	111.2(9)	O(3)-Cl(1)-O(2)	109(3)
C(7)-C(6)-C(5)	129.3(10)	O(4)-Cl(1)-O(2)	107(3)

Table F.4.3: Atomic coordinates ($\times 10^4$) and equivalent isotropic displacement parameters ($\text{\AA}^2 \times 10^3$) for **PtL3-Pyz**. $U(\text{eq})$ is defined as one third of the trace of the orthogonalized U_{ij} tensor.

	x	y	z	U(eq)
Pt	5124(1)	-831(1)	2678(1)	47(1)
N(5)	6598(6)	-389(17)	2570(7)	76(4)
N(2)	4131(5)	-512(11)	2606(4)	46(2)
N(1)	4644(5)	-1751(12)	1736(5)	50(2)
C(7)	2892(6)	-1021(13)	2013(5)	41(2)
C(8)	2720(6)	-446(13)	2571(5)	40(2)
O(6)	5841(6)	-3415(18)	4499(6)	95(3)
N(4)	6171(6)	-1307(15)	2810(5)	62(3)
O(7)	7004(7)	-4394(19)	4705(8)	115(5)

	x	y	z	U(eq)
O(4)	5975(7)	1301(17)	1191(9)	114(5)
O(1)	5869(10)	4256(17)	948(9)	125(6)
O(5)	6747(5)	-2054(12)	5331(6)	91(4)
C(16)	1954(6)	-482(12)	2532(6)	45(2)
C(10)	4005(6)	99(14)	3150(5)	42(2)
C(9)	3301(6)	154(14)	3138(5)	44(2)
C(19)	492(7)	-554(15)	2399(7)	59(3)
N(3)	5295(4)	305(13)	3574(5)	49(2)
C(13)	5338(8)	2077(16)	4730(6)	65(3)
C(11)	4671(6)	632(13)	3700(5)	45(2)
O(2)	4894(6)	2800(30)	964(8)	138(6)
O(8)	6526(11)	-4800(20)	5464(6)	134(6)
C(1)	4933(6)	-2313(19)	1303(6)	62(3)
C(17)	1421(6)	55(16)	1933(6)	54(3)
C(22)	2255(7)	-1700(19)	3728(6)	63(3)
C(6)	3592(6)	-1078(13)	2042(5)	41(2)
O(1S)	7659(8)	-8750(20)	4543(10)	138(6)
C(14)	5971(7)	1746(18)	4611(7)	66(3)
N(1S)	7895(9)	-7570(20)	4273(8)	99(4)
C(21)	1747(6)	-1061(14)	3069(6)	47(2)
C(23)	6603(7)	-2513(19)	3212(7)	69(3)
O(3)	5854(8)	3050(20)	1950(6)	126(5)
C(18)	692(6)	10(19)	1855(7)	62(3)
C(1S)	8574(13)	-6910(40)	4664(13)	151(9)
C(12)	4687(7)	1530(17)	4274(6)	56(3)
C(24)	7296(7)	-2350(20)	3228(8)	80(4)
C(5)	3889(5)	-1712(15)	1522(5)	44(2)
C(4)	3466(6)	-2235(17)	883(6)	59(3)
Cl(2)	6520(20)	-3580(40)	4910(15)	660(30)
C(15)	5931(6)	836(14)	4033(7)	58(3)
C(3)	3798(7)	-2770(19)	451(6)	69(4)
C(20)	1019(8)	-1099(15)	2987(8)	64(4)
C(25)	7275(8)	-970(20)	2821(10)	84(5)
C(2)	4522(8)	-2870(20)	640(7)	80(4)
Cl(1)	5671(17)	2980(40)	1274(19)	630(30)
O(2S)	7583(14)	-7100(30)	3729(10)	210(10)

Table F.4.4: Anisotropic displacement parameters ($\text{\AA}^2 \times 10^3$) for **PtL3-Pyz**. The anisotropic displacement factor exponent takes the form: $-2\pi^2 [h^2 a^{*2} U^{11} + \dots + 2 h k a^* b^* U^{12}]$

	U^{11}	U^{22}	U^{33}	U^{23}	U^{13}	U^{12}
Pt	36(1)	54(1)	49(1)	6(1)	11(1)	0(1)
N(5)	53(7)	88(9)	98(9)	21(7)	41(7)	1(6)
N(2)	45(5)	48(5)	36(4)	-5(4)	3(4)	-2(4)
N(1)	49(5)	37(5)	63(6)	9(4)	18(5)	-5(4)
C(7)	39(5)	48(6)	36(5)	3(4)	12(4)	1(4)
C(8)	41(6)	35(5)	43(6)	5(4)	12(5)	3(4)
O(6)	57(6)	115(8)	79(7)	8(6)	-16(5)	-7(6)
N(4)	45(6)	81(7)	53(6)	19(5)	10(5)	1(5)
O(7)	85(9)	151(13)	120(11)	-55(9)	49(8)	8(8)
O(4)	89(9)	82(8)	175(14)	3(8)	53(9)	41(6)
O(1)	155(14)	110(10)	143(13)	56(9)	93(12)	47(8)
O(5)	47(5)	66(6)	145(10)	-45(6)	17(6)	-5(4)
C(16)	45(6)	35(5)	55(6)	-9(4)	18(5)	-4(4)
C(10)	45(6)	37(5)	40(6)	6(4)	10(5)	-9(5)
C(9)	46(6)	39(5)	46(6)	0(5)	13(5)	3(5)
C(19)	44(6)	61(8)	74(8)	-18(6)	24(6)	2(5)
N(3)	24(4)	67(6)	53(5)	-1(4)	8(4)	-4(4)
C(13)	78(9)	60(8)	48(7)	-10(6)	12(6)	-11(6)
C(11)	45(6)	44(6)	44(6)	0(4)	12(5)	-5(4)
O(2)	38(5)	218(16)	136(11)	-2(11)	5(6)	29(8)
O(8)	234(18)	104(9)	43(6)	18(6)	25(8)	-5(11)
C(1)	39(6)	94(9)	60(7)	7(7)	28(5)	4(6)
C(17)	52(7)	49(6)	58(7)	-7(6)	15(6)	-8(6)
C(22)	72(8)	73(8)	49(7)	3(6)	27(6)	-7(7)
C(6)	39(5)	44(6)	38(5)	1(4)	11(4)	-9(4)
O(1S)	87(10)	143(12)	188(18)	29(12)	55(11)	-8(9)
C(14)	52(7)	66(8)	57(7)	-1(6)	-8(6)	-5(6)
N(1S)	112(12)	107(11)	67(8)	-17(9)	18(8)	-4(10)
C(21)	48(6)	51(6)	46(6)	-11(5)	23(5)	-5(5)
C(23)	56(7)	82(9)	66(8)	28(7)	20(6)	15(7)
O(3)	132(11)	179(14)	60(7)	5(8)	26(7)	10(10)
C(18)	35(6)	68(7)	74(9)	-21(7)	5(6)	4(6)
C(1S)	118(18)	190(20)	134(19)	-19(18)	35(16)	-70(18)
C(12)	52(7)	58(6)	51(7)	-4(6)	9(5)	-2(6)
C(24)	47(7)	102(11)	80(9)	14(9)	8(7)	23(8)

	U ¹¹	U ²²	U ³³	U ²³	U ¹³	U ¹²
C(5)	33(5)	59(6)	43(6)	12(5)	17(4)	4(5)
C(4)	47(6)	80(9)	47(6)	0(6)	14(5)	-7(6)
Cl(2)	820(60)	470(30)	380(40)	-210(30)	-150(40)	240(40)
C(15)	37(6)	62(7)	63(7)	5(6)	4(5)	-4(5)
C(3)	66(8)	94(10)	46(6)	-13(7)	19(6)	-15(7)
C(20)	70(9)	60(7)	86(10)	-18(7)	56(8)	-7(6)
C(25)	47(8)	108(13)	100(12)	6(9)	30(8)	15(7)
C(2)	75(10)	107(12)	68(9)	4(8)	38(8)	16(8)
Cl(1)	480(50)	700(60)	560(50)	290(50)	10(40)	150(50)
O(2S)	300(30)	158(18)	111(14)	-3(13)	4(16)	11(16)

Table F.4.5: Hydrogen coordinates ($\times 10^4$) and isotropic displacement parameters ($\text{\AA}^2 \times 10^3$) for**PtL3-Pyz.**

	x	y	z	U(eq)
H(7)	2522	-1366	1620	49
H(9)	3210	594	3509	53
H(19)	8	-555	2359	71
H(13)	5355	2671	5120	78
H(1)	5436	-2348	1439	74
H(17)	1556	450	1580	65
H(22A)	2367	-732	4046	94
H(22B)	2693	-2119	3678	94
H(22C)	2036	-2664	3887	94
H(14)	6415	2129	4915	79
H(23)	6452	-3365	3454	82
H(18)	340	347	1449	75
H(1S1)	8920	-7872	4784	226
H(1S2)	8548	-6373	5065	226
H(1S3)	8723	-6021	4413	226
H(12)	4259	1760	4349	67
H(24)	7694	-3050	3469	96
H(4)	2963	-2224	748	70
H(15)	6357	581	3959	70
H(3)	3515	-3075	12	82
H(20)	884	-1504	3339	77
H(25)	7667	-504	2731	100
H(2)	4743	-3285	348	96
H(100)	6430(80)	730(100)	2360(70)	80(50)

Table F.4.6: Torsion angles

Bond:	Angle (deg):	Bond:	Angle (deg):
N(3)-Pt-N(2)-C(10)	-5.7(8)	N(2)-C(10)-C(11)-C(12)	170.5(11)
N(1)-Pt-N(2)-C(10)	177.2(8)	C(9)-C(10)-C(11)-C(12)	-9.6(18)
N(4)-Pt-N(2)-C(10)	62(5)	C(5)-N(1)-C(1)-C(2)	0.1(19)
N(3)-Pt-N(2)-C(6)	-179.0(8)	Pt-N(1)-C(1)-C(2)	-177.6(11)
N(1)-Pt-N(2)-C(6)	3.9(8)	C(21)-C(16)-C(17)-C(18)	-0.7(17)
N(4)-Pt-N(2)-C(6)	-111(5)	C(8)-C(16)-C(17)-C(18)	178.3(10)
N(2)-Pt-N(1)-C(1)	177.3(11)	C(10)-N(2)-C(6)-C(7)	0.6(15)
N(3)-Pt-N(1)-C(1)	167.8(12)	Pt-N(2)-C(6)-C(7)	173.6(7)
N(4)-Pt-N(1)-C(1)	-6.8(11)	C(10)-N(2)-C(6)-C(5)	-179.0(9)
N(2)-Pt-N(1)-C(5)	-0.5(7)	Pt-N(2)-C(6)-C(5)	-6.1(11)
N(3)-Pt-N(1)-C(5)	-10.0(16)	C(8)-C(7)-C(6)-N(2)	-2.4(15)
N(4)-Pt-N(1)-C(5)	175.5(7)	C(8)-C(7)-C(6)-C(5)	177.2(10)
C(6)-C(7)-C(8)-C(9)	3.5(14)	C(12)-C(13)-C(14)-C(15)	-1(2)
C(6)-C(7)-C(8)-C(16)	-177.2(9)	C(17)-C(16)-C(21)-C(20)	0.6(15)
C(25)-N(5)-N(4)-C(23)	-1.2(18)	C(8)-C(16)-C(21)-C(20)	-178.3(9)
C(25)-N(5)-N(4)-Pt	172.9(11)	C(17)-C(16)-C(21)-C(22)	178.8(11)
N(2)-Pt-N(4)-N(5)	-169(5)	C(8)-C(16)-C(21)-C(22)	-0.1(17)
N(3)-Pt-N(4)-N(5)	-101.6(13)	N(5)-N(4)-C(23)-C(24)	0.3(17)
N(1)-Pt-N(4)-N(5)	76.7(13)	Pt-N(4)-C(23)-C(24)	-173.9(10)
N(2)-Pt-N(4)-C(23)	4(6)	C(16)-C(17)-C(18)-C(19)	1.4(18)
N(3)-Pt-N(4)-C(23)	71.2(12)	C(20)-C(19)-C(18)-C(17)	-2.0(18)
N(1)-Pt-N(4)-C(23)	-110.5(12)	C(14)-C(13)-C(12)-C(11)	0.7(19)
C(9)-C(8)-C(16)-C(17)	138.7(11)	N(3)-C(11)-C(12)-C(13)	-1.1(18)
C(7)-C(8)-C(16)-C(17)	-40.6(13)	C(10)-C(11)-C(12)-C(13)	-175.2(11)
C(9)-C(8)-C(16)-C(21)	-42.4(14)	N(4)-C(23)-C(24)-C(25)	0.7(18)
C(7)-C(8)-C(16)-C(21)	138.3(10)	C(1)-N(1)-C(5)-C(4)	-0.2(16)
C(6)-N(2)-C(10)-C(9)	0.0(15)	Pt-N(1)-C(5)-C(4)	177.8(9)
Pt-N(2)-C(10)-C(9)	-173.0(8)	C(1)-N(1)-C(5)-C(6)	179.4(10)
C(6)-N(2)-C(10)-C(11)	179.9(9)	Pt-N(1)-C(5)-C(6)	-2.6(11)
Pt-N(2)-C(10)-C(11)	6.9(12)	N(2)-C(6)-C(5)-C(4)	-174.9(11)
N(2)-C(10)-C(9)-C(8)	1.1(15)	C(7)-C(6)-C(5)-C(4)	5.4(18)
C(11)-C(10)-C(9)-C(8)	-178.7(10)	N(2)-C(6)-C(5)-N(1)	5.5(13)
C(7)-C(8)-C(9)-C(10)	-2.8(15)	C(7)-C(6)-C(5)-N(1)	-174.2(10)
C(16)-C(8)-C(9)-C(10)	177.9(9)	N(1)-C(5)-C(4)-C(3)	-1.1(18)
N(2)-Pt-N(3)-C(15)	-173.5(10)	C(6)-C(5)-C(4)-C(3)	179.3(11)
N(1)-Pt-N(3)-C(15)	-164.0(10)	C(11)-N(3)-C(15)-C(14)	-2.2(17)
N(4)-Pt-N(3)-C(15)	10.6(10)	Pt-N(3)-C(15)-C(14)	174.3(9)

Bond:	Angle (deg):	Bond:	Angle (deg):
N(2)-Pt-N(3)-C(11)	3.2(7)	C(13)-C(14)-C(15)-N(3)	1.8(19)
N(1)-Pt-N(3)-C(11)	12.7(17)	C(5)-C(4)-C(3)-C(2)	3(2)
N(4)-Pt-N(3)-C(11)	-172.7(8)	C(18)-C(19)-C(20)-C(21)	2.0(18)
C(15)-N(3)-C(11)-C(12)	1.9(16)	C(16)-C(21)-C(20)-C(19)	-1.2(16)
Pt-N(3)-C(11)-C(12)	-175.2(9)	C(22)-C(21)-C(20)-C(19)	-179.6(11)
C(15)-N(3)-C(11)-C(10)	176.5(9)	N(4)-N(5)-C(25)-C(24)	2(2)
Pt-N(3)-C(11)-C(10)	-0.5(11)	C(23)-C(24)-C(25)-N(5)	-1.4(19)
N(2)-C(10)-C(11)-N(3)	-3.9(13)	C(4)-C(3)-C(2)-C(1)	-3(2)
C(9)-C(10)-C(11)-N(3)	175.9(10)	N(1)-C(1)-C(2)-C(3)	1(2)

Symmetry transformations used to generate equivalent atoms.